UNIVERSITAT DE BARCELONA

FACULTAT DE BIOLOGÍA

DEPARTAMENTO DE BIOQUÍMICA I BIOLOGÍA MOLECULAR

“Role of DOR/TP53INP2 in the control of muscle protein degradation”

“Papel de DOR/TP53INP2 en el control de la degradación de proteínas en el músculo esquelético”

PAULA MARTÍNEZ CRISTÓBAL

BARCELONA, 2016

UNIVERSITAT DE BARCELONA

FACULTAT DE BIOLOGIA

DEPARTAMENT DE BIOQUÍMICA I BIOLOGIA MOLECULAR

PROGRAMA DE DOCTORAT DE BIOMEDICINA

"Role of DOR/TP53INP2 in the control of muscle protein degradation"

"Papel de DOR/TP53INP2 en el control de la degradación de proteínas en el músculo esquelético"

Memoria presentada por Paula Martínez Cristóbal
para optar al título de doctor por la Universitat de Barcelona

ANTONIO ZORZANO OLARTE PAULA MARTÍNEZ CRISTÓBAL

BARCELONA, 2016

Hay tantas cosas que tendrás que descubrir.
Las cosas invisibles, las difíciles,
la brecha que te espera entre el deseo y el mundo:
apretarás los dientes, resistirás,
nunca pedirás nada.
No, no se vive para ganarle a nadie.
Se vive para darse.

Eduardo Galeano

A quienes me han hecho crecer

AGRADECIMIENTOS

Muchísimas gracias Antonio por brindarme la oportunidad de empezar esta tesis. Estos cuatros años han sido una experiencia intelectual increíblemente enriquecedora. Gracias por tu optimismo, tu ayuda, tus consejos y tu motivación. Gracias por el seguimiento constante de este proyecto y todas tus correcciones. Manuel, muchas gracias por tus infinitas ganas de preguntar en los seminarios, por todas tus contribuciones, ideas y tu buen humor.

JP y Fabio, me considero la doctoranda más afortunada del Universo por haber aprendido de vosotros y trabajado a vuestro lado. Sois unos científicos brillantes y unas buenísimas personas, esta tesis no hubiera sido posible sin vuestra ayuda, alegría, consejos y discusiones científicas, me habéis dado toda la energía y fuerza necesaria para llegar hasta aquí y me habéis enseñado que cualquier experimento puede esperar si es para ayudar a los demás.

Al equipito de "Lost in DOR", gracias por vuestra generosidad, ayuda y amistad. Ha sido un gusto compartir ciencia, risas y estreses a vuestro lado. A todos los compañeros del lab que me habéis acompañado en esta aventura, gracias por todo el apoyo y todas las charlas de ciencia y de la vida, me habéis enseñado mucho y habéis sido un gran pilar en el día a día de esta tesis, por hacerme sonreir, por todas las cenas, celebraciones, videos de tesis, viajes, noches ravaleras, por los room escapes ficticios... y no tan ficticios, por todo, todo, gracias.

Jordi y Celia, muchísimas gracias: el laboratorio no sería posible sin vuestra incuantificable ayuda, gracias de corazón por todo vuestro trabajo y buena predisposición para ayudarme siempre. Me siento feliz por haber sido vuestra compañera de pasillo. Natalia Plana y Vanessa, todos los estudios de ratones no hubieran sido posibles sin vosotras, sois unas grandes profesionales y ha sido un placer trabajar a vuestro lado. A todo el personal del estabulario, de las facilities y de administración que han estado siempre que lo he necesitado, y a Natalia Molner y Olga, por toda la ayuda con los papeleos y organización, muchas gracias.

A los recientes doctores, muchas gracias por todos los consejos y apoyo moral con los formatos, la burocracia y los metaarchivos mejorados. A Blanca, por tu ayuda con el diseño y maquetación. Y en especial, a María i Xavi, fuisteis mis primeros amigos aquí y ha sido un gusto compartir hasta la escritura con vosotros. Os estoy eternamente agradecida por vuestra bondad y armonía, por compartirlo todo, sois unos amores y os voy a echar muchísimo de menos. A Valeria y Alessio, por hacerme sentir siempre como en casa, porque parece como si nos conociéramos de toda la vida. María (delaF), muchas gracias por hacerme reir tanto en esta etapa de escritoras, me ha dado mucha fuerza correr juntas esta maratón. Jose, gracias a ti estoy ahora escribiendo esta tesis, muchas gracias por confiar en mí.

Gracias a todos los que hicieron realidad la aventura de la Ruta Quetzal 2002, en especial Anne y Lore, ese viaje confirmó mi pasión por el estudio de la naturaleza y de la vida y fue muy determinante en la elección de esta carrera. Hoy sigo haciendo mi ruta, orgullosa de echar la vista atrás y contemplar a todos los maestros y experiencias que me han acompañado (y lo seguirán por siempre) a ser quien quiero y quien puedo ser.

Muchas gracias por los amigos que se volvieron familia. Con vosotros, he pasado muchos de los mejores momentos de mi vida. A mis amigas del alma Ana y Cris, muchas gracias por estar siempre ahí y haber crecido juntas. Marija, Zoran, Luka e Ian, porque me derrito de ternura a vuestro lado, me habéis hecho la tía más feliz. A Caro, gracias por tus buenas vibraciones, tu paz y tu cariño. A Javi y Tere, mis compañeros de carrera, de aventuras, de amores y dramas, porque pase lo que pase, a vuestro lado puedo estar riendo sin parar, porque sois unos compañeros de vida inmejorables.

Muchas gracias a mi pequeña gran familia. A mis abuelas porque sois unas auténticas y unas valientes, por todo lo que me enseñáis cada día y por lo que me hacéis reir, os admiro. En la memoria de mis abuelos, especialmente de mi abuelo Rafa, que ha sido para mí como un segundo padre. A Gabriel, por hacerme un huequito en tu corazón. Pero sobre todo, esta tesis os la dedico a vosotros, mamá y papá, por vuestro apoyo incondicional, por creer siempre en mí y confiar en todas mis decisiones por muy alocadas que sean, porque siempre me lo habéis hecho todo más fácil, ofreciéndolo todo sin exigir nada a cambio y porque gracias a vosotros he podido tener la educación que he querido. Esta tesis también es vuestra, no hubiera podido llegar hasta aquí sin vosotros.

Y finalmente, gracias a ti, muchas gracias por todos los sueños hechos realidad. Por darme la mano y lanzarte al vacío, y desde ese entonces, convertirte en mi piedra angular en la que se ha sostenido toda la carga emocional de esta tesis. Contigo he caminado en los momentos más difíciles. Tus palabras y tus abrazos, siempre cargadas de paciencia, optimismo y cariño, fueron mi mejor bálsamo. Contigo también he compartido alegrías, millones de risas e infinitas aventuras, gracias por creer en lo imposible y por el amor, la ilusión y la motivación que pones en cada cosa que haces. Gracias por sacarme una sonrisa cada día de nuestras vidas. Sólo puedo decirte una y mil veces ¡GRACIAS!

Muchas gracias a todos de corazón

Paula Martínez Cristóbal
Barcelona, 5 de septiembre del 2016

INDEX

INDEX OF FIGURES

INTRODUCTION

RESULTS

DISCUSSION

MATERIALS & METHODS

RESUMEN

APPENDIX I

INDEX OF TABLES

CHAPTER 1 ABBREVIATIONS

1. ABBREVIATIONS

A

Ac-ANW-R110: Ac-Ala-Asn-Trp-rhodamine 110
Ac-PAL-R110: Ac-Pro-Ala-Leu-rhodamine 110
Akt: also known as protein kinase B or PKB
AMC: 7-amino-4-methylcoumarin
ATF4: activating transcription factor 4
Atg: autophagy-related gene
ATP: adenosine triphosphate

B

Baf: bafilomycin
BAG: Bcl-2-associated athanogene
Bag1: BAG family molecular chaperone regulator 1
Bag3: BAG family molecular chaperone regulator 3
BCA: bicinchoninic acid
βGF: beta-grasp folded
BMP: bone morphogenetic protein
BSA: bovine serum albumin

C

cDNA: coding DNA
Cf: final concentration
CFA: complete Freund's adjuvant
ChIP : chromatin immunoprecipitation
CHIP: C-terminus of Hsp70-interacting protein
CMA: chaperone-mediated autophagy
CPM: counts per minute
CQ: chloroquine
C26: colon 26 tumor

D

DMEM: Dulbecco Modified Eagle´s Medium

DNA: deoxyribonucleic acid
DOR: Diabetes and Obesity regulated gene
DTT: dithiothreitol
DUB: deubiquitinating enzyme

E

4E-BP1: Eukaryotic translation initiation factor 4E-binding protein 1
EcR: ecdysone receptor
EDL: extensor digitorum longus
EDTA: ethylenediaminetetraacetic acid
eIF2α: eukaryotic initiation factor 2 alpha
eIF3-f: eukaryotic translation initiation factor 3 subunit F
eIF4F: eukaryotic initiation factor 4F
ER: endoplasmic reticulum
ERAD: endoplasmic reticulum-associated degradation
E1: ubiquitin-activating enzyme
E2: ubiquitin-conjugating enzyme
E3: ubiquitin ligase

F

FBS: fetal bovine serum
FoxO: forkhead box protein O

G

GABARAP: gamma-aminobutyric acid receptor-associated protein
GABARAPL1: GABA type A receptor associated protein like 1
GADD34: growth arrest and DNA damage-inducible protein
GATE16: GABARAPL2: GABA type A receptor associated protein like 2
GFP: green fluorescent protein
GR: glucocorticoid receptor

H

HAT: hypoxathine, aminopterin, thymidine
HCL: hairy cell leukemia
HDAC6: histone deacetylase 6
Hela: Henrietta Lacks cervical cancer cells
HEK: human embryonic kidney cells
HFCS hybridoma fusion and clonning supplement

Hsc70: heat shock cognate 71 kDa protein
HSJ1: heat shock protein J1
HSP: heat shock protein
HSPA8: heat shock 70 kDa protein 8
HspBP: HSPA (heat shock 70 kDa) binding protein
Hsp70: 70 kilodalton heat shock protein
Hsp90: 90 kilodalton heat shock protein
HSR: heat shock response
HUGO: Human Genome Organization

I

I.B.W: initial body weight
IFA: incomplete Freund's adjuvant
IGF-II: Insulin-like growth factor 2
INS: insulin
IRE1: endoplasmatic reticulum to nucleus signaling 1

K

KO: knock out

L

LAMP1: lysosome-associated membrane protein type 1
LAMP2A: lysosome-associated membrane protein type 2A
LB: Luria Bertani
LC3B: MAP1LC3B: Microtubule-associated proteins 1A/1B light chain 3B
LIR: LC3-interacting region
LLC: Lewis Lung Carcinoma
LSB: laemmli sample buffer

M

3-MA: 3-methyladenine
MAFbx: muscle atrophy F-box protein
MAPK8/JNK1: mitogen-activated protein kinase 8
MG132: carbobenzoxyl-L-leucyl-L-leucyl-L-leucine
MLC1: myosin light chain 1
moi: multiplicity of infection
mRNA: messenger RNA
mTOR: mammalian target of rapamycin

mTORC1: mammalian target of rapamycin complex 1
MuRF1: muscle RING-finger protein-1
MUSA1: muscle ubiquitin ligase of SCF complex in atrophy-1
MyoD: myogenic differentiation protein

N

NBR1: neighbor of the *BRCA1* gene
NES: nuclear export signal
NLS: nuclear localization signal
NoLS: nucleolar localization signal
NP-40: nonyl phenoxypolyethoxylethanol 40

O

OSR: oxidative stress response

P

PAC: proteasome assembling chaperone
PBS: phosphate-buffered saline
PBSE: PBS containing EDTA
PCR: Polymerase Chain Reaction
PEG: polyethylene glycol
PEI: polyethylenimine
P-EIF2α: phospho-eukaryotic initiation factor 2 alpha
PFA: paraformaldehyde
Pfu: plaque-forming unit
PFHM: protein free hybridoma medium
PML: promyelocytic leukemia
PMSF: phenylmethane sulfonyl fluoride or phenylmethylsulfonyl fluoride
POLR1 PIC: RNA polymerase I preinitiation complex
PPARγ: peroxisome proliferator-activated receptor gamma
P-S6: phospho - S6 ribosomal protein
P-S6K: phospho - p70 S6 kinase
P-4EBP1: phospho - eukaryotic translation initiation factor 4E-binding protein 1
P62/SQSTM1: p62 protein/sequestosome

R

R110: rhodamine 110
rDNA: ribosomal DNA

RIPA: radio-immunoprecipitation assay
RNA: ribonucleic acid
Rpm: rotations per minute
RPMI: Roswell Park Memorial Institute medium
rRNA: ribosomal RNA
RT-PCR: real time PCR

S

19S: regulatory particle
20S: core particle
26S/30S: 26/30 Svedberg sedimentation coefficient proteasome
scrRNA: scrambled RNA
SDS: sodium dodecyl sulfate
siRNA: small interfering RNA
SIRT1: sirtuin 1
SKM: skeletal muscle
SKM-KO: skeletal muscle knock out mice
SKM-Tg: skeletal muscle transgenic mice
Suc-LLVY-AMC: N-Succinyl-Leu-Leu-Val-Tyr- aminoluciferin
SUMO: small ubiquitin-like modifier
SUnSET: SUrface SEnsing of Translation
S6: S6 ribosomal protein
S6K: 70 ribosomal protein S6 kinase-1

T

TBP: TATA Box Binding Protein
TBS: tris-buffered saline
TBS-T: tris-buffered saline and Tween 20
TP53INP1: tumor protein 53 interacting protein 1
TP53INP2: tumor protein 53 interacting protein 2
TRα1: thyroid hormone receptor alpha 1
TRAF6: tumor necrosis factor (α) receptor adaptor protein 6
TRIM32: tripartite motif-containing protein 32
tRNA: transfer RNA

U

Ub: ubiquitin
UBA: ubiquitin-associated domain

UBD: ubiquitin-binding domain
UBL: ubiquitin-like domain
UCP: mitochondrial uncoupling proteins
UPR: unfolded protein response
UPS: ubiquitin proteasome system
UTR: untranslated region

V

VDR: vitamin D receptor

W

WAT: gonadal white adipose tissue

Y

YTH: Yeast Two Hybrid

Z

ZDF: Zucker diabetic fatty

CHAPTER 2 INTRODUCTION

2. INTRODUCTION

2.1. Mechanisms of protein degradation

Protein homeostasis (or proteostasis) resulting from the fine regulation of synthesis and degradation, is a key mechanism by which cells rapidly respond to their environment to maintain cellular proteins in a state that allows optimum biological activity (Anfinsen, 1973). It does not involve just a single pathway or process but is maintained by a highly inter-connected network comprising many complex pathways that control the synthesis (transcription and translation), folding, trafficking, aggregation, disaggregation, and degradation of proteins. The network is additionally adjusted by signalling pathways, such as the heat shock response (HSR), the unfolded protein response (UPR) and the oxidative stress response (OSR) (Morimoto & Cuervo, 2014; Roth & Balch, 2011).

For decades, studies have focused on the analysis of protein synthesis, particularly in understanding transcriptional and translational signals. However, the other side of protein steady-state, i.e. degradation, has been overlooked. Two major pathways of degradation have been described for most cellular proteins in eukaryotic cells: 1) the Ubiquitin Proteasome System (UPS), responsible for degrading 80-90% of proteins including many regulated, short-lived, abnormal, denatured, or, in general, damaged proteins (Lecker *et al*, 2006); and 2) autophagy, which, by contrast, is primarily responsible for the degradation of most long-lived proteins, but also for aggregated proteins as well as cellular organelles (Johansen & Lamark, 2011).

2.1.1. Ubiquitin proteasome system

2.1.1.1. *Ubiquitin*

Post-translational modifications extend the functional diversity and dynamics of the proteome. Proteins in eukaryotic cells can be modified by small molecules such as phosphate, methyl or acetyl groups as well as by certain proteins (Hochstrasser, 2000).

Ubiquitin (Ub) is the first such protein-based modification to be identified when a reticulocyte proteolytic system was described (Ciechanover *et al*, 1980).

The ubiquitin system is a key component of the protein quality control needed to terminate damaged or misfolded proteins and is also involved in the regulation of several cellular processes, such as cell cycle and division, stem cell function, differentiation and development, signal transduction, metabolism, gene transcription and DNA repair, biogenesis of organelles, senescence, apoptosis, antigen processing, immune response and inflammation, neural and muscular degeneration, morphogenesis of neural networks, the secretory pathway, stress response, ribosome biogenesis or viral infection (Finley, 2009; Okita & Nakayama, 2012; Raiborg & Stenmark, 2009; Tanaka, 2013; Ulrich & Walden, 2010; Wong & Cuervo, 2010). To fulfill this wide variety of functions, ubiquitin uses two molecular mechanisms: covalent attachment to other proteins or to itself (process known as ubiquitination) and specific binding to surfaces (ubiquitin-binding domains-UBD-) that form transient, non-covalent interactions either with ubiquitin moieties or with the linkage regions in their chains (Dikic *et al*, 2009; Pickart & Fushman, 2004).

Ubiquitin is highly conserved among all different kingdoms. It is a 76 amino acid residue polypeptide that only has a difference of three amino acids between the yeast and human polypeptides at position 19, 24 and 28 (Clamp *et al*, 2004). It belongs to the superfamily of beta-grasp folded (βGF) proteins, consistent in 4 or 5 β strands forming an anti-parallel sheet and one α helix region; this structural pattern is stabilized by hydrophobic interactions, providing a compact architecture, highly resistant to proteolytic processing, stable to temperature and pH changes (Burroughs *et al*, 2007).

2.1.1.2. *The ubiquitin signaling pathway*

The Ubiquitin Proteasome System (UPS) is a key component of the protein quality control system needed to degrade damaged or misfolded proteins (Wong & Cuervo, 2010). The conjugation of ubiquitin to the substrate protein is the first step of the UPS-mediated degradation; this process is known as ubiquitination and is achieved through an enzymatic sequential mechanism involving three distinct classes of enzymes (Finley, 2009) (Figure 1).

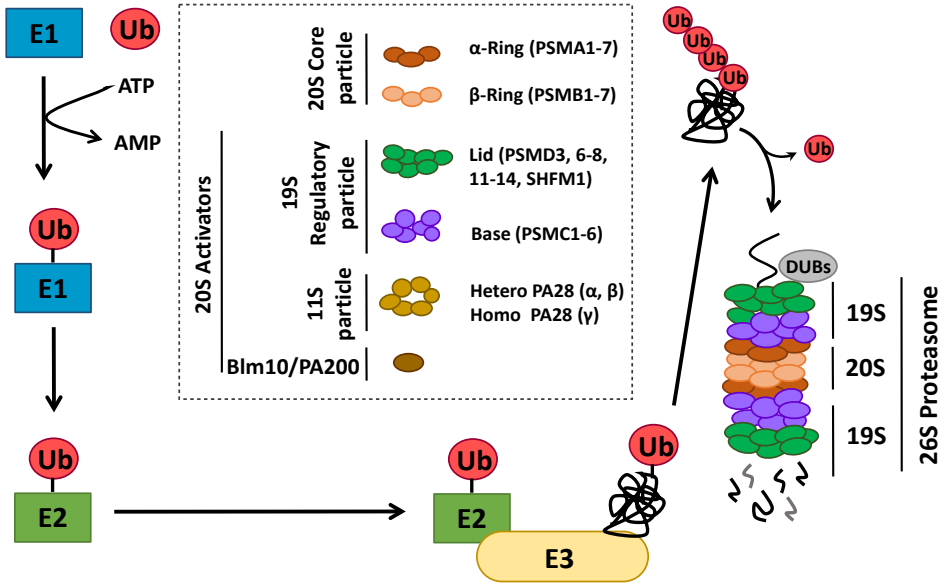

Figure 1. The Ubiquitin-Proteasome System (UPS). The sequential conjugation of ubiquitins to the target protein generates a poly-ubiquitin chain, which acts as a signal for the protein to be degraded through the proteasome. Active proteasomes are formed by the interaction of proteasomal regulatory particles with a core particle (20S). Free intracellular 20S are normally found in an inactive/closed state and require the binding of regulatory particles to degrade proteins such as the 19S and also the PA28 complex (also known as 11S) or by the Blm10/PA200 protein. Finally, the protein is cleaved into short peptides.

First, the ubiquitin-activating enzyme (E1) activates the C-terminal glycine residue of an ubiquitin in an ATP-dependent manner to generate a high-energy thioester ubiquitin intermediate. The activated ubiquitin moiety from E1 is next transferred to a cysteine site of the ubiquitin-conjugating enzyme (E2), via an additional high-energy thioester intermediate. And then it is transferred to the substrate that is specifically bound to a member of the ubiquitin ligase family (E3). In the third step, the E3 specifically catalizes the covalent attachment of ubiquitin to the substrate. The ubiquitin is attached to protein substrates through an amide linkage between its C-terminal end and a primary amino group of the acceptor polypeptide (Pickart, 2001). The successive E3 activity on the substrates produces polyubiquitinated proteins containing chains of ubiquitin (Figure 1). In some cases, a specific E3 ubiquitin ligase confers only initial oligoubiquitination and the chain is later extended by another type of Ub ligase. This Ub chain extending enzymes are termed E4 ligases (Crosas *et al*, 2006; Koegl *et al*, 1999). In the other way, the reversal of

that process is controlled by the deubiquitinating enzymes (DUBs). DUBs are isopeptide proteases which specifically cleave ubiquitin from Ub-conjugated protein substrates and polyubiquitin chains (Dambacher *et al*, 2016; Ventii & Wilkinson, 2008).

While it has been described only two E1 in humans, there are several E2 enzymes and many E3 ubiquitin ligases, each of which are responsible for the selectivity of the process. Therefore, E3 ubiquitin ligases recognizes one or several of specific protein motifs targeting them to degradation by the proteasome (Pickart, 2001). Nevertheless, ubiquitin has seven lysine residues, all of which can form polymer chains, forming polyubiquitilated or monoubiquitilated proteins. The primary signal for proteasomal degradation is a chain of at least four lysine 48-linked ubiquitins (Thrower *et al*, 2000), while other linear ubiquitin chains participate in different processes such as signal transduction, lysosomal degradation, DNA repair regulation, cell-cycle progression, innate immunity or inflammation among others (Peng *et al*, 2003) (Figure 2). After the sequential ubiquitination, the polyubiquitylated protein is now recognized by the machinery responsible for its degradation, the proteasome.

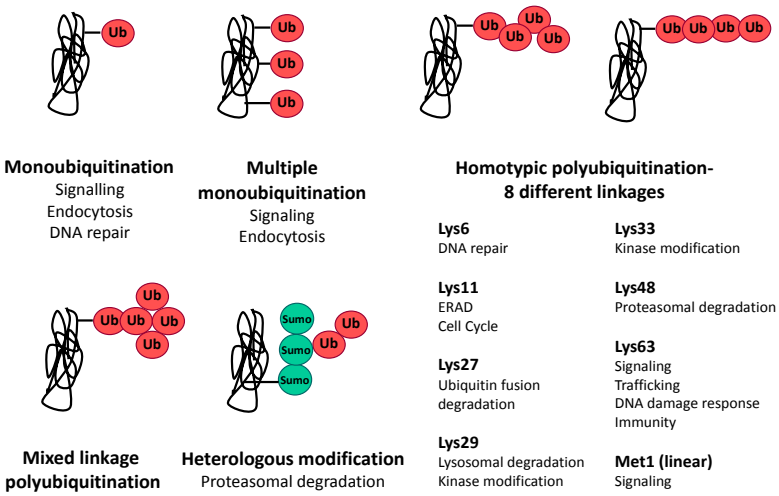

Figure 2. Summary of the major cellular processes whereby specific ubiquitin linkages play roles. Abbreviations: ERAD, endoplasmic reticulum-associated degradation; SUMO, small ubiquitin-like modifier.

2.1.1.3. *The proteasome*

The proteasome is a complex proteolytic machine formed by the assembly of several subunits (Finley, 2009). On the one hand, the **core particle (20S)** of the proteasome is a barrel-like structure formed by 28 subunits that are assembled into four stacked rings of seven subunits (Finley, 2009). The composition of the two outer rings are seven α subunits (named α1 to α7 in yeast or PSMA1-7 in rodents and humans), while the two inner rings are composed by seven β subunits (named β1 to β7 in yeast or PSMB1-7 in rodents and humans) (Groll *et al*, 1997) (Figure 1). The function of the α-rings is to control the substrate entry into the catalytic cavity. In reference to the function of the β-rings, three of the β subunits contain the proteolytic active sites: caspase-like (β1), trypsin-like (β2) and chymotrypsin-like (β5) activities (Orlowski, 1990; Orlowski *et al*, 1993). Concerning the proteolitic activity of the β1, β2 and β5 subunits, its end termini define active sites, which contain a threonine residue that promotes nucleophylic attack in the proteolytic reaction. It exists a specialized form of the 20S proteasome generated by replacement of the catalytic subunits by β1i, β2i and β5i; this form is known as the **immunoproteasome** because of its prevalence in antigen-presenting cells (Gaczynska *et al*, 1993; Monaco & McDevitt, 1984).

There are 20S particles in a free form, however its conformation is closed and requires the binding of proteasome activators to open the gate and degrade polyubiquitylated proteins. Although 20S particles alone have been considered to be inactive, unable to degrade polyubiquitylated proteins (Kisselev & Goldberg, 2005), posterior studies show that free 20S particles have a detectable activity independent of ubiquitination and ATP towards small proteins (Baugh *et al*, 2009; Choi *et al*, 2016).

On the other hand, several forms of active proteasome exists in the cells, but most frequently, the assembly is formed through the 20S and **the regulatory particle 19S**, a subunit that also participates in the regulation of the activity of the holo-complex, named 26S or 30S proteasomes. The 26S proteasome is arranged into two subcomplexes: a 20S core particle capped with a 19S regulatory particle. Whereas the elongated 30S proteasome (determined by density-gradient centrifugation analysis) contains two 19S regulatory particle attached to both ends of the 20S core particle (Hoffman *et al*, 1992;

Hough *et al*, 1987; Waxman *et al*, 1987). The 19S recognizes polyubiquitylated proteins and unfolds and translocates these proteins to the 20S for degradation in an ATP dependent process (Deveraux *et al*, 1994). The 19S is composed of, at least 19 subunits and is organized in two subcomplexes: the base and the lid. The base is adjacent to the 20S, and the lid sits on top of the base (Deveraux *et al*, 1994) (Figure 1). The base contains six ATPases, which are members of the AAA family of ATPases (named Rpt1-Rpt6 in yeast also known as PSMC1-PSMC6 in rodents and humans), and four non ATPases subunits (named Rpn1, Rpn2, Rpn10 and Rpn13 in yeast and PSMD2, PSMD1, PSMD4 and ADRM1 respectively in rodents and humans) (Beyer, 1997; Finley, 2009). The lid complex forms the distal mass of the 19S and is critical for substrate recognition and deubiquitination (Finley, 2009). The 19S lid is formed by nine subunits (Rpn3, Rpn5, Rpn6, Rpn7, Rpn8, Rpn9, Rpn11, Rpn12 and Rpn15/Sem1 in yeast and PSMD3, PSMD12, PSMD11, PSMD6, PSMD7, PSMD13, PSMD14, PSMD8 and SHFM1 respectively in rodents and humans) (Udvardy, 1993). In the Table 1 are listed all these subunits. The topology of the yeast regulatory particle has been recently elucidated by electron microscopy tools, revealing the special rearrangement of the diverse subunits (Lander *et al*, 2012; Luan *et al*, 2016).

Table 1. Proteasome subunits and proteasome-interacting proteins (PIPs) known to function as auxiliary factors.

Category	Systematic Nom.	HUGO	Human Nomenclature	Yeast Nomenclature	Function
20S CP					
α Type subunits	α1	PSMA6	Iota	Scl1, YC7	
	α2	PSMA2	C3	Pre8, Y7	
	α3	PSMA4	C9	Pre9, Y13	
	α4	PSMA7	C6	Pre6	
	α5	PSMA5	Zeta	Pup2, DOA5	
	α6	PSMA1	C2	Pre5	
	α7	PSMA3	C8	Pre10, YC1	
	α8	PSMA8	-	-	
β Type subunits	β1	PSMB6	Y, delta	Pre3	Caspase-like
	β2	PSMB7	Z	Pup1	Trypsin-like
	β3	PSMB3	C10	Pup3	
	β4	PSMB2	C7	Pre1	
	β5	PSMB5	X, MB1, epsilon	Pre2, Doa3	Chymotrypsin-like
	β6	PSMB1	C5	Pre7	
	β7	PSMB4	N3, beta	Pre4	
	β1i	PSMB9	LMP2, RING12	-	Chymotrypsin-like
	β2i	PSMB10	MECL1, LMP10	-	Trypsin-like
	β5i	PSMB8	LMP7, RING10	-	Chymotrypsin-like
	β5t	PSMB11	-	-	Chymotrypsin-like
19S RP (PA700)					
ATPase subunits	Rpt1	PSMC2	S7, Mss1	Cim5, Yta3	ATPase
	Rpt2	PSMC1	S4, p56	Yta5/mts2	ATPase, gate opening
	Rpt3	PSMC4	S6, S6b, p48, TBP7	Yta2	ATPase
	Rpt4	PSMC6	S10b, p42	Sug2, Pcs1, Crl3	ATPase
	Rpt5	PSMC3	S6, S6a, TBP1	Yta1, Tbp1/ pam2, tbp1	ATPase, gate opening
	Rpt6	PSMC5	S8, p45, TRIP1	Sug1, Cim3/ let1	ATPase

Table 1. (Continued).

Category	Systematic Nom.	HUGO	Human Nomenclature	Yeast Nomenclature	Function
19S RP					
Non-ATPase subunits	Rpn1	PSMD2	S2, p97, TRAP2	Hrd2, Nas1/ mts4	PIPs scaffold
	Rpn2	PSMD1	S1, p112	Sen3	PIPs scaffold
	Rpn3	PSMD3	S3, p58	Sun2	
	Rpn5	PSMD12	p55	Nas5	
	Rpn6	PSMD11	S9, p44.5	Nas4	
	Rpn7	PSMD6	S10a, p44		
	Rpn8	PSMD7	S12, p40, MOV34	Nas3	
	Rpn9	PSMD13	S11, p40.5	Nas7/mts1	
	Rpn10	PSMD4	S5a, MBP1	Sun1, Mcb1/ pus1	Ub receptor
	Rpn11	PSMD14	S13, Poh1	Mpr1/pad1, mts5	DUB
	Rpn12	PSMD8	S14, p31	Nin1/mts3	
	Rpn13	ADRM1	ADRM1	Daq1	Ub receptor, UCH37 recruiting
	Rpn15	SHFM1	DSS1, SHFM1	Sem1/dss1	
PA28-11S REG					
PA28α/β		PSME1	PA28α, REGα	-	PSM activator
PA28γ		PSME2	PA28β, REGβ	-	PSM activator
		PSME3	PA28γ, REGγ, Ki	-	PSM activator
PA200		PSME4	PA200, TEMO	Blm10	PSM activator
PI31		PSMF1	PI31	-	PSM inhibitor?

Table 1. (Continued).

Category	Systematic Nom.	HUGO	Human Nomenclature	Yeast Nomenclature	Function
Assembling chaperones					
CP-chaperone	hUmp1	POMP	Proteassemblin	Ump1	CP formation
	PAC1	PSMG1	DSCR2, c21-LRP	Pba1, Poc1	CP formation
	PAC2	PSMG2	C7orf86	Pba2, Poc2, Add66	CP formation
	PAC3	PSMG3	C6orf86	Pba3, Poc3, Dmp2	CP formation
	PAC4	PSMG4	-	Pba4, Poc4, Dmp1	CP formation
RP-chaperone	-	PSMD10	p28, gankyrin	Nas6	Base formation
	Rpn14	PAAF1	FLJ11848	Rpn14	Base formation
		PSMD9	p27	Nas2	Base formation
		PSMD5	S5b, p50.5	Hsm3	Base formation
PIPs					
	-	RAD23A/B	hH23A/b	Rad23	Shuttling factor
	-	UBQLN1/2	hPLIC-1/2	Dsk2	Shuttling factor
	BAG6	BAG6	BAT3, G3	-	Shuttling factor
	USP14	USP14	USP14	Ubp6/ubp6	DUB
	UCH37	UCHL5	UCH37	-/uch2	DUB
	UBE3C	UBE3C	KIAA10	Hul5	Ub ligase
		TRIP12	KIAA0045	Ufd4	Ub ligase
		UBR1	E3α1	Ubr1	Ub ligase
		UBE3A	E6-AP	-	Ub ligase
		PARK2	Parkin	-	Ub ligase
	Txnl1	TXNL1	TRP32	-	Thioredoxin
	Ecm29	KIAA0368	ECM29	Ecm29	PSM stabilizer
	AIRAP	ZFAND2A	-	-	PSM stabilizer?
	AIRAPL1	ZFAND2B	-	-	PSM stabilizer?
Transcription	Rpn4	-	-	SON1, UFD5	PSM gene transcription
	TCF11	NFE2L1	Nrf1, HBZ17	-	PSM gene transcription

In addition, the core particle can be activated by other regulatory particles (Figure 1). For example, in the case of the immunoproteasome, instead of the 19S regulatory particle, the PA28 particle attaches to the core particle. PA28, also known as 11S (Ma *et al*, 1992), is composed by hetero-heptameric rings of the 28-kDa proteins PA28α and PA28β or homo-heptameric rings of PA28γ (Ahn *et al*, 1996). To open the chanel of the proteasome, PA28 binds to the cylinder end of the core particle (Demartino & Gillette, 2007; Förster *et al*, 2005). However, in contrast to the 19S regulatory particle, PA28 has neither ATPase activity nor the ability to bind to ubiquitin conjugates (Dubiel *et al*, 1992; Ma *et al*, 1992). On the one hand, PA28αβ is inducible by interferon-γ (Realini *et al*, 1997) and modulates the presentation and generation of specific viral antigens (Sijts *et al*, 2002). On the other hand, PA28γ is involved in cell cycle regulation promoting the degradation of small proteins such as p21 (Li *et al*, 2007). Another regulatory mechanism of the 20S proteasome is the activation by Blm10/PA200, a monomeric protein of 250 kDa (Ustrell *et al*, 2002). Blm10/PA200 has the ability to form hybrid complexes in which this protein binds to one end of the 20S proteasome and the 19S to the opposite end (Blickwedehl *et al*, 2008; Schmidt *et al*, 2005). Taken together, different proteasome activators are tightly modulating proteasome activity (Table 1).

2.1.2. Autophagy

Autophagy (from Greek, "self-eating") is a cellular process that mediates the degradation of intracellular components—misfolded proteins and damaged, dysfunctional or aged organelles—inside lysosomes (Martinez-Vicente & Cuervo, 2007; Mizushima *et al*, 2008; Wesselborg & Stork, 2015). Along with other proteolytic systems, autophagy is involved in the maintenance of cellular homeostasis, in this sense, degradation of cellular aged components produce substrates for the synthesis of new components. Autophagy is also required for processes such as growth control, differentiation, development, pathogen-to-host defense and adaptation to adverse environments (Kobayashi, 2015).

Different types of autophagy have been described. On the one hand, they can be categorized into two types, namely nonselective or selective. Nonselective autophagy takes randomly a portion of cytoplasm into autophagosomes. Conversely, selective autophagy

is required for remodeling to adapt to changing environmental or nutritional conditions and for removal of damaged organelles. An example of selective autophagy is mitophagy, essential for the maintenance of mitochondrial quality (Jin *et al*, 2013). (Figure 3C). On the other hand, depending on how the intracellular components are delivered to lysosomes for degradation, there are three main types of autophagy in mammals: macroautophagy, microautophagy and chaperone-mediated autophagy (CMA) (Cuervo, 2004) (Figure 3).

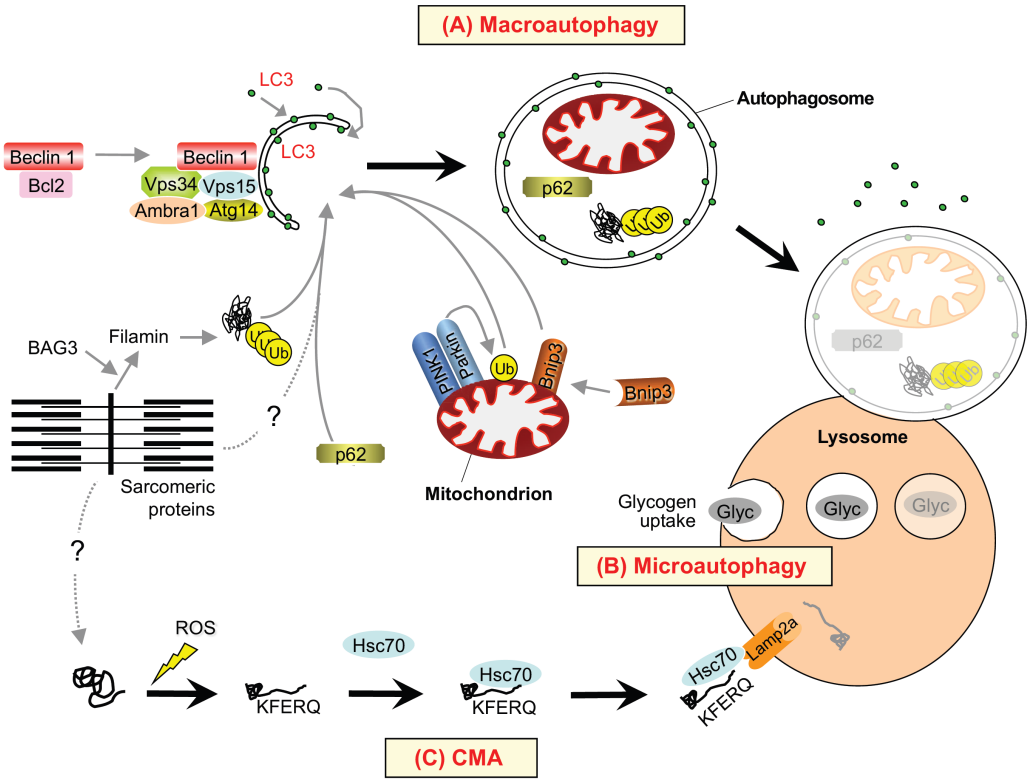

Figure 3. Schematic model of the three main types of autophagy and their contribution to protein degradation and organelle removed in skeletal muscle (Bonaldo & Sandri, 2013).

Macroautophagy (hereafter referred to as autophagy) is the best characterized type of lysosomal degradation. In this process, cytosolic components or organelles are nonspecifically sequestered to the lysosomes for degradation. During autophagy, a small vesicular sac called the isolation membrane or phagophore elongates and subsequently encloses a portion of cytoplasm (including organelles). It results in the formation of a double-

membraned structure, the autophagosome. This membrane necessary for the autophagosome formation arises from the endoplasmic reticulum (ER) and the Golgi; recently it has been also described that mitochondria appears to provide a membrane source (Tooze & Yoshimori, 2010). Then, the outer membrane of the autophagosome fuses with a lysosome (to form an autolysosome), leading to the degradation of the enclosed materials together with the inner autophagosomal membrane. The endosome can also fuse with the autophagosome (to form an amphisome) before fusion with the lysosome. Amino acids and other small molecules that are generated by autophagic degradation are delivered back to the cytoplasm for recycling or energy production (Hamasaki *et al*, 2013; Mizushima & Klionsky, 2007) (Figure 3A).

The diverse steps in macroautophagy are orchestrated by a group of proteins, generically known as Atg (autophagy-related) proteins, which were first characterized in yeast, and are conserved throughout the phylogenetic scale (Klionsky *et al*, 2003). These proteins mediate some mechanisms such as induction, vesicle formation, and breakdown of the autophagic body, therefore, to determine their expression levels is useful to monitor autophagy. Beclin1/Atg7 is a scaffold protein that regulates the autophagic sequestration (Funderburk *et al*, 2010). This protein activates LC3B/Atg8, which is synthesized in an unprocessed form, LC3B-I, that is converted to its lipidated form LC3B-II by phosphatidylethanolamine (PE)-conjugation. LC3B-II is required for autophagosome formation and closure and binds throughout the process of autophagy from the autophagosome membrane until the fusion of the autophagosome with the lysosome (Sou *et al*, 2008; Tanida *et al*, 2005). Another important component of the process of autophagy is the adaptor p62/SQSTM1, which plays a critical role in recognizing and loading certain cargo proteins that will be degraded by autophagic-lysosomal proteolysis.

Less information is currently available on microautophagy. This process allows direct engulfment of small areas of cytosol, inclusions (e.g., glycogen) and organelles (e.g., ribosomes, peroxisomes in case of pexophagy) by lysosomal membrane invagination (Huber & Teis, 2016) (Figure 3B). The molecular mechanisms that mediate lysosomal membrane invaginations and the delivery of cytosolic cargo to lysosomes are unknown.

In contrast to macro- and microautophagy, soluble cytosolic proteins can be targeted selectively for degradation in lysosomes by chaperone-mediated autophagy (CMA). Target proteins have a specific amino acid sequence (the KFERQ-like motif) that is recognized by chaperonines such as heat shock protein 70 (Hsc70) and HSPA8. Subsequently, a protein from the lysosomal membrane, named lysosome-associated membrane protein type 2A (LAMP2A), binds the complex formed by the target protein and the chaperonine; in this way, it can be internalized into the lysosomal lumen and degraded (Bonaldo & Sandri, 2013; Jin *et al*, 2013). Irrespective of the type of autophagy, degradation is performed by acidic proteases named cathepsins that are activated at pH usually comprised between 3.5 and 6.5.

2.1.3. Crosstalk autophagy and UPS

For a long time, autophagy and UPS were viewed as independent of each other (Ciechanover, 2005; Pickart, 2004). However, evidences generated during recent years, challenge this view and offer a glance into a complex interplay between these two cellular pathways.

One of the proposed links observed between the UPS and autophagy is that impairment of the UPS leads to increased autophagic function (Ding *et al*, 2007; Iwata *et al*, 2005; Pandey *et al*, 2007). This is commonly considered to be a compensatory mechanism, allowing cells to reduce the accumulated UPS substrates. The regulation of autophagy by the UPS involves many intracellular mediators or cascades, including histone deacetylase 6 (HDAC6), mechanistic target of rapamycin complex 1 (MTORC1), activating transcription factor 4 (ATF4), and the endoplasmatic reticulum to nucleus signaling 1 (IRE1)- mitogen-activated protein kinase 8 (MAPK8/JNK1) pathway (Wu *et al*, 2010).

However, direct evidence for the regulation of the UPS by autophagy is lacking. For instance, in neurons of autophagy-null mice, autophagy deficiency leads to the impaired degradation of specific UPS substrates and induces the accumulation of polyubiquitinated proteins, but no obvious alterations in proteolitic activities (Hara *et al*, 2006; Komatsu *et al*, 2006). In neuroblastoma SHSY5Y cells, inhibition of lysosomal activities enhanced chaperone-mediated autophagy instead of upregulating proteasomal functions (Qiao &

Zhang, 2009). Furthermore, autophagy inhibition has been shown to produce an excess of p62/SQSTM1 and delay the delivery of polyubiquitinated proteins to the proteasome without affecting proteasome activity and thereby inhibiting their clearance (Korolchuk *et al*, 2009a, 2009b). Only one study has reported that inhibition of autophagy by a pharmacological or RNA interference approach could induce proteasome activity in colon cancer cells (Wang *et al*, 2013). Moreover, it has been described a coordinated upregulation of both the UPS and autophagy that involves the coordinating action of the FoxO transcription factors on both pathways; this has been reported to contribute to muscle atrophy in physiological conditions, like fasting, as well as in diseases characterised by muscle wasting (Zhao *et al*, 2007).

In addition to these data, the cytoskeleton protein filamin has been described as a client recognized by chaperones (Hsp70, Hsc70 or Hsp90) and co-chaperones (Bag1, Bag3, CHIP, HspBP1, HSJ1, etc.) that attempt to refold or degrade this substrate protein in mechanically strained cells and tissues. Mechanical tension results in unfolding of filamin, leading to recognition by the chaperone complex. CHIP (C-terminus of Hsp70-interacting protein) is a co-chaperone with an E3 ubiquitin ligase activity associated to Hsp70. It contains two functional domains and may mediate substrate degradation by both degradative pathways: the tetratricopeptide repeat domain is involved in proteasomal degradation, whereas the U-box domain directs substrates toward the lysosomal degradation pathway. Other co-chaperones known to be involved in switching between the UPS and autophagy are members of the BAG (Bcl-2-associated athanogene) protein family. BAG1 constitutes a link between Hsp70 and the proteasome. It also interacts with CHIP, and may therefore direct Hsc/Hsp70 substrate to the proteasome. In contrast, BAG3 facilitates the degradation of substrates such as mutated Huntingtin with expanded glutamine repeats via the autophagic process. BAG3, will favor K63- (Lysine 63) over K48-polyubiquitination (Lysine 48), and direct the substrate protein to autophagic degradation (Arndt *et al*, 2010; Gamerdinger *et al*, 2009; Kettern *et al*, 2011; Ulbricht, 2013).

Then, the tagged protein is usually recognized by several types of adaptor proteins, such as p62/SQSTM1 that bring them to the proteasome or to autophagic vesicles. p62

is able to link ubiquitinated proteins to the autophagic machinery through its ubiquitin-associated (UBA) domain on one side, and can also interact with the intrinsic subunits of the proteasome via an N-terminal ubiquitin-like (UBL) domain (Komatsu & Ichimura, 2010). At a higher level of integration, the degradative pathways are probably coordinated with more general homeostatic programs, such as response to stress factors; one example of coordination of signaling pathways directing the activity of both degradative pathways is the ER stress response (Buchberger *et al*, 2010).

2.2. Skeletal muscle

Skeletal muscle is crucial for movement and whole body metabolism, and therefore, the maintenance of skeletal muscle mass is essential for mobility, disease prevention and quality of life. Skeletal muscle mass is determined by the net balance between the rate of protein degradation and protein synthesis. Thus, identifying the molecular mechanisms that regulate protein degradation and protein synthesis is critical for the development of effective exercise programs and potential pharmacological interventions that could inhibit muscle atrophy and / or promote hypertrophy (Goodman *et al*, 2011a)

2.2.1. Regulation of skeletal muscle mass

Skeletal muscle mass and muscle fiber size is determined by physiological and pathological conditions. An increase in muscle mass and fiber size is named **muscle hypertrophy**, and it happens during development and in response to mechanical overload (incapacitation or ablation of synergistic muscles, strength training, reloading after unloading) or anabolic hormonal stimulation (testosterone or β2-adrenergic agonists). In contrast, **muscle atrophy** is the decrease in muscle mass and fiber size, and it results from aging, starvation, cancer, diabetes, bed rest, loss of neural input (denervation, motor neuron disease) or catabolic hormonal stimulation (corticosteroids). The balance between protein synthesis and degradation regulates the protein turnover within muscle fibers. However, skeletal muscle fibers are multi-nucleated structures, thus, cell or nuclear turnover may affect this equilibrium, i.e. addition of new myonuclei, due to fusion

of satellite cells, or loss of myonuclei, due to nuclear apoptosis. The molecular signalling mechanisms regulating these processes have been the subject of several recent reviews (Cohen *et al*, 2014; Egerman & Glass, 2014; Schiaffino *et al*, 2013).

In this work, I will focus mainly in the degradation pathways that regulates protein turnover. The mechanisms that regulate muscle protein homeostasis are four: Ca^{2+} dependent calpains, caspases, ubiquitin-proteasome system and autophagy-lysosome system.

First, the Ca^{2+}-dependent proteolytic system is driven by calpains, a family of ubiquitous and tissue-specific cysteine proteases. Three calpain isoforms are active in the skeletal muscle: μ-calpain (calpain 1) and m-calpain (calpain 2), both expressed ubiquitously, and the muscle-specific calpain 3. They are activated depending on intracellular Ca^{2+} concentrations: for example, calpain 1 is sensitive to low Ca^{2+} concentration, while high levels of free Ca^{2+} activate calpain 2 (Huang & Wang, 2001). Moreover, the endogenous specific inhibitor calpastatin is able to regulate all these calpain isoforms. Calpain 3 has been described to regulate myofibril homeostasis. Indeed, muscle dystrophies are associated with reduction of its activity. It also has been reported that calpains are required for maintaining the sarcomeric structure and its contraction, in fact, calpains are able to cleave big muscle proteins such as titin and nebulin that form the Z-line, α-actin and desmin that link the sarcolema to the Z-line and also troponins, tropomyosin, myosin and actin (Garnham *et al*, 2009; Huang *et al*, 2008; Richard *et al*, 1995).

Second, caspases belong to the family of cytoplasmic cystein-aspartic endoproteases and are a key component of programmed cell death (apoptosis) and inflammation. In skeletal muscle, caspase-3 activation is able to uncouple the actin-myosin complex, generating substrates which can be subsequently degraded by other proteolytic systems (Du *et al*, 2004).

Third, in reference to the Ubiquitin-Proteasome System, the deubiquitinase expression could be a regulatory step in skeletal muscle. Indeed, reduced deubiquitinase gene expression has been reported in different conditions associated with muscle atrophy such as denervation, fasting and cachexia. But also, in the other way, up-regulation of deubiquitinases can stimulate protein degradation (Combaret *et al*, 2005; Wing, 2013).

In addition, several muscle-specific E3 ubiquitin ligases have been identified. The most relevant are atrogin-1/MAFbx (Muscle Atrophy F-box protein) and MuRF1 (Muscle RING-finger protein-1), described in skeletal muscle following transcript profiling in fasting and immobilisation models of rodent muscle atrophy (Bodine *et al*, 2001). Atrogin-1 is regulated by FoxO transcription factors and promotes the degradation of the muscle transcription factor MyoD and the activator of protein synthesis eIF3-f (Csibi *et al*, 2010; Lagirand-Cantaloube *et al*, 2008). MuRF1 ubiquitylates preferentially muscle structural proteins such as troponin I, myosin heavy chain, actin, myosin binding protein C and myosin light chain 1 and 2, directly inducing muscle atrophy (Sandri, 2013). Another muscle specific E3 ubiquitin ligase is TRIM32 , which is constitutively active and has the ability to bind and degrade thin filaments (actin, tropomyosin, troponins) and Z-band (Cohen *et al*, 2012). However, its absence is not able to prevent muscle atrophy (Kudryashova *et al*, 2012). Tumor necrosis factor (α) receptor adaptor protein 6 (TRAF6) has been also reported to control ubiquitination and autophagy regulating muscle atrophy (Paul *et al*, 2010). Furthermore, the absence of the E3 ubiquitin ligase ZNF216 protects mice from denervation-induced atrophy and accumulation of polyubiquitylated proteins in the skeletal muscle (Hishiya *et al*, 2006). And most recently, the E3 ubiquitin ligase SCF complex in atrophy-1 (MUSA1) has been identified, whose induction is required for atrophy and is regulated by the bone morphogenetic protein (BMP) pathway (Sartori *et al*, 2013).

Finally, autophagy was described to be involved in skeletal muscle atrophy for the first time in 2004 by Mizushima and collaborators (Mizushima *et al*, 2004). The expression of the lysosomal proteases and the activity of the autophagy process are increased during muscle wasting (Bonaldo & Sandri, 2013; Sala *et al*, 2014). Many myopathies and some types of dystrophies are associated with reduced autophagy capacity, resulting in accumulation of useless substrates (Bonaldo & Sandri, 2013).

2.2.2. Cancer cachexia

Cancer patients frequently develop a condition of general wasting known as cachexia. This is a multifactorial syndrome that complicates patient management, increases

morbidity and mortality rates, reduces the tolerance to antineoplastic therapies, and results in poor quality of life (Fearon *et al*, 2011; von Haehling & Anker, 2010; Penna *et al*, 2013, 2015; Pin *et al*, 2015).

Cachexia is particularly prominent in gastric, colorectal, pancreatic and lung cancers, while it is less common in sarcoma, head and neck, or breast cancer hosts (DeWys *et al*, 1986). The 54% to 70% of cancer patients develop cachexia. However, this percentage increases in lung cancer patients and may reach 80% in subjects affected by gastrointestinal tumors (Inui, 2008). Prognosis and survival of patients affected by cancer is dependent of the presence of cachexia and up to 20% of all cancer deaths are caused directly by cachexia, usually because of cardiac or respiratory failure (Stewart *et al*, 2006).

The most relevant feature of the pathophysiology of cancer cachexia is the ongoing loss of skeletal muscle mass, not necessarily associated with the loss of fat mass. Such a pattern results in progressive reduction of muscle strength, endurance and exercise capacity, and cannot be fully reversed by conventional nutritional support. Moreover, cachexia also includes increased protein catabolism, systemic inflammation, hormonal disturbances and down-regulation of anabolic signals (Argilés *et al*, 2014; Fearon *et al*, 2011).

In addition to skeletal muscle and adipose tissues wasting, cancer cachexia promotes alterations such as anorexia (loss of appetite, early satiety), pain and nausea, which are the primary causes of reduction in food intake and malnutrition (Vigano *et al*, 2012). Besides malabsorption, negative nitrogen balance, metabolic competition between the host and the tumor, alteration of the humoral homeostasis, and increase catabolism are as well involved in the pathogenesis of cancer cachexia (Argilés *et al*, 2014). Many of the primary events driving cachexia are likely mediated via the central nervous system and include inflammation-related anorexia, hypoanabolism and/or hypercatabolism (Fearon *et al*, 2012). These abnormalities cannot be fully reversed by conventional nutritional support (oral, enteral or parenteral nutrition) and lead to functional impairment (Muscaritoli *et al*, 2010). Finally also systemic inflammation, insulin resistance and anemia occur.

Cancer cachexia is invariable associated with muscle wasting and atrophy, but the mechanisms underlying it are still unclear. Many metabolic alterations are responsible

for the loss of muscle mass (Fearon *et al*, 2012). Thus, abnormalities in protein (synthesis and degradation) and amino acid metabolism (transport and branched-chain amino acid oxidation) are observed in cachectic muscle. While protein synthesis has been described to be depressed in skeletal muscle of animal models of cachexia (Eley *et al*, 2008; Smith & Tisdale, 1993), the pathway that is most reported to be involved in the wasting process is protein degradation that is mediated by the UPS (Acharyya & Guttridge, 2007; Attaix *et al*, 2008; Bossola *et al*, 2001; Costelli *et al*, 1995; Khal *et al*, 2005; Zhang *et al*, 2011). Indeed, experimental and clinical studies have shown that hyperactivation of the ubiquitin-proteasome-dependent proteolytic system plays a key role. For example, it has been observed an overexpression of muscle Ub mRNA in gastric cancer patients with cachexia (Bossola *et al*, 2001); also, it has been determined an upregulation of the ubiquitin ligase Atrogin-1/MAFbx in C2C12 myotubes treated with LLC-conditioned medium (Zhang *et al*, 2011) or an increasing on chymotrypsin-like activity in gastrocnemius muscle of mice bearing the MAC16 tumour as well as an upregulated expression of the α subunit C2 and the β subunit C5 of the proteasome (Khal *et al*, 2005).

However, in the past few years, the involvement of autophagic-lysosomal proteolisis has also been proposed. Studies suggest that autophagy is activated in the muscle of animals bearing Lewis lung carcinoma (LLC) or colon 26 (C26) tumors, two models highly used to study cancer cachexia. Indeed, Beclin-1, LC3B and p62/SQSTM1 protein levels, as well as autophagic flux are increased in the skeletal muscle of murine models of cachexia. Consistent with these results, increased protein levels of Beclin-1 and LC3B-II are observed in skeletal muscle of cancer patients. (Aversa *et al*, 2016; Penna *et al*, 2013).

2.3. DOR/ TP53INP2

Our laboratory has identified an additional component of the autophagic pathway, thereby providing further insight into this evolving field (Mauvezin *et al*, 2010). It is the nuclear cofactor DOR (named Diabetes and Obesity Regulated gene) or also referred to as TP53INP2 (tumor protein p53 inducible nuclear protein 2); please note that the mouse

nomenclature is TRP53INP2. However, we use TP53INP2 hereafter to refer to both the human and mouse genes/proteins for simplicity).

TP53INP2 was first discovered searching for new candidate genes involved in the pathophysiology of type II *Diabetes mellitus* by PCR-select cDNA subtraction. In a screening of genes differentially expressed in muscle from Zucker diabetic fatty (ZDF) and non-diabetic lean (control) rats, a cDNA library was substracted and the cDNA of *TP53INP2* was isolated, amplified and sequenced. Besides, studies of *TP53INP2* mRNA expression showed a reduction of 77% in its expression in the skeletal muscle of ZDF rats, thereby corroborating the original substraction hybridization assay (Baumgartner *et al*, 2007). Consistent with these data, it was also described that muscle *TP53INP2* expression was 70% lower in both type 2 diabetic patients and in obese nondiabetic subjects compared with that in controls (Sala *et al*, 2014) (Figure 4A). In addition, transcripts from human, rats and mice are predominant in skeletal muscle and heart while lower expression was detected in other tissues such as white adipose tissue, brain, kidney and liver (Figure 4B).

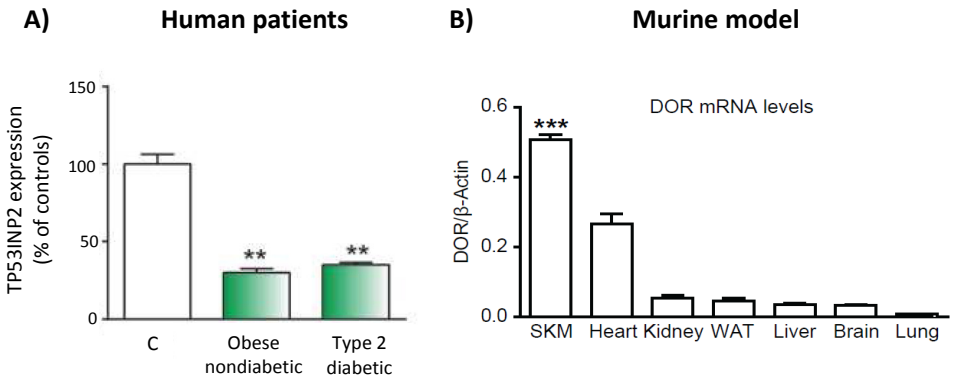

Figure 4. TP53INP2 mRNA expression. A) TP53INP2 expression is downregulated in skeletal muscle from obese and type 2 diabetic patients. TP53INP2 mRNA levels in skeletal muscle from type 2 diabetic and obese subjects (Lyon study). B) TP53INP2 mRNA levels in different mouse tissues. The skeletal muscle (SKM) used for mRNA analysis was tibialis anterior, and tissues from 3 different male mice were used. Data represent mean ± SEM. **p<0,01***p<0,001 versus control group. From Sala *et al*, 2014.

This gene encodes a protein of 220 (human) or 221 (mouse, rat) residues and it is well conserved among all these species (84% identity between human and mouse, 83% between human and rat, 85% between rat and mouse). Interestingly, two conserved

regions are identified in all sequences of TP53INP2 gene family members. In the region 1 (position 28 to 42 in humans), a nuclear export sequence (NES) motif and a functional and conserved LC3-interacting region (LIR) have been identified (Mauvezin *et al*, 2010; Sancho *et al*, 2012). The region 2 (position 66 to 112) has a highly hydrophobic C-terminal region and is hypothesized to maintain some secondary/tertiary structure required for the protein function (Sancho *et al*, 2012). In the N-terminal region, a nuclear localization signal (NLS) has been described (Figure 5).

Figure 5. TP53INP2 sequence in mice. The nuclear export signal (NES) is highlighted in red, nuclear localization signal (NLS) in orange, and LC3-interacting region (LIR) in yellow. The two highly conserved regions are highlighted in green. The position of the α-helix is marked between amino acids 86 and 112. From Sancho, 2011.

Moreover, in parallel to mRNA studies, it has been reported that TP53INP2 protein is abundantly expressed in tissues with high metabolic rate like the skeletal muscle and the heart and is strongly repressed in obese diabetic murine models and in muscle from patients with type 2 diabetes and obesity (Figure 6) (Baumgartner *et al*, 2007; Sala *et al*, 2014).

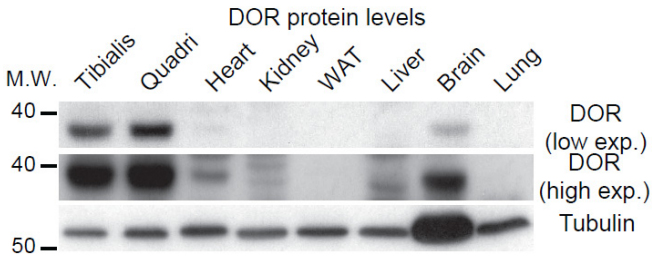

Figure 6. TP53INP2 protein levels in different mice tissues. From Sala *et al*, 2014.

The only homologous protein described to date is a human p53-dependent apoptosis regulator named Tumor Protein 53 Interacting Protein 1 (TP53INP1, also named SIP) with an identity of 36%, which is a regulator of p53 and p73 tumor proteins. Based on phylogenetic and comparative analysis from our laboratory (Sancho *et al*, 2012), TP53INP2 has been identified in metazoan species. In organisms older than cartilaginous fish, only one of the two homologous genes is present and data from Sancho *et al*, 2012 have demonstrated that *TP53INP2* is the ancestral gene and *TP53INP1* may have arisen by gene duplication (Figure 7).

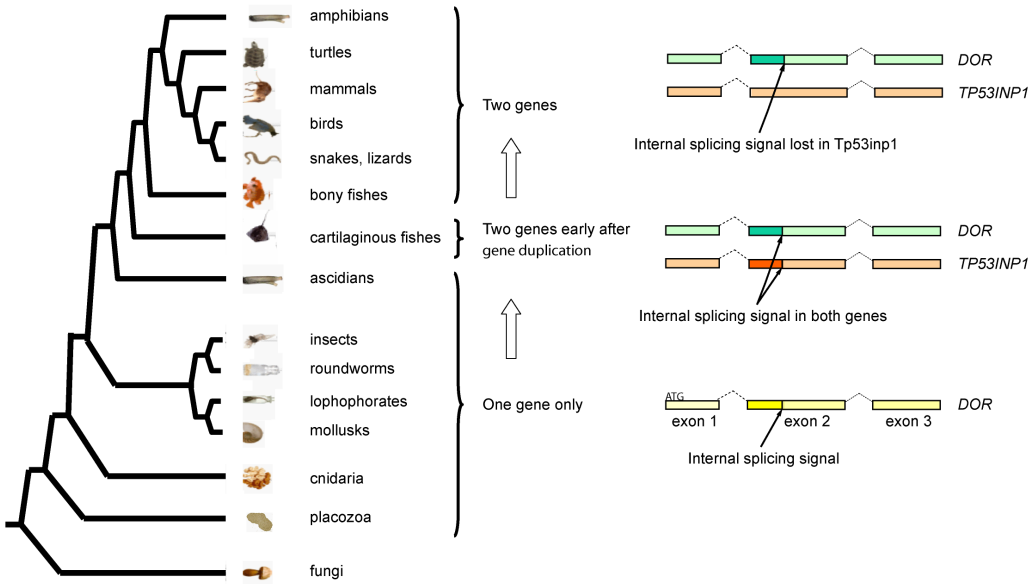

Figure 7. Phylogenetic analysis of the *TP53INP2* gene family. Diagram depicting the absence of an alternative exon 2 internal splicing signal in *TP53INP1* genes. Exons shown correspond to the coding exons of the human genes. An alternative splicing signal present in exon 2 of *TP53INP2* and absent in *TP53INP1* genes from bony fish to mammals suggests *TP53INP2* is the ancestral gene. From Sancho *et al*, 2012.

Interestingly, *TP53INP2* was identified in a genomic screening for genes involved in mammalian cranio-facial development (Fowles *et al*, 2003). It was shown by in situ hybridization that *TP53INP2* is in the human chromosome band 20q11.2 (Nowak *et al*, 2005). It is described to be expressed in the mouse embryonic facial primordia (Bennetts *et al*, 2006) and unaltered in autosomal recessive non-progressive infantile ataxia (Bennetts *et al*, 2007). Furthermore, *TP53INP2* has been characterized in another screening of genes in hairy cell leukemia (HCL) population where a 700 kb deletion of the region 20q11.22 was detected encompassing ten characterized genes, among them *TP53INP2* (Nordgren *et al*, 2010). Also, matrix-specific alternative splicing of exon 2 in the 5' UTR (untranslated region) of *TP53INP2* has been demonstrated to be a key event necessary for cancer cells to invade the extracellular matrix (Moran-Jones *et al*, 2009). *TP53INP2* down-regulation has been described in liver cells during acute phase response, which is related to the decreased serum level of thyroid hormones and to the direct action of the main acute-phase cytokines (Malik *et al*, 2010). Finally, *TP53INP2* expression levels in adipose tissue change depending on the diet (Fromm-Dornieden *et al*, 2012) and *TP53INP2* has been identified as a target of mir638, which promotes melanoma metastasis and protects melanoma cells from apoptosis and autophagy (Bhattacharya *et al*, 2014).

Nevertheless, TP53INP2 function was not characterized until 2007 (Baumgartner *et al*, 2007). And nowadays we know that TP53INP2 has a dual role, on the one hand in the nucleus acts as a coactivator of different nuclear receptors and on the other hand, in the cytosol is an autophagy regulator.

2.3.1. TP53INP2 as a nuclear coactivator

TP53INP2 was identified originally as a protein expressed in promyelocytic leukemia (PML) nuclear bodies of insulin-sensitive tissues (Baumgartner *et al*, 2007) which coactivates different nuclear receptors. In fact, the co-transfection of TP53INP2 and nuclear hormone receptors such as TRα1, GR, PPARγ or VDR enhanced the transcriptional activity of the reporter gene in a dose-dependent manner and only in the presence of the ligand (Sancho *et al*, 2012).

Regarding the fact that TP53INP2 potentiates the activity of TRα1, the authors have demonstrated a physical interaction between TP53INP2 and TRα1 and to T3-responsive promoters. As a consequence, TP53INP2 loss-of-function reduces the action of thyroid hormones and its activity is modulated during myogenesis and osteoblast differentiation (Baumgartner *et al*, 2007; Linares *et al*, 2011). In fact, in C2C12 cells, the expression of genes such as *myogenin, creatine kinase, caveolin-3, α-actin 1, UCP* and *IGF-II* is reduced in the absence of TP53INP2, suggesting a role of TP53INP2 as a regulator of early stages of TR-mediated cellular response.

In concordance with these evidences, it has been demonstrated that the transcriptional coactivator function of TP53INP2 is conserved in *Drosophila* (Francis *et al*, 2010). The orthologous gene of *TP53INP2* in the fly (*dTP53INP2*) presents four isoforms and one of them acts as a coactivator of nuclear receptors such as ecdysone receptor (EcR), which shares many commonalities with type II nuclear receptors. Moreover the authors generated dTP53INP2 knockout flies and demonstrated that these flies show ecdysone activity defects (retardation of salivary gland death and spiracle eversion defects), reduced ecdysone receptor target gene expression, partial lethality during pupation, autophagy defects and reduced triglyceride contents. They establish a mutual antagonistic relationship between ecdysone and insulin signaling in the fly fat body. Furthermore, because ecdysone signaling inhibits insulin signaling in the fat body, this also uncovers a feed-forward mechanism whereby ecdysone potentiates its own signaling via dTP53INP2 (Francis *et al*, 2010) (Figure 8).

A recent study from this year (Xu *et al*, 2016) have described a novel function of TP53INP2 in protein synthesis indicating that TP53INP2 promotes ribosome biogenesis through facilitating ribosomal RNA (rRNA) synthesis. It has been detected an association of TP53INP2 with the ribosomal DNA (rDNA) in HeLa and MCF-7 cells by chromatin immunoprecipitation (ChIP) assays, which suggested that TP53INP2 was a promoter of rDNA transcription under adequate nutrition condition. This role of TP53INP2 was conferred by its localization at the nucleolus through its nucleolar localization signal (NoLS) and its interaction with the components of the POLR1/RNA polymerase I preinitiation complex (PIC) facilitating the assembly of the complex at rDNA promoters.

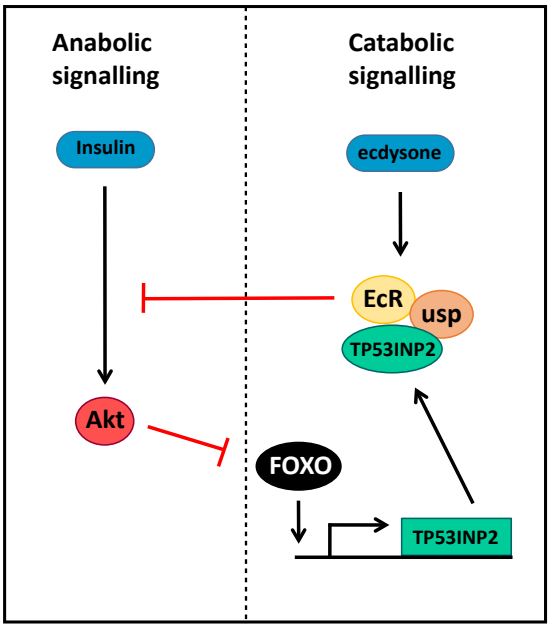

Figure 8. Schematic diagram of the proposed model for TP53INP2 function in *Drosophila*.

2.3.2. TP53INP2 as a regulator of autophagy

Originally TP53INP2 has been described as a nuclear protein in basal conditions. However, it has been reported that TP53INP2 exits the nucleus in response to cellular stress or activation of autophagy, and relocates to punctate cytoplasmic structures (Mauvezin *et al*, 2010, 2012; Nowak *et al*, 2009). Besides, cytoplasmic TP53INP2 localizes to early autophagosomes and interacts directly with autophagosome-membrane-associated proteins LC3, GABARAP, GABARAPL1 and GATE16, but not with autolysosome-associated protein LAMP1 (Figure 9) (Mauvezin *et al*, 2010; Nowak *et al*, 2009; Sancho *et al*, 2012). In addition, later data demonstrate that TP53INP2 is a dynamic protein under normal conditions that continuously shuttles in and out of the nucleus, localizes at the nucleolus and has an effect on activating basal autophagy (Mauvezin *et al*, 2012).

Moreover, TP53INP2 enhance the degradation of proteins through autophagy under basal conditions and amino acid starvation (Mauvezin *et al*, 2010). In experiments with TP53INP2 gain-of function HeLa cells, protein degradation rates increase and there are higher numbers of LC3-GFP-positive puncta per cell, as well as major accumulation of autophagosomes. In contrast, when TP53INP2 expression is suppressed by siRNA in

C2C12 myoblasts, cells have a substantial inhibition of protein degradation compared with control cells, fewer LC3-GFP-positive puncta and fewer autophagosomes. Together, this provides convincing evidence for the positive role of TP53INP2 in stress-induced autophagy in cellular models.

Last year, it was demonstrated that the starvation-induced LC3 translocation is controlled by the deacetylase SIRT1 (Huang *et al*, 2015). Utilizing mass spectroscopy, site-directed mutagenesis, protein-protein interaction and protein acetylation analysis, it was determined that activated SIRT1 deacetylates LC3 at Lys49 and Lys51 allowing LC3 specifically to interact with nuclear TP53INP2 and be exported together with TP53INP2 from the nucleus (Figure 9).

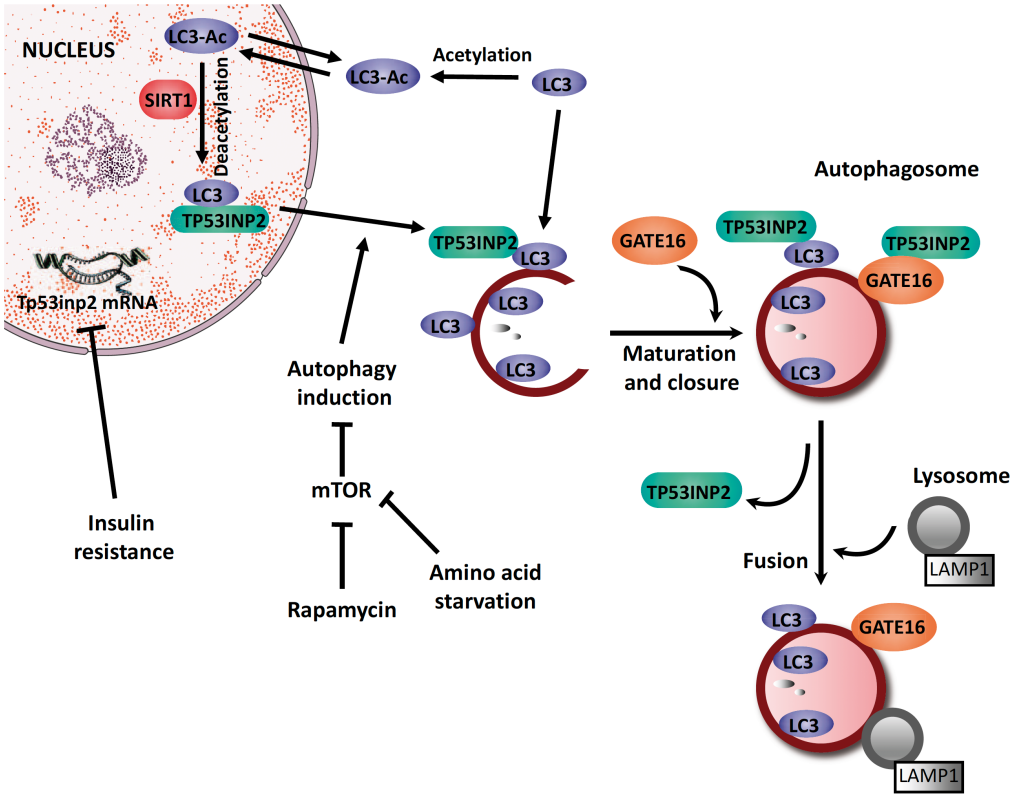

Figure 9. Functional role of TP53INP2 in autophagy. In response to nutrient depletion, SIRT1 deacetylates nuclear LC3. TP53INP2 interacts with deacetylated LC3 in the nucleus. Upon autophagy induction, TP53INP2 translocates from the nucleus to the cytosol together with deacetylated LC3. In the cytosol, TP53INP2 also interacts with other Atg8 family members such as GATE16, and promotes autophagosome formation. Upon closure, TP53INP2 leaves the autophagosome before the fusion with the lysosome. Under insulin resistant conditions, TP53INP2 gene expression is repressed, to downregulate an excessive autophagy.

The role of TP53INP2 as a regulator of autophagy has been also described in *Drosophila*. Having identified a homologue of TP53INP2 in flies (dTP53INP2), siRNA was used to suppress the expression of dTP53INP2 in larval fat bodies, an organ with high levels of autophagy. Control larvae had a greater number of Lysotracker-positive puncta in the fat body, as well as more autophagosomes and autolysosomes than the larvae deficient in dTP53INP2 (Mauvezin *et al*, 2010).

Recent studies from our laboratory (Sala *et al*, 2014) have shown that TP53INP2 promotes muscle wasting in mice. In fact, muscle-specific overexpression of TP53INP2 causes a reduction in muscle mass while TP53INP2 ablation causes muscle hypertrophy. Data indicate that this phenotype is because TP53INP2 activates basal autophagy in skeletal muscle (SKM) by increasing the formation of autophagosomes through the interaction with LC3. Not only that, but TP53INP2 also is involved in the autophagic degradation of ubiquitinated proteins, colocalizes with ubiquitinated protein aggregates and interacts with ubiquitin.

The authors (Sala *et al*, 2014) also conclude that TP53INP2 favors muscle wasting specifically in those catabolic conditions in which autophagy is activated, for example, streptozotocin-induced diabetes activates autophagy and therefore contributes to muscle wasting and TP53INP2 gain-of-function accelerates muscle atrophy in diabetic mice. On the other hand, TP53INP2 ablation mitigates muscle loss during streptozotocin-induced diabetes together with reduced autophagy activation. These results suggest that muscle TP53INP2 expression is modulated as an adaptative mechanism to preserve homeostasis in highly anabolic or catabolic conditions.

CHAPTER 3 OBJECTIVES

3. OBJECTIVES

In September 2012 when I joined Antonio's Zorzano laboratory, a substantial amount of information had been obtained about the protein DOR/TP53INP2. *TP53INP2* was first discovered searching for new candidate genes involved in the pathophysiology of type 2 diabetes mellitus. Further research had demonstrated that *TP53INP2* was repressed in pathological conditions such as the skeletal muscle of type 2 diabetes and in obese Zucker rats or diabetic mice (Baumgartner *et al*, 2007; Sala *et al*, 2014). In reference to the functional role of TP53INP2, published data originally identified TP53INP2 as a protein expressed in PML of nuclear bodies with capacity to coactivate different nuclear receptors in mammalian cells and in flies (Baumgartner *et al*, 2007; Francis *et al*, 2010; Sancho *et al*, 2012). Besides, TP53INP2 had been also described to exit the nucleus and to regulate autophagy in response to cellular stress (Mauvezin *et al*, 2010, 2012). When I came into the laboratory, Dr. David Sala had demonstrated that TP53INP2 participated in muscle wasting by the activation of basal autophagy in skeletal muscle (Sala *et al*, 2014), but the role of TP53INP2 in the regulation of the main mechanism of protein degradation in muscle, the Ubiquitin Proteasome System, was unknown. That was the starting point of my PhD project. Interestingly, some observations linked TP53INP2 with the UPS: a) TP53INP2 has been identified as a binding partner of PSMD4 and PSMA6 (subunits from the proteasome) by Yeast Two Hybrid assays (Nowak *et al*, 2009); b) TP53INP2 has been reported to be degraded through the proteasome in cellular models (Mauvezin *et al*, 2010); and c) TP53INP2 has been described to interact with ubiquitinated proteins (Sala *et al*, 2014).

According to this background, the main aim of my PhD thesis was to analyze the role of TP53INP2 in combining the regulation of autophagy with the Ubiquitin- Proteasome System.

3.1. Specific objectives

The following specific objectives have been pursued:

1) To study the effects of TP53INP2 on the Ubiquitin Proteasome System in skeletal muscle. To this end, we have analyzed whether TP53INP2 is involved in the modulation of the proteasome and the immunoproteasome activity. In addition, we have studied the participation of TP53INP2 in the regulation of the expression of proteasome subunits and some of the mechanisms by which TP53INP2 regulates the proteasome.

2) To study whether TP53INP2 regulates a muscle wasting condition such as cancer cachexia.

CHAPTER 4 RESULTS

4. RESULTS

4.1. Description of the experimental models

In this study we have used different cellular and *in vivo* experimental models. On the one hand, we have used C2C12 myoblasts knock down or overexpressing DOR/TP53INP2, performed either by using a lentiviral or adenoviral delivery system or either by transfection of cells with plasmids or siRNA oligos. On the other hand, the mouse strains used for this project are skeletal muscle DOR/TP53INP2 knockout mice (SKM-KO) and transgenic mice overexpressing DOR/TP53INP2 in skeletal muscle (SKM-Tg) (Sala *et al*, 2014).

4.1.1. TP53INP2 in skeletal muscle

TP53INP2 is highly expressed in tissues with high metabolic rate; in fact, the skeletal muscle shows the highest expression of TP53INP2 mRNA and protein compared with other mouse tissues (Sala *et al*, 2014). In 2014, our laboratory reported that TP53INP2 is a regulator of muscle wasting by the activation of basal autophagy (Sala *et al*, 2014). However, some evidences (described in the Objectives section) suggested that TP53INP2 is also involved in other mechanisms of protein degradation such as the Ubiquitin-Proteasome System (UPS). To determine the role of TP53INP2 in skeletal muscle UPS, different studies have been performed in this thesis.

On the one hand, the muscle-specific TP53INP2 knockout mouse line (Sala *et al*, 2014) was generated by crossing homozygous TP53INP2$^{loxP/loxP}$ mice with a mouse strain expressing Cre recombinase under the control of the myosin light chain 1 (MLC1) promoter in a C57BL/6J pure genetic background (Bothe *et al*, 2000). Deletion of exons 3 and 4 driven by Cre recombinase caused the ablation of *TP53INP2* expression, and, indeed, TP53INP2 protein was undetectable in skeletal muscle from SKM-KO mice. However, other tissues showed a normal TP53INP2 expression in SKM-KO mice (Sala *et al*, 2014).

On the other hand, the transgenic mice overexpressing TP53INP2 specifically in skeletal muscle under the control of the MLC1 promoter in a C57BL/6J pure genetic background showed higher *TP53INP2* expression and protein levels in skeletal muscle compared with that in controls (WT), whereas TP53INP2 expression was unaltered in other tissues (Sala *et al*, 2014).

4.1.2. TP53INP2 in a muscle cell model

In parallel, we have carried out experiments in C2C12 muscle cells. C2C12 loss-of-function cells were generated by stably expressing siRNA against TP53INP2 or scrRNA (used as control) via lentiviral transduction in myoblasts (Figure 10). However, C2C12 gain-of-function model was generated by transduction of adenoviruses coding for TP53INP2 or LacZ (used as control) for 30 hours of infection (Figure 11).

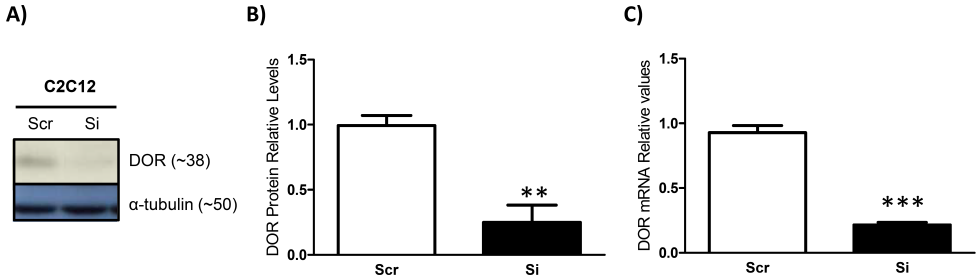

Figure 10. Down-regulation of DOR/TP53INP2 in C2C12 cells. (A) Analysis of western blot and (B) quantification (n=3) of total homogenates of C2C12 myoblasts stably expressing a siRNA against DOR (si) or a scramble siRNA (scr) as a control. White bars represent C2C12 scr cells, black bars represent C2C12 si cells. Total levels of DOR/TP53INP2 were detected by immunoblotting and α-tubulin was used as loading control. (C) Analysis of *DOR/TP53INP2* mRNA levels were studied in total homogenates of C2C12 scr and si. ARP and β-actin were used as housekeeping. Data represent mean ± SEM. **p<0,005, ***p<0,001 vs. control (scr).

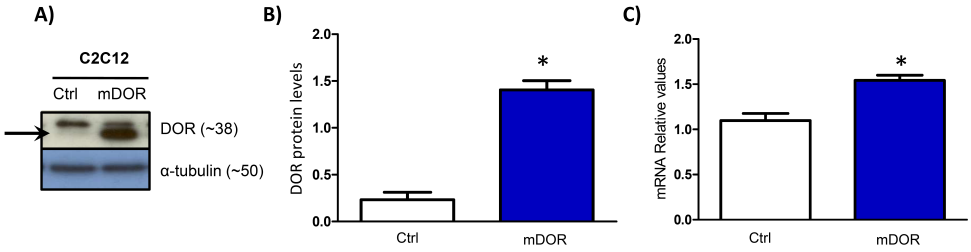

Figure 11. Overexpression of DOR/TP53INP2 in C2C12 cells. (A) Analysis of western blot and (B) quantification (n=3) of total homogenates of C2C12 myoblasts infected with the adenoviral system expressing wild type DOR (mDOR) or lacZ as a control (Ctrl). White bars represent Ctrl C2C12 cells, blue bars represent mDOR C2C12 cells. Total levels of DOR/TP53INP2 were detected by immunoblotting and α-tubulin was used as loading control. (C) Analysis of DOR/TP53INP2 mRNA levels were studied in total homogenates of C2C12 Ctrl and mDOR. ARP and β-actin were used as housekeeping. Data represent mean ± SEM. *p<0,05 vs. control (Ctrl).

4.2. Effects of TP53INP2 on the UPS

Previous observations show that TP53INP2 interacts with ubiquitinated proteins (Sala *et al*, 2014). Besides, this protein binds in Yeast Two Hybrid assays (YTH) to proteasome subunits PSMD4 and PSMA6. Based on these data, we decided to explore whether TP53INP2 influences UPS. To this end, we analyzed the effect of TP53INP2 ablation on skeletal muscle Ubiquitin Proteasome System.

4.2.1. Role of TP53INP2 on proteasome activity

In the first set of experiments, we analyzed the role of TP53INP2 in the modulation of the proteasome activity. Eukaryotic proteasomes have six active sites: two chymotrypsin-like, two trypsin-like and two caspase-like sites, each type differ in their specificity toward model fluorogenic peptide substrates (Orlowski, 1990; Orlowski *et al*, 1993). We have analyzed the chymotrypsin-like site, which is often considered the most important in protein breakdown (Chen & Hochstrasser, 1996; Heinemeyer *et al*, 1997).

For this purpose, we monitored the degradation of a fluorogenic peptide substrate specific for the chymotrypsin-like activity of the 26S/30S proteasome (Kisselev & Goldberg, 2005) in skeletal muscle of TP53INP2 KO versus control (loxP) fed mice. This fluorogenic substrate is a four amino acid residue peptide with a fluorogenic reporter group at the C terminus (AMC). The proteasome cleaves an amino bond between an

4.3. TP53INP2 modulates protein degradation during cancer cachexia

This second part of my doctoral thesis has been carried out in collaboration with Dr. Fabio Penna (University of Turin, Italy). As mentioned in the Introduction section, the most relevant feature of the pathophysiology of cancer cachexia is the ongoing loss of skeletal muscle mass. TP53INP2 has been described to be a negative regulator of muscle mass (Sala *et al*, 2014), indeed, TP53INP2 expression is repressed in wasting conditions such as diabetes (Baumgartner *et al*, 2007; Sala *et al*, 2014). To further analyze whether TP53INP2-induced exacerbation of muscle loss is a unique feature of the pathophysiology of diabetes or it also occurs in other catabolic conditions, we studied whether modulating TP53INP2 expression could affect muscle wasting caused by cancer cachexia.

In previous studies from David Sala's doctoral thesis, the experimental model used for the induction of cancer cachexia was the Lewis Lung Carcinoma (LLC), implanted intramuscularly in C57BL/6J mice and characterized by the growth of a large solid primary tumor and the appearance of cachexia 14 days after tumor implantation. However, the size of the tumor is approximately 20% of total body weight, very large to be compared with common human tumors or in comparison with the experimental model adopted for the study of cancer cachexia in this thesis. Consequently, the remarkable LLC tumor mass did not allow to appreciate exactly body weight loss until the animals were killed (Penna *et al*, 2015).

For that reason, we decided to use mice implanted with the murine colon carcinoma C26. In contrast to LLC model, C26 tumor mass represents approximately 1.5% of total body weight (Penna *et al*, 2013), representing a condition more similar to human cancer cachexia. C26 tumor was originally chemically induced in BALB/c mice and it does not grow in C57BL/6J so it was necessary to backcross the mice into the BALB/c strain to allow tumor engraftment. However, published data show that even an F2 generation of C57BL/6J mice backcrossed to a BALB/c strain is permissive for C26 growth and induction of body weight loss, as compared to pure BALB/c mice in both male and female animals (Penna *et al*, 2013, 2015). Besides, in the C26 model, a rapid and progressive cachectic phenotype occurs in tumor-bearing mice from day 9 of tumor growth.

To analyze whether TP53INP2 was regulated in such catabolic condition of cancer cachexia in muscles of WT mice, we first induced cancer cachexia by implantation of C26 cells in two month old WT mice and evaluated the mRNA expression (Figure 45). *TP53INP2* mRNA levels were significanly decreased in the skeletal muscle of C26-tumor bearing mice.

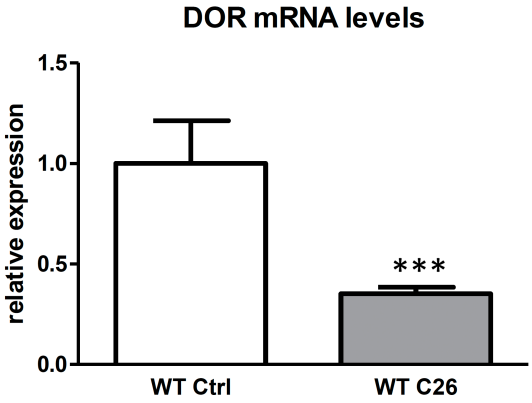

Figure 45. DOR/TP53INP2 decrease during the development of cancer cachexia induced by C26 tumor implantation. Gene expression analysis of TP53INP2 transcripts. mRNA abundance was corrected for β-actin levels on individual samples. Data represent mean ± SEM. ***p<0,001 vs. control mice. Ctrl (n=5) and C26 (n=6).

Thus, we induced cancer cachexia in two-month old (referred to as 60 days in the Figure 46) WT and TP53INP2 SKM-Tg animals. We decided to use this transgenic mouse colony overexpressing TP53INP2 in order to block the repression of the gene induced by catabolic conditions, cancer cachexia in this case. For simplicity, muscle-specific TP53INP2-overexpressing animals are referred to as "DOR" in the figures. Two experiments were carried out in parallel, the first one using males that were killed 14 days after C26 implantation, whereas in the second experiment, females were divided randomly into two groups and killed at 10 days and 13 days after C26 implantation. In this way, we could observe whether TP53INP2 exerts its effect in early or advanced stages of cachexia. We monitored the effect of C26 implantation in both experimental series as indicated in Figure 46.

First, we analyzed the loss of body weight of animals from the experimental serie I. C26 growth promoted a significant body weight reduction from day 8, consistently with previous results (Penna *et al*, 2013) in both WT and TP53INP2 SKM-Tg. However,

TP53INP2 SKM-Tg mice showed a more pronounced reduction (p=0.07 vs C26 WT) of body weight (Figure 47A and B), despite no significant changes were observed in food intake between WT and TP53INP2 SKM-Tg animals (Figure 47C and D) in both control conditions and after C26 implantation.

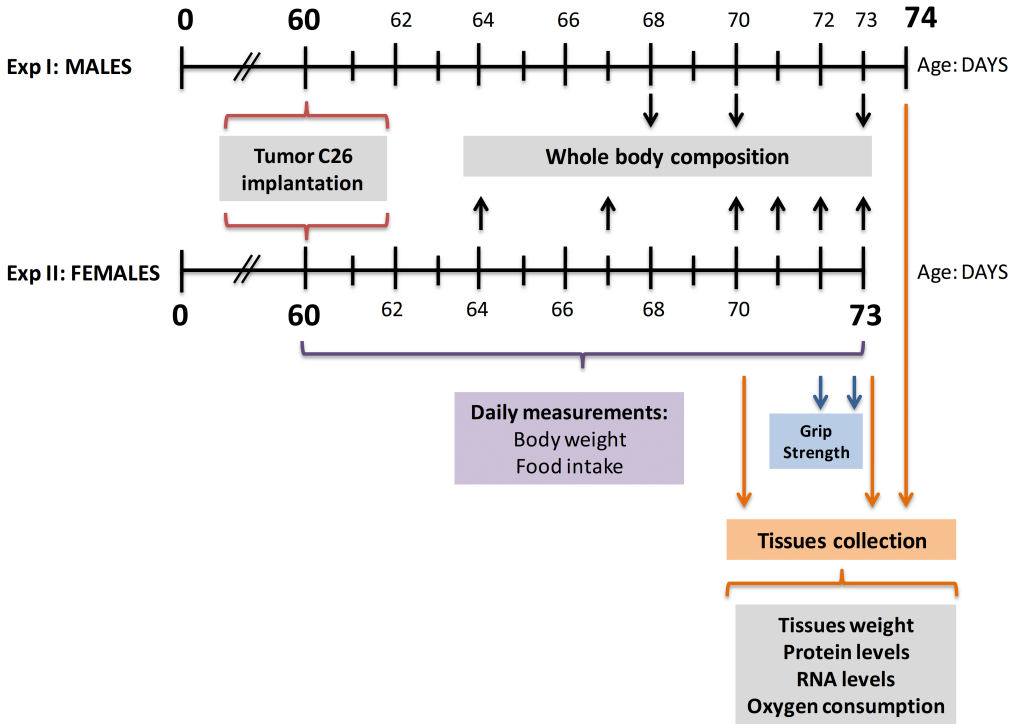

Figure 46. Chronologic layout of experiments I and II. Experiment I was carried out with male mice killed at one point (day 14). However experiment II was carried out with females mice killed at two different points (day 10 and 13).

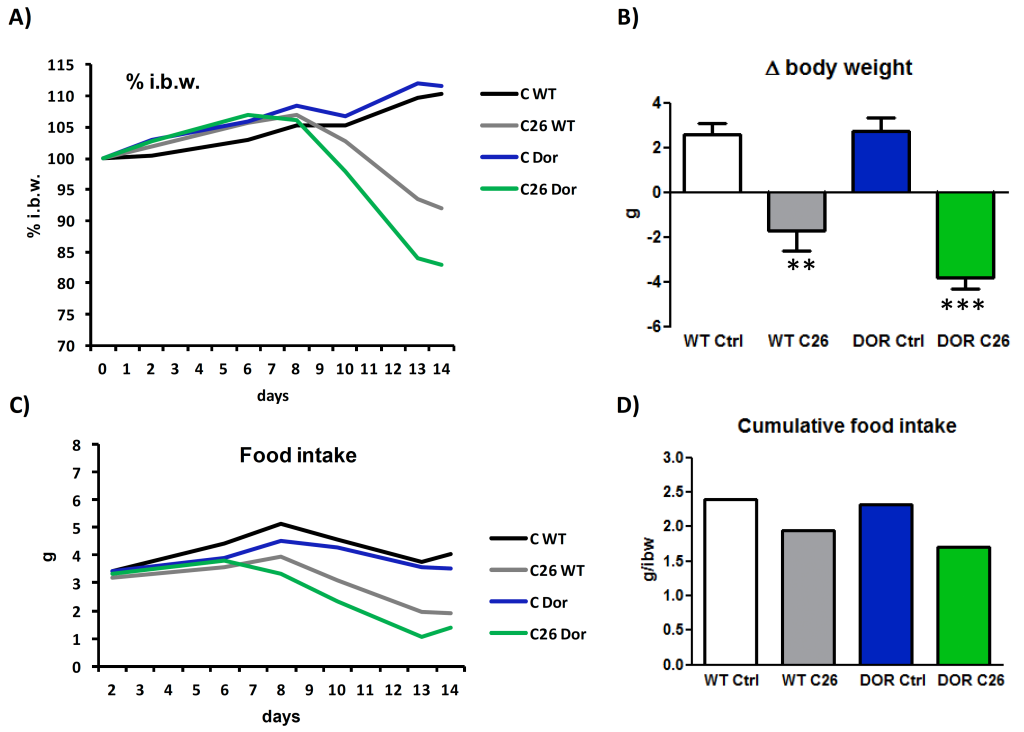

Figure 47. Effects of C26 implantation on body weight and food intake of BALB/c mice WT and TP53INP2 SKM-Tg. Body weight of control (C; n=6) and C26-bearing male mice (C26; n=9) reported as (A) % of initial body weight (% i.b.w.) and (B) variation of body weight at the end of the experimental period. (C) grams of daily food intake during the 14 days after C26 implantation. (D) Cumulative food intake. Data represent mean (A, C and D) and mean ± SEM (B). **p<0,01 ***p<0,001 vs. control mice (WT Ctrl).

Next, body composition in live animals was analyzed by magnetic resonance in experiment I at tumor injection and three time points before sacrifice. Despite the lack of change in body weight in control conditions, body fat mass was reduced at the end of the experiment in TP53INP2 SKM-Tg mice compared to WT mice (Figure 48A). In contrast, fat mass of WT animals were markedly reduced in comparison with TP53INP2 SKM-Tg upon C26 implantation at day 8. Besides, at the end of the experimental period, fat mass decreased dramatically in both WT and TP53INP2 SKM-Tg tumor-bearing animals in comparison with control conditions (Figure 48A). Nevertheless, no significative changes were detected in lean mass of WT and TP53INP2 SKM-Tg animals (Figure 48B).

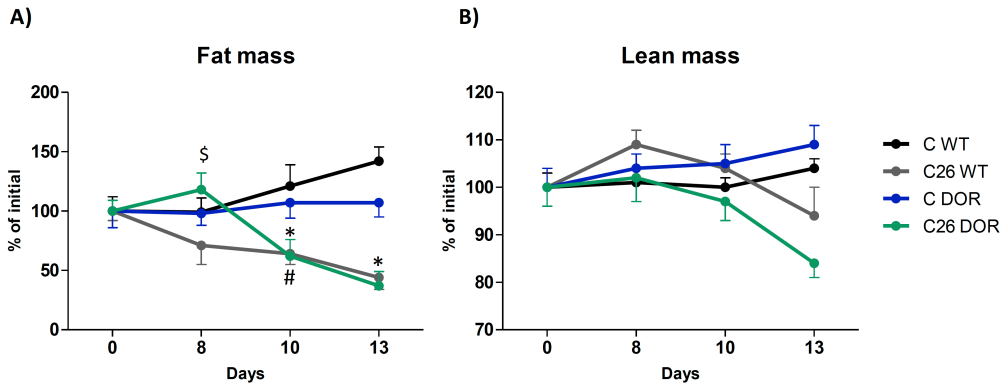

Figure 48. Effects of C26 implantation on fat and lean mass of BALB/c mice WT and TP53INP2 SKM-Tg. Fat mass and lean mass were analyzed at given time points (x axis) in males using the EchoMRI-100TM System. WT Ctrl and DOR Ctrl (n=6) and WT C26 ad DOR C26 (n=9). Data represent mean ± SEM of the % of initial value. * $p<0.05$ vs WT control. # $p<0.05$ vs. DOR Ctrl. $ $p<0.05$ vs. tumor bearing WT mice (C26 WT).

Moreover, to support the hypothesis that the reduction of TP53INP2 expression in wasting conditions is an adaptive mechanism to protect muscle mass, gastronemius muscle weight was analyzed in WT and TP53INP2 SKM-Tg mice. Muscles underwent a weight reduction in WT and TP53INP2 SKM-Tg mice upon C26 implantation. However, TP53INP2 SKM-Tg mice showed a more dramatic muscle loss (Figure 49A). Overall, these data indicate that TP53INP2 exacerbates muscle wasting in C26-induced cancer cachexia. Gonadal white adipose tissue (WAT) was also analyzed and a similar significant reduction was observed after C26 implantation in WT and TP53INP2 SKM-Tg mice (Figure 49B). This endpoint measure does not allow to document the kinetic of tissue loss, that might be distinc between WT and TP53INP2 SKM-Tg mice, as suggested by EchoMRI analyses. Finally, no significant changes were found in tumor mass in both animal groups, meaning that the changes in body and muscle weight observed do not rely on different tumor load (Figure 49C).

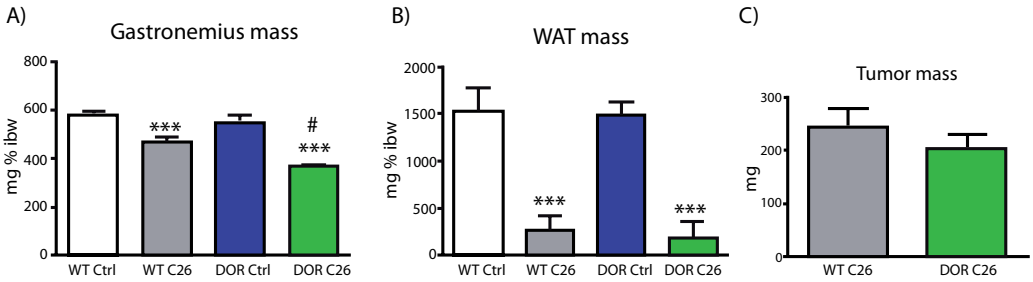

Figure 49. Effects of C26 implantation on tissues weight in BALB/c WT and TP53INP2 SKM- Tg mice. Muscle weight (gastronemius) (A), white adipose tissue (WAT) (B) and tumor weight (C) were analyzed in males at day 14 of tumor growth. Data are reported as milligrams/100 grams of initial body weight (I.B.W.). Data represent mean ± SEM. ***p<0,001 vs. control mice (WT Ctrl). #p<0,05 vs. tumor bearing control mice (WT C26). WT Ctrl and DOR Ctrl (n=6) and WT C26 ad DOR C26 (n=9).

In parallel, the same measurements were carried out in experiment II in which females were analyzed at initial and advanced stages of the development of cancer cachexia. First, we analyzed the loss of body weight of WT and TP53INP2 SKM-Tg animals. Similar to previous data and with experiment I, C26 promoted body weight reduction from day 10 of tumor growth in both WT and TP53INP2 SKM-Tg (Figure 50A and B). Even in this dataset, TP53INP2 SKM-Tg mice showed a tendency to a further reduction of body weight, although no significant changes were detected, probably, because the *n* of this of experiment was not sufficient to demonstrate statistical changes (Figure 50A and B). As expected, no significant changes were observed in food intake between WT and TP53INP2 SKM-Tg animals (Figure 50C) in control conditions and after C26 implantation.

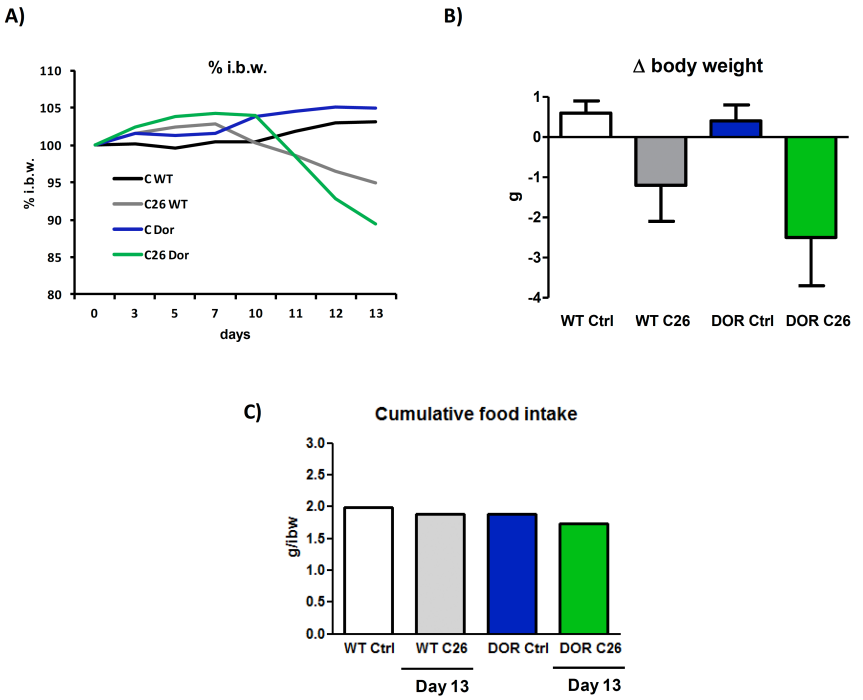

Figure 50. Effects of C26 implantation on body weight and food intake of BALB/c mice WT and SKM-TP53INP2 Tg. (A) Body weight of control and C26 bearing female mice reported as (A) % of initial body weight and (B) variation of body weight. (C) Cumulative food intake. Data represent mean in panel A and C. Data represent mean ± SEM in panel B. WT Ctrl and DOR Ctrl (n=6), WT C26 (n=3) and DOR C26 (n=4).

Next, body composition was analyzed in the experimental serie II. In accordance to the lack of change in body weight in control conditions, no differences were observed in fat and lean mass. In contrast, fat mass was markedly reduced upon C26 implantation at day 13 without significant differences between WT and TP53INP2 mice (Figure 51A and B).

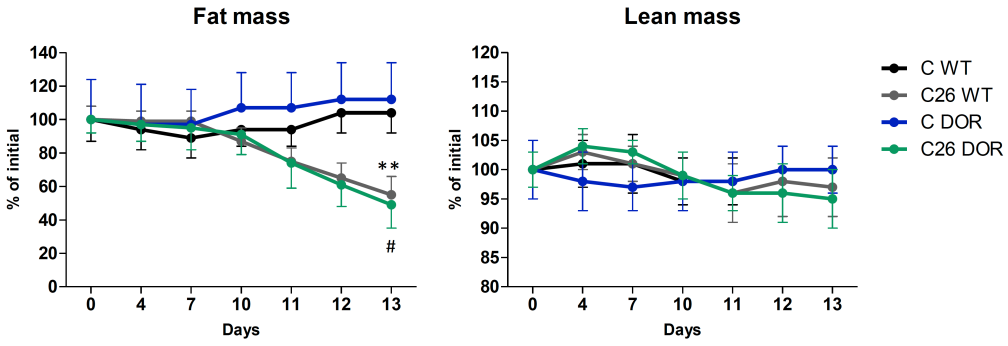

Figure 51. Effects of C26 implantation on fat and lean mass of BALB/c mice WT and TP53INP2 SKM-Tg. Fat mass and lean mass were analyzed at given points (x axis) in females using EchoMRI-100TM System. WT Ctrl and DOR Ctrl (n=6) and WT C26 and DOR C26 (n=7). Data represent mean ± SEM. ** p<0.01 vs WT control. # p<0,05 vs. DOR Ctrl.

Besides, gastrocnemius muscle weight was analyzed in WT and TP53INP2 SKM-Tg mice. Muscles underwent a weight reduction in WT and TP53INP2 SKM-Tg mice upon C26 implantation while the comparison between WT and TP53INP2 tumor-bearing mice shows a tendency to a more reduced muscle weight, however no significant changes were detected because of the small *n* in the experimental groups (Figure 52A).

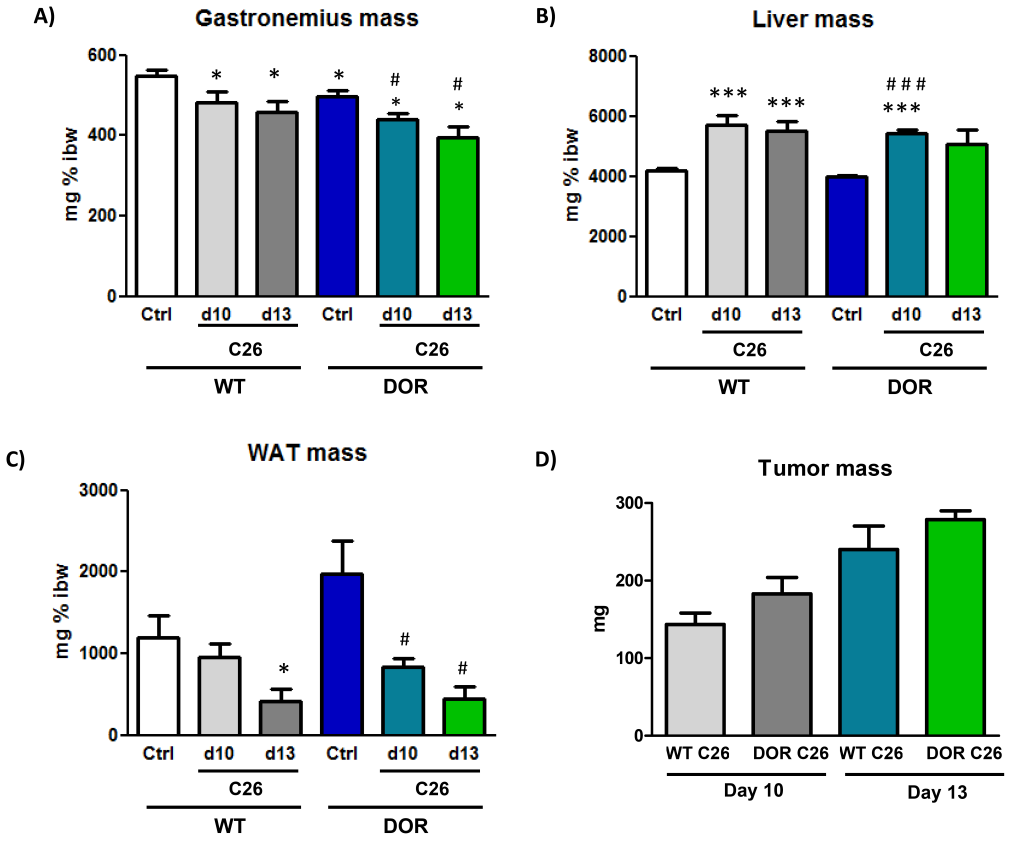

Figure 52. Effects of C26 implantation on tissues weight of BALB/c WT and TP53INP2 SKM-Tg mice. Muscle weight (gastronemius) (A), liver (B), white adipose tissue (C) and tumor mass (D) were analyzed in females at control conditions and after implantation of C26 tumor at given points (x axis). Data are reported as milligrams/100 grams of initial body weight (I.B.W.). WT Ctrl and DOR ctrl (n=6), WT C26 at day 10 and 13 (n=3) and DOR C26 at day 10 and day 13 (n=4). Data represent mean ± SEM. *p<0.05 and ***p<0,001 vs. control mice. #p<0,05 and ###p<0,001 vs. tumor bearing control mice (WT C26).

Liver and white adipose tissue (WAT) were also measured at the end of the experimental period when animals were killed. In reference to the liver mass, it increases upon C26 tumor development in both WT and TP53INP2 SKM-Tg mice (Figure 52B), likely due to the massive inflammatory acute phase response associated with tumor growth. In contrast, WAT is markedly reduced in the C26-bearing mice with respect to control animals. Besides, TP53INP2 SKM-Tg mice showed bigger WAT mass in control conditions in comparison with WT mice, suggesting that TP53INP2 regulation of muscle mass triggers a crosstalk with the adipose tissue stimulating a stronger accumulation (Figure 52C). Nevertheless, no significant changes were found in tumor mass in both animals (Figure 52D).

To better characterize the effect of cachexia on skeletal muscle function of these mice, muscle strength was measured using the grip strength test in WT and TP53INP2 SKM-Tg mice. Muscle strength in control groups is not affected by the presence of the transgene, however, a reduction of voluntary strength is observed after C26 implantation in TP53INP2 SKM-Tg mice (Figure 53).

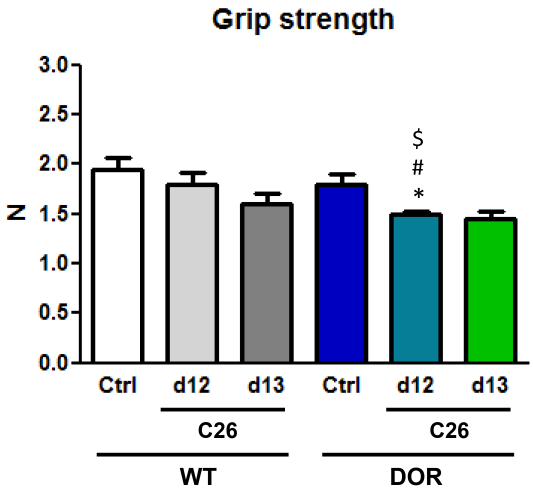

Figure 53. Effects of C26 implantation in females BALB/c WT and SKM-Tg mice on skeletal muscle strength. Grip strength was measured in females at day 12 and day 13 as a voluntary grasping strength test data and expressed in Newton. WT Ctrl and DOR Ctrl (n=6) and WT C26 and DOR C26 at day 12 and day 13 (n=7). Data represent mean ± SEM. *p<0,05 vs. control mice. # p <0,05 vs. DOR Ctrl. $ p<0,05 vs. WT C26 d12.

Taken together, the data from experiments I and II supports the concept that TP53INP2 negatively regulates muscle mass in catabolic conditions. In order to study the mechanisms by which TP53INP2 overexpression enhances C26-induced muscle atrophy at day 14, we evaluated the involvement of relevant protein degradation pathways in muscles from the experiment I. We analyzed the mRNA expression of the atrogenes *MURF1* and *Atrogin-1/FbxO32*. We observed that atrogenes *MURF1* and *Atrogin-1* were upregulated in C26-tumor bearing mice (Figure 54). Consistent with the effect of TP53INP2 on muscle atrophy, *MURF1* is significantly increased in tumor bearing transgenic mice in comparison with tumor bearing WT mice (Figure 54B). A tendency of higher levels of *Atrogin-1* is also observed in tumor bearing transgenic mice, however no significant changes were detected, probably because of the error bars of the experiment (Figure 54A).

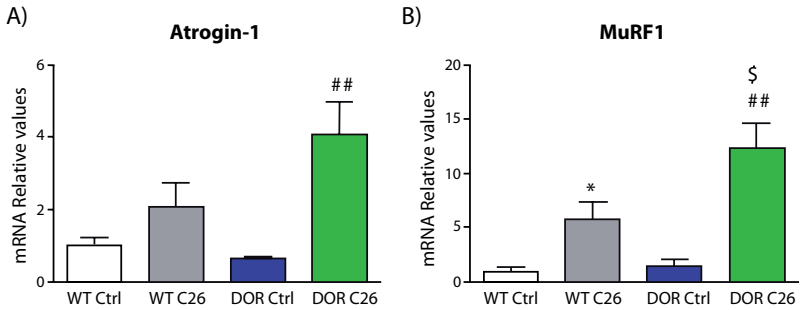

Figure 54. Tumor- driven muscle expression of atrogenes is exacerbated in SKM-Tg mice. Gene expression analysis of (A) *Atrogin-1* and (B) *MURF1* measured in tibialis muscle. mRNA abundance was corrected for β-actin levels on individual samples. Ctrl (n=6) and C26 (n=9). Data represent mean ± SEM. *p<0,05 vs. control mice. # p<0,05 and ## p<0,005 vs. DOR Ctrl. $ p<0,05 vs. WT C26.

To assess whether changes in autophagy may be responsible for these effects of enhanced muscle wasting in C26 tumor bearings TP53INP2 SKM-Tg mice, autophagy markers have been evaluated in the tibialis muscle of males in control conditions and on day 14 of tumor growth, representing the advanced stage of muscle wasting. *Beclin-1*, a main upstream regulator of autophagic sequestration tend to increase in tumor-bearing mice, but not significant changes were detected (Figure 55A). Next, levels of *LC3B*, a

marker of autophagosome formation, were significantly elevated in tumor-bearing mice of both WT and TP53INP2 without differences upon TP53INP2 manipulation (Figure 55B). The same behavior had *p62/SQSTM1*, p62 has been assayed as a measure of substrate sequestration into autophagosomes, binding to LC3 and to substrates marked for degradation by ubiquitylation. In accordance to *LC3*, *p62* accumulates in tumor bearing mice, in both WT and TP53INP2-overexpressing mice (Figure 55C). In addition, *NBR1*, another ubiquitin-binding scaffold protein participating in autophagic degradation of ubiquitinated proteins was analyzed and the same tendency of increasing upon C26 implantation is observed however no significant changes were detected (Figure 55D). *GABARAPL1*, essential for later stages of autophagosomal maturation, is also upregulated under cachectic conditions (Figure 55E). In reference to the expression of *LAMP2A*, the receptor for substrates degraded through Chaperone-Mediated Autophagy, it was upregulated upon C26 implantation but, surprisingly, higher expression is detected in muscles of WT animals in comparison with TP53INP2-overexpressing cachectic animals (Figure 55F). Finally, the lysosomal endopeptidase *Cathepsin L*, in accordance with the previous markers of autophagy analyzed, showed increased levels in C26-induced muscle atrophy muscles, without significant changes between both genotypes (Figure 55G).

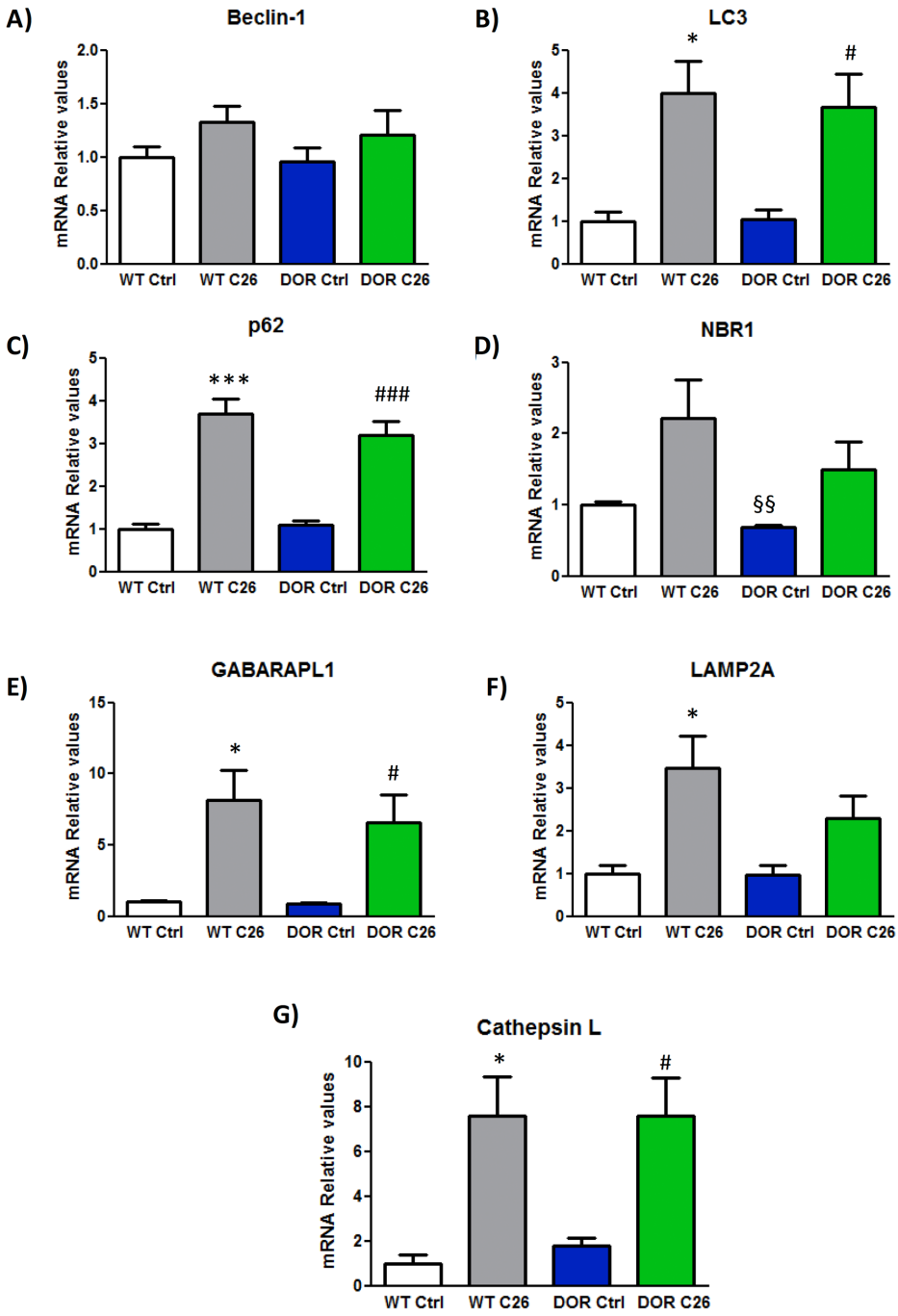

Figure 55. Autophagy related genes are induced by C26 growth though not affected by DOR/TP53INP2 expression. Gene expression analysis of (A) *Beclin-1*, (B) *p62*, (C) *LC3*, (D) *NBR1*, (E) *GABARAPL1* (F) *LAMP2A* and (G) *Cathepsin L* measured in tibialis muscle. mRNA abundance was corrected for β-actin levels on individual samples. Ctrl (n=6) and C26 (n=9). Data represent mean ± SEM. *p<0,05 and ***p<0,001 vs. control mice. # p <0,05 and ### p<0,001 vs. DOR Ctrl. $ p<0,05 and $$ p<0,005 vs. WT C26.

The mitophagy markers *Bnip3* and *Bnip3L* were also analyzed (Figure 56A and B) and the results indicated that *Bnip3* is induced in tumor bearing mice independently from the genotype (Figure 56A). Overall, our data indicate that an increased expression of autophagic degradation and mitophagy markers are induced in muscle upon 14 days of C26 tumor implantation. In some cases, such as *LAMP2A*, the induction of autophagic genes is reduced in transgenic animals, which might be an adaptive mechanism to buffer autophagic activity.

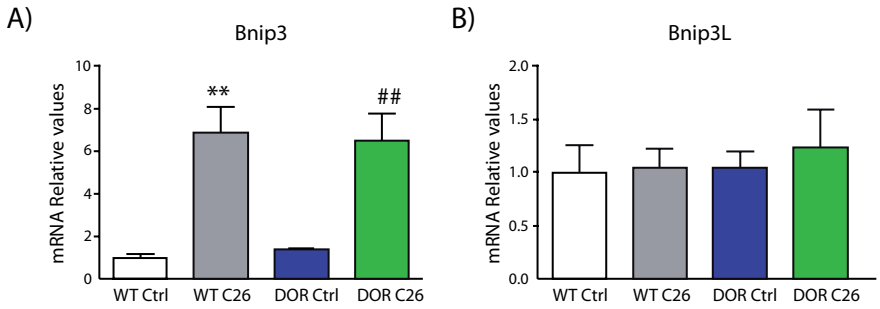

Figure 56. Mitophagy is induced in tumor-bearing SKM-Tg mice. Gene expression analysis of (A) *Bnip3* and (B) *Bnip3L* measured in tibialis muscle. mRNA abundance was corrected for β-actin levels on individual samples. Ctrl (n=6) and C26 (n=9). Data represent mean ± SEM. **p<0,005 vs. control mice (WT Ctrl). ## p<0,005 vs. DOR Ctrl.

Because of the close functional relationship between mitochondria and autophagy, we studied the master mitochondrial transcriptional regulator *PGC1α* (Figure 57A) and the mitochondrial dynamics related genes such as *Mfn2*, *Opa1* and *Drp1* (Figure 57B, C and D). We discovered that *Mfn2*, *Opa1* and *Drp1* expression was reduced in transgenic mice overexpressing TP53INP2 upon C26 implantation. Taken together, these data indicate that muscle wasting promoted by TP53INP2 overexpression in muscle alters mitochondrial dynamics.

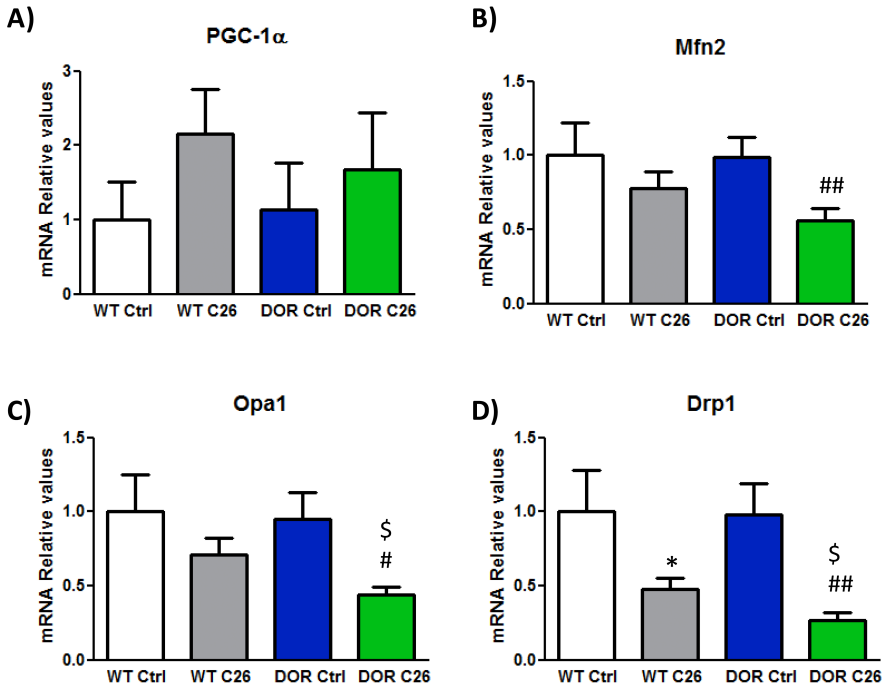

Figure 57. Mitocohondrial dynamics related genes are downregulated in tumor-bearing SKM-Tg mice. Gene expression analysis of (A) *PGC-1α*, (B) *Mfn2*, (C) *Opa1* and (D) *Drp1* measured in tibialis muscle. mRNA abundance was corrected for β-actin levels on individual samples. Ctrl (n=6) and C26 (n=9). Data represent mean ± SEM. *p<0,05 vs. control mice. # p <0,05 and ## p<0,005 vs. DOR Ctrl. $ p<0,05 vs. WT C26.

Cancer cachexia enhances global energy expenditure (Petruzzelli *et al*, 2014). However, whether muscle participates in this process is unknown and studies performed in C2C12 myotubes indicate a reduced mitocondrial respiration in response to incubation with Lewis Lung carcinoma conditioned medium (McLean *et al*, 2014). Therefore, we analyzed mitochondrial oxygen consumption in isolated muscle fibers from WT and TP53INP2 transgenic animals. Interestingly, the maximal respiration capacity induced by FCCP is increased in muscle fibers from transgenic mice in basal conditions (Figure 58). Moreover, cancer cachexia reduced mitochondrial respiration in both genotypes, in fact both complexes I and II are reduced upon C26 implantation. This effect does not seem to be dependent of TP53INP2 regulation.

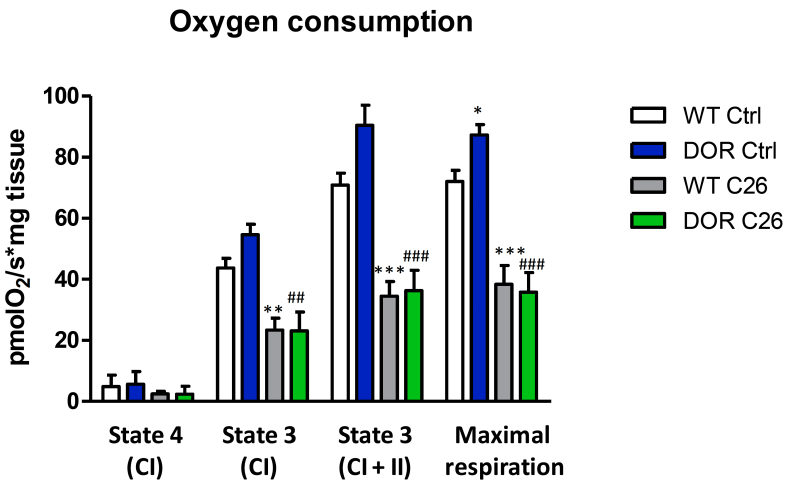

Figure 58. Effects of C26 implantation on muscle oxygen consumption of WT and SKM-Tg BALB/c mice. Oxygen consumption in state 3 and state 4 was measured in permeabilized fibers from EDL muscles, with complex I (glutamate + malate) and complex II (succinate) substrates. Maximal respiratory capacity was assessed after the addition of the uncoupler FCCP. All measurements were taken in control conditions (white and blue bars) and after implantation of C26 tumor (grey and green bars) (n=6 mice per group). Data represent mean ± SEM; **p<0.005, ***p<0.001 vs. control mice (WT Ctrl). ## p<0.005, ### p<0.001 vs. DOR Ctrl.

Finally, we analyzed the expression of *TP53INP2*. Surprisingly, *TP53INP2* mRNA expression is dramatically reduced not only in WT animals after 14 days of C26 growth, but also, in transgenic mice. Figure 59 shows the effects of the tumor growth on endogenous levels of *TP53INP2* (Figure 59A) and also including the expression of the transgene (Figure 59B).

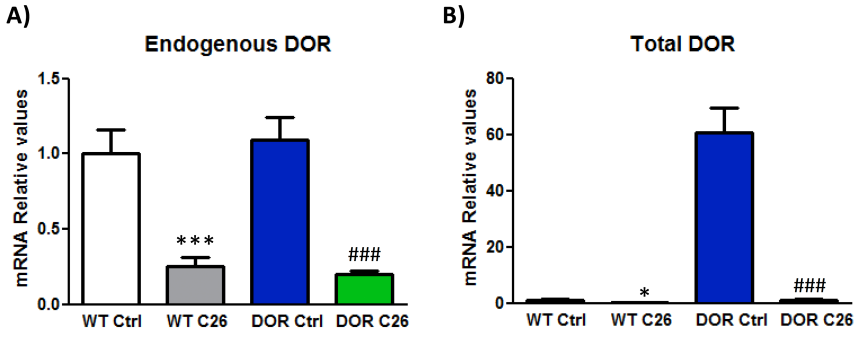

Figure 59. Total DOR/TP53INP2 mRNA levels are lowered to physiologic levels after C26 growth for 14 days. Gene expression analysis of (A) endogenous DOR and (B) total DOR transcripts measured in tibialis muscle. mRNA abundance was corrected for β-actin levels on individual samples. Ctrl (n=6) and C26 (n=9). Data represent mean ± SEM. *p<0,05 and ***p<0,001 vs. control mice. ### p<0,001 vs. DOR Ctrl.

Consistently with gene expression, protein levels were also analyzed in all the experimental conditions and a dramatic reduction of TP53INP2 was observed in TP53INP2 SKM transgenic animals at 14 days of tumor bearing (Figure 60). Thus, we can confirm that this condition of muscle wasting induced by tumor implantation was triggering a reduction in the levels of endogenous and exogenous expression of TP53INP2 (Figure 60). In all, our data indicate that TP53INP2 overexpression at initial stages is enough to promote muscle loss in this model of cancer cachexia induced by C26.

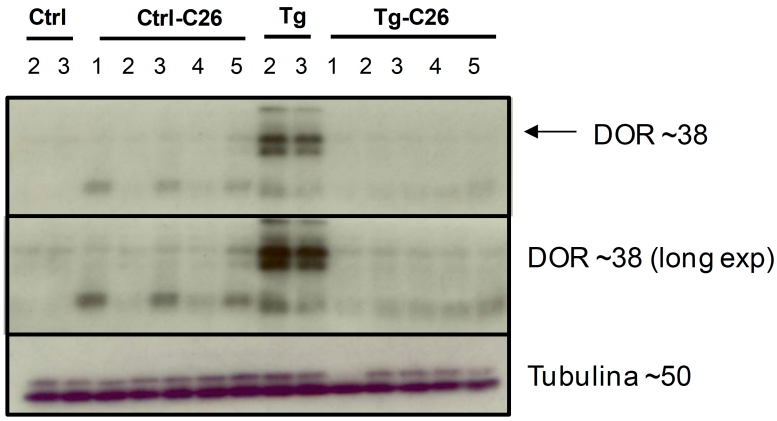

Figure 60. Total DOR/TP53INP2 protein is lowered to physiologic levels after C26 growth for 14 days. Western blot analysis of total DOR in total homogenates of tibialis from WT and DOR SKM-Tg male animals in control conditions and after implantation of C26 tumor. Protein levels were corrected for α-tubulin levels on individual samples. Ctrl (n=6) and C26 (n=9).

To conclude this part, based on the functional role of TP53INP2 in controlling muscle mass, we analyzed whether the expression of *TP53INP2* gene was regulated in human muscles biopsies from control patients (n=8), and from cancer patients (n=29) from M.G. Vannini Hospital in Rome (Italy) and Azienda Ospedaliera Universitaria Senese in Siena (Italy). The samples from cancer patients were sub-classified into two groups: patients with body weight loss <5% (cancer no cachexia, n=17) and patients with body weight loss >5% (cancer cachexia, n=12). Interestingly, *TP53INP2* mRNA levels underwent an 85% reduction in cancer patients with cachexia in comparison with healthy patients and also in relation to non-cachectic cancer patients (Figure 61). Overall, these data strongly supported the view that TP53INP2 is repressed in wasting conditions such as cancer

cachexia. These data are coherent with the *TP53INP2* gene repression observed in diabetic and obese patients (Sala *et al*, 2014), suggesting that TP53INP2 may have a relevant role in the attempt to spare muscle mass that takes place under these pathological states.

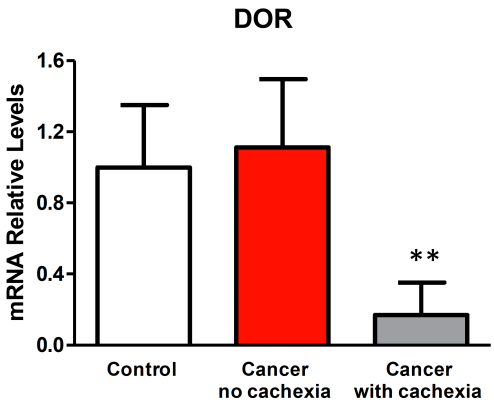

Figure 61. DOR/TP53INP2 decreases in cancer cachectic patients although are maintained in not cachectic cancer patients. Gene expression of TP53INP2 transcript was analyzed in healthy, cancer (not cachectic) and cancer cachectic patients. mRNA abundance was corrected for TBP levels on individual samples. Data represent mean ± SEM. **p<0,01 vs. control patients. Ctrl (n=8), not cachectic cancer (n=17) and cancer cachectic patients (n=12).

CHAPTER 5 DISCUSSION

5. DISCUSSION

5.1. Effects of TP53INP2 on the Ubiquitin Proteasome System

TP53INP2 has been previously described in our laboratory as a protein with two different functions, i.e., a nuclear coactivator and an autophagy regulator (Baumgartner *et al*, 2007; Francis *et al*, 2010; Mauvezin *et al*, 2010, 2012; Sancho *et al*, 2012). During this PhD we have demonstrated that TP53INP2 is a regulatory protein that links autophagy with the Ubiquitin Proteasome System in muscle. Thus, TP53INP2 deficiency, which causes a reduction in autophagy, in parallel also enhances the proteasome activity as well as the abundance of the subunits PSMD11 and PSMA1-7 both in skeletal muscle and in muscle cells (Figure 62).

Currently available data indicate that PSMD11 is necessary for proteasome assembly (Vilchez *et al*, 2012). Indeed, human embryonic stem cells (hESC) exhibit high proteasome activity, compared with differentiated cells, and this increased proteasome activity correlates with increased levels of the 19S proteasome subunit PSMD11. This is an essential subunit for the activity of the 26S/30S proteasome because stabilizes the otherwise weak interaction between the 20S core and the 19S cap particles (Pathare *et al*, 2012). In this study, we observe that PSMD11 is upregulated upon TP53INP2 deficiency in muscle cells and in skeletal muscle, and besides, PSMD11 is the only subunit of the proteasome which is downregulated by TP53INP2 gain of function. Taken together, our data permit us to conclude that TP53INP2 has an effect on the expression of PSMD11. In this connection, when muscle cells are treated with autophagy inhibitors no changes were detected in the levels of PSMD11. This supports the view that the effects of TP53INP2 deficiency are not just an indirect consequence of autophagy inhibition, but instead that TP53INP2 is also involved in the regulation of the ubiquitin proteasome system.

Because of the increased PSMD11 abundance, we suggest that TP53INP2 deficiency facilitates proteasome assembly. To confirm this hypothesis, studies using native gel analysis of the proteasome followed by western blot with PSMA1-7 (20S subunit) need to be done, in order to detect the abundance of assembled proteasome complexes (26S and 30S).

The immunoproteasome, referred also as the inducible form of the proteasome, plays a role in generating peptides for antigen presentation by MHC I, but it has also been described in all tissues as an active participant in the response to oxidative stress (Pickering & Davies, 2012b). Optimal functioning of both the immunoproteasome and the 26S/30S appears to be critical for cellular function (Johnston-Carey *et al*, 2016; Tanaka *et al*, 2012). For that reason, we measured the impact of TP53INP2 on immunoproteasome ativity, and our data clearly reveals that TP53INP2 loss-of-function also upregulates the immunoproteasome.

There are different mechanisms that promote increased proteasome and immunoproteasome activities, however, it is not necessarily accompanied by an increase in the β5/β5i proteasome subunits expression. In the particular case of the immunoproteasome, it can bind to the 11S (PA28) regulatory particle, which may increase its activity without any change of the proteasomal mass. Besides, stress-induced phosphorylation of the proteasome might also trigger detaching of the 19S regulatory particle, thus providing more 20S and less 26S capacity. This fact could promote that free 20S core particles bind to 11S particle increasing the ATP-independent proteasomal degradation, which may provide a shift in proteolytic capacity without any change in the levels of proteasome subunits (Johnston-Carey *et al*, 2016). In this sense, it will be of interest to analyze whether TP53INP2 modulates the 11S particle through the expression of PSME1, PSME2 or PSME3 (proteasome activators).

Emerging evidences have demonstrated that autophagy and UPS are coordinated to mediate the degradation of polyubiquitinated proteins. Most published results show that inhibition of proteasomal activities induce autophagy (Ding *et al*, 2007; Iwata *et al*, 2005; Pandey *et al*, 2007). However, less information is available about the regulation of the UPS by autophagy (Hara *et al*, 2006; Komatsu *et al*, 2006; Korolchuk *et al*, 2009a, 2010;

Wu *et al*, 2010). Contrary to what happened in other studies (Komatsu *et al*, 2006; Qiao & Zhang, 2009), we report that an impairment of autophagy mediated by TP53INP2 deficiency induces proteasome activity in muscle cells and skeletal muscle in the absence of nutritional stress or amino acid starvation. Only one study has reported this relation in which inhibition of autophagy by treatment with chloroquine or by knockdown of autophagy-related genes such as PIK3C3, ATG5 and ATG7 could induce proteasomal activity in colon cancer cells (Wang *et al*, 2013). In fact, induction of proteasome activity was only detected in conditions of starvation-induced autophagy but not under basal conditions (Wang *et al*, 2013). It is unclear whether this regulation occurs in other cellular contexts.

As it has been mentioned in the introduction, the possible relationship between the UPS and autophagy has been reported in different studies. In addition, Cuervo et al reported that the autophagic pathway degrades the proteasomes in rat liver (Cuervo *et al*, 1995), which supports the possibility that inhibition of autophagy might enhance the accumulation of proteasomes. This finding is in concordance with our data indicating that TP53INP2 deficiency enhances proteasome activity. However, our results also indicate that the proteasome subunits PSMD11, PSMD4 and PSMA1-7 are not degraded by autophagy. Instead, we have documented that PSMD11 and PSMA1-7 subunits are degraded through the proteasome. Opposite evidence also exists in the literature supporting that autophagy blockade has no effect on neuronal proteasomal activity in vitro and in vivo (Komatsu *et al*, 2006; Qiao & Zhang, 2009). The regulatory mechanisms that operate between autophagy and proteasomal activity have to be elucidated.

In this study, we have documented that TP53INP2 loss-of-function causes an increased proteasome activity in muscle cells. We also demonstrated that some proteasome subunits are degraded through the proteasome since PSMD11 and PSMA1-7 proteins increased upon proteasome blockade. The precise mechanisms by which the regulation of the proteasome subunits occurs in response to TP53INP2 deficiency remain unknown. Recent global proteomic studies reveal that a majority of cellular proteins are substrates for ubiquitination, including some proteasomal components (Danielsen *et al*, 2011; Kim *et al*, 2011; Wagner *et al*, 2011). A model has been proposed (Jacobson *et al*,

2014) by which ubiquitination of some subunits of the 26S proteasome serves to regulate proteasome activity. Indeed, ubiquitination of the 26S proteasome impairs binding of ubiquitinated proteins, a process that is regulated by oxidative stress or serum starvation (Jacobson *et al*, 2014). Four subunits were described to be subjected to *in situ* ubiquitination, one of them was the human homologue of PSMD4, named S5a. Besides, Rpn10, the yeast homologue of PSMD4, was found to be monoubiquitinated and/or multiple monoubiquitinated on the yeast 26S proteasome (Crosas *et al*, 2006; Isasa *et al*, 2010). Similar modification was also found in *Drosophila* (Lipinszki *et al*, 2012) which indicates that ubiquitination of this subunit is conserved among different species. These studies permit us to suggest that TP53INP2 regulates the levels of ubiquitination of proteasome subunits, to test this hypothesis, we are planning to measure the ubiquitination level of PSMD4 or PSMD11 subunits upon immunoprecipitation.

Related to the mechanism of regulation, our data suggest that TP53INP2 does not regulate the expression of the proteasome subunits at a transcriptional level. Instead, TP53INP2 repression stabilizes the proteasome subunits PSMD11, PSMD4 and PSMA1-7 (Figure 62). Further studies should be done to determine the precise half-life of the proteasome subunits by using [^{35}S]methionine labeling approaches.

TP53INP2 is a nuclear-cytoplasmic shuttling protein. It is actively transported between both compartments at a high rate, however, mutation of the nuclear export sequence (NES) located at residues 32-40 blocks the protein in the nucleus (Mauvezin *et al*, 2010; Sancho *et al*, 2012). This pattern of TP53INP2 is reminiscent of p62 protein, which also shuttles between nuclear and cytosolic compartments upon cellular stress. As TP53INP2, p62 is also found in nuclear promyelocytic leukemia bodies (PML) and contains two nuclear localization signals (NLS) and a nuclear export signal (NES) (Pankiv *et al*, 2010). Recent data from our laboratory demonstrated that TP53INP2 colocalizes with ubiquitinated proteins, interacts with ubiquitin and promotes the degradation of ubiquitinated proteins independently of p62 and NBR1. In fact, TP53INP2 overexpression displaces p62 from autophagosomes, probably, due to the fact that TP53INP2 interacts with LC3 with higher affinity that p62 (Sala *et al*, 2014). On the other hand, p62 has been described to recruit nuclear polyubiqutinated proteins or protein aggregates to

PML bodies and may help in their proteasomal degradation in the nucleus (Pankiv *et al*, 2010). In contrast to the effects of p62, our results indicate that a NES mutant form that retains TP53INP2 in the nucleus no longer shows ability to regulate the proteasome subunits. Our data suggest that cytosolic TP53INP2 regulates the stability of proteasome subunits through mechanisms that are not directly linked to autophagy modulation.

A coordinated effort of the three groups of enzymes E1, E2 and E3s results in the attachment of ubiquitin to a substrate protein, with multiple lysine 48-linked ubiquitin molecules serving as a signal for that protein to be degraded by the 26S proteasome (Chau *et al*, 1989). MuRF1 and Atrogin-1 have been identified as muscle specific E3 ubiquitin ligases. In skeletal muscle, increases in proteasome activity are generally associated with muscle atrophy, a process characterized by the induction of MuRF1 and Atrogin-1 (Auclair *et al*, 1997; Bodine *et al*, 2001; Gomes *et al*, 2012, 2001; Hobler *et al*, 1999). The role of MuRF1 and Atrogin-1 in muscle hypertrophy, such as the situation induced in muscles with TP53INP2 gain-of-function is unknown (Sala *et al*, 2014). It is generally assumed that an increase in proteasome activity is linked to an increase in MuRF1 and Atrogin-1 expression, as a greater quantity of ubiquitin ligases should increase the number of polyubiquitinated proteins. Nevertheless, our data indicate that TP53INP2 activates gene expression of the atrogene MuRF1 in muscle cells but no activation was detected in skeletal muscle and no differences were observed in atrogenes protein levels. These observations reveal that MuRF1 and Atrogin-1 are not always good markers of proteasome activity. Other studies also described this apparent disconnection between MuRF1 and Atrogin-1 expression and proteasome activity. Thus, acute alcohol intoxication increased MuRF1 and Atrogin-1 expression but did not increase skeletal muscle proteolysis (Vary *et al*, 2008). Similarly, 14 days of glucocorticoid treatment did not result in increase proteasome activity despite significant upregulation of MuRF1 and Atrogin-1 expression (Baehr *et al*, 2011). Conversely, MuRF1 and Atrogin-1 expression was not increased when mice were allowed to recover following 7 days of hindlimb unloading but proteasome activity was significantly increased in the first day of recovery (Lang *et al*, 2012). Furthermore, under denervation conditions, the lack of MuRF1 resulted in greater activation of the proteasome (Gomes *et al*, 2012). Lastly, muscle hypertrophy

caused by functional overload (Baehr *et al*, 2014) is associated with elevated proteasome activity even after MuRF1 and Atrogin-1 expression has returned to baselines levels. In all, the levels of MuRF1 and Atrogin-1 does not appear to regulate in all conditions the proteasome activity in skeletal muscle and muscle cells upon TP53INP2 modulation. These findings highlight the need for a better understanding of the roles of MuRF1 and Atrogin-1 in the function of skeletal muscle.

As described before, changes in protein turnover that lead to muscle hypertrophy or atrophy do not always proceed according to the most logical equations (Baehr *et al*, 2011, 2014; Gomes *et al*, 2012; Lang *et al*, 2012; Vary *et al*, 2008). Hypertrophy does not always result from increased protein synthesis and decreased protein degradation, while muscle atrophy is not always produced by decreased protein synthesis and increased protein degradation (Goldberg, 1969; Schiaffino *et al*, 2013). Indeed, our data indicate that TP53INP2 deficiency seems to promote protein synthesis in muscle cells as assessed by the SUnSET method. As to the signals involved, no changes in mTOR signaling pathway were detected. Surprisingly, the phosphorylation of eIF2α was upregulated in TP53INP2 deficient cells, which it is known to repress global translation coincident with translation of ATF4. This suggests the activation of the eIF2α-mediated stress response pathway. However it is the first time that a dysregulation between pEIF2α and increased levels of protein synthesis is described. A study has recently reported that TP53INP2 plays a role in rDNA transcription promoting ribosome biogenesis in HeLa and MCF-7 cancer cells (Xu *et al*, 2016). The potential mechanisms by which TP53INP2 regulates protein synthesis remain unclear.

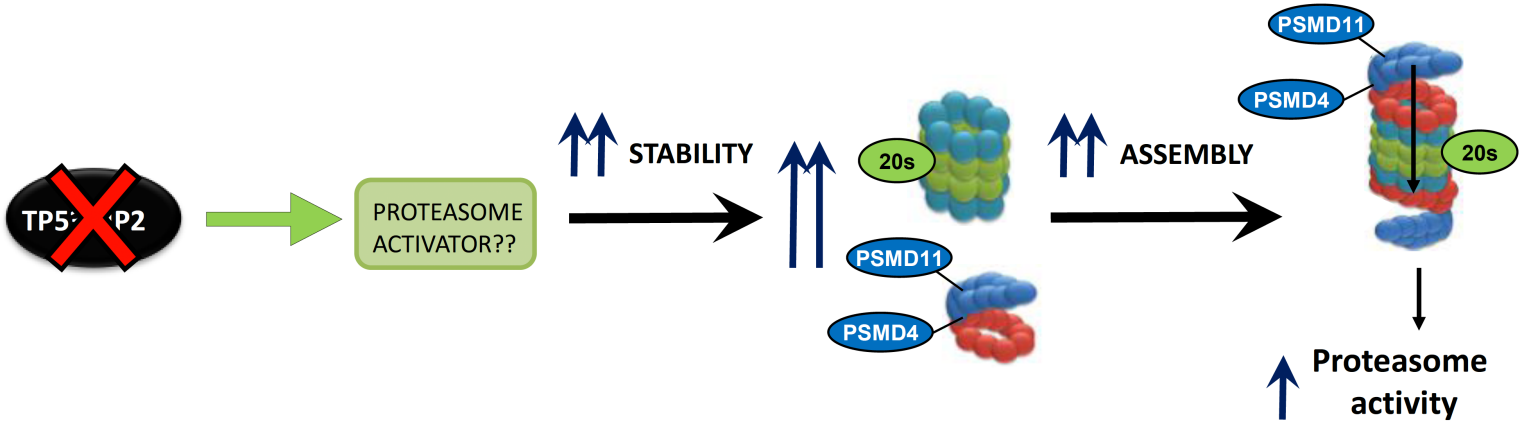

Figure 62. Schematic model of the regulation of the ubiquitin proteasome system by TP53INP2.

5.2. Effects of TP53INP2 on cancer cachexia.

Cachexia is a complex syndrome characterized by body weight loss – mainly from loss of skeletal muscle and body fat - and inflammation (Argilés *et al*, 2014; DeWys *et al*, 1986). The most studied players in the onset of this paraneoplastic pathology are several pro-inflammatory cytokines including TNFα, IL-1, IL-6 and IFNγ, and also of tumor derived factors, such as PIF and LMF. All of them influence skeletal muscle protein metabolism through modulations of both protein synthesis and degradation machinery (Fearon *et al*, 2012).

In this thesis, we have confirmed that the autophagy process plays an essential role in the skeletal muscle of C26 cachectic mice. Some data supporting such hypothesis are already published in previous studies carried out by the laboratory of Dr. Fabio Penna (Aversa *et al*, 2016; Penna *et al*, 2013). Indeed, it was demonstrated that muscle wasting is associated with the increase of the markers of autophagy including Beclin-1, LC3B and p62 (Penna *et al*, 2013).

Previous studies from our laboratory have shown that muscle expression of TP53INP2 was reduced in catabolic conditions such as diabetes and obesity (Baumgartner *et al*, 2007; Sala *et al*, 2014) and favors muscle wasting in those catabolic conditions in which autophagy is activated such as in diabetic mice (Sala *et al*, 2014). For that reason we thought that TP53INP2 could play a role in muscle wasting mediated by cancer cachexia. Indeed, the major conclusion of this work is that the forced activation of TP53INP2 accelerates body weight loss and muscle wasting in cancer cachectic mice (Figure 63). Furthermore, we have observed that *TP53INP2* mRNA levels are reduced in muscles from C26 tumor bearing mice and cancer cachectic patients.

Thus, our data are consistent with the idea that *TP53INP2* expression is modulated as an adaptive mechanism to preserve muscle homeostasis. This means that *TP53INP2* repression that occurs in tumor bearing mice represents an attempt to limit muscle loss in this pathological condition as it happens in obesity or type 2 diabetes. For that reason we suggest TP53INP2 as a good target in people at risk of muscle loss because TP53INP2 inhibition may save muscle mass.

To further strengthen the effects on cachexia, body composition and muscle strength were measured. Consistent with previous results, the reduction in muscle strength observed in TP53INP2 SKM-Tg mice upon C26 implantation is faster than WT animals; suggesting a decrease in muscle quality. Measurements of cross-sectional area are required to confirm the alterations in muscle fibers size.

According to autophagy markers, the results shown in the present study confirm and further extend those of previous reports (Aversa *et al*, 2016; Penna *et al*, 2013), showing that *LC3*, *p62*, *GABARAPL1*, *cathepsin L* and *Bnip3* mRNA levels are increased in the skeletal muscle of tumor bearing mice. Although all the markers of autophagy mentioned previously do not share the same pattern of expression in the cachexia models, data indicate an increased autophagic degradation in cachectic mice. However no significant differences could be detected in autophagic genes upon TP53INP2 manipulation. Interestingly, the induction of *LAMP2A*, a chaperone-mediated autophagy marker was reduced in transgenic mice, which might be an adaptive mechanism to buffer autophagic activity.

Muscle wasting in cancer cachexia was considered to depend mainly on hyperactivation of proteasomal degradation (Acharyya & Guttridge, 2007; Attaix *et al*, 2008; Khal *et al*, 2005; Zhang *et al*, 2011). In our study the ubiquitin ligases *MuRF1* and *Atrogin-1* expression levels were measured and both of them were increased in tumor bearing animals. In addition, we observed that *MuRF1* is upregulated in TP53INP2 SKM-Tg mice upon C26 implantation. This is consistent with previous data in which we showed that muscle atrophy is increased in transgenic animals.

A previous report has demonstrated that global energy expenditure is enhanced in cancer cachexia (Petruzzelli *et al*, 2014). They have observed that white adipose tissue (WAT) browning contributes to the increased energy expenditure and is associated with activation of a thermogenic program in adipocytes characterized by increased mitochondrial content and uncoupling activity. However, whether muscle participates in this process is unknown and studies performed in C2C12 myotubes indicate a reduced mitocondrial respiration in response to incubation with Lewis lung carcinoma conditioned medium (McLean *et al*, 2014). Furthermore, mitochondrial dysfunction has been

reported in several models of cancer cachexia; but conflicting data regarding the nature of alterations to the mitochondrial electron transport chain have been described (Aria Tzika *et al*, 2013; Busquets *et al*, 2005; Constantinou *et al*, 2011; Julienne *et al*, 2012; Khamoui & Kim, 2012). In our study, we have confirmed that cancer cachexia reduced mitochondrial oxygen consumption in isolated muscle fibers from C26 tumor bearing mice independently of TP53INP2 manipulation.

Our data also suggest for the first time that TP53INP2 is involved in the alteration of mitochondrial dynamics upon C26 tumor implantation, because Mfn2, Opa1 and Drp1 expression was reduced in cachectic mice overexpressing TP53INP2.

As it has been mentioned before, the levels of TP53INP2 are regulated in catabolic states such as in cachectic mice and patients and also in diabetic, obese mice (Baumgartner *et al*, 2007; Sala *et al*, 2014) and in type 2 diabetes (Sala *et al*, 2014). Surprisingly, regarding the regulation of TP53INP2 expression in cancer cachexia, when testing the mRNA and protein levels of TP53INP2, we observed that the endogenous levels and also the expression of the transgen were dramatically reduced not only in WT animals after 14 days of C26 growth, but also, in transgenic mice. This suggests that C26 implantation has an effect on the muscle promoter MLC1. The MLC1 or Myosin Light Chain 1 is a muscle promoter. Besides, in these conditions of cancer cachexia, muscle wasting is often triggered by a decrease in protein synthesis and an increase in protein degradation (Attaix *et al*, 2008; Aversa *et al*, 2016; Bossola *et al*, 2001; Eley *et al*, 2008; Khal *et al*, 2005; Penna *et al*, 2013; Smith & Tisdale, 1993). Thus, this promoter could not be active anymore in this catabolic condition or it might be a decrease in the levels of all muscle mRNA genes. To confirm this hypothesis, it would be interesting to perform a time course analysis of MLC1 expression in C26-bearing mice in order to understand when the expression of the transgene is suppressed.

To further confirm whether TP53INP2 expression was downregulated in early stages of the development of cancer cachexia induced by C26, we plan to measure TP53INP2 mRNA and protein levels in mice which were killed after tumor growth for 10 days. Interestingly, our preliminary assay (data not shown) confirms that TP53INP2 protein is not lowered behind physiologic levels after 10 days of tumor growth. Overall, our results

confirm the hypothesis that TP53INP2 is triggering its effect in muscle wasting since early stages of the development of cancer cachexia.

As a conclusion, the knowledge of the molecular mechanisms underlying cancer cachexia may allow for therapeutic approaches that ameliorate or even successfully cure the syndrome.

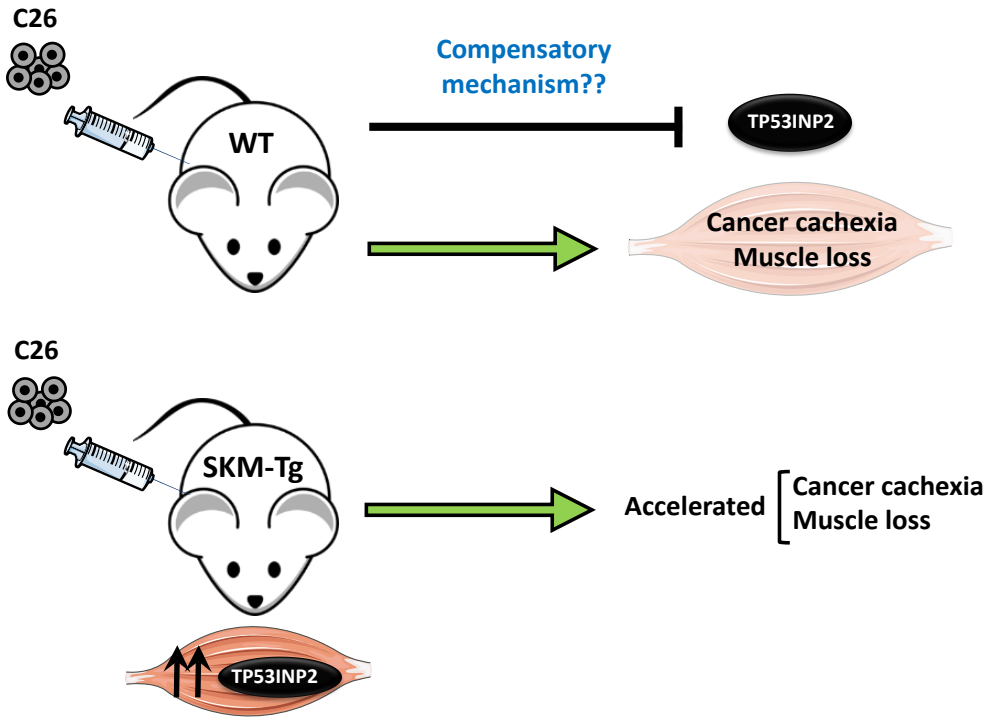

Figure 63. Schematic model of the effects of TP53INP2 on cancer cachexia.

CHAPTER 6 CONCLUSIONS

6. CONCLUSIONS

I. TP53INP2 negatively regulates the Ubiquitin Proteasome System in mouse skeletal muscle. Muscle-specific TP53INP2 ablation increases proteasome activity and the expression of proteasome subunits PSMD11, PSMD4 and PSMA1-7.

II. TP53INP2 loss-of-function upregulates both the immunoproteasome and the proteasome activity, and increases the generation of K48 polyubiquitilated proteins as well as the expression of proteasome subunits PSMD11 and PSMA1-7 in muscle cells.

III. Proteasome subunits PSMD11 and PSMA1-7 are degraded through the Ubiquitin Proteasome system in muscle cells. TP53INP2 deficiency enhances the stability of these subunits by reducing its proteasomal degradation without altering gene expression.

IV. TP53INP2 gain-of-function reduces the expression of PSMD11 protein in muscle cells. This effect requires the cycling of TP53INP2 from the nucleus to the cytosol; indeed, a mutant form of TP53INP2 lacking the nuclear export signal, and retained in the nucleus has no capacity to repress PSMD11.

V. TP53INP2 gene expression is reduced in skeletal muscle from patients with cancer cachexia and in tumor-bearing cachectic mice. TP53INP2 gain-of-function exacerbates muscle loss in parallel with increased atrogenes expression in C26 tumors-bearing cachectic mice. These data strongly support the concept that TP53INP2 negatively regulates skeletal muscle mass. Furthermore, we propose that TP53INP2 repression is part of an adaptive mechanism aimed at preserving muscle mass under cancer cachexia conditions.

Chapter 7

MATERIALS AND METHODS

7. MATERIALS AND METHODS

7.1. Material

The following material was used during this PhD thesis. In the tables below, it is listed the useful information concerning: a) reagents used in cell culture experiments (Table 2); b) the plasmids used for transient transfections (Table 3); c) the plasmids used for adenoviral and lentiviral infections (Table 4); d) Sybr Green primers and Taqman probes used in the real time PCR (Table 5); and e) the primary antibodies (Table 6) for western blot and immunofluorescence.

Table 2. Reagents used in this thesis.

Reagents						
Name	**Solubility**	**Stock**	**Conditions of use**	**Application**	**Storage**	**Source**
3MA	Water	200 mM	10 mM	Class III-PI3K inhibitor. Inhibits initial steps of autophagy	20°C	Sigma M9281
Bafilomycin A1	Ethanol	1 mM	200 nM (6h, 16h)	Inhibitor of vacuolar type H+-ATPase (V-ATPase) blocking fusion between autophagosomes and lysosomes	20°C	Sigma A9415
Cloroquine	Water	100 mM	10 µM	Inhibitor of fusion between autophagosomes and lysosomes	4°C	Sigma C6628
Cyclohexi-mide	DMSO	100 mg/ml	50 µg/µl (1-3-5-7h)	Inhibitor of protein tras-lation	4°C	Sigma C4859
MG132	DMSO or Ethanol	15 mM	10 µM	Reversible Proteasome Inhibitor	20°C	Calbiochem 474790
Puromycin	Water	10 mg/ml	1 µM	Inhibitor of Protein synthe-sis. Inhibits translation by causing premature release of nascent polypeptide chains	20°C	sc-108071b
Insulin	Water	1 mM	100 nM	Activates protein synthesis by activating components of the translational machi-nery including eIFs and eEFs	20°C	Sigma 91077C

Table 3. Plasmids for transient transfections used in this thesis.

Plasmids for transient transfections				
Name	**Vector**	**Insert**	**Resistence**	**Source**
mDOR	pcDNA3	mDOR	Ampicillin	Berchard Baumgarter
NES mutant	pcDNA3	mDOR L36A/ I38A/L40A	Ampicillin	Meritxell Orpinell
GFP	pEGFP	eGFP	Ampicillin	Clonetech
Myc-MuRF1	pCMV-Tag3b-M1	pCMV	Neomycin/ Kanamycin	Gift from Monte S Willis
FLAG-DOR	pcDNA3	FLAG-DOR	Ampicillin	Saska Ivanova
pcDNA3.1	pcDNA3.1	None	Ampicillin	Invitrogen V790-20

Table 4. Plasmids for adenoviral and lentiviral infections used in this thesis.

ADENOVIRAL PLASMIDS					
Name	**Vector**	**Insert**	**Selection**	**Source**	**Function**
pDONR 221	pDONR 221	None	Kanamycin	Invitrogen 12536-017	Entry Vector for Gateway technologies
pAdeno/ CMV/V5-dest	pAdeno/CMV/ V5-dest	None	Ampicillin	Invitrogen V493-20	Destination vector for Gateway technologies
pAd-FLAG-mDOR	pAdeno/CMV/ V5-dest	FLAG-mDOR	Ampicillin	Ana Sancho	Gateway cloning

LENTIVIRAL PLASMIDS					
Name	**Vector**	**Insert**	**Selection**	**Source**	**Function**
pMD2.G	pMD2.G	VSV-G	Ampicillin	gift from D.Trono	Helper vector for lentivirus (envelope)
pCMV-dR8.74	pCMV	gag,pol, tat,rev	Ampicillin	gift from D.Trono	Helper vector for lentivirus (packaging)
pLVTHM	pLVTHM	None	Ampicillin	gift from D.Trono	Transfer vector
pLVTHM scr RNA	pLVTHM	scr DOR	Ampicillin	Vicent Ribas	
pLVTHM si RNA	pLVTHM	si DOR	Ampicillin	Vicen Ribas	

Table 5. Sybre Green primers and Taqman probes used for RT-PCR in this thesis. Continue to next page.

Sybr Green primers			
Symbol	**Name**	**Forward**	**Reverse**
ARP	Acidic Ribosomal protein, large, PD	AAGCGCGTCCTGGCATTGTCT	CCGCAGGGGCAGCAGTGGT
Atrogin 1	Atrogin 1	GCAAACACTGCCACATTCTCTC	CTTGAGGGGAAAGTGAGACG
Beclin 1	Beclin 1, autophagy related	TCGATTTTGTCTTCCGTACAGGA	GCATGAACTTGAGCGCTTTTG
β-actin	Beta-actin	GGTCATCACTATTGGCAACGA	GTCAGCAATGCCTGG
Bnip3	BCL2/adenovirus E1B 19 kd-interactin protein 3	CACCTTTATCACTCTGCTGAATTCTCT	GATTTTGTTTTTCATTTCCAGTCTTTTAA
Bnip3L	BCL2/adenovirus E1B 19 kd-interactin protein 3-like	AGTTTTGCCATTTTTGAAAGTATTAGTAAA	GTTTCACCCAACAAGAATCTGTGTA
Cathepsin L	Cathepsin L	GCAGCAAGAACCTCGACCAT	GTTGTCCCGGTCTTTGGCTA
DOR	Diabetes and Obesity Regulated gene (endogenous)	AACCACAGCCTGCTTCTAATACCTT	TCAGCCAGTCTCAACACAAAACAC
DORORF	Diabetes and Obesity Regulated gene (endogenous + transgene)	GCCCTCCTTGATGGATGAGA	ACATGCTGGGATGCTCAATG
DRP-1	Dynamin Related protein 1	AGCCAATCCATCTCAAGGTTTTCTC	ATCGCCTACAGGTACTTTGGTCATTC
GABARAPL1	Gamma-amnobutyric acid receptor-associated protein like 1	CACCATCCCTCCCACCAGT	GGCTTCTGCCTCATTTTCCAT
GAPDH	Glyceraldehyde-3-Phophate Dehydrogenase	CATGGCCTTCCGTGTTCCTA	GCGGCACGTCAGATCCA
LAMP2A	Lysosome-associated membrane glycoprotein 2 alpha	CACATATGCAATGTTTTAAGGTCTGTC	TCAAGCAGTGTTTATTAATTCCAGTAAGAT
LC3B	Microtubule-associated proteins 1A/1B light chain beta	AGCTCTTTGTTGG TGTGTAACTGTCT	TTGTCCTCACAGCTGACATGTATG
MFN2	Mitofusin 2	AGAACTGGACCCGGTTACCA	CACTTCGCTGATACCCCTGA
MURF1	Muscle RING-finger protein 1	CATTGTGTGACTGGCGATTGT	TCTCTAGGCCACCGAGTGAGA
NBR1	Neighbor of BRCA1 gene protein 1	CCCCAGATTGGTTTACAAGC	TCCACCGTTTCCTTAACCAC

Table 5. (Continued).

Sybr Green primers			
Symbol	**Name**	**Forward**	**Reverse**
PGC-1α	Peroxisome Proliferative activated receptor, gamma, coactivator1 alpha	GAAAGGGCCAAACAGAGAGA	GTAAATCACACGGCGCTCTT
PSMA1	Proteasome Subunit Alpha 1	GCCTGTGTCTCGTCTTGTATCTCTAA	TCCGGCCATATCGTTGTGTT
PSMA2	Proteasome Subunit Alpha 2	TGAATATGCTTTGGCTGCTGTAG	CCACACCATTTGCAGCTTTAATT
PSMA3	Proteasome Subunit Alpha 3	GAATGACGGTGCGCAACTCT	CAGCCCCAATAACCGTATGAA
PSMA5	Proteasome Subunit Alpha 5	CCAGAGTGGAGACACAGAACCA	GGGTCACACTCTCCACTGTCATT
PSMA6	Proteasome Subunit Alpha 6	CCCGAGGGTCGGCTCTA	GATGTAAGGCCACCCTGGTTAA
PSMA7	Proteasome Subunit Alpha 7	GCCAGTCTGAAGCAGCGTTAT	TGAGGGCAGAGATGCCAAAC
PSMD4	Proteasome 26S Subunit, Non-ATPase 4	AGAGCACTATGGTTTGTGTGG	GTGGGAAGGAAGTCTCCGT
p62/SQSTM1	62 Kda/Sequestosome 1	CCCAGTGTCTTGGCATTCTT	AGGGAAAGCAGAGGAAGCTC
TBP	TATA box Binding Ptotein	TGCACAGGAGCCAAGAGTGAA	CACATCACAGCTCCCCACCA
Taqman probes			
TAQMAN	**Name**	**ID Number**	
PSMD11	Proteasome 26S Subunit, Non ATPase 11	Mm00780758_sH	
OPA1	Optic atrophy gene 1	Mm00453879_m1	

Table 6. Primary Antibodies used in this thesis. MW: molecular weight, kDa: kiloDalton, Cat. Num: catalogue number, WB: western blot, IF: immunofluorescence; IP: immunoprecipitation.

Primary Antibodies							
Antibody	**Host**	**Isotype**	**Dilution**	**MW (Da)**	**Supplier**	**Cat. Num**	**Applications**
β-actin	Mouse	IgG1	1/10000	42	Sigma Aldrich	A1978	WB
ATF4	Rabbit		1/1000	42	Aviva System Biology	ARP37017_P0S0	WB
Atrogin-1	Rabbit	IgG	1/1000	42	Abcam	ab168372	WB
DOR/TP53INP2	Mouse	IgG2a	WB: 1/50, 1/500. IF: 1/150	38	Generated in the Lab	DOR 3.15	WB/IF
4E-BP1	Rabbit		1/1000	15-20	Cell Signalling	9452	WB
eIF2a	Rabbit		1/1000	38	Cell Signalling	9772	WB
GADD34	Rabbit	IgG	1/1000	73	Santa Cruz	sc-8327	WB
LC3	Rabbit	IgG	1/1000	18/16	MBL	PM036	WB
Murf1	Rabbit	IgG	1/1000	41	abcam	ab77577	WB
Proteasome 20S α	Mouse	IgG1	1/1000	28	abcam	ab22674	WB
Proteasome PSMD4	Rabbit	IgG	1/1000	55	Thermo Scientific	PAS-30136	WB/IP
Proteasome PSMD11	Mouse	IgG1 k	1/1000	47,5	Novus Biologicals	NBP1-30252	WB
p-4EBP1 (Ser65)	Rabbit		1/1000	15-20	Cell Signalling	9451	WB
p-eIF2 α (Ser51)	Rabbit	IgG	1/1000	38	Cell Signalling	3597	WB
p-S6 (Ser 235/236)	Rabbir		1/1000	32	Cell Signalling	2211	WB
p-S6K (Thr389)	Rabbit	IgG	1/1000	70-85	Cell Signalling	9234	WB
pUb (FK2)	Mouse	IgG1	1/1000	Smear	ENZO Life Sciences	BML-PW8810	WB
pUb K48	Rabbit		1/1000	Smear	Cell Signalling	4289	WB
Puromycin	Mouse	IgG2ak	1/1000	Smear	Millipore	MABE343	WB
S6	Mouse	IgG2b	1/1000	32	Santa Cruz	sc-74459	WB
S6k	Rabbit		1/1000	70/85	Cell Signalling	9202	WB
α-tubulin	Mouse	IgG1	1/10000	50	Sigma Aldrich	T5168	WB

7.2. Methods

7.2.1. Cell culture protocols

7.2.1.1. *Cell culture*

During this thesis, C2C12 muscle cells have been used as the cellular model, furthermore, for adenoviral and lentiviral infections as far as for immunoprecipitation assays (described below) HEK 293A and HEK 293T cells have been also used.

Cells were cultured at 37°C and 5% of CO2 in DMEM (*Dulbecco Modified Eagle´s Medium*, Gibco) supplemented with 10% of fetal bovine serum (FBS, Gibco), 100 U/ml of penicillin/streptomycin (Gibco) and 25 mM Hepes pH 7.3 (Panreac) in an humidified incubator. Different treatments have been utilized in cell cultures as specified in Table 2.

7.2.1.2. *Transient transfections*

For transient transfection assays, cells were plated onto a 100-mm cell plate and transfected with 5 μg of DNA plasmids using polyethylenimine (PEI) solution. The DNA:PEI polyplexes were prepared in 5% of the initial culture volume with a total of 1 μg DNA/ml of culture to be transfected. An equal volume of diluted PEI was added to the DNA. The mixture was inverting and incubated for 20 minutes at room temperature before its addition to cell culture. After 18 hours of incubation at 37°C in 5% CO_2, the medium was removed and fresh DMEM was added to the cells. Transfection efficiency was determined by analysis of GFP expression in transfected cells with GFP constructs as a control.

In this thesis, we have used the full-length TP53INP2 cDNA, which was PCR-amplified and cloned in pcDNA3 vectors as previously described (mDOR) (Baumgartner *et al*, 2007) and the TP53INP2mut plasmid (NES mutant form), generated by mutagenesis (L36A, I37A, I38A and L40A) (*QuickChange Site-Directed Mutagenesis Kit*, Stratagene); also, we have used Myc-MuRF1 (Li *et al*, 2011) and FLAG-TP53INP2 (FLAG-DOR, generated in the laboratory) plasmids. As a positive control of transfection a GFP vector was used, while an empty pcDNA3 plasmid was used as a negative control (Table 3).

7.2.1.3. *Adenoviral infection*

Adenoviral infection was used in experiments of TP53INP2 overexpression in C2C12 cells. 80% confluent myoblasts were transduced for 30 hours at a multiplicity of infection (moi) of 50 pfu/cell. Cells were infected with adenoviruses coding for TP53INP2 or LacZ (used as control). Adenoviruses were generated by transfection of the adenoviral expression vectors (Virapower System, Invitrogen) in human embryonic kidney cell line (HEK 293A) (Table 4). The adenoviruses generated were then amplified in HEK 293A cells, titrated using the Adeno-XTM Rapid Titer kit (Clontech) and used directly for cell transduction to the cells of interest (in our case C2C12 cells).

7.2.1.4. *Lentiviral infection and siRNA generation*

The generation of C2C12 cells stably expressing siRNA against TP53INP2 or scrRNA (used as control) by lentiviral transduction, was based in the protocol previously described (Baumgartner *et al*, 2007).

TP53INP2 siRNA was obtained from sFold software (http://sfold.wadsworth.org). The sequence for TP53INP2 siRNA is GTGGATGGCTGGCTCATCA. Scrambled siRNA was obtained by scrambling a functional TP53INP2 siRNA sequence. All HIV-1 derived lentiviral constructs (pLVTHM transfer vector, pCMVdR8.74 helper packaging construct and pMD2G vector encoding for envelope protein) (Table 4) were kindly provided by Dr. Didier Trono from the Ecole Polytechnique Federale de Lausanne (Switzerland) and used as reported (Wiznerowicz & Trono, 2003).

The pLVTHM vector contains a GFP expression cassette and two restriction sites (ClaI and MluI) after the H1 promoter, thereby allowing direct siRNA cloning. Lentiviruses encoding scrambled and TP53INP2 siRNA were produced by triple transient transfection of HEK 293T cells using the PEI solution.

Lentiviral viruses were produced by transfecting subconfluent HEK 293T cells with 10 μg of pLVTHM encoding scrambled or TP53INP2 siRNA, 7 μg of pCMVdR8.74 and 3 μg of pMD2G. Culture medium containing lentiviruses was collected 48h and 72h after transfection and filtered using a 0.44 μm filter. Lentiviruses were concentrated by

ultracentrifugation (26,000 rpm, 1 hour 30 min at 4°C, using a 4 ml sucrose 20% solution) and resuspended in 100 ml fresh medium. We stored lentiviral aliquots at -80°C.

Titration was performed transducing 105 HEK 293T cells grown in 12-well plates with 1, 10 or 100 ml of a 1/100 dilution of the concentrated lentiviruses. After 48 h, the percentage of transduced HEK 293T cells (% GFP positive cells) were selected with puromycin (2 μg/ml) or sorted for GFP positive cells using an EPIC hour S XL flow cytometer (Beckman Coulter H).

Fifteen million C2C12 myoblasts grown on 12-well plates were transduced at moi 100 and cells were amplified during 5–7 days. Transduced cells (GFP-positive) were then sorted with a MoFloH flow cytometer (DakoCytomationH, Summit v 3.1 software), obtaining between 93%–99% GFP-positive cells.

7.2.2. General molecular biology protocols

7.2.2.1. *Transformation of competent cells*

The *E.Coli* DH5α, XL-Blue or TOP10 competent cells (50 μl) were transformed with 5 μl of the desired plasmid by the heat shock protocol. Competent cells were routinely generated by the technical lab assistance.

The heat shock protocol consists in incubation of the DNA and the competent cells on ice for 15 minutes, a heat shock step at 42°C for 45 seconds and 5 minutes incubation on ice.

Subsequently, 1 ml of Luria-Bertani (LB) medium is added and transformed cells are shacked (600 rpm) at 37°C for 45 minutes. Cells are spinned down for 4 minutes at 8,000 rpm and 900 μL of the supernatant is discarded. 100 μl of the resuspended cells are plated on LB plates with Ampicilin (Cf= 100 μg/ml) or Kanamicin (Cf= 30 μg/ml) (for selection of positive clones) and incubated at 37°C overnight. A single colony is picked the next day and incubated for 8 hours with agitation in 3 ml of LB medium with the adequate antibiotic selection.

7.2.2.2. *Plasmid DNA purification*

To purify plasmids from bacterial cultures, different commercial kits are commonly used. These systems of purification are based on bacterial alkali lyses and several purification ranges are available, depending on the quality and quantity of DNA required. For both mini- and maxi-scale DNA preparation, Qiagen kits were used (*Plasmid Mini Kit* and *Plasmid Maxi Kit*, respectively). The procedure is indicated in the relevant manual of each kit.

7.2.3. Manipulation and detection of nucleic acids protocols

7.2.3.1. *Gene expression analysis*

Following the supplier's instruction, RNA from tissues and cell culture was extracted using a protocol combining TRIzol reagent (Invitrogen) and *RNAeasy® minikit* columns (Qiagen), including DNAse I digestion to avoid potential contaminations of DNA. 1 μg of RNA was reverse-transcribed into cDNA with the *SuperScript RTIII kit* (Invitrogen). The expression of target genes of interest was quantified by quantitative real-time PCR (RT-PCR) and was performed using the ABI Prism 7900 HT real-time PCR machine (Applied Biosystems) and the SYBR® Green PCR Master Mix or the Taqman Probes 20X (Applied Biosystems). Primers used for amplification are listed in Table 5. All measurements were normalized to the expression of housekeeping genes ARP, β- actin and GAPDH.

7.2.4. Manipulation and detection of protein protocols

7.2.4.1. *Protein Extraction*

On the one hand, protein whole cell extracts were obtained by lysis of harvested cells with radio-immunoprecipitation assay (RIPA) buffer composed by 150 mM NaCl, 10 mM Tris HCl, pH 7.2, 0.1% w/v SDS, 1% w/v Triton X-100, 1% w/v deoxycholate, 5 mM EDTA, 1 mM NaVO4, 5 mM NaF, 1 mM PMSF and protease inhibitor mixture (Roche). Protein lysates were passed through 25 gauge needle attached on a 1 ml syringe and centrifuged at 10,000xg for 15 min at 4°C.

On the other hand, tissue samples were homogenized in 10 volumes of RIPA buffer using an ultraturex. Homogenates were rotated for 1 hour at 4°C in an orbital shaker and centrifuged at 10,000x*g* for 15 min at 4°C.

Finally, protein extracts were quantified using the bicinchoninic acid (BCA) method (Thermo Scientific Pierce) with bovine serum albumin (BSA) as standard.

7.2.4.2. *Immunoblot*

40 µg of protein extracts were mixed with 4X Loading Sample Buffer (LSB) and DTT 100 mM, heated for 5 minutes and resolved on SDS-PAGE gels of different acrylamide percentage depending on the molecular weight of the working protein, at 90V and 110V in 1X Running Buffer (25 mM Tris-base, 200 mM glycine, 0.1% w/v SDS). Proteins were then transferred onto PVDF Transfer Membranes (Millipore) at 350 mA for 1 hour 30 minutes on ice in 1X Transfer Buffer (25 mM Tris-HCl pH 8.3, 200 mM glycine and 20% v/v methanol). In some cases, protein transfer is checked by staining with Ponceau S (Sigma). Transferred membranes were blocked for 1 hour at room temperature in 3% w/v skimmed milk in TBS-T (10 mM Tris-HCl pH 7.5, 100 mM NaCl and 0.1% Tween-20). Then, the membrane is incubated overnight at 4°C with the corresponding primary antibody diluted in 3% skimmed milk or BSA in TBS-T (see Table 6 for antibody dilutions in Western Blot). After three washes of 5 minutes with TBS-T, membranes were incubated for 1 hour at room temperature with the corresponding secondary antibody conjugated to horseradish peroxidase (1/10000) diluted in TBS-T: goat anti mouse, goat anti-rabbit IgG-HRP (Santa Cruz) and donley anti-goat IgG-HRP (Jackson). After three washes of 10 minutes with TBS-T, protein detection is performed by enhanced chemiluminiscence with Pierce ECL Western Blotting Substrate (Thermo Scientific).

7.2.4.2.1. *Immunoblot analysis for catalitic subunits β5 and β5i*

To detect the protein expression of the catalytic subunits of the proteasome and immunoproteasome, it is followed the protocol described before (Grimm *et al*, 2012). 2×10^6 control (scr C2C12) or knock down cells (si C2C12) were harvested, lysed and the protein concentration was measured as described above. Protein extract (20–50 µg) was

subjected, in Laemmli buffer, to SDS/PAGE (12% gel) and the separated proteins were transferred on to nitrocellulose transfer membranes (Whatmann). Blots were blocked in 5% non-fat milk/PBS buffer at room temperature (22°C) for 1 hour. Before detection of phosphorylated proteins, the blots were blocked in Odyssey® blocking buffer (LI-COR Biosciences) at 4°C overnight. Blocking was followed by incubation with primary antibodies that were diluted according to the recommendations of the manufacturers under constant agitation for another hour. The following primary antibodies were used: anti-β5 (PSMB5) (Abnova), anti-β5i (proteasome 20S LMP7) (Abcam), and anti-GAPDH (glyceraldehyde-3-phosphate dehydrogenase) (Abcam). After being washed three times, the blots were incubated with the appropriate secondary antibody: goat anti-rabbit (IRDye® 800CW conjugated) or donkey anti-mouse (IRDye® 680LT conjugated) (LI-COR Biosciences) for 1 hour. Blots were washed and analysed for their near-infrared fluorescence signals with the Odyssey® infrared imaging system (LI-COR Biosciences).

7.2.4.3. *Immunoprecipitation assays*

In co-immunoprecipitation assays, HEK 293T cells were plated onto a 100-mm cell plate and transfected using 5 μg of the plasmids MuRF1-Myc and Flag-TP53INP2 per plate in a ratio of 4.5 μg polyethylenimine (PEI) (Polyscience) per 1 μg DNA. The mix with DNA and PEI was added to cell plates at a 70% of confluence and after 16 hours media was removed and changed for new medium. Experiments were performed after 24 hours.

For Flag immunoprecipitation assays, cell lysates were prepared in ice-cold lysis buffer (50 mM Tris HCl pH 7.4 with 150 mM NaCl, 1 mM EDTA, 0.5% NP-40, 50 mM NaF, 5 mM $Na_4P_2O_7$ and 2 mM Na3VO4) supplemented with Complete protease inhibitors (Roche), rotated for 1 hour at 4°C and centrifuged at 13000 rpm for 15 min at 4°C. Protein concentration was determined using Pierce BCA protein assay kit (Thermo scientific) and 2 mg of protein extracts were used. Flag-TP53INP2 protein was immunoprecipitated by using the FLAG Tagged Protein Immunoprecipitaton Kit (Sigma) following the manufacturer's instructions (Figure 64). MuRF1-Myc was detected by α-myc antibody.

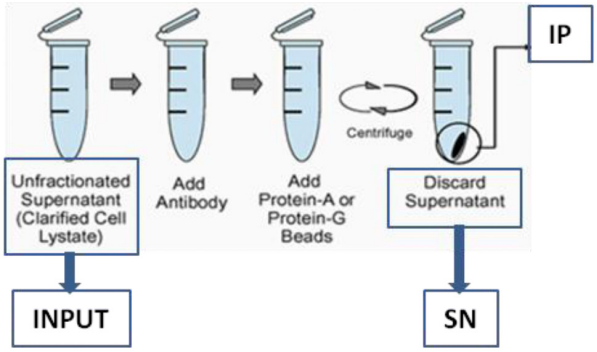

Figure 64. Scheme of the steps of the immunoprecipitation process and the different collected fractions. SN: supernatant fraction, IP: immunoprecipitated fraction.

7.2.4.4. *Immunofluorescence*

C2C12 cells grown in sterile cover slips were fixed in 4% paraformaldehyde (PFA) for 15 minutes at room temperature. After two washes in PBS for 10 minutes, cells were incubated in NH4Cl (50 mM) and glycine (20 mM) to reduce the autofluorescence and permeabilized with a solution of 0.1% Triton x- 100 in PBS during 10 minutes at room temperature. After two washes in PBS for 10 minutes and blocking during 30 minutes in Blocking solution (PBS- 10% FBS), slides were incubated with the corresponding primary antibodies diluted in blocking solution during 1 hour.

After three washes in PBS for 10 minutes, samples were further incubated with the corresponding secondary antibodies for 1 hour, followed again by three, 10 minutes washes in PBS. DAPI (1/2000; Sigma) was used to label DNA. Finally, cells were covered using Fluoromount-G (Electron Microscopy Sciences) and let to dry overnight (O/N) before being stored at 4°C. Leica TCS SP2 AOBS Systems confocal scanning microscope was used to analyze the immunofluorescence.The following primary antibody was used: monoclonal TP53INP2/DOR (1/150 dilution, generated in our laboratory). The following secondary antibody was used: goat anti-mouse conjugated with Alexa-Fluor 568 (1/250 dilution, Invitrogen).

7.2.5. Proteasome protocols

7.2.5.1. *Proteasome inhibition*

C2C12 cells were grown overnight until reach 80% confluency. The proteasome inhibitor MG132 (Sigma) was solubilized in DMSO (Table 2) and added to final concentration

of 10 μM at indicated time points. Protein levels were analyzed by immunoblotting with specific antibodies.

7.2.5.2. *Measurement of proteasome activity*

7.2.5.2.1. *C2C12 cells*

For measuring the proteasome activity in C2C12 myoblasts, it was carried out the 26S proteasome fluorogenic peptidase assays (Figure 65). The in vitro assay of 26S proteasome activities was performed as previously described (Kisselev & Goldberg, 2005). Cells were collected in proteasome activity assay buffer (50 mM Tris-HCl, pH 7.5, 250 mM sucrose, 5 mM $MgCl_2$, 0.5 mM EDTA, 2 mM ATP and 1 mM DTT) and lysed by passing ten times through a 27-gauge needle. ATP has to be added to the buffer to prevent dissociation of the 26S proteasome into its components, to ensure that it has maximal activity, and that indeed 26S but not 20S activity is measured.

Lysate was centrifuged at 10,000x*g* for 10 min at 4°C. 15-25 μg of total protein of cell lysates (in a maximum volume of 40 μl) were transferred to a 96-well microtiter plate (BDFalcon) and incubated with 100 μl of the assay buffer with fluorogenic substrate for chymotrypsin-like activity (Suc-LLVY-AMC). Fluorescence (380 nm excitation, 460 nm emission) was monitored on a microplate fluorometer (Infinite M1000, Tecan) every 5 minutes for 1 hour at 37°C.

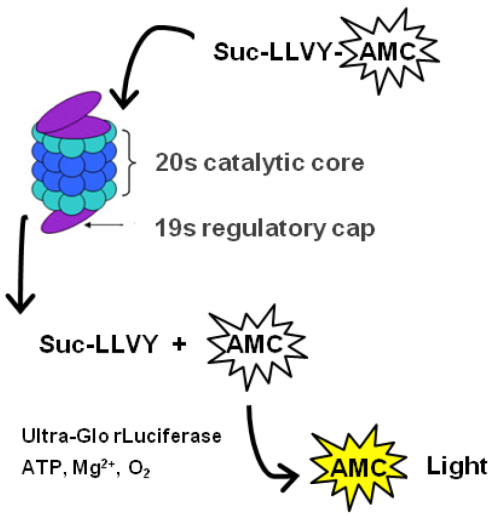

Figure 65. Basis of the bioluminescent proteasome activity assay. Proteasome substrate Suc-LLVY interacts with the β5 subunit releasing aminoluciferin, which is used by luciferase to generate light. The amount of light generated is directly proportional to the activity of the proteasomal subunits.

7.2.5.2.2. *Skeletal muscle*

For the setup of the proteasome activity assay in skeletal muscle tissue, a commercially available indirect enzyme-based luminescent assay was modified (Promega, cat. num. G8621 with substrate for chymotrypsin-like activity [Suc- LLVY-aminoluciferin]). This assay kit is designed and established to measure the proteasomal activity in purified proteasome using a luminogenic substrate. Thus, the original purpose of this commercially available assay is to detect the effect of test compounds on purified proteasome. In contrast, we modified the assay setup to enable the measurement of the proteasomal activity using soluble total protein extracts from skeletal muscle tissue as described below.

Proteasome activity in total homogenates from EDL muscles were measured as reported (Strucksberg *et al*, 2010). Briefly, 100 µl of ice-cold PBS containing 5 mM EDTA (PBSE) was added to 1 mg of skeletal muscle tissue and sonicated on ice for 20 seconds with a pulse length of 1 second two times using a pulsed homogenizer. Tissue lysates were centrifuged at 13,000x*g* for 5 minutes at 4°C, and supernatants were subjected to protein quantification employing the bicinchoninic acid (BCA) method with bovine serum albumin as standard. Protein extraction buffer PBSE was used as blank.

The supernatants (soluble protein extracts) prepared from skeletal muscle tissue as described above, were diluted to a concentration of 0.2 mg/ml total protein with ice-cold PBSE. Then, 50 µl corresponding to 10 µg of total protein were added to 50 µl of the luminescent reagent containing the Ultra-Glo Luciferase and the signal peptide for chymotrypsin-like activity coupled to luciferin (Promega). After mixing of the components and preincubation for 60 minutes in a black 96-well plate at room temperature, the resulting luminescence was measured every 5 minutes for 1 hour using the Infinite M1000 (Tecan) reader in luminometry mode at 37°C. As a negative control, the supernatants were incubated previously with the proteasome inhibitor MG132 10 µM for 1 hour.

7.2.5.3. *Measurement of immunoproteasomal activity*

On the one hand, for the determination of the immunoproteasomal activity and the preparation of cell lysates for immunoblotting, 2×10^6 cells were harvested, centrifuged for 5 minutes at 1900 rpm at 4°C and the cell pellet was resuspended in lysis buffer

(250 mM sucrose, 25 mM Hepes, 10 mM magnesium chloride, 1 mM EDTA and 1.7 mM DTT). Cells were lysed using a syringe, followed by repeated freeze–thaw cycles.

On the other hand, muscle homogenates were prepared from EDL muscles. Briefly, EDL muscles were homogenized in 500 µl of the same lysis buffer with ultraturex until no tissue pieces are visible and followed by centrifugation at 12,000 rpm, 4°C for 20 minutes. The supernatant was collected.

In both cases, cell lysates and the homogenates were used for the measurement of the immunoproteasome activity assay and western blots for proteasome subunits. Protein concentrations of cell lysates and homogenates were determined using BCA protein assay kit (Pierce) with bovine serum albumin as the standard.

The substrates for the immunoproteasome were chosen according to the bibliography (Blackburn *et al*, 2010). The substrates were obtained from AAT Bioquest to monitor the activity of the immunoproteasome (i): β1i, Ac-PAL-R110; and β5i, Ac-ANW-R110 (where R110 is rhodamine 110). R110 liberation was measured using the TECAN fluorescence reader at 485 nm excitation and 528 nm emission for 30 min at 37°C. Free R110 was used as a standard for quantification.

7.2.6. Protein turnover and synthesis protocols

7.2.6.1. *Cicloheximide assays*

To determine the stability of the proteasome subunits, their abundance was monitored by blocking protein translation with cicloheximide (Table 2) in scr *versus* siRNA C2C12 cells. Equal numbers of C2C12 cells were seeded into 6-well plates and allowed to attach for 18 hours. The cells were then treated with cycloheximide (20 µg/ml) and harvested at indicated time points. The cell lysates were prepared in LSB sample buffer directly, and an equal amount of lysates was analyzed by immunoblotting.

7.2.6.2. Measurement of protein turnover by radioactivity

In order to measure the proteasome subunits turnover with more accuracy, we used a radioactive method based in the protocol previously described (Bartoccioni *et al*, 2008; González-Muñoz *et al*, 2009; Liu *et al*, 2007) (Figure 66). C2C12 cells in a 60-mm dish

were washed twice with PBS and incubated in methionine-free DMEM for 30 min at 37°C (Figure 66, step 1), followed by pulse labeling in methionine-free DMEM containing 10% dialyzed fetal bovine serum and 100 µCi/dish of [35S]methionine (Perkin Elmer Life Science) (Figure 66, step 2) for different times depending on the experiment (1h, 5h or 12h). To begin with, the first trials were pulses of 1 and 5 hours, however the % of 35S incorporation per plate was from 1-6%; then, in a posterior trial of 12 hours of pulse, the incorporation was 18-20% of 35S. Afterwards, to study the synthesis, the cells were washed with PBS and incubated in complete DMEM supplemented with 10% fetal bovine serum and 100 µg/ml of L-methionine. For the chase experiments, cells were washed twice with PBS at the indicated times (0, 3 and 24 hours) (Figure 66, step 3), but pulse-chase experiments didn't function correctly, and we only have data from the synthesis experiments.

Next, the labeled cells were washed with ice-cold PBS and homogenized in 500 µl lysis buffer (150 mmol/l NaCl, 1.0% NP-40, 0.1% SDS, 1 mmol/l EDTA/Na, and 50 mmol/l TrisHCl, pH 8.0), followed by centrifugation at 10,000x*g* for 10 min at 4°C. 1 mg of the supernatant was precleared by incubation for 30 min at 4°C with 40 µl protein A-Sepharose beads (25% vol/vol) loaded with rabbit nonimmune serum. The beads were sedimented by centrifugation at maximum speed for 30 seconds. The supernatant was incubated for 12 hours at 4°C with an IP matrix prepared the day before composed by 40 µl protein A-Sepharose beads and 5 µg rabbit anti-PSMD4 or nonimmune serum. After incubation of the matrix and lysate, the beads were washed once with lysis buffer containing 0.5% NP-40, once with lysis buffer containing 1 mol/l NaCl, twice with lysis buffer containing 0.5% NP-40, and once with PBS (Figure 66, step 4). The proteins were eluted from the beads by incubation in LSB sample buffer for 5 min at 95°C and subjected to SDS-PAGE and autoradiography (Figure 66, step 5 and 6) using the BAS-1800 II bio-imaging analyzer (Fuji Photo Film). The % of [35S]methionine incorporation in this step was also measured and levels are around 1% for the pulse, but in the chase of 3 and 24 hours no signal was detected, for that reason, only preliminary pulse experiments were carried out.

The PSMD4 bands were identified by immunoblotting the lysate of unlabeled cells. The radioactivities of the PSMD4 bands were quantified with Image Gauge software (Fuji Photo Film). The radioactivity of immunoprecipitated PSMD4 was calculated by subtracting the radioactivity obtained with nonimmune serum.

Preliminar immunoprecipitation experiments were performed without radioactivity to control for the efficiency and specificity of the immunoprecipitating antibodies.

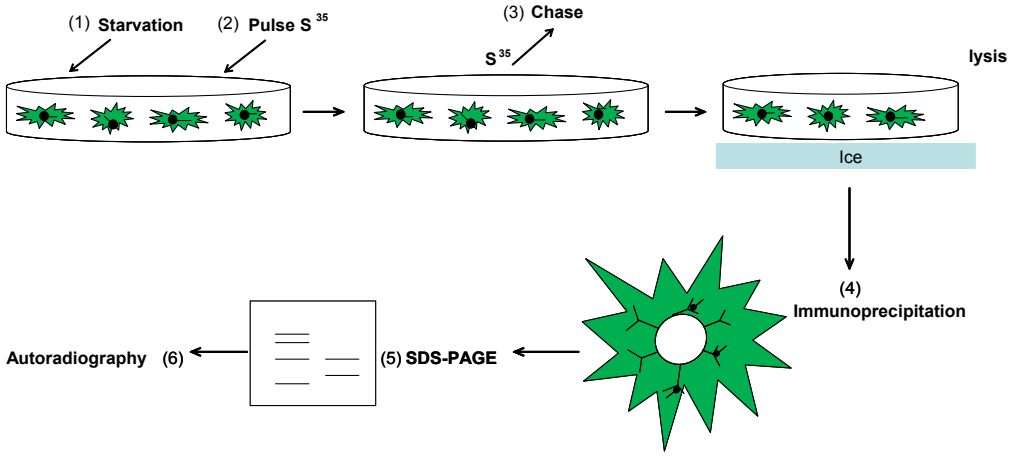

Figure 66. Scheme of the protocol for measuring protein turnover with [35S] methionine. Adapted from Paola Bartoccioni's thesis.

7.2.6.3. *SUnSET: non-radioactive method for measuring protein synthesis*

Protein synthesis rates commonly were measured using isotopic tracers to quantify the incorporation of a labeled amino acid into muscle proteins as explained before, however there are an alternative nonisotopic SUnSET technique which is a valid and accurate method for the measurement of in vivo changes in protein synthesis (Goodman & Hornberger, 2013; Goodman *et al*, 2011b) (Figure 67).

C2C12 myoblasts were cultured on a 6-well dish as described previously (Goodman & Hornberger, 2013; Goodman *et al*, 2011b). On confluence, cells were switched to serum-free DMEM for 16 hours. The medium was then replaced with fresh serum-free DMEM with or without 100 nM insulin (Sigma). After 60 minutes, 1 μM puromycin was added to all wells, and the cells were incubated for an additional 30 minutes. Cells

were then collected and subjected to WB analysis or RNA measurements as described previously.

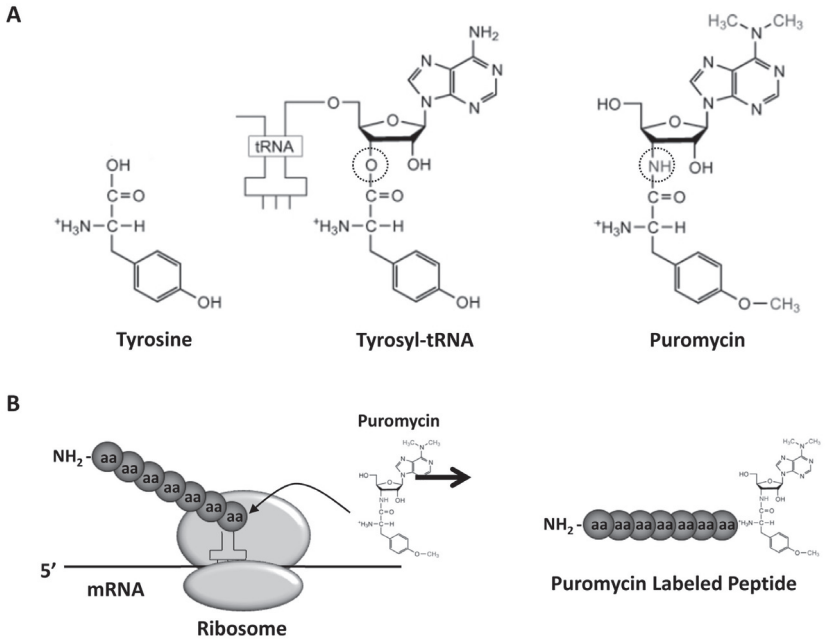

Figure 67. Puromycin structure and mechanism of action. (A) Comparison of the molecular structure of tyrosine, tyrosyl-tRNA and puromycin. The hydrolyzable ester bond in tyrosyl-tRNA and the non-hydrolyzable amide bond in puromycin are highlighted with a circle. (B) Puromycin's mechanism of action involves its incorporation into growing peptide chains via the formation of a peptide bound. Once bound, the puromycin-labelled peptide is unable to undergo further elongation and is released from the ribosome (Goodman & Hornberger, 2013).

7.2.7. Animal studies

7.2.7.1. *Animal care*

All animal experiments were performed in compliance with guidelines established by the Barcelona Science Park's Committee on Animal Care. Mice were maintained on a regular dark-light cycle (light from 8AM to 8PM), with free access to food and water during the whole experimental period.

7.2.7.2. *Generation of animal models*

In this project, we used a SKM-KO TP53INP2 mouse line, which was generated by crossing homozygous TP53INP2 $^{loxP/loxP}$ mice with a mouse strain expressing Cre recombinase under the control of the Myosin- Light Chain 1 promoter (Bothe *et al*, 2000; Sala *et al*, 2014). Non-expressing Cre TP53INP2 $^{loxP/loxP}$ littermates were used as controls for knockout animals. Four-month-old male mice were used in all experiments. Mice were in a C57BL/6J pure genetic background.

Besides, a transgenic mouse line (SKM-Tg) overexpressing TP53INP2 in skeletal muscle under the control of the Myosin-Light Chain 1 promoter/enhancer was generated as described before (Sala *et al*, 2014). The open reading frame of TP53INP2 was introduced in an EcoRI site in the MDAF2 vector, which contains a 1.5 kb fragment of the MLC1 promoter and 0.9 kb fragment of the MLC1/3 gene containing a 3' muscle enhancer element (Otaegui *et al*, 2003; Rosenthal *et al*, 1989). The fragment obtained after the digestion of this construct with BssHII was the one used to generate the transgenic mouse line. Nontransgenic littermates were used as controls for the transgenic animals. Mice were in a C57BL/6J pure genetic background. Four-month-old male mice were used in all experiments.

For modeling cancer-induced cachexia, in collaboration with Fabio Penna (University of Torino, Italy), the SKM-Tg mouse line was backcrossed with Balb/c mice in order to obtain successful C26 carcinoma engraftment and a reproducible cachectic phenotype. Based on previously published data (Penna *et al*, 2015), the F2 generation of C57BL/6J mice backcrossed to BALB/c strain is permissive for C26 growth, and is comparable for induction of body weight loss, as compared to pure BALB/c mice in both male and female animals.

7.2.7.3. *Cancer cachexia induction*

Mice were randomized and divided into two groups, namely controls (C, n=12) and tumor bearers (C26, n=16). Tumor bearing (C26) mice were inoculated subcutaneously in the back with $5x10^5$ Colon26 (C26) cells. C26 cells were maintained in vitro in DMEM (Invitrogen) supplemented with 10% FBS, 100 U/ml penicillin, 100 μg/ml streptomycin,

100 µg/ml sodium pyruvate, 2 mM L-glutamine, at 37°C in a humidified atmosphere of 5% CO2 in air. The day of tumor implantation, cells were trypsinized, resuspended in sterile saline, and implanted in the back of the animals.

Animal weight and food intake were recorded daily, starting from the day of tumor implantation. Control and tumor-bearing mice were killed under anesthesia 14 days after C26 implantation, respectively. Several muscles and tissues were rapidly excised, weighed, frozen in melting isopentane cooled with liquid nitrogen and stored at -80°C.

7.2.7.4. Measurement of whole body composition

Body composition was evaluated in living awake, conscious animals in triplicate using a magnetic resonance whole-body composition analyzer (EchoMRI) (Taicher *et al*, 2003). Mice were restrained but not anesthetized during measurements, and lean mass, fat mass and total water mass were determined based on radio pulse emission properties to differentiate between tissue types.

7.2.7.5. Grip force assessment

Skeletal muscular strength in mice was quantified by the grip-strength test (Penna *et al*, 2011; Sinis *et al*, 2008; Zangarelli *et al*, 2006). The grip-strength device (Panlab/ Harvard Apparatus) comprised a triangular pull bar connected to an isometric force transducer (dynamometer). Basically, the grip-strength meter was positioned horizontally, and the mice are held by the tail and lowered towards the device. The animals are allowed to grasp the triangular pull bar and were then pulled backwards in the horizontal plane. The force applied to the bar just before it lost grip was recorded as the peak tension. At least three measurements were taken per mouse on both baseline and test days, and the results were averaged for analysis.

7.2.7.6. *Mitochondrial respiration*

7.2.7.6.1. *Isolation and permeabilization of muscle fibers.*

In a distinct set of control (C, n=6) and tumor bearing (C26, n=10) mice, EDL muscles were excised and immediately placed in ice-cold biopsy containing preservation

medium (BIOPS; OROBOROS Instruments) (Table 7). Muscle fiber bundles weighing around 3 mg were mechanically separated using thin tweezers and permeabilized with 50 µg/ml saponin for 30 minutes at 4°C according to the technique of Veksler *et al* (Veksler *et al*, 1987). After completion of the permeabilization protocol, muscle fibers were transferred into ice-cold mitochondrial respiration buffer (MiRO5; OROBOROS Instruments) (Table 7). Subsequently, the muscle fibers were transferred to the oxygraph to perform high-resolution respirometry corrected for wet weight.

Table 7. Composition of buffers BIOPS and MiRO5 to measure mitochondrial respiration in skeletal muscle.

BIOPS composition		MiRO5 composition	
CaK_2EGTA_3	2,77 mM	EGTA	0,5 mM
K_2EGTA_4	7,23 mM	$MgCL_2 \cdot 6H_2O$	3 mM
Na_2ATP	5,77 mM	K-lactobionat$_1$	60 mM
$MgCl_2 \cdot 6H_2O$	6,56 mM	Taurina	20 mM
Taurina	20 mM	KH_2PO_4	10 mM
Na_2Fosfocreatina	15 mM	HEPES	20 mM
Imidazol	20 mM	Sacarosa	110 mM
DTT	0,5 mM	BSA_2	1 g/l
MES	50 mM		

7.2.7.6.2. *High resolution respirometry*

Thereafter, the respiration chambers were hyperoxygenated and closed at an O_2 concentration of approximately 500 µM. Oxygen limitation of respiration was prevented by maintaining the oxygen levels in the respirometer above air saturation in the range of 500 to 200 µM.

Mitochondrial respiratory rates were measured at 37°C by polarographic oxygen sensors in a 2-chamber Oxygraph (OROBOROS Instruments) equipped with a Peltier thermostat and electromagnetic stirrers. The oxygen concentration was recorded at 2.0-second intervals using the acquisition software DatLab 4 (OROBOROS Instruments). The first derivative of the oxygen tension changes is displayed as oxygen flux, and mean values during about 1 minute were obtained from these recordings for calculation of stable oxygen flux rates.

To evaluate oxidative phosphorylation, different substrate inhibition protocols were used. In every protocol applied, first, 2 mM malate was added for depletion of endogenous substrates followed by addition of 10 mM glutamate as a substrate for complex I. In addition, an excess of 2.5 mM ADP was added to evaluate state 3 respiration of complex I. Then 10 mM succinate was added to obtain state 3 respiration by activating both complex I and II. With these substrates, maximal physiological capacity is obtained, reconstituting the operation of the tricarboxylic acid cycle and preventing depletion of key metabolites from the mitochondrial matrix (Gnaiger, 2009). Cytochrome c (10 μM) was added to check the integrity of the outer mitochondrial membrane. Finally, maximal oxygen flux rates were measured with the chemical uncoupler carbonylcyanide-4-(trifluoromethoxy)-phenylhydrazone (FCCP), which was titrated (0.5 μM per addition) until no further stimulation of respiration could be detected.

In order to evaluate complex II respiration, complex I inhibitor Rotenone (0.5 μM) was added. Finally, Antimycin A (2.5 μM) was added for completely disrupting mitochondrial respiration. The obtained O_2 consumption rate was subtracted to all measurements in order to exclude non-mitochondrial respiration from the analysis. Mitochondrial respiration measured ex vivo in permeabilized muscle fibers obtained from the same muscle biopsy can show some variation (Gnaiger, 2009). Therefore, all measurements were done in duplicate.

7.2.8. Human samples

7.2.8.1. *Patients*

The methods were carried out in accordance with the approved guidelines and regulations. After approval of the local ethical committees at M.G. Vannini Hospital in Rome (Italy) and Azienda Ospedaliera Universitaria Senese in Siena (Italy), and after the obtainment of written informed consent, twenty-nine consecutive cancer patients (17 males and 12 females) were enrolled among those undergoing abdominal surgery (Aversa *et al*, 2016). The samples for cancer patients belong to colon rectum (n=14), pancreas (n=5), stomach (n=4) and miscellaneous (n=6) cancers. Eight control patients were recruited among those undergoing abdominal surgery for non-neoplastic diseases.

Reasons for abdominal surgery in controls were: incisional hernia, cholelithiasis, benign prostatic hyperplasia, epigastric hernia and mesenteric cyst. Exclusion criteria for both cancer patients and controls were: liver failure, diabetes, metabolic acidosis, acute and chronic renal failure, sepsis, AIDS, inflammatory bowel diseases, acute and chronic hepatitis, autoimmune disorders and chronic obstructive pulmonary disease. The average age was 68 ± 2 for caner patients and 63 ± 4 for control patients.

The % of body weight loss was evaluated during the previous six months. Patients were defined according to the ESPEN Special Interest Group (SIG) on cachexia-anorexia in chronic wasting diseases consensus definition (Fearon *et al*, 2011; Muscaritoli *et al*, 2010). They were classified as non cachectic patients when the weight loss is ≤ 5% of usual body weight in the last 6 months but as cachectic patients when they showed body weight loss > 5% in the previous 6 months according the International Consensus definition on cancer cachexia (Fearon *et al*, 2011).

7.2.8.2. *Muscle biopsy*

Based in the protocol previously described (Aversa *et al*, 2016), biopsy specimens were obtained during the initial phase of the operation from the rectus abdominis muscle. After skin incision and dissection through the subcutaneous fat, the anterior sheet of the rectus abdominis muscle was opened with scissors and a muscle biopsy specimen was obtained (approximately 0.5 g). Small bleeding vessels were carefully controlled with ligatures and cautery after the muscle biopsy had been obtained; thereafter the operation continued in a routine fashion. No complications occurred from the biopsy procedure. Biopsy specimens were immediately frozen in liquid nitrogen and stored at – 80 °C until analysis; part of the specimens was used for the present study and part was kept stored for further, subsequent investigations.

7.2.8.3. *Real-time PCR*

Total RNA was obtained using TriReagent (Sigma Aldrich) following the manufacturer's instructions and the protocol previously described (Aversa *et al*, 2016). RNA concentration was determined fluorometrically using the RiboGreen rea-

gent (Invitrogen). Total mRNA was retrotranscribed using the iScript cDNA synthesis kit (Bio-Rad). Transcript levels were determined by real-time PCR using the SsoFast EvaGreen Supermix and the MiniOpticon Thermal Cycler (Bio-Rad). Ten seconds of denaturation at 95 °C was followed by 30 seconds of annealing/extension at 60 °C and repeated for 40 cycles. Every qPCR was validated by analyzing the respective melting curve. Only one peak was detectable, indicating the presence of just one amplicon. Gene expression was normalized to both GAPDH and TATA-binding protein (TBP) expression and calculated using the $2-\Delta\Delta Ct$ method. Primers sequences used (forward and reverse) are indicated in Table 5.

7.2.9. Expression of results and statistical analysis

Data are presented either as mean ± SEM of a number of independent experiments (ranging from 3 to 15). Statistical significance was assessed by a two-tailed paired Student's t-test and One-way Anova analysis. A value of $p< 0.05$ was chosen as the limit of statistical significance.

CHAPTER 8

RESUMEN EN CASTELLANO

8. RESUMEN

8.1. Introducción

El músculo esquelético es fundamental para funciones tan importantes como el movimiento y el metabolismo de nuestro cuerpo, por ello, el mantenimiento de la masa muscular es esencial para aspectos básicos como la movilidad, la prevención de enfermedades y una buena calidad de vida. La masa muscular se encuentra regulada de manera global por el balance neto entre la tasa de degradación de proteínas y la tasa de síntesis de proteínas (Goodman *et al*, 2011a).

La homeostasis de proteínas (*o proteastasis*) resulta de la regulación de la síntesis y degradación proteica y es un mecanismo clave por el cual las células rápidamente responden a su entorno para mantener las proteínas de la célula con una actividad biológica óptima (Anfinsen, 1973).

Desde hace décadas, los investigadores se han centrado en estudiar la síntesis de proteínas, particularmente en entender las señales transcripcionales y traduccionales. Sin embargo, la degradación de proteínas ha sido menos caracterizada. Dos rutas de degradación principales se han descrito en la mayoría de proteínas en células eucariotas: 1) el sistema ubiquitina proteosoma (UPS), responsable de degradar entre el 80 y 90% de proteínas incluyendo la mayoría de proteínas de vida media corta, anormales, desnaturalizadas o en general proteínas dañadas (Lecker *et al*, 2006) y 2) la autofagia, que por el contrario, es principalmente responsable de la degradación de la mayoría de proteínas de vida media larga, pero también de agregados de proteínas así como órganos celulares (Johansen & Lamark, 2011).

Aunque el estudio del proceso de autofagia ha aumentado sustancialmente en los últimos años, aún existe mucho desconocimiento sobre la identidad de los componentes de la ruta de autofagia así como de su regulación. En nuestro laboratorio, se ha identificado un nuevo componente de la ruta de autofagia, el cofactor nuclear DOR (gen regulado

en diabetes y obesidad) también conocido por el nombre de TP53INP2 (Mauvezin *et al*, 2010).

TP53INP2 fue identificado originalmente como una proteína que se expresaba en cuerpos nuncleares de tejidos sensibles a la insulina (Baumgartner *et al*, 2007). Sin embargo, en respuesta a estrés celular o activación de la autofagia, TP53INP2 sale del núcleo y colocaliza con estructuras citoplasmáticas en forma de puntos. Además, se ha descrito que la proteína TP53INP2 citoplasmática localiza con autofagosomas tempranos e interacciona directamente con proteínas asociadas a membrana de los autofagosomas (Baumgartner *et al*, 2007; Huang *et al*, 2015; Mauvezin *et al*, 2010; Nowak *et al*, 2009) (Figura 1). También se ha demostrado que TP53INP2 favorece la degradación de proteínas a través de la autofagia en condiciones basales así como en ayuno de aminoácidos (Mauvezin *et al*, 2010).

TP53INP2 se expresa abundantemente en tejidos con alta tasa metabólica como el músculo esquelético (SKM) y el corazón. Además, la expresión de TP53INP2 está reprimida en músculos de pacientes obesos, con diabetes tipo II y en modelos de ratones de diabetes. Estudios recientes de nuestro laboratorio demuestran que TP53INP2 desencadena pérdida de masa muscular. De hecho, la ganancia de función de TP53INP2 provoca atrofia, mientras que la pérdida de función de TP53INP2 desencadena hipertrofia en el músculo. Estos datos sugieren que este fenotipo es debido a que TP53INP2 activa la autofagia basal en el músculo esquelético incrementando la formación de autofagosomas a través de la interacción con LC3 (Sala *et al*, 2014).

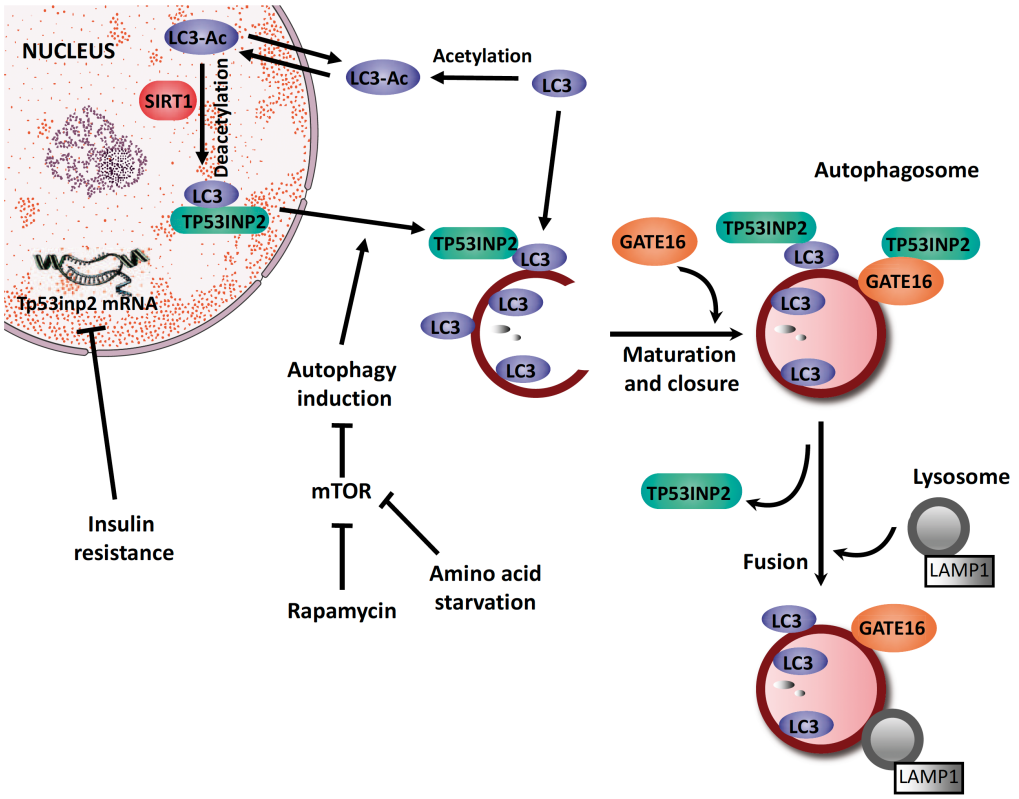

Figura 1. Papel functional de TP53INP2 en autofagia. En respuesta a diferentes estreses celulares como la ausencia de nutrientes, SIRT1 desencadena la desacetilación de LC3 nuclear. TP53INP2 interacciona con LC3 deacetilado en el núcleo. La inducción de autofagia provoca la translocación de TP53INP2 del núcleo al citosol junto con LC3 deacetilado. En el citosol, TP53INP2 también interacciona con otros miembros de la familia Atg8 como GATE16 y promueve la formación de autofagosomas. A continuación, TP53INP2 abandona el autofagosoma antes de la fusión con el lisosoma. Bajo condiciones de resistencia a insulina, la expresión génica de TP53INP2 está reprimida para permitir la disminución de un exceso de autofagia.

Hay muchas investigaciones que demuestran que la autofagia y el sistema ubiquitina proteosoma (UPS) son procesos fundamentales en el mantenimiento de la homeostasis celular, lo cual sugiere que estos dos procesos tienen que estar regulados coordinadamente. Durante mucho tiempo, estos procesos se han estudiado como independientes el uno del otro (Ciechanover, 2005; Pickart, 2004). Sin embargo, hay evidencias recientes que sugieren una interrelación de estas dos rutas celulares.

Uno de los mecanimos propuestos que interconecta el UPS y la autofagia está basado en la observación de que una deficiencia de UPS provoca un incremento de la función autofágica (Ding *et al*, 2007; Iwata *et al*, 2005; Pandey *et al*, 2007). Esto está considerado

comúnmente como un mecanismo compensatorio, lo cual permite a las células reducir los sustratos acumulados del UPS. Sin embargo, estudios genéticos en ratones demuestran que, por otro lado, una deficiencia de autofagia también conlleva a una deficiente degradación de sustratos específicos de UPS (Hara *et al*, 2006; Komatsu *et al*, 2006; Korolchuk *et al*, 2009a, 2009b; Qiao & Zhang, 2009). Además, se ha descrito una *upregulación* coordinada de ambos procesos que contribuyen a la atrofia muscular en condiciones fisiológicas, como ayuno, o en enfermedades caracterizades por la pérdida de masa muscular (Zhao *et al*, 2007).

Una patología asociada a la pérdida de masa muscular y la atrofia es la caquexia cancerosa. La caquexia cancerosa suele darse en pacientes con cáncer gástrico, colorectal, pancreático y de pulmón (DeWys *et al*, 1986) . Es considerado un síndrome multifactorial caracterizado por la anorexia, la pérdida de peso y atrofia muscular que aumenta la tasa de morbilidad y de mortalidad y reduce la tolerancia a terapias antineoplásicas provocando una baja calidad de vida (Fearon *et al*, 2011; von Haehling & Anker, 2010; Penna *et al*, 2013, 2015; Pin *et al*, 2015).

Los mecanismos que regulan esta patología aún no son muy conocidos. Se han observado muchas alteraciones metabólicas que son responsables de la pérdida de masa muscular (Fearon *et al*, 2012). De hecho, en músculos caquécticos se han identificado anormalidades en la síntesis y degradación de proteínas así como en el metabolismo de aminoácidos. Mientras que se ha descrito que la síntesis proteica se encuentra reducida en el músculo esquelético de modelos animales de caquexia (Eley *et al*, 2008; Smith & Tisdale, 1993), el mecanismo que más se ha estudiado que está implicado en la pérdida de masa muscular es la degradación de proteínas mediada por el UPS. Estudios experimentales y clínicos han demostrado que la hiperactivación del UPS juega un papel muy importante (Bossola *et al*, 2001; Costelli *et al*, 1995). Sin embargo, recientemente, se ha propuesto la implicación de la proteólisis mediada por autofagia y lisosomas como un posible mecanismo para explicar la caquexia. Estudios sugieren que la autofagia está activada en músculos de animales portadores del carcinoma pulmonar de Lewis (LLC) y tumores de colon C26, dos modelos muy usados para el estudio de la caquexia cancerosa (Penna *et al*, 2015). De hecho, los niveles proteicos de Beclin-1, LC3B y p62/SQSTM1 así

como el flujo autofágico se ve aumentado en el músculo esquelético de modelos de ratones de caquexia. En relación con estos resultados, elevados niveles proteicos de Beclin-1 y LC3B se observan en músculo esquelético de pacientes con cáncer (Aversa *et al*, 2016; Penna *et al*, 2013).

8.2. Resultados y discusión

8.2.1. Efecto de TP53INP2 en el Sistema ubiquitina proteasome.

De acuerdo con estos antecedentes, el principal objetivo de la presente tesis es analizar el papel de DOR/TP53INP2 como regulador que interconecta la autofagia con otros procesos homeostáticos como el sistema de ubiquitina proteosoma (UPS) en el músculo esquelético.

Para evaluar esto, lo primero que hemos medido es la actividad del proteosoma mediante unos ensayos que determinan la degradación de sustratos específicos peptídicos fluorogénicos (Kisselev *et al*, 2006) en el músculo esquelético de ratones *knock out* para TP53INP2 en comparación con los controles loxP así como en células musculares C2C12 deficientes para TP53INP2 en comparación con células WT. Los resultados indican que existe un incremento de la actividad del proteosoma cuando hay una pérdida de función de TP53INP2 en ratones (Figura 2) y en células musculares (Figura 3). Para confirmar estos resultados, en células musculares, se ha determinado la tasa de proteínas poliubiquitinadas en el residuo K48 (residuo específico para la degradación de proteínas mediada por proteosoma), y se ha observado que está aumentada en células deficientes en TP53INP2. Además, los niveles de la actividad del immunoproteosoma se estudiaron también en colaobración con el equipo de Tilman Grüne y se observó que estaba regulado coordinamente con la actividad del proteosoma en células musculares, es decir, la actividad del inmunoproteosoma estaba aumentada en células C2C12 deficientes en TP53INP2.

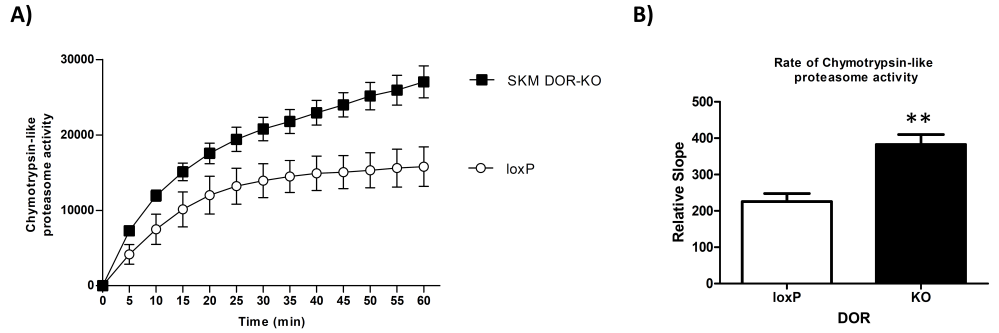

Figura 2. La actividad del proteosoma está incrementada en el músculo esquelético de ratones deficientes en TP53INP2. (A) La actividad del proteosoma específica Chymotrypsin-like (Z- Gly-Gly-Leu-AMC) en extractos totales de músculo EDL de ratones control (loxP) (blanco, n=4) y ratones knock out para TP53INP2 (negro, n=5). (B) Tasa de la actividad chymotrypsin-like expresada como pendiente relativa. Los datos representan la media ± SEM. **p<0,005 vs ratones control (loxP).

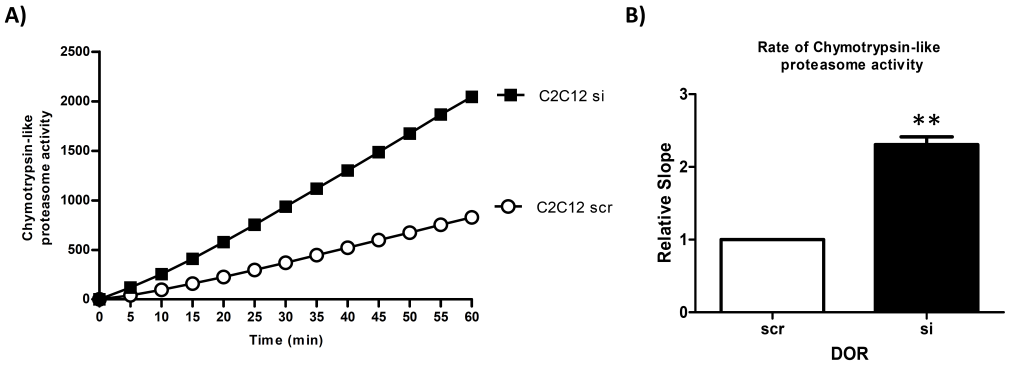

Figura 3. La actividad del proteosoma está incrementada células C2C12 deficientes en TP53INP2. (A) La actividad del proteosoma específica Chymotrypsin-like (Z- Gly-Gly-Leu-AMC) en extractos totales de células C2C12 scrDOR (blanco) en comparación con siDOR (negro), n=4. (B) Tasa de la actividad chymotrypsin-like expresada como pendiente relativa. Los datos representan la media ± SEM. **p<0,005 vs células control (C2C12 scr).

El proteosoma 26S/30S consiste en una estructura central que contiene los sitios de actividad proteolítica y la estructura 19S que regula la actividad del holo-complejo (26S con una subunidad reguladora y 30S con dos subunidades reguladoras). Para empezar, examinamos la expresión de PSMD4 y PSMD11 (ambas pertenecientes a la estructura reguladora 19S) y de PSMA1-7 y β5 (perteneciente a la estructura central 20S). PSMD4 está descrito que interacciona con TP53INP2 en ensayos de doble híbrido en levadura

(YTH) (Nowak *et al*, 2009) y es el receptor de ubiquitina mejor caracterizado que se une y probablemente selecciona conjugados ubiquitinados para ser degradados (Deveraux *et al*, 1994). PSMD11 tiene un papel principal en la estabilización de la interacción débil entre la estructura central 20S y la reguladora 19S. PSMA1-7 está implicado en el desplegamiento de los sustratos y su traslocación y la subunidad β5 fue estudiada en colaboración con el equipo de Tilman Grüne del Instituto Alemán de Nutrición Humana. β5 es responsable de la actividad proteolítica chymotrypsin-like.

Nuestros resultados confirman que existe un incremento de las subunidades PSMD11, PSMD4 y PSMA1-7 en el músculo esquelético de ratones deficientes en TP53INP2 (Figura 4). Cuando analizamos la expresión de estas subunidades en células musculares C2C12 también pudimos observar un incremento de los niveles de PSMD11 y PSMA1-7 en las células musculares C2C12 deficientes para TP53INP2 (Figura 5). Por el contrario, no encontramos diferencias significativas en la expresión de la subunidad β5 en células musculares.

En contraposición a estos resultados, también se llevaron a cabo experimentos para determinar los niveles de expresión de las subunidades del proteosoma en células musculares que sobrexpresan TP53INP2. En conformidad con lo que habíamos estudiado previamente, los niveles de PSMD11 estaban reducidos cuando TP53INP2 estaba aumentado, sin embargo, no se encontraron diferencias significativas para el resto de subunidades (PSMD4 y PSMD1-7).

Para confirmar si el efecto de TP53INP2 sobre el proteosoma es una respuesta general del sistema en la que se activa la vía UPS cuando la autofagia está inhibida, llevamos a cabo unos experimentos en los cuales tratamos células musculares C2C12 WT con diferentes inhibidores de autofagia y medimos los niveles de las subunidades del proteosoma. Los resultados demuestran que los efectos de TP53INP2 en el proteosoma no son una consecuencia de tener el proceso de la autofagia alterada, sino que nuestra proteína de estudio está ejerciendo una regulación específica sobre el UPS.

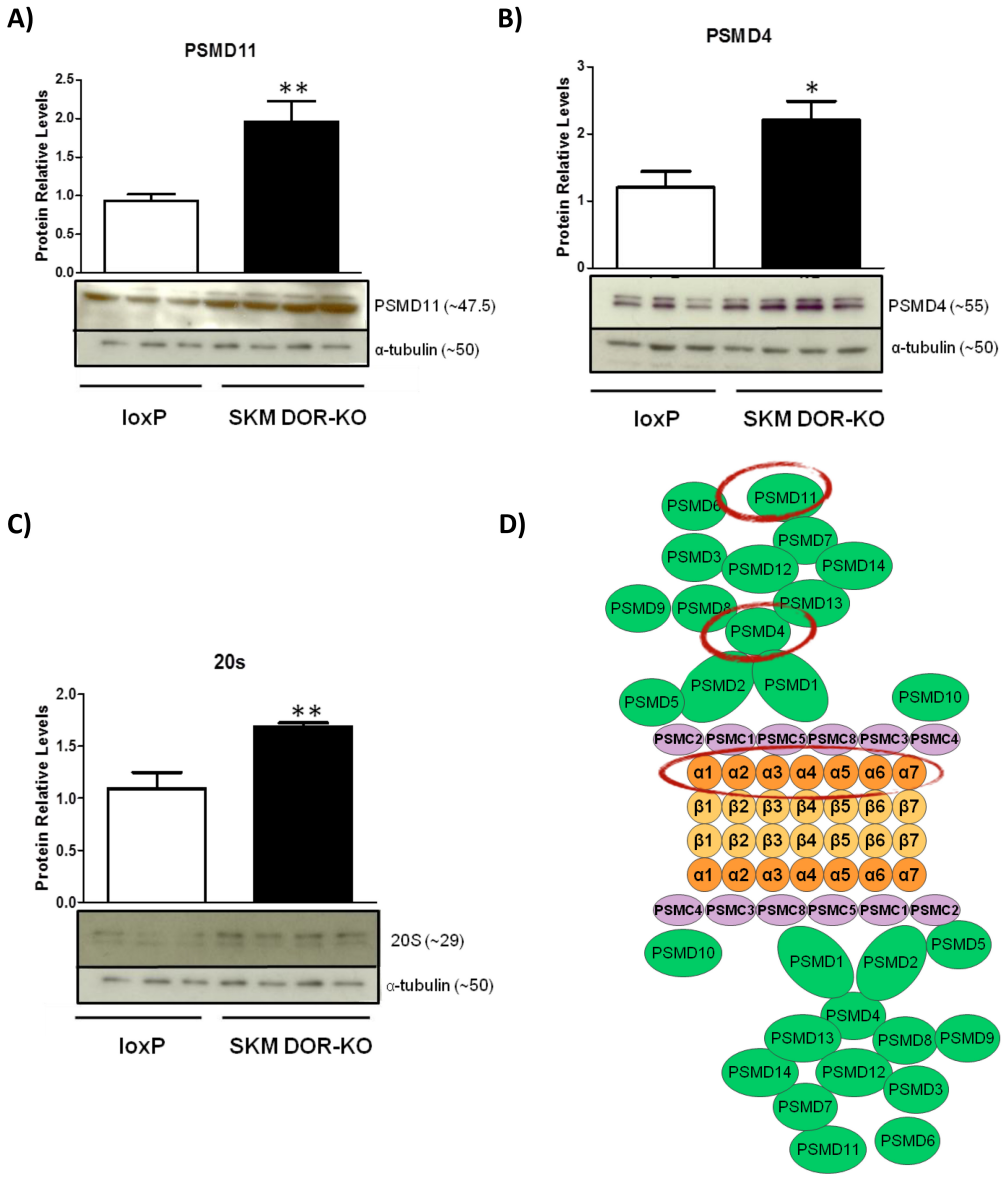

Figura 4. La deficiencia de DOR/TP53INP2 en músculo esquelético aumenta la expresión de PSMD11 (A), PSMD4 (B) y 20S (C). Análisis de western blot y cuantificación de las subunidades del proteosoma PSMD11 (A), PSMD4 (B) and PSMA1–7 (20S) (C) en homogenados totales de gastrocnemius de animales WT (n=6) y SKM DOR-KO (n=8). La α-tubulina es el control de carga. Las barras blancas de los gráficos representan ratones control (loxP) mientras que las negras representan ratones SKM DOR-KO. Los datos representan la media ± SEM. *p<0,05, **p<0,005 vs. ratones control (loxP). (D) Ilustración del proteosoma 26S. Las subunidades en verde son no-ATPasas de la partícula reguladora 19S, las subunidades en morado son ATPasas de la partícula 19S y las subunidades en naranja representan la partícula central 20S. Círculos en rojo remarcan las subunidades de nuestro estudio.

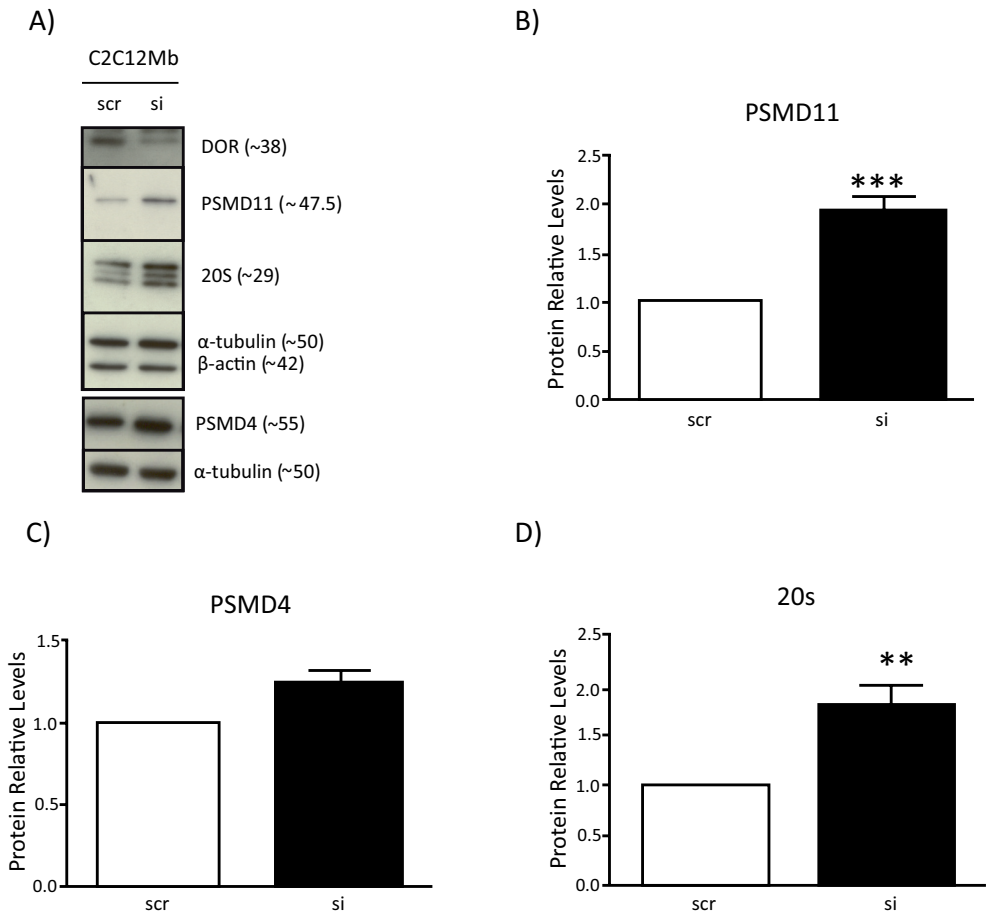

Figura 5. La deficiencia de DOR/TP53INP2 en células musculares aumenta la expresión de PSMD11 (A), PSMD4 (B), and 20S (C). Análisis de western blot (A) y la cuantificación de las subunidades del proteosoma PSMD11 (B, n=12), PSMD4 (C, n=4) and PSMA1–7 (20S) (D, n=12) en homogenados totales de células musculares C2C12 scr y si. α-tubulina es el control de carga. Las barras blancas de los gráficos representan células C2C12 scr mientras que las negras representan células C2C12 si. Los datos representan la media ± SEM. **p<0,005, ***p<0,001 vs. control (scr).

Por el contrario, para averiguar si las subunidades del proteosoma eran degradadas por la vía UPS analizamos la expresión de las subunidades de nuestro estudio en células tratadas con el inhibidor del proteosoma MG132. Podemos confirmar que MG132 aumenta los niveles de las subunidades PSMD11 y pSMA1-7 en células control, sugiriendo que estas subunidades son degradadas por el proteosoma. Sin embargo, células deficientes en TP53INP2 muestran una respuesta diferente al tratamiento con MG132 ya que los niveles de PSMD11 y PSMA1-7 no se ven alterados, lo cual confirma la hipótesis de que

la pérdida de función de TP53INP2 reduce la degradación proteosomal de las subunidades PSMD11 y PSMA1-7.

A continuación estudiamos si la localización subcelular de TP53INP2 regulaba el UPS, para ello, estudiamos los efectos de una forma mutante de TP53INP2 que es nuclear y no circula entre el núcleo y citoplasma como la forma WT de TP53INP2. Nuestros datos demuestran que TP53INP2 requiere estar circulando entre núcleo y citosol para llevar a cabo la regulación de la expresión de las subiunidades del proteosoma. Además, estudios de expresión génica corroboran que TP53INP2 no regula transcripcionalmente los niveles de las subunidades del proteosoma en células musculares y el músculo esquelético de ratones.

Por tanto, la siguiente pregunta que nos hicimos era si TP53INP2 regulaba la estabilidad de las subunidades del proteosoma y para ello las células musculares C2C12 scr y si se trataron con cicloheximida (50 μg/ml), un inhibidor de la traducción y, a continuación, se realizaron análisis de western blot en extractos celulares totales. El estudio se limitó a 6 horas de tratamiento con cicloheximida en base a la vida media descrita de TP53INP2 que es de aproximadamente 4 horas (Mauvezin *et al*, 2010). Los resultados muestran que las células control presentan una caida de los niveles de las subunidades PSMD11, PSMD4 y PSMA1-7 después del bloqueo de la traducción. Sin embargo, las células deficientes en TP53INP2 muestran una estabilización de esas subunidades y no se observó ninguna caída en la abundancia de estas proteínas (Figura 6).

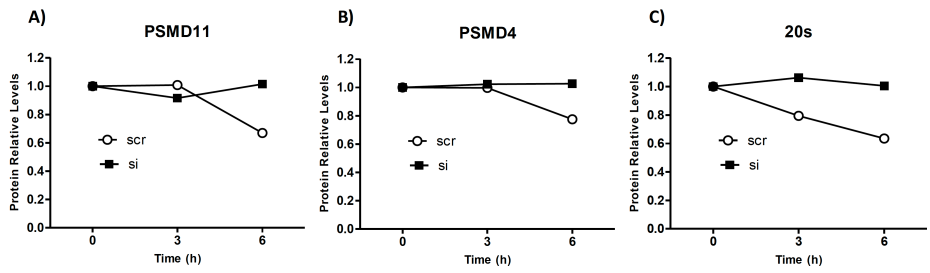

Figura 6. La estabilidad de las subunidades del proteosoma está aumentada en células deficientes en TP53INP2. Experimentos representativos de la cuantificación del western blot de homogenados totales de células musculares C2C12 (scr y si) tratadas con 50 μg/ml de cicloheximida para inhibir la síntesis proteica a 3 y 6 horas. Fueron detectadas las subunidades del proteosoma PSMD11 (A), PSMD4 (B) and 20S (C) por inmunoblotting (n=4). α-tubulina y β-actina son el control de carga. Las barras blancas representan células C2C12 scr y las barras negras representan células C2C12 si.

En base a los datos que demuestran que las células C2C12 deficientes en TP53INP2 generan mayores niveles de proteína ubiquitinada en el residuo K48, decidimos explorar si TP53INP2 estaba implicada en la regulación de las enzimas ligasas ubiquitina E3. En el músculo, las ubiquitina ligasas E3 más estudiadas son MuRF1 y Atrogin-1, las cuales, además, se han descrito que están aumentadas en modelos in vivo de ratones con atrofia muscular (Bodine *et al*, 2001; Gomes *et al*, 2012). Además, algunas evidencias de nuestro laboratorio sugieren que MuRF1 y MuRF2 podrían estar actuando en el mismo complejo que TP53INP2 ya que TP53INP2 se une en el ensayo de *Yeast Two Hybrid* a las mismas proteínas que se han escrito para MuRF1 y MuRF2. Por esta razón, decidimos estudiar la participación de TP53INP2 en la regulación de las ubiquitina ligasas E3. Algunos resultados preliminares muestran que TP53INP2 regula transcripcionalmente e interacciona con MuRF1.

Finalmente, datos previos de nuestro laboratorio demuestran que la deficiencia de TP53INP2 causa hipertrofia muscular, mientras que la sobrexpresión de TP53INP2 promueve la atrofia muscular (Sala *et al*, 2014). En base a esto y teniendo en cuenta el incremento del sistema ubiquitina proteasome en el músculo y células deficientes en TP53INP2, a continuación hemos analizado si la síntesis de proteínas también estaba regulada por TP53INP2. La síntesis de proteínas se midió con el método SUnSET, una técnica no radiactiva en la que los cambios en la tasa de síntesis proteica se estiman en relación a la cantidad de puromicina incorporada en nuevas proteínas sintetizadas (Goodman & Hornberger, 2013; Goodman *et al*, 2011b; Schmidt *et al*, 2009). Nuestros resultados sugieren que las células musculares deficientes en TP53INP2 tienen aumentada la síntesis proteica. Sin embargo, en contra de lo esperado, no hemos encontrado cambios en los niveles de los componentes de la vía de mTOR, una ruta muy conocida como reguladora de la síntesis proteica. Y, sorprendentemente, resultados preliminares muestran que TP53INP2 aumenta la fosforilación de la subunidad α del factor eIF2, el cual se conoce como un mecanismo que disminuye la síntesis proteica bajo condiciones de estrés celular.

8.2.2. TP53INP2 modula la degradación proteica en caquexia cancerosa

La segunda parte de la tesis se ha realizado en colaboración con el Dr. Fabio Penna (universidad de Torino, Italia). Como se mencionó en la sección de la introducción, la caracterísitica más relevante de la patología de la caquexia cancerosa es la continuada pérdida de masa muscular. TP53INP2 se ha descrito como un regulador negativo de la masa muscular (Sala *et al*, 2014), de hecho la expresión de TP53INP2 está reprimida en condiciones de pérdida muscular (Baumgartner *et al*, 2007; Sala *et al*, 2014). Con el objetivo de analizar si el incremento de pérdida muscular inducido por TP53INP2 es una característica peculiar de la patofisiología de la diabetes o también ocurre en otras condiciones catabólicas, decidimos estudiar si modulando la expresión de TP53INP2 se veía afectada la pérdida de masa muscular causada por cáncer caquexia.

Para ello, el modelo experimental que usamos fueron ratones a los que habíamos inoculado células de carcinoma de colon C26; el tumor que desarrollan es aproximadamente el 1.5% del peso total del animal (Penna *et al*, 2013), lo cual representa una condición similar a la caquexia cancerosa humana. El tumor C26 fue originariamente inducido químicamente en ratones BALB/c y no crece en C57/BL6, por lo que fue necesario cruzar los ratones transgénicos para TP53INP2 con un background C57/BL6 con la cepa BALB/C para permitir el crecimiento del tumor. Además, en este modelo, el fenotipo de caquexia es rápido y progresivoy se puede observar en ratones portadores del tumor a partir del día 9. Estudiamos en paralelo dos series experimentales, en la primera usamos machos que fueron sacrificados a día 14 de ser portadores del tumor, mientras que en la segunda serie experimental, se usaron hembras que fueron divididas al azar en dos grupos y sacrificadas a día 10 y a día 13 de haber sido portadoras del tumor C26, de esta manera pudimos observar si TP53INP2 ejercía un efecto en etapas tempranas o avanzadas de la caquexia cancerosa. La monitorización de los experimentos se describe a continuación (Figura 7).

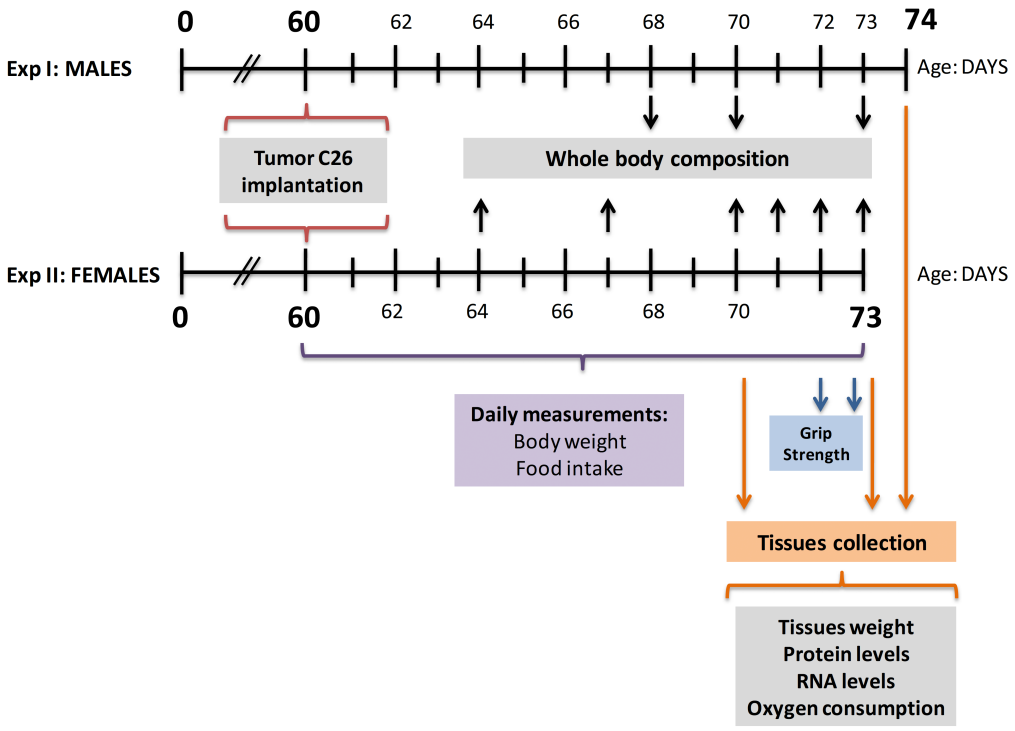

Figura 7. Esquema cronológico de la serie experimental I y II. El experimento I se llevó a cabo con ratones machos sacrificados a día 14. Sin embargo, el experimento II se llevó a cabo con hembras sacrificadas a día 10 y a día 13.

Primero, analizamos la pérdida de peso de los animales del experimento I. El desarrollo del tumor C26 provocó una pérdida de peso muy acusada a partir del día 8, lo cual es consistente con resultados previos (Penna *et al*, 2013) en ratones WT y TP53INP2 SKM-Tg. Sin embargo, los ratones TP53INP2 SKM-Tg muestran una mayor caída de peso (p=0.07 vs C26 WT) a pesar de que no se observaron diferencias en la ingesta de comida en los ratones WT y TP53INP2 SKM-Tg después de la implantación del tumor C26 (Figura 8).

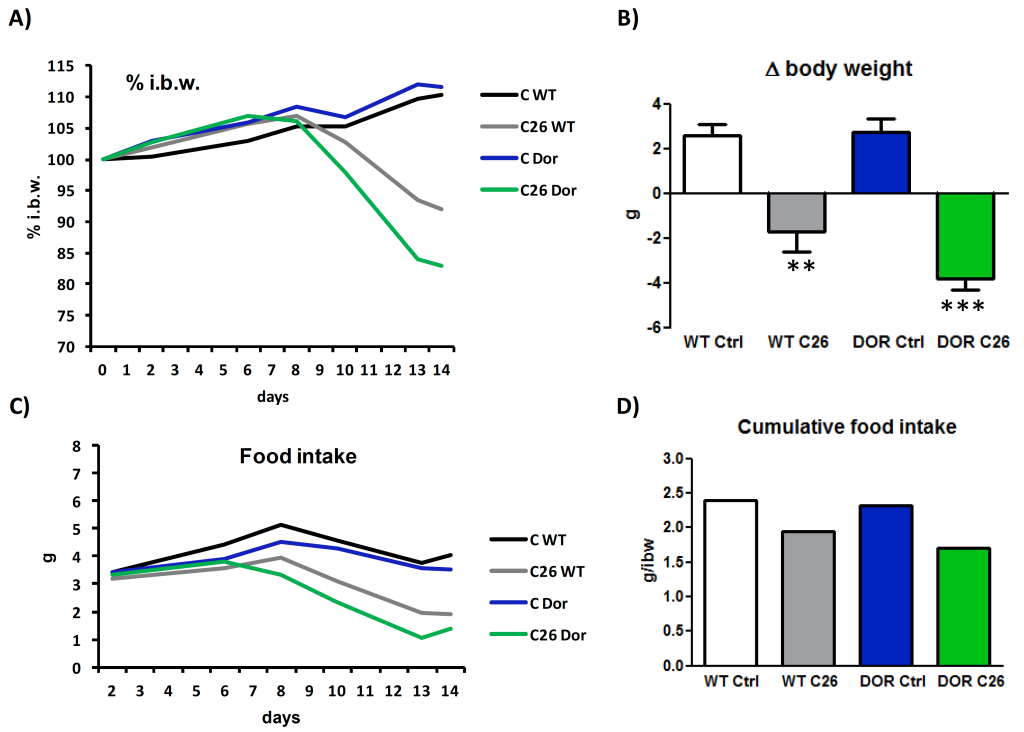

Figura 8. Efectos de la implantación de C26 en el peso corporal y la ingesta de comida en ratones Balb/c y TP53INP2 SKM Tg. El peso corporal de ratones macho control (C, n=6) y portadores del tumor C26 (C26, n=9) está graficado como (A) % del peso corporal inicial y (B) variación del peso corporal al final del periodo experimental. (C) gramos de ingesta de comida diaria durante los 14 días después de la implantación del tumor. (D) acumulación de comida ingerida. Los datos se representan como media (A, C y D) y como mean ± SEM (B). **p<0,01 ***p<0,001 vs. ratones control.

A continuación, para confirmar la hipótesis de que la disminución de la expresión de TP53INP2 en condiciones de pérdida de masa muscular es un mecanismo adaptativo de protección, el peso de los músculos gastrocnemios fue analizado en ratones WT y TP53INP2 SKM-Tg. Podemos observar que los músculos habían disminuido después de la implantación del tumor C26. Sin embargo, los ratones TP53INP2 SKM-Tg mostraban una pérdida muscular más dramática, lo cual indica que TP53INP2 agrava la pérdida de músculo en condiciones de caquexia cancerosa. El tejido adiposo blanco también fue analizado y se observó que tenía una disminución similar después de la implantación del tumor C26 en WT y en ratones trangénicos, así como la masa del tumor, en el cual no se vieron cambios significativos (Figura 9).

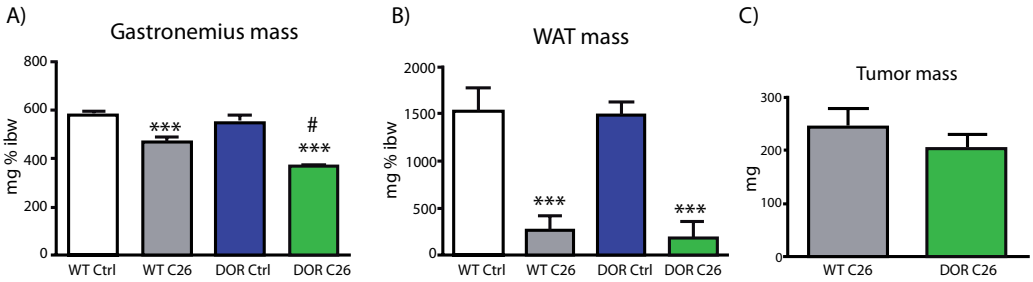

Figura 9. Efecto de la implantación del tumor C26 en el peso de los tejidos en ratones Balb/c y TP53INP2 SKM Tg. El peso del músculo (gastronemios) (A), del tejido adiposo blanco gonadal (WAT, B) y del tumor (C) fue analizado en machos a día 14 del crecimiento del tumor. Los datos están graficados como medias ± SEM. ***p<0,001 vs. ratones control. #p<0,05 vs. raones control portadores del tumor (WT C26). WT Ctrl and DOR Ctrl (n=6) and WT C26 ad DOR C26 (n=9).

En paralelo, se fueron registrando las mismas medidas en la serie experimental II, en la que las hembras fueron analizadas en una etapa inicial y otra etapa avanzada del desarrollo de la caquexia cancerosa. De la misma manera, primero se analizaron la pérdida de peso corporal de ratones WT y ratones transgénicos TP53INP2 SKM-Tg y de forma similar se pudo observar que el tumor C26 provocaba una pérdida de peso corporal a partir del día 10 de ser portador del tumor en ratones WT y TP53INP2 SKM-Tg. Incluso también en esta serie experimental se ve una tendencia a tener una mayor pérdida de peso corporal los ratones trangénicos que sobrexpresan TP53INP2 aunque no se detectan diferencias significativas, probablemente porque la n experimental no era lo suficientemente grande. Como esperábamos, tampoco se detectaron cambios en los niveles de ingesta de comida entre ratones WT y transgénicos TP53INP2 SKM-Tg en condiciones controles y portadores del tumor.

Además, observamos que el peso de los músculos gastrocnemios de la serie experimental II también estaba disminuido en ratones WT y trangénicos portadores de tumor y, aunque se distinguía una tendencia en la que el peso muscular de ratones transgénicos estaba reducida en mayor medida que los ratones WT, no había diferencias significativas debido a la n experimental, la cual no era lo suficientemente grande. La masa del hígado también fue analizada y se veía aumentada en presencia del tumor C26, probablemente debido a una respuesta de inflamación aguda asociada con el crecimiento del tumor. Por el contrario, la masa del tejido adiposo blanco estaba disminuida en presencia del tumor

en comparación con ratones control. No sólo eso, sino que además, los animales transgénicos tenían mayor cantidad de tejido adiposo blanco en comparación con los ratones WT, probablemente porque la regulación de la masa muscular por parte de TP53INP2 desencadenó una comunicación cruzada con el tejido adiposo blanco desencadenando una mayor acumulación. Por último, tampoco se observaron diferencias significativas en la masa del tumor, como en la serie experimental analizada previamente.

Para una mejor caracterización del efecto de la caquexia cancerosa, en esta serie experimenal, pudimos analizar la fuerza muscular usando un test de fuerza muscular (fuerza de prensión) en ratones WT y transgénicos TP53INP2 SKM-Tg. En condiciones control, no se veía afectada la fuerza muscular en presencia del transgén, mientras que sí que se podía observar una fuerza voluntaria reducida después de la implantación del tumor C26 en ratones transgénicos TP53INP2 SKM-Tg.

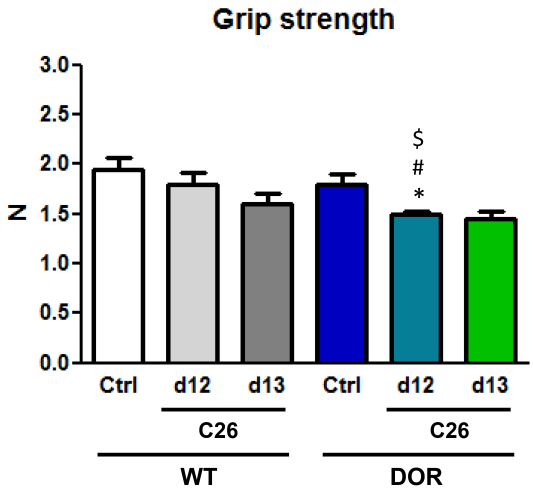

Figura 10. Efectos de la implantación del tumor C26 en la fuerza del músculo esquelético de ratones hembras Balb/c WT y SKM-Tg. El test de grip strength se midió en hembras a día 12 y día 13 de la implantación del tumor como un test de fuerza muscular voluntaria y se expresó en Newton. WT Ctrl y DOR ctrl (n=6) y WT C26 y DOR C26 a día 10 y día 13 (n=7). Los datos se grafican como media ± SEM. *p<0,05 vs. ratones control. # p <0,05 vs. DOR Ctrl. $ p<0,05 vs. WT C26 d12.

En conjunto, los datos de la serie experimental I y I apoyan la idea de que TP53INP2 regula negativamente la masa muscular en condiciones catabólicas. Con el objetivo de estudiar los mecanismos por los que la sobrexpresión de TP53INP2 promueve la atrofia muscular inducida por la implantación del tumor C26 a día 14, hemos estudiado la implicación de diferentes rutas de degradación relevantes en la serie experimental I. Cuando analizamos la expresión de los atrogenes MuRF1 y Atrogen1/FbxO32, se obsevaba un

aumento de su expresión en ratones inducidos con el tumor en comparación con ratones WT, y, además de esto, en ratones transgénicos se puede diferenciar una mayor inducción de MuRF1 en el músculo de ratones que sobrexpresan TP53INP2 en comparación con ratones WT inducidos por el tumor C26, la misma tendencia se obseva para Atrogin-1, pero por la variabilidad experimental no se pudieron detectar cambios significativos. También realizamos el análisis de genes de autofagia y observamos que la presencia del tumor C26 siempre induce la expresión de genes de autofagia, y en algunos casos esa inducción es menor (para el caso de LAMP2A) en ratones transgénicos que sobrexpresan TP53INP2; lo cual nos podría sugerir que es un efecto adaptativo.

Debido a la relación funcional que existe entre autofagia y mitocondria, estudiamos el regulador transcripcional PGC1α así como genes relacionados con la dinámica mitocondrial. De este análisis descubrimos que la expresión de Mfn2, Opa1 y Drp1 estaba reducida en ratones transgénicos que sobrexpresan TP53INP2 portadores del tumor. La caquexia cancerosa promueve un mayor gasto energético (Petruzzelli *et al*, 2014). Sin embargo, aún no se sabe si el músculo participa o no en este proceso y estudios llevados a cabo en miotubos C2C12 demuestran que existe una dismiunción en la regulación mitocondrial en respuesta a la incubación con medio condicionado del carcinoma de pulmón de Lewis. Por ello, analizamos el consumo de oxígeno mitocondrial en fibras musculares aisladas de ratones WT y transgénicos que sobrexpresan TP53INP2, hemos podido observar que la ganancia de función de TP53INP2 aumenta la respiración mitocondrial en músculo y, además, la caquexia cancerosa disminuye la regulación mitocondrial, en concreto del complejo I, aunque este efecto no parece depender de TP53INP2. Por último, analizamos la expresión de TP53INP2 y para nuestra sorpresa, pudimos observar una reducción dramática de los niveles de este gen en animales portadores del tumor durante 14 días, por lo que sugerimos que esta condición de atrofia provocada por el tumor C26 está desencadenando una reducción de los niveles del promotor MLC1. En conclusión, se podría decir, que los efectos de la sobrexpresión de TP53INP2 en etapas iniciales son suficientes para promover la pérdida de masa muscular en este modelo de caquexia cancerosa inducida por C26.

Para finalizar este apartado, también analizamos si la expresión del gen TP53INP2 estaba regulada en biopsias de músculos humanos de pacientes sanos (n=7) y de pacientes con cáncer (n=29), los cuales se subdividieron en dos grupos, pacientes que habían perdido un porcentaje de peso menor del 5% (n=17, cancer sin caquexia) y pacientes que habían perdido un porcentaje de peso corporal mayor del 5% (cáncer con caquexia). Los resultados indican que los niveles de mRNA de TP53INP2 se vieron reducidos un 85% en pacientes con cáncer y caquexia, lo cual no se podía observar en pacientes con cáncer sin caquexia. Globalmente, podríamos concluir que la expresión de TP53INP2 puede tener un papel muy relevante en el mantenimiento de la masa muscular que tiene lugar en estados patológicos.

8.3 Conclusiones

I. TP53INP2 regula negativamente el Sistema Ubiquitina Proteosoma en el músculo esquelético. La ausencia de TP53INP2 en músculo incrementa la actividad proteosomal y la expresión de las subunidades PSMD11, PSMD4 and PSMA1-7.

II. La deficiencia de TP53INP2 aumenta la actividad del proteosoma y del inmunoproteosoma, e incrementa la generación de proteínas poliubiquitinadas en el residuo K48 así como la expresión de las subunidades del proteosoma PSMD11 y PSMA1-7 en células musculares.

III. Las subunidades del proteasome PSMD11 y PSMA1-7 están degradadas a través del sistema Ubiquitina-Proteosoma en células musculares. La deficiencia de TP53INP2 favorece la estabilidad de estas subunidades mediante la reducción de su degradación por parte del proteosoma sin alterarse la expresión génica.

IV. La ganancia de función del TP53Inp2 disminuye la expresión de PSMD11 en células musculares. Estos efectos requieren la recirculación de TP53INP2 del núcleo al citoplasma, y la forma mutante de TP53INP2 que pierde la señal de exportación nuclear y se mantiene en el núcleo no tiene la capacidad de reprimir PSMD11.

V. La expresión génica de TP53INP2 está reducida en el músculo esquelético de pacientes con cáncer caquexia así como en ratones caquécticos portadores del tumor C26. La ganancia de función de TP53INP2 agrava la pérdida muscular y la expresión de atrogenes en ratones caquécticos portadores del tumor C26. Estos datos apoyan fuertemente la hipótesis de que TP53INP2 regula negativamente la masa del músculo esquelético. Además, proponemos que la represión de TP53INP2 es parte de un mecanismo adaptativo que pretende preservar la masa muscular bajo condiciones de caquexia cancerosa.

Chapter 9 BIBLIOGRAPHY

9. BIBLIOGRAPHY

Acharyya S & Guttridge DC (2007) Cancer cachexia signaling pathways continue to emerge yet much still points to the proteasome. *Clin. Cancer Res.* **13:** 1356–1361

Ahn K, Erlander M, Leturcq D, Peterson PA, Fruh K & Yang Y (1996) In Vivo Characterization of the Proteasome Regulator PA28. *J. Biol. Chem.* **271:** 18237–18242

Albert V & Hall MN (2015) mTOR signaling in cellular and organismal energetics. *Curr. Opin. Cell Biol.* **33C:** 55–66

Anfinsen CB (1973) Principles that Govern the Folding of Protein Chains. *Science* **181:** 223–230

Argilés JM, Busquets S, Stemmler B & López-Soriano FJ (2014) Cancer cachexia: understanding the molecular basis. *Nat. Rev. Cancer* **14:** 754–62

Arndt V, Dick N, Tawo R, Dreiseidler M, Wenzel D, Hesse M, Fürst DO, Saftig P, Saint R, Fleischmann BK, Hoch M & Höhfeld J (2010) Chaperone-assisted selective autophagy is essential for muscle maintenance. *Curr. Biol.* **20:** 143–8

Attaix D, Combaret L, Bechet D & Taillandier D (2008) Role of the ubiquitin-proteasome pathway in muscle atrophy in cachexia. *Curr. Opin. Support. Palliat. Care* **2:** 262–266

Auclair D, Garrel DR, Chaouki Zerouala A & Ferland LH (1997) Activation of the ubiquitin pathway in rat skeletal muscle by catabolic doses of glucocorticoids. *Am. J. Physiol.* **272:** C1007–C1016

Aversa Z, Pin F, Lucia S, Penna F, Verzaro R, Fazi M, Colasante G, Tirone A, Fanelli FR, Ramaccini C, Costelli P, Muscaritoli M, Fearon K, Muscaritoli M, Molfino A, Gioia G, Laviano A, Fanelli FR, Muscaritoli M, Lucia S, et al (2016) Autophagy is induced in the skeletal muscle of cachectic cancer patients. *Sci. Rep.* **6:** 30340

Baehr LM, Furlow JD & Bodine SC (2011) Muscle sparing in muscle RING finger 1 null mice: response to synthetic glucocorticoids. *J. Physiol.* **589:** 4759–76

Baehr LM, Tunzi M & Bodine SC (2014) Muscle hypertrophy is associated with increases in proteasome activity that is independent of MuRF1 and MAFbx expression. *Front. Physiol.* **5:** 69

Bartoccioni P, Rius M, Zorzano A, Palacín M & Chillarón J (2008) Distinct classes of trafficking rBAT mutants cause the type I cystinuria phenotype. *Hum. Mol. Genet.* **17:** 1845–1854

Baugh JM, Viktorova EG & Pilipenko E V (2009) Proteasomes can degrade a significant proportion of cellular proteins independent of ubiquitination. *J. Mol. Biol.* **386:** 814–27

Baumgartner BG, Orpinell M, Duran J, Ribas V, Burghardt HE, Bach D, Villar AV, Paz JC, González M, Camps M, Oriola J, Rivera F, Palacín M & Zorzano A (2007) Identification of a novel modulator of thyroid hormone receptor-mediated action. *PLoS One* **2:** e1183

Bennetts JS, Fowles LF, Butterfield NC, Berkman JL, Teasdale RD, Simpson F & Wicking C (2006) Identification and analysis of novel genes expressed in the mouse embryonic facial primordia. *Front Biosci* **11:** 2631–2646

Bennetts JS, Rendtorff ND, Simpson F, Tranebjaerg L & Wicking C (2007) The coding region of TP53INP2, a gene expressed in the developing nervous system, is not altered in a family with autosomal recessive non-progressive infantile ataxia on chromosome 20q11-q13. *Dev. Dyn.* **236:** 843–852

Beyer A (1997) Sequence analysis of the AAA protein family. *Protein Sci.* **6:** 2043–2058

Bhattacharya A, Schmitz U, Raatz Y, Schönherr M, Schauer M, Franz S, Saalbach A, Anderegg U, Schadendorf D, Simon JC, Magin T, Vera J & Kunz M (2014) miR-638 promotes melanoma metastasis melanoma cells from apoptosis and autophagy and protects. *Oncotarget* **6:** 2966–2980

Blackburn C, Gigstad KM, Hales P, Garcia K, Jones M, Bruzzese FJ, Barrett C, Liu JX, Soucy TA, Sappal DS, Bump N, Olhava EJ, Fleming P, Dick LR, Tsu C, Sintchak MD & Blank JL (2010) Characterization of a new series of non-covalent proteasome inhibitors with exquisite potency and selectivity for the 20S beta5-subunit. *Biochem. J.* **430:** 461–476

Blickwedehl J, Agarwal M, Seong C, Pandita RK, Melendy T, Sung P, Pandita TK & Bangia N (2008) Role for proteasome activator PA200 and postglutamyl proteasome activity in genomic stability. *Proc. Natl. Acad. Sci. U. S. A.* **105:** 16165–16170

Bodine SC, Latres E, Baumhueter S, Lai VK, Nunez L, Clarke BA, Poueymirou WT, Panaro FJ, Na E, Dharmarajan K, Pan ZQ, Valenzuela DM, DeChiara TM, Stitt TN, Yancopoulos GD, Glass DJ, Jagoe RT, Goldberg AL, Cooney RN, Kimball SR, et al (2001) Identification of ubiquitin ligases required for skeletal muscle atrophy. *Science* **294:** 1704–8

Bonaldo P & Sandri M (2013) Cellular and molecular mechanisms of muscle atrophy. *Dis. Model. Mech.* **6:** 25–39

Bossola M, Muscaritoli M, Costelli P, Bellantone R, Pacelli F, Busquets S, Argilès J, Lopez-Soriano FJ, Civello IM, Baccino FM, Rossi Fanelli F & Doglietto GB (2001) Increased muscle ubiquitin mRNA levels in gastric cancer patients. *Am. J. Physiol.* **280:** R1518–23

Bothe GW, Haspel JA, Smith CL, Wiener HH & Burden SJ (2000) Selective expression of Cre recombinase in skeletal muscle fibers. *Genesis* **26:** 165–166

Buchberger A, Bukau B & Sommer T (2010) Protein Quality Control in the Cytosol and the Endoplasmic Reticulum: Brothers in Arms. *Mol. Cell* **40:** 238–252

Burroughs AM, Balaji S, Iyer LM, Aravind L, Glickman M, Ciechanover A, Goldstein G, Scheid M, Hammerling U, Schlesinger D, Niall H, Boyse E, Wilkinson K, Vijay-Kumar S, Bugg C, Cook W, Vijay-Kumar S, Bugg C, Wilkinson K, Cook W, et al (2007) Small but versatile: the extraordinary functional and structural diversity of the β-grasp fold. *Biol. Direct* **2:** 18

Busquets S, Almendro V, Barreiro E, Figueras M, Argilés JM & López-Soriano FJ (2005) Activation of UCPs gene expression in skeletal muscle can be independent on both circulating fatty acids and food intake: Involvement of ROS in a model of mouse cancer cachexia. *FEBS Lett.* **579:** 717–722

Chau V, Tobias JW, Bachmair A, Marriott D, Ecker DJ, Gonda DK & Varshavsky A (1989) A multiubiquitin chain is confined to specific lysine in a targeted short-lived protein. *Science* **243:** 1576–1583

Chen P & Hochstrasser M (1996) Autocatalytic subunit processing couples active site formation in the 20S proteasome to completion of assembly. *Cell* **86:** 961–972

Choi WH, de Poot SAH, Lee JH, Kim JH, Han DH, Kim YK, Finley D & Lee MJ (2016) Open-gate mutants of the mammalian proteasome show enhanced ubiquitin-conjugate degradation. *Nat. Commun.* **7:** 1–12

Ciechanover A (2005) Proteolysis: from the lysosome to ubiquitin and the proteasome. *Nat. Rev. Mol. Cell Biol.* **6:** 79–87

Ciechanover A, Elias S, Heller H, Ferber S & Hershko A (1980) Characterization of the Heat-stable Polypeptide of the ATP- dependent Proteolytic System. *J. Biol. Chem.* **255:** 8–11

Clamp M, Cuff J, Searle SM & Barton GJ (2004) The Jalview Java alignment editor. *Bioinforma. Appl. NOTE* **20:** 426–427

Cohen S, Nathan JA & Goldberg AL (2014) Muscle wasting in disease: molecular mechanisms and promising therapies. *Nat. Rev. Drug Discov.* **14:** 58–74

Cohen S, Zhai B, Gygi SP & Goldberg AL (2012) Ubiquitylation by Trim32 causes coupled loss of desmin, Z-bands, and thin filaments in muscle atrophy. *J. Cell Biol.* **198:** 575–89

Combaret L, Adegoke OAJ, Bedard N, Baracos V, Attaix D & Wing SS (2005) USP19 is a ubiquitin-specific protease regulated in rat skeletal muscle during catabolic states. *Am. J. Physiol. Endocrinol. Metab.* **288:** E693–700

Constantinou C, De Oliveira CCF, Mintzopoulos D, Busquets S, He J, Kesarwani M, Mindrinos M, Rahme LG, Argilés JM & Tzika AA (2011) Nuclear magnetic resonance in conjunction with functional genomics suggests mitochondrial dysfunction in a murine model of cancer cachexia. *Int. J. Mol. Med.* **27:** 15–24

Costelli P, García-Martínez C, Llovera M, Carbó N, López-Soriano FJ, Agell N, Tessitore L, Baccino FM & Argilés JM (1995) Muscle protein waste in tumor-bearing rats is effectively antagonized by a β2-adrenergic agonist (clenbuterol): Role of the ATP-ubiquitin-dependent proteolytic pathway. *J. Clin. Invest.* **95:** 2367–2372

Crosas B, Hanna J, Kirkpatrick DS, Zhang DP, Tone Y, Hathaway NA, Buecker C, Leggett DS, Schmidt M, King RW, Gygi SP & Finley D (2006) Ubiquitin Chains Are Remodeled at the Proteasome by Opposing Ubiquitin Ligase and Deubiquitinating Activities. *Cell* **127:** 1401–1413

Csibi A, Cornille K, Leibovitch M-P, Poupon A, Tintignac LA, Sanchez AMJ & Leibovitch SA (2010) The translation regulatory subunit eIF3f controls the kinase-dependent mTOR signaling required for muscle differentiation and hypertrophy in mouse. *PLoS One* **5:** e8994

Cuervo AM (2004) Autophagy: In sickness and in health. *Trends Cell Biol.* **14:** 70–77

Cuervo AM, Palmer A, Rivett AJ & Knecht E (1995) Degradation of proteasomes by lysosomes in rat liver. *FEBS J.* **227:** 792–800

Dambacher CM, Worden EJ, Herzik MA, Martin A & Lander GC (2016) Atomic structure of the 26S proteasome lid reveals the mechanism of deubiquitinase inhibition. *Elife* **5:** 1–17

Danielsen JMR, Sylvestersen KB, Bekker-Jensen S, Szklarczyk D, Poulsen JW, Horn H, Jensen LJ, Mailand N & Nielsen ML (2011) Mass spectrometric analysis of lysine ubiquitylation reveals promiscuity at site level. *Mol. Cell. Proteomics* **10:**

Demartino GN & Gillette TG (2007) Proteasomes: machines for all reasons. *Cell* **129:** 659–62

Deveraux Q, Ustrell V, Pickart C & Rechsteiner M (1994) A 26 S protease subunit that binds ubiquitin conjugates. *J. Biol. Chem.* **269:** 7059–61

DeWys WD, Malone WF, Butrum RR & Sestili MA (1986) Clinical trials in cancer prevention. *Cancer* **58:** 1954–62

Dikic I, Wakatsuki S & Walters KJ (2009) Ubiquitin-binding domains - from structures to functions. *Nat. Rev. Mol. Cell Biol.* **10:** 659–671

Ding W-X, Ni H-M, Gao W, Yoshimori T, Stolz DB, Ron D & Yin X-M (2007) Linking of autophagy to ubiquitin-proteasome system is important for the regulation of endoplasmic reticulum stress and cell viability. *Am. J. Pathol.* **171:** 513–24

Du J, Wang X, Miereles C, Bailey JL, Debigare R, Zheng B, Price SR & Mitch WE (2004) Activation of caspase-3 is an initial step triggering accelerated muscle proteolysis in catabolic conditions. *J. Clin. Invest.* **113:** 115–23

Dubiel W, Pratt G, Ferrell K & Rechsteiner M (1992) Purification of an 11 S regulator of the multicatalytic protease. *J. Biol. Chem.* **267:** 22369–77

Egerman MA & Glass DJ (2014) Signaling pathways controlling skeletal muscle mass. *Crit. Rev. Biochem. Mol. Biol.* **49:** 59–68

Eley HL, Skipworth RJE, Deans DAC, Fearon KCH & Tisdale MJ (2008) Increased expression of phosphorylated forms of RNA-dependent protein kinase and eukaryotic initiation factor 2alpha may signal skeletal muscle atrophy in weight-losing cancer patients. *Br. J. Cancer* **98:** 443–9

Fearon K, Strasser F, Anker SD, Bosaeus I, Bruera E, Fainsinger RL, Jatoi A, Loprinzi C, MacDonald N, Mantovani G, Davis M, Muscaritoli M, Ottery F, Radbruch L, Ravasco P, Walsh D, Wilcock A, Kaasa S & Baracos VE (2011) Definition and classification of cancer cachexia: an international consensus. *Lancet. Oncol.* **12:** 489–95

Fearon KCH, Glass DJ & Guttridge DC (2012) Cancer cachexia: mediators, signaling, and metabolic pathways. *Cell Metab.* **16:** 153–66

Finley D (2009) Recognition and processing of ubiquitin-protein conjugates by the proteasome. *Annu. Rev. Biochem.* **78:** 477–513

Förster A, Masters EI, Whitby FG, Robinson H & Hill CP (2005) The 1.9 A structure of a proteasome-11S activator complex and implications for proteasome-PAN/PA700 interactions. *Mol. Cell* **18:** 589–99

Fowles LF, Bennetts JS, Berkman JL, Williams E, Koopman P, Teasdale RD & Wicking C (2003) Genomic screen for genes involved in mammalian craniofacial development. *Genesis* **35:** 73–87

Francis VA, Zorzano A & Teleman AA (2010) dDOR is an EcR coactivator that forms a feed-forward loop connecting insulin and ecdysone signaling. *Curr. Biol.* **20:** 1799–808

Fromm-Dornieden C, Lytovchenko O, von der Heyde S, Behnke N, Hogl S, Berghoff J, Köpper F, Opitz L, Renne U, Hoeflich A, Beissbarth T, Brenig B & Baumgartner BG (2012) Extrinsic and intrinsic regulation of DOR/TP53INP2 expression in mice: effects of dietary fat content, tissue type and sex in adipose and muscle tissues. *Nutr. Metab. (Lond).* **9:** 1–11

Funderburk SF, Wang QJ & Yue Z (2010) The Beclin 1-VPS34 complex - at the crossroads of autophagy and beyond. *Trends Cell Biol.* **20:** 355–362

Gaczynska M, Rock KL & Goldberg AL (1993) Gamma-interferon and expression of MHC genes regulate peptide hydrolysis by proteasomes. *Nature* **365:** 264–7

Gamerdinger M, Hajieva P, Kaya AM, Wolfrum U, Hartl FU & Behl C (2009) Protein quality control during aging involves recruitment of the macroautophagy pathway by BAG3. *EMBO J.* **28:** 889–901

Garnham CP, Hanna RA, Chou JS, Low KE, Gourlay K, Campbell RL, Beckmann JS & Davies PL (2009) Limb-girdle muscular dystrophy type 2A can result from accelerated autoproteolytic inactivation of calpain 3. *Biochemistry* **48:** 3457–67

Gnaiger E (2009) Capacity of oxidative phosphorylation in human skeletal muscle: New perspectives of mitochondrial physiology. *Int. J. Biochem. Cell Biol.* **41:** 1837–1845

Goldberg AL (1969) Protein Turnover in Skeletal Muscle I. Protein Catabolism during work-induced hypertrophy and growth induced with growth hormone. *J. Biol. Chem.* **244:** 3217–3222

Gomes A V, Waddell DS, Siu R, Stein M, Dewey S, Furlow JD & Bodine SC (2012) Upregulation of proteasome activity in muscle RING finger 1-null mice following denervation. *FASEB J.* **26:** 2986–99

Gomes A V. (2013) Genetics of proteasome diseases. *Scientifica (Cairo).* **2013:** 1–30

Gomes MD, Lecker SH, Jagoe RT, Navon A & Goldberg AL (2001) Atrogin-1, a muscle-specific F-box protein highly expressed during muscle atrophy. *Proc. Natl. Acad. Sci. U. S. A.* **98:** 14440–5

González-Muñoz E, López-Iglesias C, Calvo M, Palacín M, Zorzano A & Camps M (2009) Caveolin-1 Loss of Function Accelerates Glucose Transporter 4 and Insulin Receptor Degradation in 3T3-L1 Adipocytes. *Endocrinology* **150:** 3493–3502

Goodman C & Hornberger T (2013) Measuring protein synthesis with SUnSET: a valid alternative to traditional techniques? *Exerc. Sport Sci. Rev.* **41:** 107–115

Goodman CA, Mabrey DM, Frey JW, Miu MH, Schmidt EK, Pierre P & Hornberger TA (2011a) Novel insights into the regulation of skeletal muscle protein synthesis as revealed by a new nonradioactive in vivo technique. *FASEB J.* **25:** 1028–39

Goodman CA, Mayhew DL & Hornberger TA (2011b) Recent progress toward understanding the molecular mechanisms that regulate skeletal muscle mass. *Cell. Signal.* **23:** 1896–1906

Grimm S, Ott C, Hörlacher M, Weber D, Höhn A & Grune T (2012) Advanced-glycation-end-product-induced formation of immunoproteasomes: involvement of RAGE and Jak2/STAT1. *Biochem. J.* **448:** 127–39

Groll M, Ditzel L, Löwe J, Stock D, Bochtler M, Bartunik HD & Huber R (1997) Structure of 20S proteasome from yeast at 2.4Å resolution. *Nature* **386:** 463–471

von Haehling S & Anker SD (2010) Cachexia as a major underestimated and unmet medical need: facts and numbers. J. Cachexia. *Sarcopenia Muscle* **1:** 1–5

Hamasaki M, Shibutani ST & Yoshimori T (2013) Up-to-date membrane biogenesis in the autophagosome formation. *Curr. Opin. Cell Biol.* **25:** 455–60

Hara T, Nakamura K, Matsui M, Yamamoto A, Nakahara Y, Suzuki-Migishima R, Yokoyama M, Mishima K, Saito I, Okano H & Mizushima N (2006) Suppression of basal autophagy in neural cells causes neurodegenerative disease in mice. *Nature* **441:** 885–889

Heinemeyer W, Fischer M, Krimmer T, Stachon U & Wolf DH (1997) The active sites of the eukaryotic 20S proteasome and their involvement in subunit precursor processing. *J. Biol. Chem.* **272:** 25200–25209

Hishiya A, Iemura S, Natsume T, Takayama S, Ikeda K & Watanabe K (2006) A novel ubiquitin-binding protein ZNF216 functioning in muscle atrophy. *EMBO J.* **25:** 554–64

Hobler SC, Williams A, Fischer D, Wang JJ, Sun X, Josef E, Hasselgren P, Fischer JE, Scott C & John J (1999) Activity and expression of the 20S proteasome are increased in skeletal muscle during sepsis Activity and expression of the 20S proteasome are increased in skeletal muscle during sepsis. *Am. J. Physiol.* **277:** R434–R440

Hochstrasser M (2000) Evolution and function of ubiquitin-like protein-conjugation systems. *Nat. Cell Biol.* **2:** E153–7

Hoffman L, Pratt G & Rechsteiner M (1992) Multiple forms of the 20 S multicatalytic and the 26 S ubiquitin/ATP-dependent proteases from rabbit reticulocyte lysate. *J. Biol. Chem.* **267:** 22362–8

Hough R, Pratt G & Rechsteiner M (1987) Purification of two high molecular weight proteases from rabbit reticulocyte lysate. *J. Biol. Chem.* **262:** 8303–8313

Huang R, Xu Y, Wan W, Shou X, Qian J, You Z, Liu B, Chang C, Zhou T, Lippincott-Schwartz J & Liu W (2015) Deacetylation of nuclear LC3 drives autophagy initiation under starvation. *Mol. Cell* **57:** 456–66

Huang Y, de Morrée A, van Remoortere A, Bushby K, Frants RR, den Dunnen JT & van der Maarel SM (2008) Calpain 3 is a modulator of the dysferlin protein complex in skeletal muscle. *Hum. Mol. Genet.* **17:** 1855–66

Huang Y & Wang KK (2001) The calpain family and human disease. *Trends Mol. Med.* **7:** 355–62

Huber EM, Basler M, Schwab R, Heinemeyer W, Kirk CJ, Groettrup M & Groll M (2012) Immuno- and constitutive proteasome crystal structures reveal differences in substrate and inhibitor specificity. *Cell* **148:** 727–738

Huber LA & Teis D (2016) Lysosomal signaling in control of degradation pathways. *Curr. Opin. Cell Biol.* **39:** 8–14

Inui A (2008) Cancer anorexia-cachexia syndrome: current issues in research and management. *CA. Cancer J. Clin.* **52:** 72–91

Isasa M, Katz EJ, Kim W, Yugo V, González S, Kirkpatrick DS, Thomson TM, Finley D, Gygi SP & Crosas B (2010) Monoubiquitination of RPN10 Regulates Substrate Recruitment to the Proteasome. *Mol. Cell* **38:** 733–745

Iwata A, Riley BE, Johnston JA & Kopito RR (2005) HDAC6 and Microtubules Are Required for Autophagic Degradation of Aggregated Huntingtin. *J. Biol. Chem.* **280:** 40282–40292

Jacobson AD, MacFadden A, Wu Z, Peng J & Liu C-W (2014) Autoregulation of the 26S proteasome by in situ ubiquitination. *Mol. Biol. Cell* **25:** 1824–35

Jin M, Liu X & Klionsky DJ (2013) SnapShot: Selective Autophagy. *Cell* **152:** 368–368.e2

Johansen T & Lamark T (2011) Selective autophagy mediated by autophagic adapter proteins. *Autophagy* **7:** 279–296

Johnston-Carey HK, Pomatto LCD & Davies KJA (2016) The immunoproteasome in oxidative stress, aging, and disease. *Crit. Rev. Biochem. Mol. Biol.* **9238:** 1–14

Julienne CM, Dumas J-F, Goupille C, Pinault M, Berri C, Collin A, Tesseraud S, Couet C & Servais S (2012) Cancer cachexia is associated with a decrease in skeletal muscle mitochondrial oxidative capacities without alteration of ATP production efficiency. *J. Cachexia. Sarcopenia Muscle* **3:** 265–75

Kettern N, Rogon C, Limmer A, Schild H & Höhfeld J (2011) The Hsc/Hsp70 co-chaperone network controls antigen aggregation and presentation during maturation of professional antigen presenting cells. *PLoS One* **6:** e16398

Khal J, Wyke SM, Russell ST, Hine a V & Tisdale MJ (2005) Expression of the ubiquitin-proteasome pathway and muscle loss in experimental cancer cachexia. *Br. J. Cancer* **93:** 774–780

Khamoui A V & Kim JS (2012) Candidate mechanisms underlying effects of contractile activity on muscle morphology and energetics in cancer cachexia. *Eur. J. Cancer Care (Engl).* **21:** 143–157

Kim W, Bennett EJ, Huttlin EL, Guo A, Li J, Possemato A, Sowa ME, Rad R, Rush J, Comb MJ, Harper JW & Gygi SP (2011) Systematic and quantitative assessment of the ubiquitin-modified proteome. *Mol. Cell* **44:** 325–340

Kisselev AF, Callard A & Goldberg AL (2006) Importance of the different proteolytic sites of the proteasome and the efficacy of inhibitors varies with the protein substrate. *J. Biol. Chem.* **281:** 8582–90

Kisselev AF & Goldberg AL (2005) Monitoring activity and inhibition of 26S proteasomes with fluorogenic peptide substrates. *Methods Enzymol.* **398:** 364–78

Klionsky DJ, Cregg JM, Dunn WA, Emr SD, Sakai Y, Sandoval I V, Sibirny A, Subramani S, Thumm M, Veenhuis M, Ohsumi Y, Abeliovich H, Darsow T, Emr SD, Barth H, Thumm M, Barth H, Meiling-Wesse K, Epple UD, Thumm M, et al (2003) A Unified Nomenclature for Yeast Autophagy-Related Genes. *Dev. Cell* **5:** 539–545

Kobayashi S (2015) Choose Delicately and Reuse Adequately: The Newly Revealed Process of Autophagy. *Biol. Pharm. Bull.* **38:** 1098–1103

Koegl M, Hoppe T, Schlenker S, Ulrich HD, Mayer TU & Jentsch S (1999) A Novel Ubiquitination Factor, E4, Is Involved in Multiubiquitin Chain Assembly. *Cell* **96:** 635–644

Köhler A, Cascio P, Leggett DS, Woo KM, Goldberg AL & Finley D (2001) The axial channel of the proteasome core particle is gated by the Rpt2 ATPase and controls both substrate entry and product release. *Mol. Cell* **7:** 1143–1152

Komatsu M & Ichimura Y (2010) Physiological significance of selective degradation of p62 by autophagy. *FEBS Lett* **584:** 1374–1378

Komatsu M, Waguri S, Chiba T, Murata S, Iwata J, Tanida I, Ueno T, Koike M, Uchiyama Y, Kominami E & Tanaka K (2006) Loss of autophagy in the central nervous system causes neurodegeneration in mice. *Nature* **441:** 880–884

Korolchuk VI, Mansilla A, Menzies FM & Rubinsztein DC (2009a) Autophagy inhibition compromises degradation of ubiquitin-proteasome pathway substrates. *Mol. Cell* **33:** 517–27

Korolchuk VI, Menzies FM & Rubinsztein DC (2009b) A novel link between autophagy and the ubiquitin-proteasome system. *Autophagy* **5:** 862–863

Korolchuk VI, Menzies FM & Rubinsztein DC (2010) Mechanisms of cross-talk between the ubiquitin-proteasome and autophagy-lysosome systems. *FEBS Lett.* **584:** 1393–8

Kudryashova E, Kramerova I & Spencer MJ (2012) Satellite cell senescence underlies myopathy in a mouse model of limb-girdle muscular dystrophy 2H. *J. Clin. Invest.* **122:** 1764–76

Lagirand-Cantaloube J, Offner N, Csibi A, Leibovitch MP, Batonnet-Pichon S, Tintignac LA, Segura CT & Leibovitch SA (2008) The initiation factor eIF3-f is a major target for atrogin1/MAFbx function in skeletal muscle atrophy. *EMBO J.* **27:** 1266–76

Lander GC, Estrin E, Matyskiela ME, Bashore C, Nogales E & Martin A (2012) Complete subunit architecture of the proteasome regulatory particle. *Nature* **482:** 6–13

Lang SM, Kazi AA, Hong-Brown L & Lang CH (2012) Delayed recovery of skeletal muscle mass following hindlimb immobilization in mTOR heterozygous mice. *PLoS One* **7:** 1–14

Lecker SH, Goldberg AL & Mitch WE (2006) Protein degradation by the ubiquitin-proteasome pathway in normal and disease states. *J. Am. Soc. Nephrol.* **17:** 1807–1819

Li HH, Du J, Fan YN, Zhang ML, Liu DP, Li L, Lockyer P, Kang EY, Patterson C & Willis MS (2011) The ubiquitin ligase MuRF1 protects against cardiac ischemia/reperfusion injury by its proteasome-dependent degradation of phospho-c-Jun. *Am. J. Pathol.* **178:** 1043–1058

Li X, Amazit L, Long W, Lonard DM, Monaco JJ & O'Malley BW (2007) Ubiquitin- and ATP-Independent Proteolytic Turnover of p21 by the REGγ-Proteasome Pathway. *Mol. Cell* **26:** 831–842

Linares GR, Xing W, Burghardt H, Baumgartner B, Chen S-T, Ricart W, Fernández-Real JM, Zorzano A & Mohan S (2011) Role of diabetes- and obesity-related protein in the regulation of osteoblast differentiation. *Am. J. Physiol. Endocrinol. Metab.* **301:** E40–8

Lipinszki Z, Kovács L, Deák P & Udvardy A (2012) Ubiquitylation of Drosophila p54/Rpn10/S5a regulates its interaction with the UBA-UBL polyubiquitin receptors. *Biochemistry* **51:** 2461–2470

Liu L Bin, Omata W, Kojima I & Shibata H (2007) The SUMO conjugating enzyme Ubc9 is a regulator of GLUT4 turnover and targeting to the insulin-responsive storage compartment in 3T3-L1 adipocytes. *Diabetes* **56:** 1977–1985

Luan B, Huang X, Wu J, Mei Z, Wang Y, Xue X, Yan C, Wang J, Finley DJ, Shi Y & Wang F (2016) Structure of an endogenous yeast 26S proteasome reveals two major conformational states. *Proc. Natl. Acad. Sci. U. S. A.* **113:** 2642–7

Ma CP, Slaughter CA & DeMartino GN (1992) Identification, purification, and characterization of a protein activator (PA28) of the 20 S proteasome (macropain). *J. Biol. Chem.* **267:** 10515–23

Malik IA, Baumgartner BG, Naz N, Sheikh N, Moriconi F & Ramadori G (2010) Changes in gene expression of DOR and other thyroid hormone receptors in rat liver during acute-phase response. *Cell Tissue Res.* **342:** 261–272

Martinez-Vicente M & Cuervo AM (2007) Autophagy and neurodegeneration: when the cleaning crew goes on strike. *Lancet Neurol.* **6:** 352–61

Mauvezin C, Orpinell M, Francis V a, Mansilla F, Duran J, Ribas V, Palacín M, Boya P, Teleman A a & Zorzano A (2010) The nuclear cofactor DOR regulates autophagy in mammalian and Drosophila cells. *EMBO Rep.* **11:** 37–44

Mauvezin C, Sancho A, Ivanova S, Palacin M & Zorzano A (2012) DOR undergoes nucleo-cytoplasmic shuttling, which involves passage through the nucleolus. *FEBS Lett.* **586:** 3179–3186

McLean JB, Moylan JS & Andrade FH (2014) Mitochondria dysfunction in lung cancer-induced muscle wasting in C2C12 myotubes. *Front. Physiol.* **5:** 503

Mizushima N & Klionsky DJ (2007) Protein turnover via autophagy: implications for metabolism. *Annu Rev Nutr* **27:** 19–40

Mizushima N, Levine B, Cuervo AM & Klionsky DJ (2008) Autophagy fights disease through cellular self-digestion. *Nature* **451:** 1069–75

Mizushima N, Yamamoto A, Matsui M, Yoshimori T & Ohsumi Y (2004) In vivo analysis of autophagy in response to nutrient starvation using transgenic mice expressing a fluorescent autophagosome marker. *Mol. Biol. Cell* **15:** 1101–11

Monaco JJ & McDevitt HO (1984) H-2-linked low-molecular weight polypeptide antigens assemble into an unusual macromolecular complex. *Nature* **309:** 797–799

Moran-Jones K, Grindlay J, Jones M, Smith R & Norman JC (2009) hnRNP A2 regulates alternative mRNA splicing of TP53INP2 to control invasive cell migration. *Cancer Res.* **69:** 9219–27

Morimoto RI & Cuervo AM (2014) Proteostasis and the aging proteome in health and disease. *Journals Gerontol.* **69:** S33–S38

Muñoz JP, Ivanova S, Sánchez-Wandelmer J, Martínez-Cristóbal P, Noguera E, Sancho A, Díaz-Ramos A, Hernández-Alvarez MI, Sebastián D, Mauvezin C, Palacín M & Zorzano A (2013) Mfn2 modulates the UPR and mitochondrial function via repression of PERK. *EMBO J.* **32:** 2348–61

Muscaritoli M, Anker SD, Argilés J, Aversa Z, Bauer JM, Biolo G, Boirie Y, Bosaeus I, Cederholm T, Costelli P, Fearon KC, Laviano A, Maggio M, Rossi Fanelli F, Schneider SM, Schols A & Sieber CC (2010) Consensus definition of sarcopenia, cachexia and pre-cachexia: joint document elaborated by Special Interest Groups (SIG) 'cachexia-anorexia in chronic wasting diseases'; and 'nutrition in geriatrics'. *Clin. Nutr.* **29:** 154–9

Nordgren A, Corcoran M, Sääf A, Bremer A, Kluin-Nelemans HC, Schoumans J & Grandér D (2010) Characterisation of hairy cell leukaemia by tiling resolution array-based comparative Genome hybridisation: A series of 13 cases and review of the literature. *Eur. J. Haematol.* **84:** 17–25

Nowak J, Archange C, Tardivel-Lacombe J, Pontarotti P, Pebusque M-J, Vaccaro MI, Velasco G, Dagorn J-C & Iovanna JL (2009) The TP53INP2 protein is required for autophagy in mammalian cells. *Mol. Biol. Cell* **20:** 870–881

Nowak J, Depetris D, Iovanna JL, Mattei MG & Pebusque MJ (2005) Assignment of the tumor protein p53 induced nuclear protein 2 (TP53INP2) gene to human chromosome band 20q11.2 by in situ hybridization. *Cytogenet Genome Res* **108:** 362

Okita Y & Nakayama KI (2012) UPS delivers pluripotency. *Cell Stem Cell* **11:** 728–30

Orlowski M (1990) The multicatalytic proteinase complex, a major extralysosomal proteolytic system. *Biochemistry* **29:** 10289–97

Orlowski M, Cardozo C & Michaud C (1993) Evidence for the presence of five distinct proteolytic components in the pituitary multicatalytic proteinase complex. Properties of two components cleaving bonds on the carboxyl side of branched chain and small neutral amino acids. *Biochemistry* **32:** 1563–72

Orpinell M (2006) Molecular Mechanisms of DOR action. *PhD Thesis*, University of Barcelona, Barcelona.

Otaegui PJ, Ferre T, Riu E & Bosch F (2003) Prevention of obesity and insulin resistance by glucokinase expression in skeletal muscle of transgenic mice. *FASEB J.* **17:** 2097–2099

Pandey UB, Nie Z, Batlevi Y, McCray BA, Ritson GP, Nedelsky NB, Schwartz SL, DiProspero NA, Knight MA, Schuldiner O, Padmanabhan R, Hild M, Berry DL, Garza D, Hubbert CC, Yao

T-P, Baehrecke EH & Taylor JP (2007) HDAC6 rescues neurodegeneration and provides an essential link between autophagy and the UPS. *Nature* **447:** 859–63

Pankiv S, Lamark T, Bruun J-A, Øvervatn A, Bjørkøy G & Johansen T (2010) Nucleocytoplasmic shuttling of p62/SQSTM1 and its role in recruitment of nuclear polyubiquitinated proteins to promyelocytic leukemia bodies. *J. Biol. Chem.* **285:** 5941–53

Pathare GR, Nagy I, Bohn S, Unverdorben P, Hubert A, Körner R, Nickell S, Lasker K, Sali A, Tamura T, Nishioka T, Förster F, Baumeister W & Bracher A (2012) The proteasomal subunit Rpn6 is a molecular clamp holding the core and regulatory subcomplexes together. *Proc. Natl. Acad. Sci. U. S. A.* **109:** 149–54

Paul PK, Gupta SK, Bhatnagar S, Panguluri SK, Darnay BG, Choi Y & Kumar A (2010) Targeted ablation of TRAF6 inhibits skeletal muscle wasting in mice. *J. Cell Biol.* **191:** 1395–411

Peng J, Schwartz D, Elias JE, Thoreen CC, Cheng D, Marsischky G, Roelofs J, Finley D & Gygi SP (2003) A proteomics approach to understanding protein ubiquitination. *Nat. Biotechnol.* **21:** 921–6

Penna F, Busquets S & Argilés JM (2015) Experimental cancer cachexia: Evolving strategies for getting closer to the human scenario. *Semin. Cell Dev. Biol.*

Penna F, Busquets S, Pin F, Toledo M, Baccino FM, López-Soriano FJ, Costelli P & Argilés JM (2011) Combined approach to counteract experimental cancer cachexia: eicosapentaenoic acid and training exercise. *J. Cachexia. Sarcopenia Muscle* **2:** 95–104

Penna F, Costamagna D, Pin F, Camperi A, Fanzani A, Chiarpotto EM, Cavallini G, Bonelli G, Baccino FM & Costelli P (2013) Autophagic degradation contributes to muscle wasting in cancer cachexia. *Am. J. Pathol.* **182:** 1367–78

Petruzzelli M, Schweiger M, Schreiber R, Campos-Olivas R, Tsoli M, Allen J, Swarbrick M, Rose-John S, Rincon M, Robertson G, Zechner R & Wagner EF (2014) A Switch from White to Brown Fat Increases Energy Expenditure in Cancer-Associated Cachexia. *Cell Metab.* **20:** 1–15

Pickart CM (2001) Mechanisms Underlying Ubiquitination. *Annu. Rev. Biochem.* **70:** 503–33

Pickart CM (2004) Back to the Future with Ubiquitin. *Cell* **116:** 181–190

Pickart CM & Fushman D (2004) Polyubiquitin chains: Polymeric protein signals. *Curr. Opin. Chem. Biol.* **8:** 610–616

Pickering AM & Davies KJA (2012a) Degradation of damaged proteins: The main function of the 20S proteasome. *Prog. Mol. Biol. Transl. Sci.* **109:** 227–248

Pickering AM & Davies KJA (2012b) Differential roles of proteasome and immunoproteasome regulators Pa28αβ, Pa28γ and Pa200 in the degradation of oxidized proteins. *Arch. Biochem. Biophys.* **523:** 181–90

Pin F, Busquets S, Toledo M, Camperi A, Lopez-Soriano FJ, Costelli P, Argiles JM & Penna F (2015) Combination of exercise training and erythropoietin prevents cancer-induced muscle alterations. *Oncotarget* **6:** 43202–43215

Pizon V, Rybina S, Gerbal F & Delort F (2013) MURF2B, a novel LC3-binding protein, participates with MURF2A in the switch between autophagy and ubiquitin proteasome system during differentiation of. *PLoS One* **8:** 1–21

Qiao L & Zhang J (2009) Inhibition of lysosomal functions reduces proteasomal activity. *Neurosci. Lett.* **456:** 15–9

Raiborg C & Stenmark H (2009) The ESCRT machinery in endosomal sorting of ubiquitylated membrane proteins. *Nature* **458:** 445–52

Realini C, Jensen CC, Zhang Z, Johnston SC, Knowlton JR, Hill CP & Rechsteiner M (1997) Characterization of recombinant REGalpha, REGbeta, and REGgamma proteasome activators. *J. Biol. Chem.* **272:** 25483–92

Richard I, Broux O, Allamand V, Fougerousse F, Chiannilkulchai N, Bourg N, Brenguier L, Devaud C, Pasturaud P & Roudaut C (1995) Mutations in the proteolytic enzyme calpain 3 cause limb-girdle muscular dystrophy type 2A. *Cell* **81:** 27–40

Rosenthal N, Kornhausert JM, Donoghue M, Rosent KM & Merliet JP (1989) Myosin light chain enhancer activates muscle-specific, developmentally regulated gene expression in transgenic mice. *Biochemistry* **86:** 7780–7784

Roth DM & Balch WE (2011) Modeling general proteostasis: Proteome balance in health and disease. *Curr. Opin. Cell Biol.* **23:** 126–134

Sala D, Ivanova S, Plana N, Ribas V, Duran J, Bach D, Turkseven S, Laville M, Vidal H, Karczewska-Kupczewska M, Kowalska I, Straczkowski M, Testar X, Palacín M, Sandri M, Serrano AL & Zorzano A (2014) Autophagy-regulating TP53INP2 mediates muscle wasting and is repressed in diabetes. *J. Clin. Invest.* **124:** 1914–27

Sancho A (2011) DOR and TP53INP1 are dual regulators for autophagy and transcription. *PhD Thesis*, University of Barcelona, Barcelona.

Sancho A, Duran J, García-España A, Mauvezin C, Alemu E a, Lamark T, Macias MJ, DeSalle R, Royo M, Sala D, Chicote JU, Palacín M, Johansen T & Zorzano A (2012) DOR/Tp53inp2

and Tp53inp1 constitute a metazoan gene family encoding dual regulators of autophagy and transcription. *PLoS One* **7:** e34034

Sandri M (2013) Protein breakdown in muscle wasting: role of autophagy-lysosome and ubiquitin-proteasome. *Int. J. Biochem. Cell Biol.* **45:** 2121–9

Sartori R, Schirwis E, Blaauw B, Bortolanza S, Zhao J, Enzo E, Stantzou A, Mouisel E, Toniolo L, Ferry A, Stricker S, Goldberg AL, Dupont S, Piccolo S, Amthor H & Sandri M (2013) BMP signaling controls muscle mass. *Nat. Genet.* **45:** 1309–18

Schiaffino S, Dyar KA, Ciciliot S, Blaauw B & Sandri M (2013) Mechanisms regulating skeletal muscle growth and atrophy. *FEBS J.* **280:** 4294–4314

Schmidt EK, Clavarino G, Ceppi M & Pierre P (2009) SUnSET, a nonradioactive method to monitor protein synthesis. *Nat. Methods* **6:** 275–7

Schmidt M, Haas W, Crosas B, Santamaria PG, Gygi SP, Walz T & Finley D (2005) The HEAT repeat protein Blm10 regulates the yeast proteasome by capping the core particle. *Nat. Struct. Mol. Biol.* **12:** 294–303

Sijts A, Sun Y, Janek K, Kral S, Paschen A, Schadendorf D & Kloetzel PM (2002) The role of the proteasome activator PA28 in MHC class I antigen processing. *Mol. Immunol.* **39:** 165–9

Sinis N, Guntinas-Lichius O, Irintchev A, Skouras E, Kuerten S, Pavlov SP, Schaller HE, Dunlop SA & Angelov DN (2008) Manual stimulation of forearm muscles does not improve recovery of motor function after injury to a mixed peripheral nerve. *Exp. Brain Res.* **185:** 469–483

Smith KL & Tisdale MJ (1993) Increased protein degradation and decreased protein synthesis in skeletal muscle during cancer cachexia. *Br. J. Cancer* **67:** 680–5

Sou Y, Waguri S, Iwata J, Ueno T, Fujimura T, Hara T, Sawada N, Yamada A, Mizushima N, Uchiyama Y, Kominami E, Tanaka K & Komatsu M (2008) The Atg8 conjugation system is indispensable for proper development of autophagic isolation membranes in mice. *Mol. Biol. Cell* **19:** 4762–4775

Stewart GD, Skipworth RJE & Fearon KCH (2006) Cancer cachexia and fatigue. *Clin. Med. J. R. Coll. Physicians London* **6:** 140–143

Strucksberg K-H, Tangavelou K, Schröder R & Clemen CS (2010) Proteasomal activity in skeletal muscle: a matter of assay design, muscle type, and age. *Anal. Biochem.* **399:** 225–9

Taicher GZ, Tinsley FC, Reiderman A & Heiman ML (2003) Quantitative magnetic resonance (QMR) method for bone and whole-body-composition analysis. *Anal. Bioanal. Chem.* **377:** 990–1002

Tanaka K (2013) The Proteasome: From Basic Mechanisms to Emerging Roles. *Keio J. Med.* **62:** 1–12

Tanaka K, Mizushima T & Saeki Y (2012) The proteasome : molecular machinery and pathophysiological roles. *Biol. Chem.* **393:** 217–234

Tanida I, Minematsu-Ikeguchi N, Ueno T & Kominami E (2005) Lysosomal turnover, but not a cellular level, of endogenous LC3 is a marker for autophagy. *Autophagy* **1:** 84–91

Tasdemir E, Galluzzi L, Maiuri MC, Criollo A, Vitale I, Hangen E, Modjtahedi N & Kroemer G (2008) Methods for assessing autophagy and autophagic cell death. *Methods Mol. Biol.* **445:** 29–76

Thrower JS, Hoffman L, Rechsteiner M & Pickart CM (2000) Recognition of the polyubiquitin proteolytic signal. *EMBO J.* **19:** 94–102

Tooze SA & Yoshimori T (2010) The origin of the autophagosomal membrane. *Nat. Cell Biol.* **12:** 831–835

Tzika A., Fontes-Oliveira CC, Shestov AA, Constantinou C, Psychogios N, Righi V, Mintzopoulos D, Busquets S, Lopez-Soriano FJ, Milot S, Lepine F, Mindrinos MN, Rahme LG & Argiles JM (2013) Skeletal muscle mitochondrial uncoupling in a murine cancer cachexia model. *Int. J. Oncol.* **43:** 886–894

Udvardy A (1993) Purification and characterization of a multiprotein component of the Drosophila 26 S (1500 kDa) proteolytic complex. *J. Biol. Chem.* **268:** 9055–62

Ulbricht A (2013) Tension-induced autophagy. *Autophagy* **9:** 920–922

Ulrich HD & Walden H (2010) Ubiquitin signalling in DNA replication and repair. *Nat. Rev. Mol. cell Biol.* **11:** 479–489

Ustrell V, Hoffman L, Pratt G & Rechsteiner M (2002) Pa200, a nuclear proteasome activator involved in DNA repair. *EMBO J.* **21:** 3516–3525

Vary TC, Frost RA & Lang CH (2008) Acute alcohol intoxication increases atrogin-1 and MuRF1 mRNA without increasing proteolysis in skeletal muscle. *Am. J. Physiol.* **294:** R1777–R1789

Veksler VI, Kuznetsov A V., Sharov VG, Kapelko VI & Saks VA (1987) Mitochondrial respiratory parameters in cardiac tissue: A novel method of assessment by using saponin-skinned fibers. *Biochim. Biophys. Acta - Bioenerg.* **892:** 191–196

Ventii KH & Wilkinson KD (2008) Protein partners of deubiquitinating enzymes. *Biochem. J.* **414:** 161–75

Vigano A, Del Fabbro E, Bruera E & Borod M (2012) The cachexia clinic: from staging to managing nutritional and functional problems in advanced cancer patients. *Crit. Rev. Oncog.* 17: 293–303

Vilchez D, Boyer L, Morantte I, Lutz M, Merkwirth C, Joyce D, Spencer B, Page L, Masliah E, Berggren WT, Gage FH & Dillin A (2012) Increased proteasome activity in human embryonic stem cells is regulated by PSMD11. *Nature* **489:** 304–8

Wagner SA, Beli P, Weinert BT, Nielsen ML, Cox J, Mann M & Choudhary C (2011) A Proteome-wide, Quantitative Survey of In Vivo Ubiquitylation Sites Reveals Widespread Regulatory Roles. *Mol. Cell. Proteomics* **10:**

Wang XJ, Yu J, Wong SH, Cheng ASL, Chan FKL, Ng SSM, Cho CH, Sung JJY & Wu WKK (2013) A novel crosstalk between two major protein degradation systems: regulation of proteasomal activity by autophagy. *Autophagy* **9:** 1500–8

Waxman L, Fagan JM & Goldberg AL (1987) Demonstration of two distinct high molecular weight proteases in rabbit reticulocytes, one of which degrades ubiquitin conjugates. *J. Biol. Chem.* **262:** 2451–7

Wesselborg S & Stork B (2015) Autophagy signal transduction by ATG proteins: From hierarchies to networks. *Cell. Mol. Life Sci.* **72:** 4721–4757

Wing SS (2013) Deubiquitinases in skeletal muscle atrophy. Int. J. Biochem. *Cell Biol.* **45:** 2130–5

Witt CC, Witt SH, Lerche S, Labeit D, Back W & Labeit S (2008) Cooperative control of striated muscle mass and metabolism by MuRF1 and MuRF2. *EMBO J.* **27:** 350–60

Wiznerowicz M & Trono D (2003) Conditional suppression of cellular genes: lentivirus vector-mediated drug-inducible RNA interference. *J. Virol.* **77:** 8957–61

Wong E & Cuervo AM (2010) Integration of clearance mechanisms: the proteasome and autophagy. *Cold Spring Harb. Perspect. Biol.* **2:** 1–19

Wu WKK, Sakamoto KM, Milani M, Aldana-Masankgay G, Fan D, Wu K, Lee CW, Cho CH, Yu J & Sung JJY (2010) Macroautophagy modulates cellular response to proteasome inhibitors in cancer therapy. *Drug Resist. Updat.* **13:** 87–92

Xu Y, Wan W, Shou X, Huang R, You Z, Shou Y, Wang L, Zhou T & Liu W (2016) TP53INP2/DOR, a mediator of cell autophagy, promotes rDNA transcription via facilitating the assembly of the POLR1/RNA polymerase I preinitiation complex at rDNA promoters. *Autophagy* **12:** 1118–1128

Zangarelli A, Chanseaume E, Morio B, Brugere C, Mosoni L, Rousset P, Giraudet C, Patrac V, Gachon P, Boirie Y & Walrand S (2006) Synergistic effects of caloric restriction with maintained protein intake on skeletal muscle performance in 21-month-old rats: a mitochondria-mediated pathway. *FASEB J.* **20:** 2439–2450

Zhang G, Jin B & Li Y-P (2011) C/EBPβ mediates tumour-induced ubiquitin ligase atrogin1/MAFbx upregulation and muscle wasting. *EMBO J.* **30:** 4323–4335

Zhang Y, Nicholatos J, Dreier JR, Ricoult SJH, Widenmaier SB, Hotamisligil GS, Kwiatkowski DJ & Manning BD (2014) Coordinated regulation of protein synthesis and degradation by mTORC1. *Nature* **513:** 440–443

Zhao J, Brault JJ, Schild A, Cao P, Sandri M, Schiaffino S, Lecker SH & Goldberg AL (2007) FoxO3 coordinately activates protein degradation by the autophagic/lysosomal and proteasomal pathways in atrophying muscle cells. *Cell Metab.* **6:** 472–83

APPENDIX I

Appendix I

APPENDIX I

I. TP53INP2 monoclonal antibody generation

In collaboration with Pablo Engel's laboratory (IDIBAPS-Hospital Clinic, Barcelona), we have generated monoclonal antibodies to detect the protein of our study, TP53INP2, because the commercial ones and the polyclonal antibody generated previously in our laboratory recognized non-specific bands.

In order to produce the monoclonal antibody against TP53INP2, we have followed the protocol below reviewed by the EuroMAbNet members (https://www.euromabnet.com/). The steps required for the production of the monoclonal antibody include: immunization, hybridoma production, screening, cloning, expanding and freezing down hybridomas and antibody validation.

I.1. Immunization

Immunization is necessary to present an antigen in a suitable form to induce the most vigorous humoral immune response to an animal. This essential step results in the production of cells secreting antibody against the chosen antigen.

The antigen concentration that we used for the immunization of the mice was 40 µg (peptide + carrier) per injection except for the final boost when 100-200 µg should be used. The sequence of the peptide was SPPAPSLMDESWFVTPPAC (Figure A1). The antigen was diluted in 150-200 µl of PBS; this solution will be named "antigen" (Ag).

At least, three immunizations were done per animal in intervals of 15 days between each one. The first immunization was done with the antigen and the complete Freund's adjuvant; next ones with the antigen and incomplete Freund's adjuvant, and the last one only with the antigen. The proportion antigen:adjuvant is 1:1.

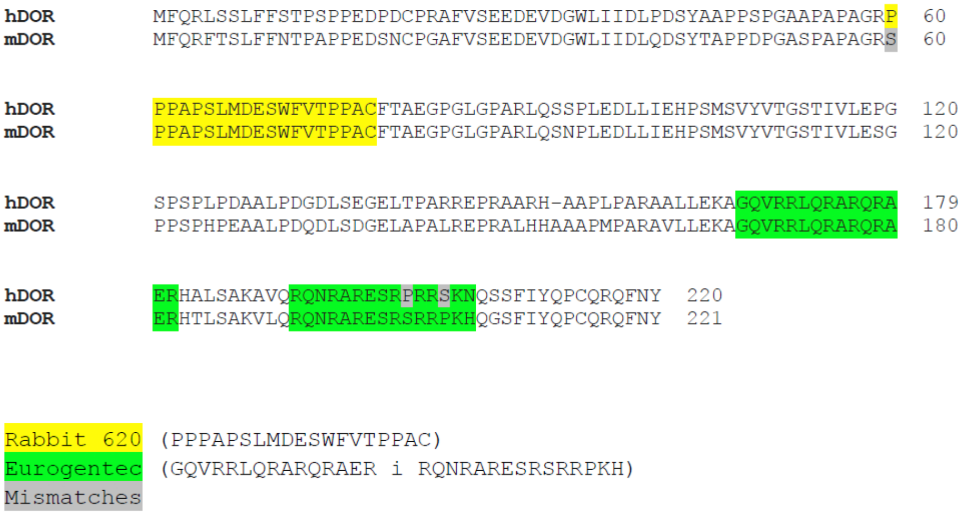

Figure A1. Sequence of human and mouse TP53INP2. In yellow it is remarked the peptide used for mice immunization, which is the same utilized in the past for the generation of the polyclonal antibody in our laboratory (Rabbit 620). In green it is selected peptides used for designing the polyclonal antibodies by Eurogentec in the past.

Adjuvants

The two main adjuvants that we used were complete (CFA) or incomplete (IFA) Freund's adjuvant (BD Difco 263810 and BD Difco 263910). CFA is a mineral oil containing a suspension of whole or pulverized heat-killed mycobacteria. When emulsified together with a solution of the antigen of interest to form a water-in-oil emulsion, CFA is effective in potentiating both cellular and humoral immune responses to the injected antigen. For most applications, CFA is usually only necessary for the initial immunization, while Incomplete Freund's Adjuvant (IFA), which lacks mycobacteria, is the adjuvant of choice for subsequent immunizations.

In our experiment, we immunize three mice. The immunization schedule is explained below:

1st day

- Dilute the antigen in 150 µl-200 µl of sterile PBS for each animal. Mix the antigen with 150 µl-200 µl of the adjuvant. The volume to be injected should be no more than 300 µl per mouse.

- Vortex the eppendorf to resuspend the adjuvant and to form an emulsion between the aqueous antigen and oil-based adjuvant. The solution should be uniformly white at this stage with no separation into two layers.
- Draw the solution into 1.0 ml syringe.
- Inject two BALB/c female mice intraperitoneally with a 23 or 25 gauge needle on the syringe.

10^{th} to 15^{th} day

- Repeat the injection.

20^{th} to 30^{th} day

- The injection this time should contain antigen in sterile PBS only (no adjuvant). This injection will be administered intraperitoneally.

30^{th} to 40^{th} day

- Collect a tail bleed from the immunised mice. Allow the blood to clot. Make serial dilutions of the resulting serum in PBS.
- Test the mouse serum samples in an ELISA against the antigen and/or another staining technique. The results should be compared with those obtained using similar dilution of normal mouse serum. This step will enable you to check if the animals have recognized the antigen and identify which mouse has the best immune response. When the title is ≥ 1/40000, means that the immunization is well done.
- Leave at least 3 weeks between the third injection and the final antigen boost before performing the fusion.
- Administer the final boost intravenously or intraperitoneally three or four days before the fusion day.
- This final boost can contain between 100-200 μg of antigen diluted in 150 μl of sterile PBS.
- Three to four days after the final boost you should sacrifice the mouse, remove the spleen aseptically and place it in a sterile container containing 5 ml medium.
- Proceed with the fusion technique.

I.2. Hybridoma production

A hybridoma is a cell line arising from one hybrid cell that is capable of secreting a monoclonal antibody specific to one epitope of your antigen permanently in culture. The hybrid cell is produced through the fusion of specific antibody producing B-cell from an immunized animal (usually a mouse, rat or rabbit; in this case a mouse) and which has a finite lifespan, with a cell from an "immortal" cultured myeloma cell line (e.g. mouse NS-1 or NS-0).

During the fusion process, B cells are isolated from the mouse spleen, mixed with the mouse myeloma cell line and fusion is induced with polyethylene glycol (PEG). The resulting hybridomas are then cultured in tissue culture medium containing Hypoxathine, Aminopterin, Thymidine (HAT), a step which kills any unfused myeloma cells that might outgrow the other weaker hybridoma cells. Unfused B cells have limited powers of division and will die off naturally in culture. Ten days after the fusion process, culture supernatant is collected and tested for the presence of the desired antibody (Figure A2).

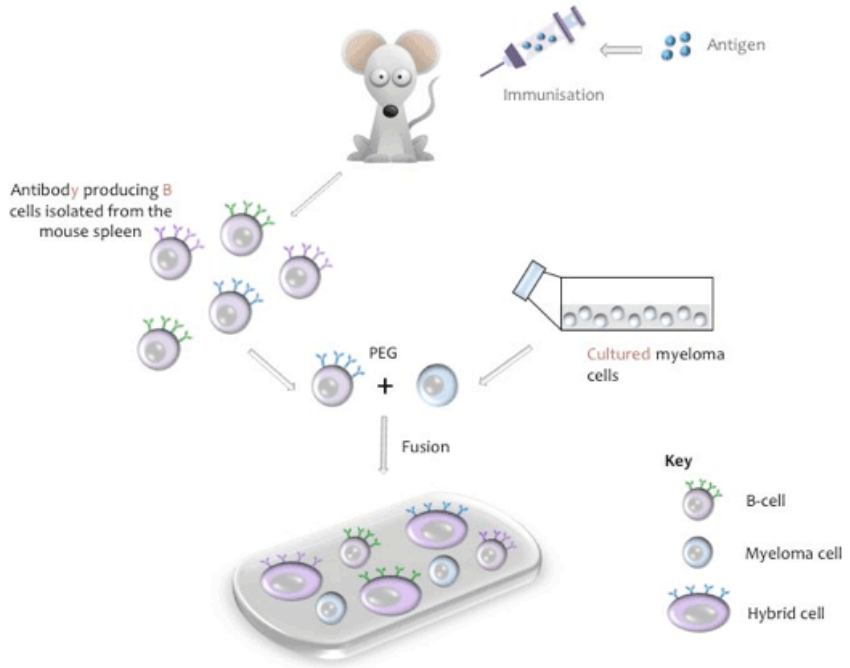

Figure A2. Schematic representation of cell fusion (https://www.euromabnet.com/).

Medium and other reagents

- RPMI medium (Sigma, R0883)
- Fetal Bovine Serum (Linus, 91S1700)
- Penicillin-Streptomycin (Biowest, L0022)
- L-Glutamina (Biowest, X0550)
- HAT (Hypoxathine, Aminopterin, Thymidine) (Sigma, H0262)
- HFCS (Hybridoma Fusion and Clonning Supplement) (Roche, 11 363 735 001)
- PEG (Sigma, P7181)
- Forane
- mHAT+HFCS:
  - 388 ml RPMI
  - 100 ml Fetal Bovine Serum
  - 5 ml Penicillin-Streptomycin
  - 5 ml L-Glutamina
  - 10 ml HAT*
    - 2.5 ml HFCS

The fusion process

Three days before - Prepare the myeloma cells for the fusion

The myeloma cells need to be in exponential growth phase when you use them. However if you set up two 75 cm^2 flasks of your myeloma cells, one at a dilution of 1:40 and one at 1:60, three days before the fusion, one of the flasks should be ideal on the day of fusion. We should have 30-40 x 10^6 cells for the day of the fusion.

One day before - prepare the medium

The following need to be made and pre-warmed to 37ºC (overnight).

- RPMI
- mHAT+HFCS
- PEG transferred to a foil wrapped (PEG is light sensitive) sterile universal

- A mini waterbath, made from a 200 ml beaker containing about 100 ml distilled water and crossed with tape wide enough so that there is an aperture to hold a 50 ml Falcon tube upright

Day of the fusion

- Kill the mouse (following institutional guidelines), extract the spleen and put it in a sterile container containing 10 ml of RPMI.

All subsequent steps must be performed in a laminar flow hood.

- Put the spleen and medium into a petri dish.
- Move the spleen with sterile forceps to wash it. Remove any adhesions and transfer the spleen to a second petri dish. Cut the spleen into two. Hold one half with blunt forceps and using another pair of curved forceps, gently tease the cells out from the spleen capsule, being careful to remove as many cells as possible. Repeat using the second half of spleen.
- Remove the spleen capsule debris and, using a sterile Pasteur pipette, mix the cells well but very gently.
- Transfer the cell suspension to a 15 ml tube and use another 5 ml of RPMI to rinse the petri dish and add to the spleen cells in the tube.
- Count the myeloma and spleen cells. You need a ratio of 1 myeloma cell to every 4 spleen cells.
- Add the myeloma cells to a 50 ml conical tube.
- Centrifuge both the spleen cells (15 ml tube) and the myeloma cells in (50 ml tube) for 1000 rpm for 10 minutes.
- Very carefully pour off the supernatant of both tubes and gently resuspend the pellets each in 10 mls of medium RPMI. The absence of FBS until the fusion process is completed is extremely important as cells will not fuse if there is FBS present.
- Combine the resuspended spleen cell and myeloma pellets into one 50 ml centrifuge tube.
- Centrifuge for 10 minutes at 1000 rpm. Very carefully pour off as much supernatant as possible. Resuspend the pellet by softly tapping the tube on the bench.

Do not flick the pellet or pipette it as this will distribute cells up around the tube reducing cell numbers that are available for fusing.

- Place the tube in the homemade water bath. Add 1.2 ml of PEG drop by drop over one minute, stirring gently every few drops.
- Add 1 ml of RPMI, drop by drop over one minute, stirring gently every few drops.
- Add first a further 2 ml of RPMI, next 5 ml, 10 ml and 20 ml, drop by drop stirring gently every few drops.
- Centrifuge the tube of cells for 10 minutes at 1000 rpm.
- Very carefully decant the supernatant and resuspend the cell pellet in medium mHAT+HFCS. The final volume will depend on the number of 96-well plates that we use taking into account that each well will have a volume of 200 µl.
- Put 200 µl of this suspension into each well of 96-well plates.
- Leave the plates in the incubator overnight (roughly 24 hours).

I.3. Screening by Elisa

After the fusion, leave the plates in the incubator. The colonies will appear between 7 to 10 days (Figure A3). In order to do a screening and select the positive clones, it is needed to carry out an enzyme-linked immuno-absorbant assay (ELISA). Once the positive clones are selected, they will be cultured in 24-wells plates.

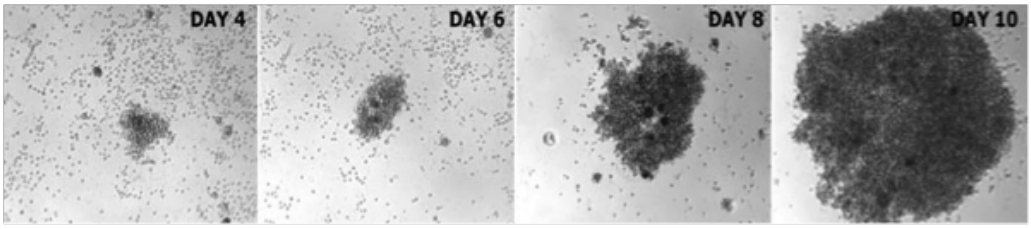

Figure A3. Growth of the colonies of hybridomas 4, 6, 8 and 10 days after the fusion (https://www.euromabnet.com/).

I.4. Cloning method

The objective of cloning the cells producing the antibody of interest is to ensure that the desired hybridoma cell line produced is obtained from an isolated single fused cell. After a fusion, many different hybrid cells will be present in a single well resulting in the growth of multiple colonies in each well. The specific antibody-secreting colony is therefore likely to be mixed with other cells that are either non-secreting or which are producing an antibody of undesired specificity.

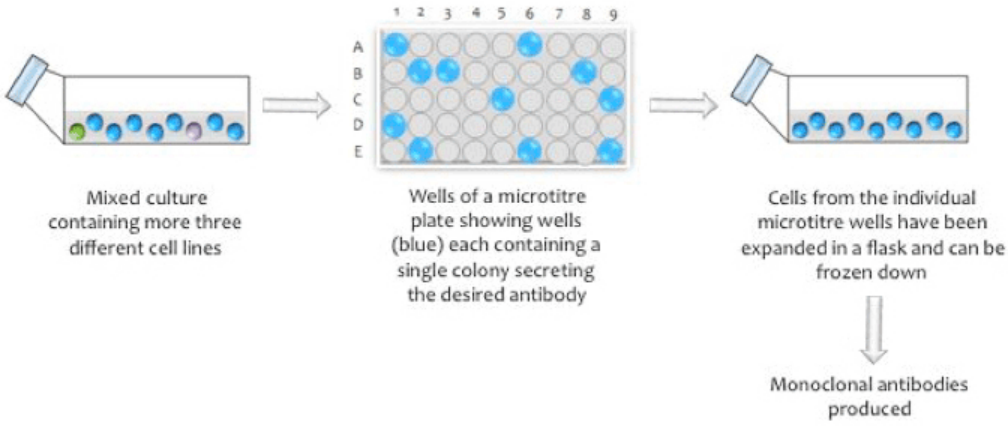

Figure A4. Outline showing the various major stages of the cloning methodology (https://www.euromabnet.com/).

The method that we use for cloning is that of limiting dilutions. This means you dilute the cells to a concentration calculated so that each well of a 96 well plate will contain one, two or no cells after plating out (Figure A4). Once the cells have begun growing to form a clone, you can view each well under the microscope and discount any well with more than one clone or no clones at all.

The cloning methodology must take into account the following steps:

- Test only single clones.
- Expand the positive clones slowly moving them into 2 ml wells still using the cloning medium. Do not mix the contents of the different original microtitre well contents as these constitute potential different cell lines.
- Expand them gradually (do not rush them), into small flasks.

Appendix I

- It is advisable to retest the supernatant at this point to ensure that the hybridoma cells are still secreting the required antibody.
- Freeze down the hybridoma cell lines.
- If you are not sure if the positive well was a single clone you must reclone the line a second time until you are sure you have achieved a cell line that has been cloned from a single cell.

In our case, after checking 8 plates of 96 wells, we selected 71 supernatants to verify the positive clones (Figure A5). From this selection, we did a screening by western blot, where we selected the clones number 15, 34, 80, 374, 455, 456, 470 and 652 (Figure A6).

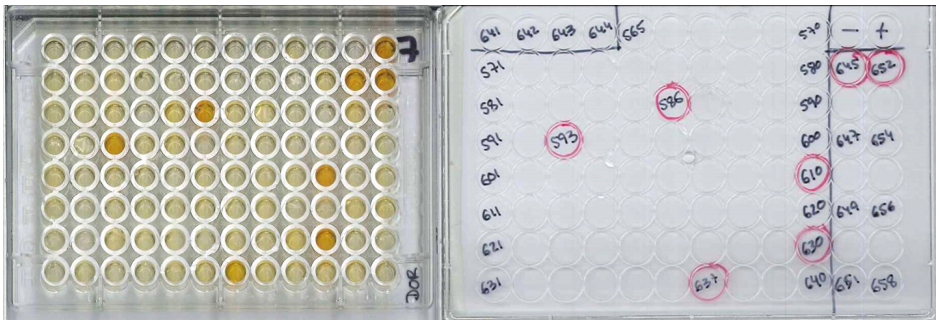

Figure A5. Example of a microtitre plate for the cloning methodology. Stronger yellow wells contain a single colony secreting the desired antibody. Circles in red refers to selected positive clones (Photo by Adriana Lázaro, IDIBAPS).

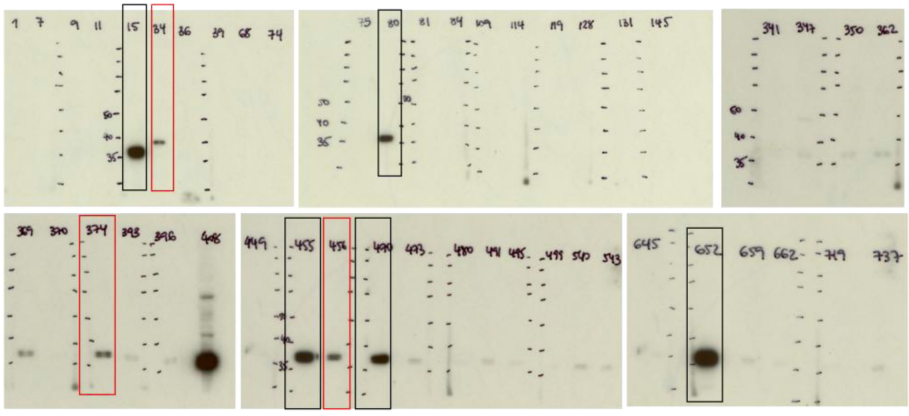

Figure A6. Screening by western blot analysis of the positive clones of the TP53INP2 antibody in Hela cells (total cell extracts) transfected with TP53INP2. Black squares refers to the ones with highest protein expression, and red squares to lower protein expression

I. 5. Production of large quantities of monoclonal antibody

In principle there are two ways to produce large quantities of antibody. We have used the technique of "slow adaptation", this option, although is not as fast as the other option, generates higher concentration of antibody than in the "fast method".

To achieve this, culture the hybridomas in normal medium containing FBS (5-10%). Since FBS contains minute amounts of IgG (depending on the batch but usually 100 μg/ml) this can interfere with subsequent labeling of the antibody.

Decrease the percentage of FBS slowly from 10 to 8; 6; 4; 2; 1 %. This can take several weeks but depends on the hybridoma. Collect the cells from the 1% FBS culture and suspend them in PFHM (Protein Free Hybridoma Medium) (Thermo Scientific). Cells sometimes go through crises but eventually start growing in this medium. Collect the quantity needed. Check for the concentration: it should be approximately the same as in FBS cultures (Usually 1-50 μg/ml).

Currently, for processing the supernatant containing the antibodies, in the laboratory of Pablo Engel, they are carrying out the purification of the monoclonal antibody by protein A chromatography following the instruction of the Affi-Prep Protein A MAPS II kit, using MAPS II buffers (BioRad). At the end of the process, the purified antibody will have high salt concentration; because of that, dialization against PBS will be necessary using the Slide-A-Lyzer™ Dialysis Cassettes (Thermofisher, 66455 or 66453).

I.6. Antibody validation

Before proceeding with the step of the purification, the antibody validation was carried out with the supernatants of the most positive clones that were identified in Figure A6. The clone number 15 was chosen. Here it is showed the antibody validation by Western blot (Figure A7 and Figure A8) and by immunofluorescence (Figure A9).

Appendix I

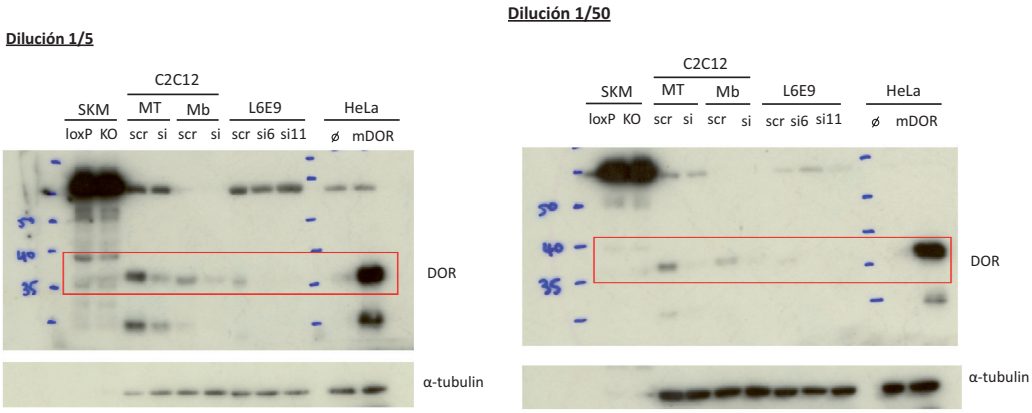

Figure A7. Screening by western blot of the positive clone number "15" of the monoclonal TP53INP2 antibody in a dilution 1/5 (A) and 1/50 (B). Protein expression is checked in skeletal muscle of loxP and KO mice (lane 1 and 2), in C2C12 myotubes scr and si cells (lane 3 and 4), C2C12 myoblasts scr and si cells (lane 5 and 6), L6E9 myoblasts cells scr, si6 and si11 (lane 7, 8, 9) and Hela transfected with an empty pcDNA3 vector and TP53INP2 overexpressed (lane 10 and 11).

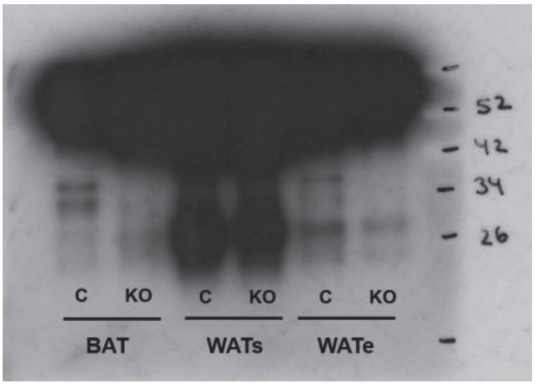

Figure A8. Screening by Western blot of the positive clone number "15" of the monoclonal TP53INP2 antibody in a dilution 1/5. Protein expression is checked in brown adipose tissue (lane 1 and 2), subcutaneous (lane 3 and 4) and epididymal (lane 5 and 6) white adipose tissue of loxP and KO mice (Photo by Alba Sabaté and Montserrat Romero, IRB).

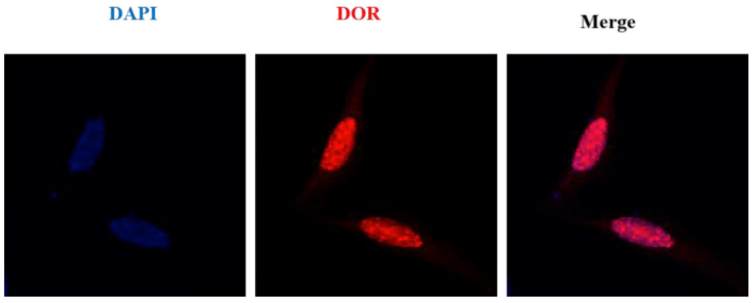

Figure A9. Screening by immunofluorescence of the positive clone num. 15 of the monoclonal TP53INP2 antibody in TP53INP2 transfected Hela cells. Nuclei in Blue, TP53INP2 in red (Photo by Ignacio Castrillón, IRB).

APPENDIX II

APPENDIX II

ARTICLE: Muñoz *et al*, EMBO Journal, 2013

Mfn2 modulates the UPR and mitochondrial function via repression of PERK

Embo Journal Vol. 32 Issue 17, pp.2348-2361, August 2013

Juan Pablo Muñoz, Saska Ivanova, Jana Sánchez-Wandelmer, Paula Martínez-Cristóbal, Eduard Noguera, Ana Sancho, Àngels Díaz-Ramos, María Isabel Hernández-Álvarez, David Sebastián, Caroline Mauvezin, Manuel Palacín, Antonio Zorzano

The EMBO Journal (2013) 32, 2348–2361
www.embojournal.org

SOURCE DATA TRANSPARENT PROCESS

THE EMBO JOURNAL

Mfn2 modulates the UPR and mitochondrial function via repression of PERK

Juan Pablo Muñoz[1,2,3], Saška Ivanova[1,2,3], Jana Sánchez-Wandelmer[1,2,3], Paula Martínez-Cristóbal[1,2,3], Eduard Noguera[1,2,3], Ana Sancho[1,2,3], Angels Díaz-Ramos[1,2,3], María Isabel Hernández-Alvarez[1,2,3], David Sebastián[1,2,3], Caroline Mauvezin[1,2,3], Manuel Palacín[1,2] and Antonio Zorzano[1,2,3,*]

[1]Institute for Research in Biomedicine (IRB Barcelona), Barcelona, Spain, [2]Departament de Bioquímica i Biologia Molecular, Facultat de Biologia, Universitat de Barcelona, Barcelona, Spain and [3]CIBER de Diabetes y Enfermedades Metabólicas Asociadas (CIBERDEM), Instituto de Salud Carlos III, Barcelona, Spain

Mitofusin 2 (Mfn2) is a key protein in mitochondrial fusion and it participates in the bridging of mitochondria to the endoplasmic reticulum (ER). Recent data indicate that Mfn2 ablation leads to ER stress. Here we report on the mechanisms by which Mfn2 modulates cellular responses to ER stress. Induction of ER stress in Mfn2-deficient cells caused massive ER expansion and excessive activation of all three Unfolded Protein Response (UPR) branches (PERK, XBP-1, and ATF6). In spite of an enhanced UPR, these cells showed reduced activation of apoptosis and autophagy during ER stress. Silencing of PERK increased the apoptosis of Mfn2-ablated cells in response to ER stress. XBP-1 loss-of-function ameliorated autophagic activity of these cells upon ER stress. Mfn2 physically interacts with PERK, and Mfn2-ablated cells showed sustained activation of this protein kinase under basal conditions. Unexpectedly, PERK silencing in these cells reduced ROS production, normalized mitochondrial calcium, and improved mitochondrial morphology. In summary, our data indicate that Mfn2 is an upstream modulator of PERK. Furthermore, Mfn2 loss-of-function reveals that PERK is a key regulator of mitochondrial morphology and function.

The EMBO Journal (2013) **32,** 2348–2361. doi:10.1038/emboj.2013.168; Published online 6 August 2013
Subject Categories: membranes & transport; signal transduction
Keywords: cell death and autophagy; cell metabolism; mitochondria

*Corresponding author. Institute for Research in Biomedicine (IRB Barcelona), C/Baldiri Reixac 10, 08028 Barcelona, Spain.
Tel.: +34 93 4037197; Fax: +34 93 4034717;
E-mail: antonio.zorzano@irbbarcelona.org

Received: 25 September 2012; accepted: 3 July 2013; published online: 6 August 2013

Introduction

Endoplasmic reticulum (ER) stress is triggered in response to a variety of stimuli that lead to a number of alterations of the ER, such as dysregulated redox homoeostasis, abnormal protein folding, and reduced calcium levels. Pathologies such as neurodegeneration, diabetes, cancer, and cardiovascular disease are characterized by the presence of ER stress (Hotamisligil, 2010). At least three proteins located in the ER membrane (PERK, IRE-1α, and ATF6) respond to ER stress stimuli by triggering the Unfolded Protein Response (UPR). These pathways activate several transcription factors involved in cell survival during the early stages of stress and in apoptotic cell death during acute or chronic stress. The PERK branch participates in the reduction of protein synthesis and activation of autophagy, apoptosis, and chaperone expression (Harding *et al*, 1999; Lu *et al*, 2004b). PERK-stimulated CHOP favors apoptosis (Harding *et al*, 2000; Rouschop *et al*, 2010), and, conversely, it has also been reported that CHOP protects neuronal cells after ischaemia reperfusion (Halterman *et al*, 2010). PERK activation decreases protein synthesis through eIF2α phosphorylation (Lu *et al*, 2004a), and, in addition, sustained PERK activation induces GADD34 expression, which relieves protein synthesis inhibition through eIF2α dephosphorylation (Novoa *et al*, 2001).

The IRE-1α branch activates the expression of XBP-1 transcription factor, which is involved in the synthesis of chaperones and other ER proteins. The IRE-1α pathway is also required for autophagy activation (Ogata *et al*, 2006). Interestingly, XBP-1 deficiency promotes autophagy in neuronal cells (Hetz *et al*, 2009). This observation points to a complex role of the IRE-1α pathway in autophagic regulation.

The transcription factor ATF6 is also stimulated during ER stress. In addition, calcium signals participate in this activation (Xu *et al*, 2004). This transcription factor induces XBP-1 and chaperones and participates in cell survival. Thus, reduced apoptosis occurs in response to ischaemia reperfusion in hearts overexpressing ATF6 (Doroudgar *et al*, 2009). Tumour cell survival also requires ATF6 through the activation of the mTOR pathway (Schewe and Aguirre-Ghiso, 2008; Doroudgar *et al*, 2009). ATF6 also mediates the synthesis of proteins and lipids required for ER biogenesis and participates in the synthesis of proteins required to activate ERAD, a mechanism for the degradation of ER proteins (Yamamoto *et al*, 2004; Maiuolo *et al*, 2011). Recent data demonstrate that PERK facilitates the stimulation of the ATF6 pathway (Teske *et al*, 2011). These studies indicate that UPR branches are exquisitely regulated and that several proteins are involved in the cross talk between branches.

Mitofusin 2 (Mfn2) is a GTPase protein localized in the outer mitochondrial membrane and in mitochondrial-associated membranes. In addition to controlling ER morphology, this protein participates in mitochondrial fusion and regulates

the transfer of calcium from the ER to mitochondria (Santel and Fuller, 2001; Legros *et al*, 2002; Bach *et al*, 2003; Ishihara *et al*, 2004; de Brito and Scorrano, 2008). Moreover, Mfn2 deficiency upregulates markers of the UPR in liver, skeletal muscle, and cultured cells (Ngoh *et al*, 2012; Sebastian *et al*, 2012), and normalization of ER stress by treatment with tauroursodeoxycholic acid ameliorates deficient insulin signalling in liver-specific Mfn2-knockout mice (Sebastian *et al*, 2012). Here we demonstrate that Mfn2 is a novel PERK regulator and that it is required for the normal activation of apoptosis and autophagy during the ER stress response. Moreover, Mfn2 deficiency causes mitochondrial dysfunction through sustained activation of PERK.

Results

Mfn2 knockout (KO) cells show massive ER expansion in response to ER stress

On the basis of the observations linking Mfn2 to ER biology, we examined the response of Mfn2-deficient cells to agents that cause ER stress. To this end, mouse embryo fibroblasts (MEFs) were incubated with 1 μM thapsigargin (Tg) for 12 h in order to induce ER stress. Under these conditions, Mfn2 KO MEFs underwent dramatic ER expansion, characterized by multilamellar structures, compared to wild-type (WT) MEFs (Figure 1A and B). To provide further evidence of the effects of ER stress on ER morphology, cells were transfected with a plasmid encoding an RFP protein that is localized in the ER luminal compartment (ER-RFP), and thereafter treated with Tg and visualized by epifluorescence microscopy. Under basal conditions, Mfn2 ablation caused ER fragmentation, which was detectable with the luminal ER marker (Supplementary Figure S1A). This finding is in keeping with prior data (de Brito and Scorrano, 2008). Supplementary Figure S1A also shows increased ER luminal expansion during ER stress (induced by Tg, tunicamycin, or brefeldin A) in Mfn2 KO cells compared to WT cells. Movie 1 (Supplementary Data) shows the formation of the expanded ER in Mfn2 KO cells upon the induction of ER stress. Labelling of the ER membrane by transfection of Sec61β-GFP also showed a dramatic ER expansion in Mfn2 KO cells in response to Tg (Figure 1C). However, labelling of ER membranes with Sec61β-GFP did not show alterations in ER morphology in these cells under basal conditions (Figure 1C), which is in keeping with prior data in COS cells (Friedman *et al*, 2011). No alterations in ER morphology were detected in Mfn1 KO cells in response to Tg (Figure 1C). Reexpression of Mfn2 in Mfn2 KO cells rescued normal mitochondrial morphology and prevented ER expansion in response to ER stress (Supplementary Figure S1B–E).

The enhanced ER expansion in Mfn2 KO cells upon Tg treatment was further documented by labelling ER–Golgi with brefeldin A-bodipy (Hetz *et al*, 2006) (Figure 1D).

Deficiency of Mfn1 or Mfn2 was also induced in MEFs by lentiviral expression of shRNAs, which caused mitochondrial fragmentation (Supplementary Figure S2A and B). Labelling of the ER membrane by transfection of Sec61β-GFP also showed marked ER expansion in Mfn2-silenced MEF cells treated with Tg (Supplementary Figure S2C). Mfn1 deficiency did not cause ER expansion upon Tg treatment (Supplementary Figure S2C).

Mfn2 KO cells show defective apoptosis in response to ER stress

On the basis of the initial observations indicating that Mfn2 ablation causes abnormal ER expansion in response to ER stress, next we examined whether Mfn2 loss-of-function also alters the biological responses driven by this stress. In this regard, apoptosis was induced through activation of caspase 3 (Rao *et al*, 2002) in response to ER stress. Mfn2 loss-of-function significantly enhanced caspase activity in MEFs and in C2C12 cells under basal conditions (Supplementary Figure S3A) (see Supplementary Figures S2 and S4 for details on Mfn2 deficiency induced in these cells). WT MEFs showed caspase 3 activation and increased caspase activity in response to tunicamycin, brefeldin A, or Tg (Figure 2A–C). Under these conditions, Mfn2 ablation greatly reduced caspase 3 processing and caspase activity (Figure 2A–C), and reexpression of Mfn2 normalized the activation of this enzyme (Supplementary Figure S3B). Reduced apoptosis was also detected by cytometry assays (subG1 DNA fragmentation) in Mfn2 KO cells (Figure 2D). Mfn1 KO cells showed reduced caspase 3 processing and caspase activity upon Tg, tunicamycin, or brefeldin A treatment, although the values observed were higher than in Mfn2 KO cells (Supplementary Figure S3C and D). Silencing of Mfn2 in 3T3-L1 or in C2C12 cells also reduced caspase 3 processing in response to ER stress (Figure 2E and Supplementary Figure S3F). In contrast, agents that induce apoptosis independently of ER stress, such as staurosporine or TNFalpha/cycloheximide (CHX), activated caspase 3 processing to a greater extent in Mfn2 KO cells compared to WT cells (Supplementary Figure S3E).

Next, we analyzed whether Mfn2 KO cells die as a result of another form of cell death upon ER stress. Lactate dehydrogenase release (an index of cell necrosis) increased in control cells during ER stress, but this did not occur in Mfn2-ablated cells (Figure 2F). We explored whether Mfn2 KO cells undergo a paraptotic-like death, which is characterized by swelling of the mitochondria and of the ER, reduced ALIX expression (Sperandio *et al*, 2000; Yoon *et al*, 2010), and involves externalization of phosphatidylserine (PS) independently of caspases (Wang *et al*, 2004). In keeping with this, Mfn2 KO cells became annexin V-positive in response to Tg, and PS externalization was not inhibited with the pan-caspase inhibitor z-VAD (Figure 2G). In addition, in response to ER stress, Mfn2 KO cells underwent vacuolization, which was rescued by CHX (Figure 2H), and showed lower ALIX protein expression (Figure 2I). Propidium iodide (PI) permeability assays coupled to annexin V labelling in control and Mfn2 KO cells showed increased PI/annexin V labelling in response to Tg. This labelling was inhibited by addition of CHX in Mfn2 KO cells but not in WT cells (Supplementary Figure 3G). In summary, our data show that Mfn2 loss-of-function impairs the normal activation of apoptosis during ER stress, and instead paraptosis-like cell death is triggered. This observation suggests that Mfn2 plays a key role in the maintenance of a normal response to ER stress.

Mfn2 KO cells show defective autophagy in response to ER stress

ER stress also activates autophagy (Ogata *et al*, 2006), and the accumulation of multilamellar ER structures detected in $Mfn2^{-/-}$ cells (Figure 1) pointed to alterations in the clearance process. To analyze autophagy in cells subjected to ER

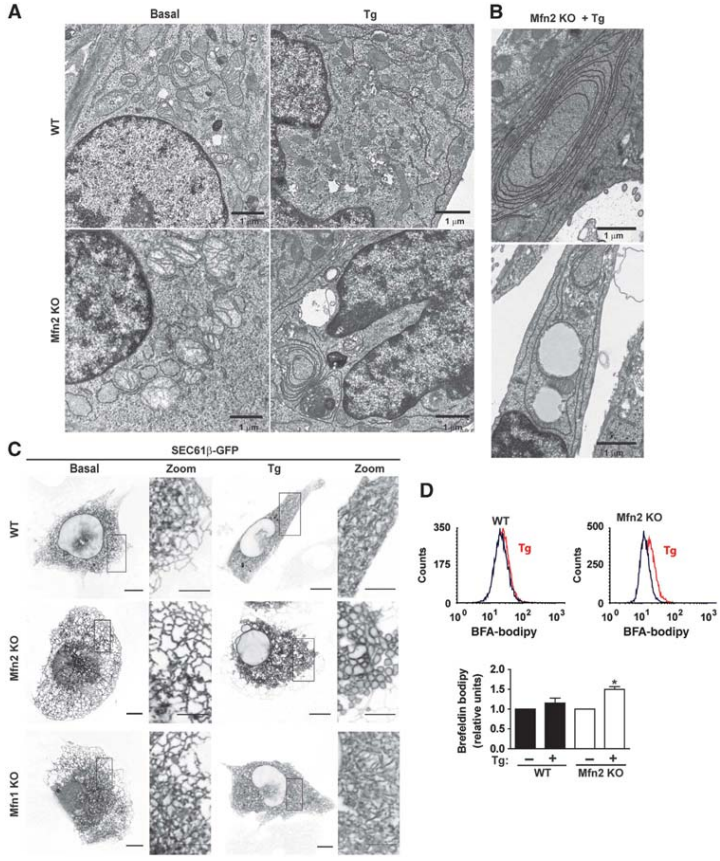

Figure 1 Mfn2 ablation promotes abnormal ER expansion during ER stress conditions. (**A**) WT or Mfn2 KO MEFs (Mfn2 KO cells) were treated with 1 μM Tg for 12 h and then processed for EM visualization of the ER morphology. Scale bar: 1 μm. (**B**) EM images of Tg-treated Mfn2 KO cells show accumulation of ER membrane stacking. Scale bar: 1 μm. (**C**) WT, Mfn2 KO or Mfn1 KO cells were transfected with the Sec61β-GFP plasmid and treated with 1 μM Tg for 24 h. Confocal microscopy images show ER vacuolization in Mfn2 KO cells treated with Tg. Scale bar: 10 μm. Insets show × 10 zoomed images. Scale bar: 5 μm. (**D**) WT and Mfn2 KO cells were treated with Tg 1 μM for 3 h and then incubated with brefeldin A-bodipy to stain ER and Golgi. Representative flow-cytometry histograms (upper panel). Mean fluorescence intensity was used to quantify ER expansion ($n = 5$) (lower panel). Data are mean ± s.e.m. $^*P < 0.05$ versus WT group.

stress, control and Mfn2 KO cells were treated with Tg for a range of times, and autophagy was assayed by immunodetection of LC3b-I and LC3b-II. ER stress caused an increased abundance of LC3b-II in control cells, which is coherent with the activation of autophagosome formation (Figure 3A). Under basal conditions, Mfn2 KO cells showed a slightly increased LC3b-II abundance (Figure 3A). ER stress-induced LC3b-II was inhibited in Mfn2 KO cells (Figure 3A), thereby suggesting a defect in autophagy progression. Incubation with the lysosomal inhibitor bafilomycin A1 increased LC3b-II levels in WT cells but not in Mfn2 KO ones (Figure 3B). Mfn2 reexpression normalized LC3b-II levels in Mfn2 KO cells treated with Tg (Supplementary Figure S5A). These observations indicate that autophagosomal formation is impaired during ER stress upon ablation of Mfn2 in MEFs.

To obtain further insight into the autophagic steps that may be altered in Mfn2-deficient cells, we expressed mCherry-EGFP-LC3 protein in these cells. ER stress markedly enhanced the abundance of acidic autophagolysosomes—detected as red punctuates in mCherry-EGFP-LC3B-expressing cells—which is consistent with increased autophagic activity (Figure 3C and D). Under these conditions, Mfn2 ablation reduced the abundance of acidic autophagolysosomes during ER stress induced by Tg, brefeldin A, or tunicamycin (Figure 3C and D). mCherry-EGFP-LC3B remained as yellow punctuate structures in Mfn2 KO cells, thereby indicating its presence in autophagosomes (Figure 3C and D). In keeping

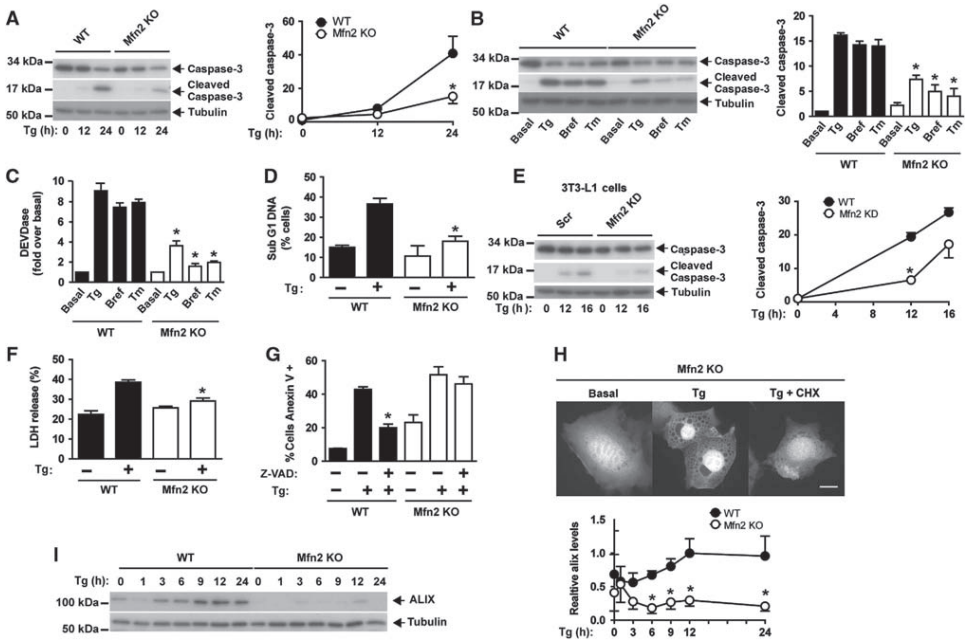

Figure 2 Mfn2 ablation prevents caspase activation during ER stress and promotes paraptosis-like cell death. (**A**) WT and Mfn2 KO cells were treated with 1 μM Tg for 12 or 24 h. Total and cleaved caspase 3 levels were detected by western blot. Data are mean ± s.e.m. ($n=3$). *$P<0.05$ versus WT group. (**B**, **C**) WT and Mfn2 KO cells were treated with 0.5 μg/ml tunicamycin (Tm), 100 ng/ml brefeldin A (Bref), or 1 μM Tg for 24 h. Total and cleaved caspase 3 levels were detected by western blot (**B**) and caspase activity (**C**) by measurement of DEVD-AFC substrate processing. Data are mean ± s.e.m. ($n=3$). *$P<0.05$ versus WT group. (**D**) Flow-cytometry analysis of the Sub G1 DNA fragmentation in methanol-fixed WT and Mfn2 KO cells after incubation with or without 1 μM Tg for 24 h. Data are given as mean ± s.e.m. ($n=3$). *$P<0.05$ versus WT group. (**E**) Scr (stably expressing scrambled shRNA) and Mfn2 knockdown (KD) (stably expressing shRNA directed against Mfn2) 3T3-L1 fibroblasts were incubated in the presence or absence of 1 μM Tg for 24 h. Total and cleaved caspase 3 were detected by western blot. Data are mean ± s.e.m. ($n=3$). *$P<0.05$ versus WT group. (**F**) WT and Mfn2 KO cells were treated with 1 μM Tg for 24 h. Lactate dehydrogenase (LDH) release was analyzed by flow cytometry to assess necrotic cell death. Data are mean ± s.e.m. ($n=3$). *$P<0.05$ versus WT group. (**G**) WT and Mfn2 KO cells were incubated for 24 h with or without 1 μM Tg in the presence or absence of z-VAD-fmk and stained for annexin V/PI. Data are mean ± s.e.m. ($n=4$). *$P<0.05$ versus WT + Tg group. (**H**) Mfn2 KO cells transfected with the pEGFP plasmid were incubated with 1 μM Tg alone or in combination with 2 μM CHX for 24 h (3 h of pre-incubation with CHX). Florescence microscopy images show that CHX prevents cytoplasmic vacuolization. Scale bar: 10 μm. (**I**) WT (black circles) and Mfn2 KO cells (white circles) were incubated with 1 μM Tg for varying times, and ALIX protein was detected by western blot. Data are mean ± s.e.m. ($n=3$). *$P<0.05$ versus WT group. Source data for this figure is available on the online supplementary information page.

with these data, reduced Lysotracker staining and LAMP1 expression were detected in these cells (Figure 3E and F). The expression of the autophagic genes LC3b or beclin-1 was also dysregulated in Mfn2 KO cells upon ER stress (Figure 3G).

In contrast to the data obtained in Mfn2 KO cells, ablation of Mfn1 did not alter ER stress-induced autophagy (Supplementary Figure S5B–D), and Lysotracker staining was enhanced compared to WT cells (Supplementary Figure S5E). Autophagy was also analyzed in 3T3-L1 fibroblasts and in C2C12 myoblasts upon Mfn2 silencing (Supplementary Figure S4). Reduced autophagic activity, assessed by LC3b-II abundance or the degradation of long-lived proteins, was detected in Mfn2-deficient cells in response to ER stress (Supplementary Figure S5F–H). In parallel, a reduced degradation rate of long-lived proteins was detected in Mfn2-deficient 3T3-L1 cells in response to tunicamycin (Supplementary Figure S5H).

In all, our data show that Mfn2 loss-of-function impairs the normal progression of autophagy during ER stress. This loss-of-function is characterized by reduced autophagosome formation, reduced lysosome abundance, and reduced autophagolysosome formation.

Mfn2 deficiency dysregulates PERK, IRE-1, and ATF6 UPR branches in response to ER stress

To understand how Mfn2 ablation leads to a disrupted biological response to ER stress, next we monitored the UPR response (Figure 4A). Mfn2 KO cells showed enhanced PERK phosphorylation as well as induced expression of downstream signalling proteins, ATF4, GADD34, and CHOP (Figure 4B and C). These observations indicate enhanced PERK branch signalling during ER stress in Mfn2 KO cells. Under these conditions, the activation of eIF2α was reduced in these cells during ER stress (Figure 4B and C).

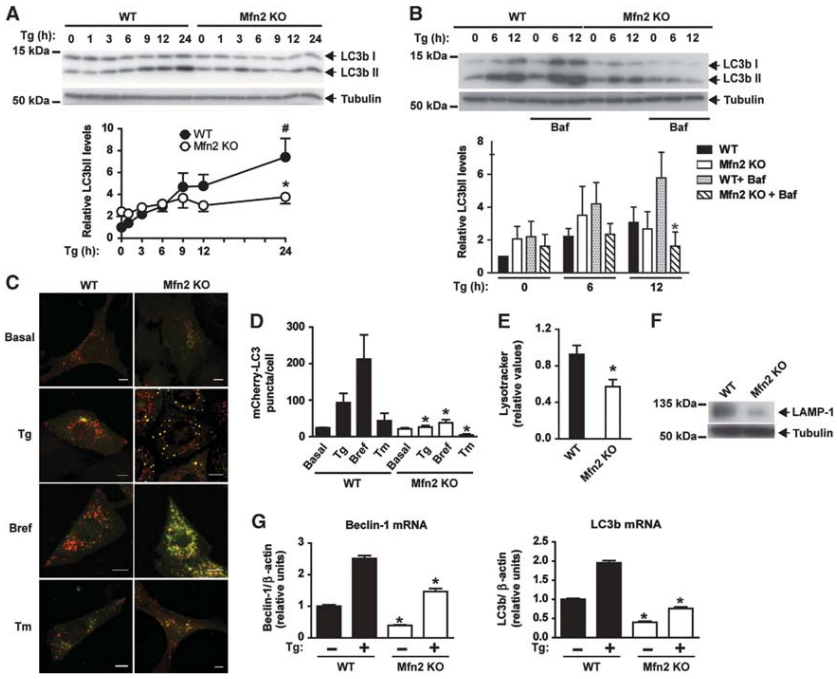

Figure 3 Mfn2 loss-of-function decreases autophagy in response to ER stress. (**A**, upper panel) WT (black circles) or Mfn2 KO cells (white circles) were treated with 1 μM Tg for a range of times. (**A**, lower) Densitometric quantification. Data are mean ± s.e.m. ($n = 3$). $^{*}P < 0.05$ versus WT group; $^{\#}P < 0.05$ versus WT non-Tg-treated group. (**B**, upper panel) WT or Mfn2 KO cells were treated with Tg for 0, 6 or 12 h, in the presence or absence of Bafilomycin (Baf, 100 nM). LC3b-I and LC3b-II expression was measured by western blot. (**B**, lower panel) Densitometric quantification of LC3b-II levels (relative to tubulin). Data are mean ± s.e.m. ($n = 3$). $^{*}P < 0.05$ versus WT + Baf + Tg group. (**C**) WT or Mfn2 KO cells stably expressing mCherry-GFP-LC3b were treated with 1 μM Tg, 100 ng/ml Brefeldin (Bref), or 0.5 μg/ml tunicamycin (Tm) for 24 h and examined by confocal microscopy. Scale bar: 10 μm. (**D**) Quantification of mCherry^{+}/GFP^{-} (mCherry-LC3) red puncta per cell (a measure of acidic autophagosomes) is shown. Data are mean ± s.e.m. ($n = 3$; 100 cells were analyzed per experiment and group). $^{*}P < 0.05$ versus WT group. (**E**) Acidic compartments of WT or Mfn2 KO cells were stained with Lysotracker Green and analyzed by flow cytometry. Data are given as mean ± s.e.m. ($n = 3$). $^{*}P < 0.05$ versus WT group. (**F**) LAMP1 expression was immunodetected in WT and Mfn2 KO cells in basal conditions. (**G**) Expression of Beclin-1 or LC3b transcripts in WT or Mfn2 KO cells treated with or without 1 μM Tg for 24 h. Data are mean ± s.e.m. ($n = 3$). $^{*}P < 0.05$ versus WT group. Source data for this figure is available on the online supplementary information page.

Tunicamycin also caused overactivation of the PERK pathway in Mfn2 KO cells, which was characterized by enhanced phosphorylation of eIF2α, and greater ATF4 expression (Figure 4D).

To determine the activity of the IRE-1α branch, we monitored protein variant XBP-1s, generated through alternative transcript processing upon Tg treatment. Mfn2 ablation caused a sustained activation of XBP-1s in response to ER stress (Figure 4B and C). Furthermore, transcriptional activity driven by ATF6 was greater in Mfn2 KO cells upon Tg treatment (Figure 4E). Analysis of UPR target genes indicated that 38 genes were induced in WT MEFs by Tg (Supplementary Table S1). Almost all these genes were additionally upregulated in Mfn2 KO cells compared to WT cells, and differences were statistically significant for 22 genes (Supplementary Table S1). In all, our data indicate that Mfn2 ablation enhances the activity of the PERK/CHOP, XBP-1, and ATF6 UPR branches in response to ER stress.

PERK deficiency improves apoptosis, and XBP-1 loss-of-function enhances autophagy during ER stress in Mfn2 KO cells

Next, we studied whether the enhanced activity of the UPR branches was responsible for the impaired responses to ER stress in Mfn2 KO cells. To this end, WT and Mfn2 KO cells were subjected to gene silencing by means of lentiviral vectors expressing shRNA directed against PERK, XBP-1, or ATF6 (Figures 5 and 6 and Supplementary Figure S6). PERK loss-of-function (Figure 5A) substantially enhanced caspase activity and caspase 3 cleavage in Mfn2 KO cells upon treatment with Tg (Figure 5B–D). In contrast, PERK silencing in WT cells did not alter either of these parameters upon treatment with this drug (Figure 5B–D). Knockdown of PERK did not enhance LC3b-II levels in response to Tg treatment in Mfn2 KO cells (Figure 5E and F).

XBP-1 loss-of-function (Figure 6A) moderately increased caspase activity but did not enhance caspase 3 cleavage in

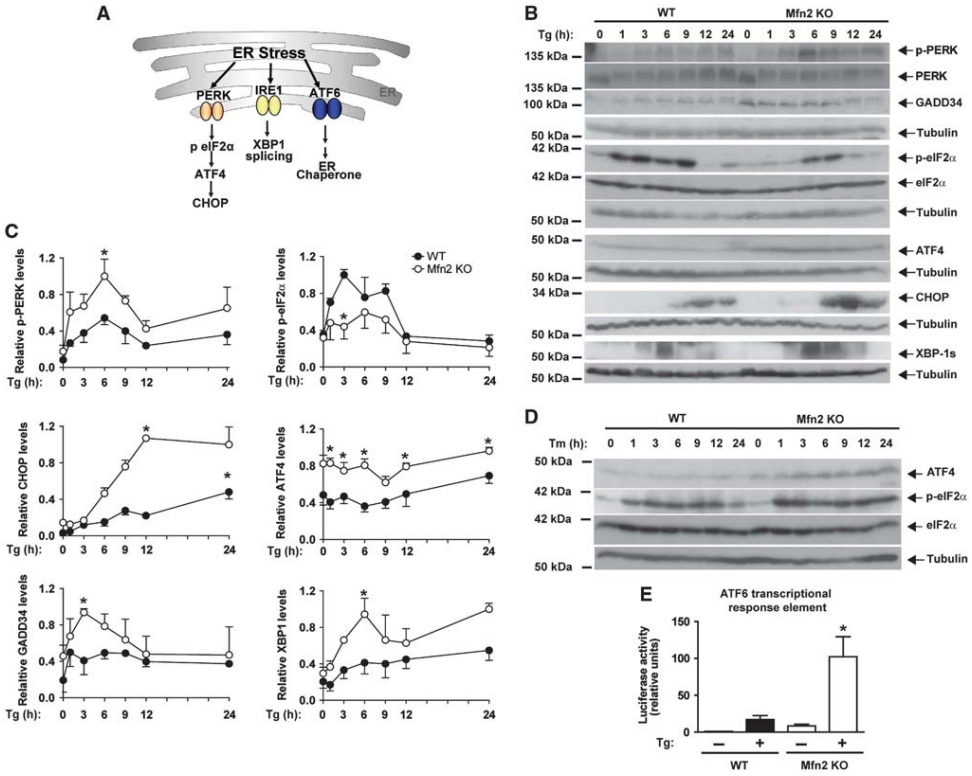

Figure 4 Mfn2 modulates the UPR response. (**A**) Scheme on UPR branches. (**B**) Immunodetection of p-PERK,PERK, GADD34, p-eIF2α, eIF2α, ATF4, CHOP, and XBP-1s in WT and Mfn2 KO cells treated with 1 μM Tg for the times indicated. (**C**) Densitometric quantifications. Data are mean ± s.e.m. ($n = 3$). *$P < 0.05$ versus WT group. (**D**) Immunodetection of p-eIF2α, eIF2α, and ATF4 in WT and Mfn2 KO cells treated with 0.5 μg/ml Tunicamycin (Tm) for the times indicated. (**E**) Transcriptional activity driven by ATF6. WT and Mfn2 KO cells were co-transfected with the 5xATF6-GL3 and TK-Renilla plasmids and treated with 1 μM Tg for 24 h after transfection. Data are mean ± s.e.m. ($n = 4$). *$P < 0.05$ versus WT group. Source data for this figure is available on the online supplementary information page.

response to 6 h of Tg treatment (Figure 6B–D). In contrast, XBP-1 knockdown markedly enhanced LC3b-II abundance in Mfn2 KO cells upon treatment with this drug (Figure 6E and F). XBP-1 did not alter any of the parameters studied in WT cells (Figure 6B–F). In keeping with these observations, XBP-1 loss-of-function increased the number of acidic autophagolysosomes, detected as red punctuates in mCherry-EGFP-LC3B-expressing Mfn2 KO cells subjected to treatment to Tg, tunicamycin, or brefeldin A (Figure 6G and H).

ATF6 loss-of-function (Supplementary Figure S6A) accelerated ER vacuolization (Supplementary Figure S6B) in Mfn2 KO cells subjected to ER stress. Under these conditions, ATF6-silenced cells showed no changes in LC3b-II levels (Supplementary Figure S6C) and underwent higher cell death (Supplementary Figure S6D), and showed unaltered caspase activity and caspase 3 cleavage upon Tg treatment (Supplementary Figure S6E and F). Knockdown of ATF6 did not alter either of these two parameters in response to Tg treatment in WT cells (Supplementary Figure S6E and F).

Mfn2 deficiency causes a sustained activation of PERK, which mediates defective mitochondrial morphology and function under basal conditions

In studies oriented to monitor the activity of UPR branches upon ER stress, data pointed to PERK stimulation under basal conditions (Figure 4B). On the basis of these data, next we studied the effect of Mfn2 loss-of-function on the basal activation state of the PERK pathway in MEFs, and in 3T3-L1 and C2C12 cells. Mfn2 loss-of-function caused sustained PERK stimulation, characterized by enhanced PERK and eIF2α phosphorylation in all three cell types (Figure 7A and B). Chronic activation of the PERK pathway was also detected in Mfn2 KO livers and skeletal muscle and was characterized by enhanced eIF2α phosphorylation and CHOP expression (Figure 7C and D). Enhanced XBP-1 abundance was also found in the liver and muscle of Mfn2 KO mice (Figure 7C and D). Furthermore, the abundance of LC3-II and p62, markers of autophagy, were enhanced in the tissues of these mice (Figure 7C and D), thereby suggesting impaired autophagy.

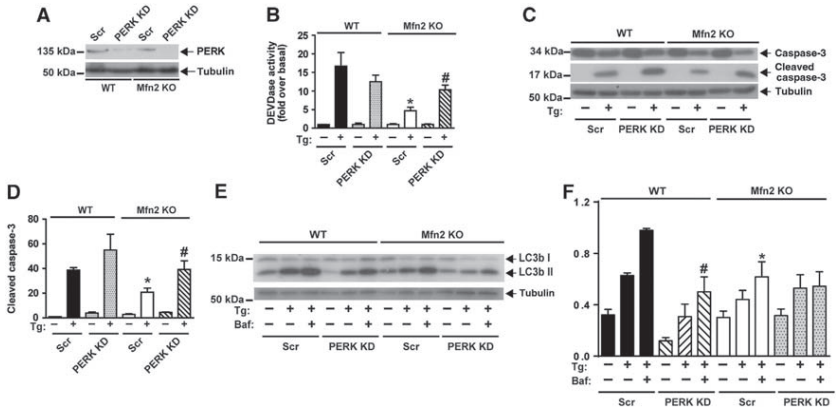

Figure 5 PERK deficiency improves apoptosis during ER stress in Mfn2-ablated cells. (**A**) Immunodetection of PERK in WT and Mfn2 KO cells stably expressing a scrambled shRNA (Scr) or a shRNA directed against PERK (PERK KD). (**B**) Caspase activity was detected by measurement of DEVD-AFC substrate processing in WT or Mfn2 KO cells subjected to PERK silencing and treated with 1 μM Tg for 24 h. Data are mean ± s.e.m. ($n = 3$). $^*P < 0.05$ versus WT; $^\#P < 0.05$ versus Scr group. (**C**, **D**) Total and cleaved caspase 3 levels were detected by western blot. Densitometric quantification is shown in **D**. Data are mean ± s.e.m. ($n = 3$). $^*P < 0.05$ versus WT; $\#P < 0.05$ versus Scr group. (**E**, **F**) Immunodetection of LC3b-I and -II in WT and Mfn2 KO cells subjected to PERK silencing and treated as indicated with Tg or Baf (1 μM Tg; 100 nM Baf) for 6 h. Densitometric quantification is shown in **F**. Data are mean ± s.e.m. (n = 3). $^*P < 0.05$ versus WT; $\#P < 0.05$ versus Scr group. Source data for this figure is available on the online supplementary information page.

The negative relationship between Mfn2 expression and PERK activity points to a physical interaction. To test this hypothesis, lysates from cells stably expressing a myc-tagged version of PERK were immunoprecipitated with anti-myc antibodies, and the immunoprecipitates were subjected to western blot assays. Immunoprecipitation assays revealed physical interaction of PERK and endogenous Mfn2 (Figure 7E). Assays were also performed in MEFs that expressed endogenous Mfn2 and PERK upon immunoprecipitation with anti-PERK antibodies. Indeed, we detected a physical interaction between endogenous PERK and Mfn2 (Figure 7F). Our data indicate that the absence of Mfn2 enhances PERK phosphorylation, which is coherent with a model in which Mfn2 negatively controls PERK.

Under basal conditions, Mfn2 KO MEFs lacked mitochondrial filaments and instead showed mitochondrial swelling, as visualized by Mitotracker Red staining (which labels the mitochondrial matrix) (Supplementary Figure S7A), or after transfection of cells with BAK-GFP (which labels the outer mitochondrial membrane) (Supplementary Figure S7B). Mfn2 ablation also caused major alterations in mitochondrial function, such as enhanced ROS production (Supplementary Figure S7C) and reduced respiration (Supplementary Figure S7D). Mitochondrial calcium overload was measured with the Rhod-2 probe, which was specifically detected in mitochondria under our experimental conditions (Supplementary Figure S7E). Mfn2 ablation caused enhanced mitochondrial Ca^{2+} overload (Supplementary Figure S7E). All these alterations in mitochondrial function are coherent with previous reports (Bach *et al*, 2003; Chen *et al*, 2005; de Brito and Scorrano, 2008). Mitochondrial alterations in morphology, ROS production, and mitochondrial respiration were reversed by reexpression of Mfn2 in Mfn2 KO cells (Supplementary Figures S1C, S7F and G).

The mitochondrial alterations secondary to Mfn2 ablation have been attributed to the role of Mfn2 as a mitochondrial fusion protein. Alternatively, we reasoned that Mfn2 deficiency may affect mitochondrial function as a result of PERK activation. To test this hypothesis, Mfn2 KO cells were subjected to PERK silencing. Surprisingly, PERK silencing ameliorated the defective mitochondrial morphology, thus swollen mitochondria were much less abundant, and instead mitochondria formed short and even long and thinner filaments (Figure 8A and B). This effect of PERK silencing was not detected in WT or Mfn1 KO cells (Figure 8C and D). Moreover, the addition of the chemical chaperones TUDCA or 4-phenyl butyric acid to Mfn2 KO cells did not alter the morphology of their mitochondria (Figure 8E). Silencing of XBP-1 or ATF6 did not modify mitochondrial morphology in WT or Mfn2 KO cells (Supplementary Figure 8A). In addition, the effects of PERK silencing on normalizing mitochondrial morphology were not associated with changes in the expression of mitochondrial fusion or fission proteins in Mfn2 KO cells (Supplementary Figure 8B and C).

PERK silencing also reduced ROS production (Figure 8F) and mitochondrial Ca^{2+} overload in Mfn2 KO cells (Figure 9A). In contrast, PERK loss-of-function did not alter ROS in WT or Mfn1 KO cells (Figure 8F and G). In addition, PERK silencing enhanced routine and maximal uncoupled respiration in Mfn2 KO cells (Figure 9B). The stimulatory effects of PERK silencing on cell respiration were also detected in WT and Mfn1 KO cells (Figure 9C and D). In keeping with these data, PERK overexpression modified mitochondrial function and morphology in WT cells. Thus, mitochondrial respiration was markedly repressed in response to PERK overexpression (Figure 9E), and mitochondria were fragmented (60% of the cells

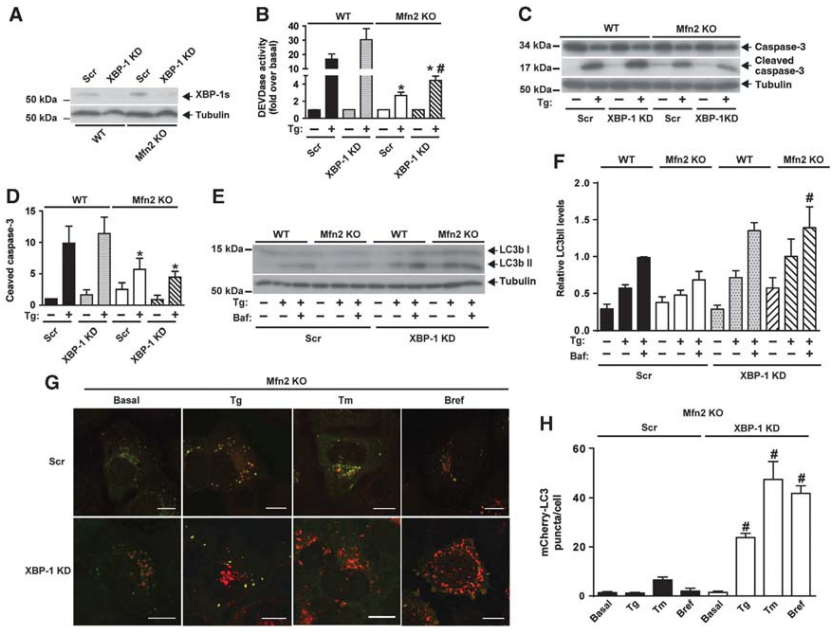

Figure 6 XBP-1 loss-of-function enhances autophagy during ER stress in Mfn2-ablated cells. (**A**) Immunodetection of XBP-1s in WT and Mfn2 KO cells stably expressing a scrambled shRNA (Scr) or a shRNA directed to XBP-1 (XBP-1 KD), and treated with Tg for 6 h. (**B**) Caspase activity was detected by measurement of DEVD-AFC substrate processing. Data are mean ± s.e.m. ($n = 3$). $^{*}P < 0.05$ versus WT group. $^{\#}P < 0.05$ versus Scr group. (**C**, **D**) Total and cleaved caspase 3 levels were detected by western blot. WT and Mfn2 KO cells subjected or not to XBP-1 silencing (Scr, and KD) and treated with 1 μM Tg for 24 h. Data are mean ± s.e.m. ($n = 3$). $^{*}P < 0.05$ versus WT group. (**E**, **F**) Immunodetection of LC3b-I and -II in Scr and XBP-1 KD WT or Mfn2 KO cells treated as indicated (1 μM Tg; 100 nM Baf) for 6 h. Densitometric quantification is shown in **F**. Data are mean ± s.e.m. ($n = 3$). $^{\#}P < 0.05$ versus Scr group. (**G**) Mfn2 KO cells stably expressing mCherry-GFP-LC3b and subjected or not to XBP-1 silencing (Scr or KD) were treated with 1 μM Tg, 100 ng/ml Bref, or 0.5 μg/ml Tm for 24 h and examined by confocal microscopy. Scale bar: 10 μm. (**H**) Quantification of mCherry + /GFP- (mCherry-LC3) red puncta per cell (a measure of acidic autophagosomes) is shown. Data are mean ± s.e.m. ($n = 3$; 100 cells were analyzed per experiment and group). $^{\#}P < 0.05$ versus Scr group. Source data for this figure is available on the online supplementary information page.

overexpressing PERK showed fragmented or round mitochondria) (Figure 9F and G).

Discussion

Mfn2 is a mitochondrial fusion protein with a lower GTPase activity than that of Mfn1 (Ishihara *et al*, 2004; Neuspiel *et al*, 2005). On the basis of the mitochondrial fusion activity of Mfn2, the alterations in mitochondrial morphology and function detected upon silencing or ablation of this gene have been attributed to reduced mitochondrial fusion (Bach *et al*, 2003; Chen *et al*, 2003; Pich *et al*, 2005). Here we provide evidence that an ER-related mechanism is responsible for the development of swollen mitochondria, enhanced Ca^{2+} overload, increased ROS production, and reduced mitochondrial respiration in Mfn2-deficient cells. This view is based on a number of observations, namely, (a) Mfn2 KO or Mfn2-silenced cells showed sustained PERK activation under basal conditions; (b) PERK silencing ameliorated the mitochondrial network and respiration and reduced ROS production and mitochondrial Ca^{2+} in Mfn2 KO cells; (c) PERK overexpression caused mitochondrial fragmentation and reduced mitochondrial respiration in cells; and (d) there is a physical interaction between Mfn2 and PERK.

Our data support the notion that Mfn2 lies upstream of PERK and that under basal conditions Mfn2 maintains PERK inactive. We detected sustained activation of PERK in skeletal muscle, liver, and pre-adipose cells under conditions of Mfn2 loss-of-function; therefore, the activation of PERK may be independent of the cellular context. We also propose that the interaction between Mfn2 and PERK occurs in mitochondrial–ER contact sites. In favour of this view, both Mfn2 and PERK are localized in this compartment (de Brito and Scorrano, 2008; Verfaillie *et al*, 2012).

Our study is also the first to demonstrate that PERK controls mitochondrial morphology and function, as well as oxidative stress in cells. In this respect, we propose that the alterations detected in tissues upon Mfn2 ablation, such as enhanced ROS production, defective mitochondrial respiration, and deficient insulin signalling and glucose handling (Sebastian *et al*, 2012), are, at least in part, the result of enhanced PERK activity.

Here we report that Mfn2 loss-of-function causes the dysregulation of UPR branches under basal or ER stress

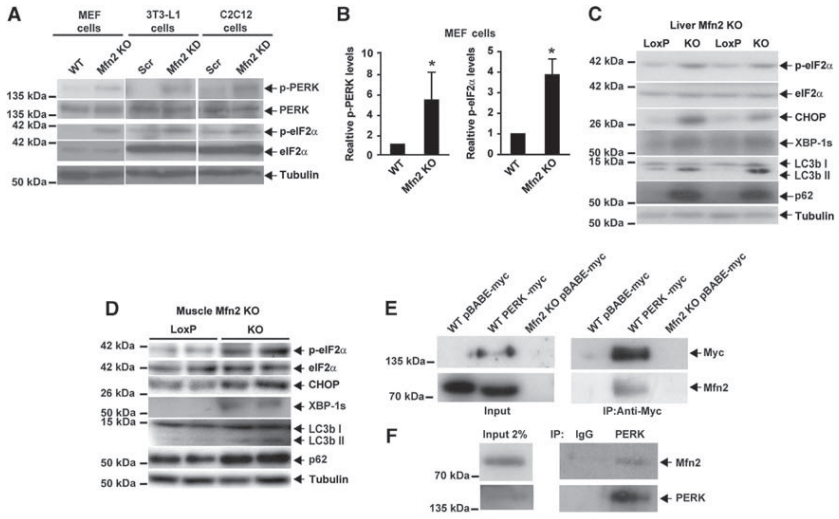

Figure 7 Mfn2 regulates PERK activity. (**A**) Immunodetection of p-PERK and p-eIF2α in Mfn2 KO MEFs, Mfn2 knockdown 3T3-L1 fibroblasts, and Mfn2 knockdown C2C12 myoblasts. (**B**) Densitometric quantification of p-PERK and p-eIF2α in MEFs. Data are mean ± s.e.m. ($n = 3$). *$P < 0.05$ versus WT cells. (**C**, **D**) Immunodetection of p-eIF2α, eIF2α, CHOP, XBP-1s, LC3b, and p62 in Mfn2-deficient liver (**C**) or skeletal muscle (**D**) from tissue-specific KO mice. (**E**) Co-immunoprecipitation of Mfn2 and PERK in WT or Mfn2 KO cells stably expressing PERK-myc or an empty vector (pBABE-myc; negative control). (**F**) Co-immunoprecipitation of endogenous Mfn2 and PERK in WT MEF lysates. PERK was immunoprecipitated with a C-terminal antibody and co-immunoprecipitation of Mfn2 was detected by western blot. Source data for this figure is available on the online supplementary information page.

conditions. Under the former, we detected enhanced PERK and eIF2α phosphorylation in Mfn2 KO cells or tissues. In addition, Mfn2-deficient cells exposed to ER stress (by incubation with agents such as Tg or tunicamycin) showed increased activation of the three major UPR branches, that is, PERK, IRE-1α, and ATF6, and enhanced expression of UPR genes. In connection with the enhanced ER stress-induced PERK pathway, which was characterized by greater expression of the proteins ATF4, GADD34, and CHOP, tunicamycin also caused enhanced phosphorylation of eIF2α, whereas Tg reduced eIF2α phosphorylation. This reduction may be explained through the complex effects of Tg on calcium homoeostasis (Inesi *et al*, 1998; Michelangeli and East, 2011), and an interaction between these effects and Mfn2 loss-of-function during ER stress. Our data agree with reports by Zhao *et al* (2012), who found increased phosphorylation of eIF2α and enhanced expression of UPR target genes in Mfn2 KO cardiac cells. In contrast, Ngoh *et al* (2012) analyzed the impact of ER stress on the PERK pathway in MEFs transduced with adenoviruses for 24 or 48 h before exposure to ER stress. They found that at short times (0.5 h) the phosphorylation of eIF2α or the expression of GADD34 or p58IPK were similarly induced in control and Mfn2-deficient cells in response to ER stress. However, at longer exposure (18 h) to ER stress, Mfn2-deficient cells showed reduced induction. These discrepancies could be attributable to differences between primary cultures, immortalized MEFs, or the use of adenoviral transduction.

ER stress activates autophagy, which is a key factor driving survival under unfavourable conditions (Ogata *et al*, 2006; Yorimitsu *et al*, 2006; Kouroku *et al*, 2007). It also induces autophagic genes via PERK/eIF2α/ATF4. Thus, ATF4 silencing, expression of a non-phosphorylatable form of eIF2α, or expression of a dominant-negative PERK inhibits ER stress-induced autophagy (Kouroku *et al*, 2007; Rzymski *et al*, 2010). There is also evidence that the IRE-1-JNK pathway is required for autophagy activation after ER stress. Thus, IRE-1α-deficient cells or cells treated with a JNK inhibitor show inhibited ER stress-induced autophagy (Ogata *et al*, 2006). In contrast, XBP-1 deficiency causes increased autophagy (Hetz *et al*, 2009). Mfn2 deficiency has been reported to impair basal autophagy in MEFs and cardiac myocytes (Hailey *et al*, 2010; Zhao *et al*, 2012). Our data indicate that Mfn2 ablation causes a deficient ER stress-induced autophagy. Mfn2-ablated cells showed a number of autophagic defects upon ER stress, namely: (a) deficient expression of autophagic genes such as beclin-1 or LC3b; (b) reduced autophagosomal proliferation; (c) reduced lysosomal abundance; and (d) decreased autophagolysosome formation. A defective response to ER stress was observed in MEFs, as well as in 3T3-L1 pre-adipocytes and C2C12 myoblasts, thereby supporting the view that these effects are independent of the cell context. We also found that the enhanced IRE-1α/XBP-1 activity upon ER stress was responsible for the reduced ER stress-induced autophagy of Mfn2-deficient cells, and silencing of XBP-1 (but not of PERK) rescued normal LC3-II formation and improved the formation of acidic autophagosomes in Mfn2-ablated cells subjected to ER stress. These effects were not detected in WT cells, thus suggesting the specificity of the Mfn2-deficient state. Neither

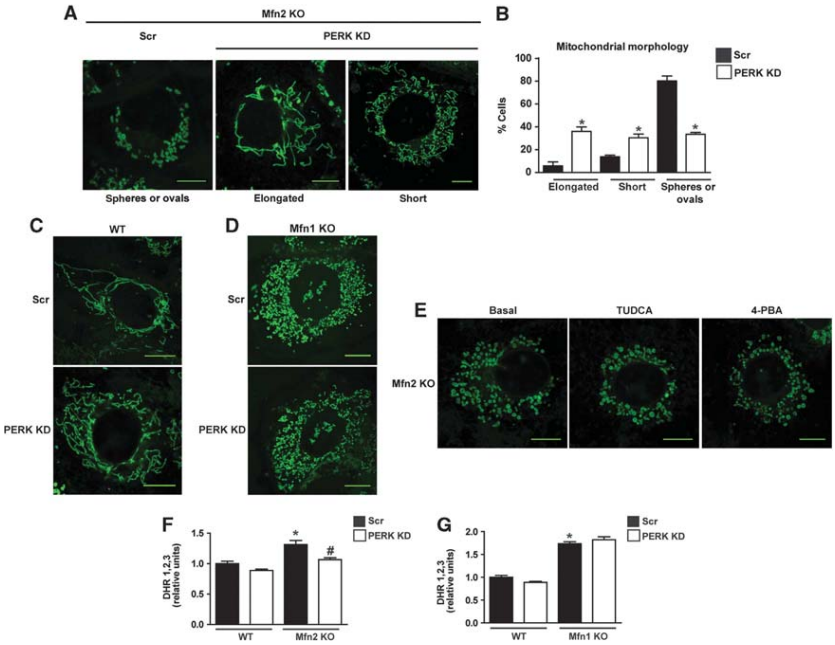

Figure 8 PERK knockdown rescues mitochondrial morphology and excessive ROS production in Mfn2 KO cells. (**A**) Representative confocal images of mitochondrial morphology in scrambled (Scr) and PERK KD Mfn2 KO cells stained with MitoTracker Green. (**B**) Mitochondrial morphology quantification. Data are mean ± s.e.m. ($n = 3$; 100 cells were analyzed per experiment and group). $^{*}P < 0.05$ versus Scr group. (**C**, **D**) Representative confocal images of mitochondrial morphology in scrambled (Scr) and PERK KD WT cells (**C**) or scrambled (Scr) and PERK KD Mfn1 KO cells (**D**) stained with MitoTracker Green. (**E**) Representative confocal images of mitochondrial morphology in Mfn2 KO cells treated with 1 μM TUDCA or 10 mM 4-phenyl butyric acid for 6 h and stained with MitoTracker Green. (**F**) Flow-cytometry quantification of ROS levels in Scr and PERK KD WT and Mfn2 KO cells (**G**) or Scr and PERK KD WT and Mfn1 cells using DHR1,2,3. Data are mean ± s.e.m. ($n = 4$). $^{*}P < 0.05$ versus WT group, $^{\#}P < 0.05$ versus Scr group. Scale bars: 10 μm.

were the effects detected under basal conditions of Mfn2 KO cells. These observations suggest that the function of XBP-1 was limited to ER stress-induced autophagy and not to basal autophagy. These data also support the notion that several mechanisms repress basal and ER stress-induced autophagy in Mfn2 KO cells.

We also report that Mfn2 KO cells are unable to stimulate apoptosis or to activate caspase 3 in response to ER stress, and instead trigger a paraptotic-like cell death pathway. Our data contrast those reported by Ngoh *et al* (2012), which indicated that ER stress exacerbated ER stress-induced apoptosis in Mfn2-deficient MEFs. Ngoh *et al* (2012) used 10-fold lower concentrations of Tg than those used in our study, and as a result they found that caspase activation was increased only 2-fold (in contrast to the 10-fold increase in our study). It is possible that the conditions used by Ngoh *et al* (2012) did not fully induce apoptosis in WT cells, as the UPR response was sufficient to deal with and resolve mild ER stress. However, under greater ER stress, cells showed a full apoptotic response.

Our data also indicate that overactivation of the PERK pathway is responsible for defective induction of apoptosis in response to ER stress. PERK loss-of-function rescued apoptosis during ER stress in the context of Mfn2 ablation. However, PERK silencing did not alter apoptosis in WT cells, and in turn apoptosis was not modified by silencing of XBP-1 or ATF6 in Mfn2 KO cells. The lack of capacity of Mfn2 KO cells to induce apoptosis during ER stress is surprising given that CHOP, one of the key regulators of apoptosis during ER stress (Tabas and Ron, 2011), is induced under these conditions. CHOP promotes BIM expression and suppresses the pro-survival protein Bcl2, which leads to the permeabilization of the mitochondrial outer membrane (McCullough *et al*, 2001; Puthalakath *et al*, 2007). Moreover, CHOP promotes mitochondrial calcium overload through the ERO1α-IP3R-CAMKII pathway (Seimon *et al*, 2006; Timmins *et al*, 2009; Li *et al*, 2010). However, this protein has also been associated with protection against cell death (Halterman *et al*, 2010; Rouschop *et al*, 2010).

Mfn2 overexpression has been reported to induce apoptosis in tumoural cells and to trigger ROS-mediated apoptosis through caspase activation (Guo *et al*, 2007; Shen *et al*, 2007; Wu *et al*, 2008). Moreover, the overexpression of this protein promotes spontaneous apoptosis and suppresses tumour growth *in vivo* (Rehman *et al*, 2012). In contrast, several reports have shown that Mfn1 or Mfn2 loss-of-function

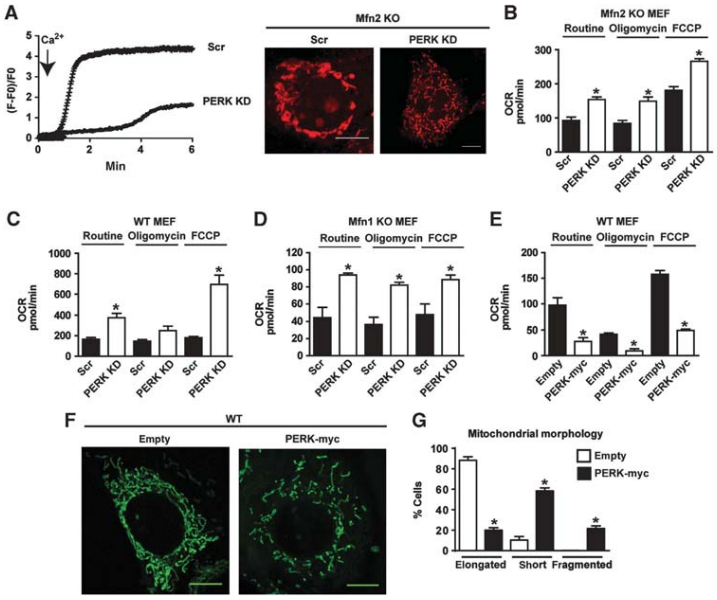

Figure 9 PERK knockdown normalizes mitochondrial Ca^{2+} overload and mitochondrial respiration. (**A**) Mitochondrial calcium overload in Scr and PERK KD Mfn2 KO cells. Cells were loaded with Rhod-2 and then treated with 2.5 mM $CaCl_2$ (left). Calcium uptake was monitored by confocal microscopy. Representative confocal images of mitochondrial morphology in WT and Mfn2 KO cells stained with Rhod-2 and incubated with 2.5 mM $CaCl_2$ for 5 min (right) . Scale bars: 10 μm. (**B**–**E**) Mitochondrial oxygen consumption (OCR) was measured in Scr and PERK KD Mfn2 KO cells (**B**), Scr and PERK KD WT cells (**C**), Scr and PERK KD Mfn1 KO cells (**D**), and WT cells stably expressing PERK-myc (**E**). Data are mean of three independent experiments. The following parameters were measured: oxygen consumption under routine conditions (DMEM with 5.5 mM glucose), maximal respiratory capacity reached after uncoupling with FCCP, and respiratory leak, measured after inhibition of ATP synthase with oligomycin. Data are mean ± s.e.m. $^*P<0.05$ versus Scr group or versus the empty plasmid group. (**F**, **G**) Representative confocal images of mitochondrial morphology in WT cells stably expressing PERK-myc stained with MitoTracker Green. Scale bars: 10 μm. Quantitative analysis of mitochondrial morphology is shown in **G**. Data are mean ± s.e.m. ($n=3$). $^*P<0.05$ versus the empty plasmid group.

increases sensitivity to apoptotic stimuli and that these proteins also interact with Bcl2 family members (Sugioka *et al*, 2004; Karbowski *et al*, 2006; Brooks *et al*, 2007; Hoppins *et al*, 2011; Leboucher *et al*, 2012). The increased sensitivity to apoptosis caused by loss-of-function is similar in both Mfn1 and Mfn2 ablation and is associated with mitochondrial fragmentation (Sugioka *et al*, 2004). Interestingly, a recent report demonstrates that Mfn2 and Bax/Bak are required for Ca^{2+}-induced mPTP opening. This novel role of Mfn2 and proteins of the Bcl2 family in necrosis indicates that mitochondrial dynamics coordinate the cell death pathway in a stimulus-dependent manner (Whelan *et al*, 2012).

Mitochondrial–ER coupling regulates metabolism, calcium signalling, and apoptosis (Simmen *et al*, 2005; de Brito and Scorrano, 2008; Bravo *et al*, 2011; Sebastian *et al*, 2012). Several reports indicate that depletion of the proteins involved in mitochondrial–ER contact sites, such as PACS-2, SERCA1T, and PML, blocks the apoptotic program (Simmen *et al*, 2005; Chami *et al*, 2008; Giorgi *et al*, 2010). Induction of the NogoB protein reduces ER–mitochondria coupling and inhibits apoptosis (Sutendra *et al*, 2011). Thus, ER–mitochondria coupling mediated by Mfn2 is crucial for metabolic homoeostasis and the regulation of cell death. On the basis of these observations, we propose that, under ER stress, Mfn2 is a key protein that determines cell fate via its role in ER–mitochondria coupling.

In all, this report uncovers a missing molecular link in the UPR. The observation that Mfn2 controls the UPR upon ER stress and that it is an upstream regulator of PERK reveals a previously unsuspected role for a protein most recognized for its key role in mitochondrial fusion. The Mfn2–PERK interaction also uncovers a new mechanism for the regulation of PERK. In keeping with the initial observations by de Brito and Scorrano (2008), our data support a major role of Mfn2 in mitochondrial–ER contact sites. Under basal conditions, Mfn2 suppresses PERK activation through direct interaction, and loss of interaction in Mfn2-eficient cells affects ROS production, mitochondrial morphology, respiration, and mitochondrial Ca^{2+} overload. Furthermore, Mfn2-deficient cells show an exaggerated activation of the UPR pathways, PERK, IRE-1α, and ATF6, and an enhanced response of PERK and XBP-1 is responsible for the deficient activation of apoptosis and autophagy, respectively. Our data show that Mfn2 plays a unique role in orchestrating mitochondrial metabolism and the UPR. These observations allow us to propose that Mfn2 senses the cellular metabolic state and coordinates the ER stress response.

Materials and methods

Reagents
See Supplementary Information.

Antibodies
See Supplementary Information.

Plasmids
See Supplementary Information.

Cells and cell culture
SV-40-transformed WT, Mfn1 KO, and Mfn2 KO MEFs were a gift from D.C. Chan (Division of Biology, California Institute of Technology, UA). Mfn KO cells, HEK293T, 3T3-L1, and C2C12 cell lines were from ATCC. MEFs, HEK293T, and C2C12 cells were grown in DMEM (Invitrogen) with 10% FBS and 100 U/ml of penicillin/streptomycin (Invitrogen), whereas 3T3L-1 cells were cultured in DMEM (GIBCO, Invitrogen 12800), 10% FBS, and 1.5 g/ml sodium bicarbonate at 37°C in a humidified atmosphere of 5% CO_2/95% O_2. Cells were starved of FBS for 3 h before the treatment with ER stress-inducing agents.

Animal care and generation of animal models
See Supplementary Information.

Western blotting assay
See Supplementary Information.

Lentivirus production and cell infection
Lentiviral vectors were packed using pMDLg/pRRE, pRSV-Rev, and pMD2.G plasmids. HEK293T cells were transfected with pLKO.1-puro plasmid or pLenti-GIII-CMV-hMFN2-HA and a third-generation packing system for 24 h at 37°C and incubated for additional 24 h at 33°C to facilitate lentiviral production. After 48 h of lentiviral particle production, MEFs, 3T3-L1, or C2C12 cells were infected with filtered lentiviral medium (derived from HEK293T cultures) supplemented with 2 μg/ml polybrene. Cells were then selected by incubation with 2.5 mg/ml puromycin in the complete medium.

Ecotropic retroviral packing
HEK293T cells were co-transfected with pCL-Eco and pBABE-puro mCherry-EGFP-LC3B, PERK-myc, or empty vector. After 48 h of retroviral particle production, MEFs, at 50% of confluence, were infected with retroviral medium (derived from HEK293T cultures) supplemented with 2 μg/ml polybrene (Sigma-Aldrich). Puromycin (2.5 μg/ml) was used to select stably transfected cells.

Confocal microscopy
For live imaging studies, cells were plated on 22-mm glass coverslips and transfected with 0.5 μg Sec61β-GFP, or BAK-GFP for 24 h using Metafectin (Bio-Rad). Cells were placed in a chamber under culture conditions (DMEM at 37°C and 5% CO2), and live cells were visualized using a Leica SP2 Confocal Microscope. Time-lapse microscopy analysis for ER expansion was performed in cells expressing ER-RFP. Cells were maintained in a chamber at 37°C equilibrated with 5% CO_2, and images were recorded every 5 min using a Nikon TE200 Inverted Microscope. Images were then processed with ImageJ software (NIH).

mCherry-GFP-LC3b confocal microscopy
WT and Mfn2 KO MEFs, as well as WT and Mfn2 KO MEFs stably transduced with lentiviruses encoding scrambled or XBP-1 shRNA, were studied. These cells were also transduced with a lentivirus expressing mCherry-GFP-LC3. mCherry/GFP-expressing cells were selected by flow cytometry, plated in 22-mm glass coverslips, and treated with ER stress inducers for 24 h. After treatment, the cells were fixed with 4% paraformaldehyde (PFA) in phosphate-buffered saline. All the cell images were obtained using SP2 Leica microscope. Autophagosomes and acidic autophagosomes were measured by confocal counting of the cells as mCherry+/GFP+ (yellow) puncta and mCherry+/GFP− (red) puncta, respectively. At least 50–100 cells/sample were counted in triplicate samples per condition and per experiment.

Labelling of mitochondrial compartment and morphological analysis
Cells were loaded with 100 nM Mitotracker Green or Mitotracker Red CMXRos for the last 20 min of incubation in culture medium. They were then washed with culture medium, and live cells were analyzed in an inverted Leica SP2 Confocal Microscope. Images were collected using a 488-nm excitation laser and 505–530-nm emission spectrum for Mitotracker Green, or excited at a wavelength of 561 nm and emission detected in red fluorescence for Mitotracker Red CMXRos. They were then processed with ImageJ software (NIH). Cells were classified on the basis of their mitochondrial morphology: oval/spheres (only observed in Mfn2 KO cells), short (<6 μm), or long (>6 μm) mitochondrial filaments. At least 100 cells/sample were counted in triplicate samples/condition/experiment.

Transmission electron microscopy
See Supplementary Information.

Cell death assays
See Supplementary Information.

Autophagy flux analysis and protein degradation assay
See Supplementary Information.

RNA extraction and Real-Time PCR
See Supplementary Information.

Luciferase reporter assay
MEFs were transfected for 24 h with 0.5 μg of 5XATF6-GL3 encoding a luciferase reporter construct for ATF6 activity and 0.5 μg TK Renilla by using Metafectin (Bio-Rad), following the manufacturer's instructions. Transfected cells were then incubated with 1 μM Tg for an additional 24 h. Luciferase activity was determined with the Dual-GLO Luciferase Assay System (Promega) in a luminometer Lumat LB 9507 (Berthold Technologies).

Oxygen consumption measurements in MEFs
MEFs (WT, Mfn1 KO, and Mfn2 KO) were plated in SeaHorse Bioscience XF24 plates. After 48 h, a Seahorse Bioscience XF24 extracellular flux analyzer was used to measure oxygen consumption. The instrument was calibrated the day before the experiment, following the manufacturer's instructions. On the day of the experiment, the injection ports on the sensor cartridge were loaded with 1.25 mM oligomycin (complex V inhibitor) to distinguish the percentage of oxygen consumption devoted to ATP synthesis and the percentage of oxygen consumption required to overcome the natural proton leak across the inner mitochondrial membrane: 1 mM FCCP was used to calculate the 'spare' respiratory capacity of cells, which is defined as the quantitative difference between maximal uncontrolled OCR and the initial basal OCR; and 0.1 mM rotenone (complex I inhibitor) and 0.1 mM antimycin A (complex III inhibitor) were used to calculate the remaining respiration caused by oxidative side reactions. During the sensor calibration, MEFs were kept in a 37°C incubator without CO_2 in 700 μl of respiration buffer (DMEM, 5 mM glucose, 2 mM glutamate, 31.6 mM NaCl and Phenol Red). Plates were immediately placed into the calibrated Seahorse XF24 flux analyzer for mitochondrial bioenergetic analysis.

Measurement of ROS
Cells were loaded with freshly prepared 10 μM dihydrorhodamine 123 ($\lambda_{excitation} = 543$ nm; $\lambda_{emission} = 560$ nm) for 30 min and then subjected to flow cytometry in a FACS Scan (Becton Dickinson, San Jose, CA).

Measurement of mitochondrial calcium
Cells were plated on coverslips and preloaded with 6 μM Rhod-2/0, 02% Pluronic F-127 in Krebs buffer without Ca^{2+} (145 mM NaCl, 5 mM KCl, 1 mM $MgCl_2$, 10 mM HEPES-Na, and 5.6 mM glucose, pH 7.4), and then incubated for 3 h at 4°C. They were washed two times with Krebs buffer. Mitochondrial Ca^{2+} uptake was monitored at 23°C in an inverted Leica SP2 confocal microscope. Cells were excited at 561 nm, and emission was detected in red fluorescence. Basal fluorescence was monitored for 1 min, and cells were then treated with 2.5 mM $CaCl_2$. Fluorescence was analyzed using Image J software. The increase in mitochondrial calcium uptake was expressed as F-F0/F0 where F is fluorescence intensity and F0 is basal fluorescence intensity.

Immunoprecipitation

Cells stably expressing retroviral PERK-myc were homogenized with IP buffer (50 mM Tris–HCl (pH 7.4), 150 mM NaCl, 1 mM EGTA, 1 mM EDTA, 1% Triton X-100, 2.5 mM $Na_4P_2O_7$, 20 mM NaF, 1 mM Na_3VO_4, 1 mM PMSF, and Roche protease inhibitor mixture) and centrifuged at 10 000 *g* for 30 min at 4°C. One milligram of protein lysate was incubated overnight at 4°C with an anti-c-Myc Agarose Affinity Gel antibody and then washed five times with IP buffer. To immunoprecipitate endogenous PERK, 1 mg of protein lysate was pre-cleared with IgG–agarose beads (Santa Cruz Biotechnology) for 2 h, and then the lysate was incubated overnight at 4°C with ImmunoCruz™ IP/WB Optima B beads (Santa Cruz Biotechnology), pre-incubated with an anti-PERK C-terminal antibody (Sigma-Aldrich) and then washed five times with IP buffer. Immunoblots were performed with specific antibodies against Mfn2 and PERK and detected with ImmunoCruz™ IP/WB secondary antibody (Santa Cruz Biotechnology).

Expression of results and statistical methods

Data are presented either as mean ± s.e.m. of a number of independent experiments (ranging from 3 to 15). Data were subjected to analysis of variance, and comparisons between groups were performed using a protected Tukey's *t*-test. A value of $P<0.05$ was chosen as the limit of statistical significance.

Supplementary data

Supplementary data are available at *The EMBO Journal* Online (http://www.embojournal.org).

Acknowledgements

EN is the recipient of a PhD scholarship from the Ministry of Science and Innovation (FPI Program). PMC is supported by a fellowship from the 'la Caixa/IRB International Ph.D. Programme. We thank I Castrillón, JC Monasterio, and J Seco for their technical assistance. We thank Ms T. Yates for editorial support. This study was funded by grants from the MEC (SAF2008-03803), the '*Generalitat de Catalunya*' (grant 2009SGR915), CIBERDEM ('*Instituto de Salud Carlos III*'), the FP7-European Commission (MITIN, HEALTH-F4-2008-223450), and INTERREG IV-B-SUDOE-FEDER (DIOMED, SOE1/P1/E178). AZ was the recipient of a Science Intensification Award from the University of Barcelona.

Authors contribution: JPM: conception and design of studies, data acquisition, analysis and interpretation, and writing the article; SI: design of studies, acquisition, analysis, and interpretation of data on apoptosis; JS-W, AS, CM, and PM-C: design of studies, acquisition, analysis, and interpretation of data on autophagy; EN and AD-R: design of studies, acquisition, analysis, and interpretation of data on respiration; MIH-A and DS: design of studies, acquisition, analysis, and interpretation of data on knockout mice; MP: analysis and interpretation of data; and AZ: conception and design of studies, data analysis and interpretation, and writing the article.

Conflict of interest

The authors declare that they have no conflict of interest.

References

Bach D, Pich S, Soriano FX, Vega N, Baumgartner B, Oriola J, Daugaard JR, Lloberas J, Camps M, Zierath JR, Rabasa-Lhoret R, Wallberg-Henriksson H, Laville M, Palacin M, Vidal H, Rivera F, Brand M, Zorzano A (2003) Mitofusin-2 determines mitochondrial network architecture and mitochondrial metabolism. A novel regulatory mechanism altered in obesity. *J Biol Chem* **278:** 17190–17197

Bravo R, Vicencio JM, Parra V, Troncoso R, Munoz JP, Bui M, Quiroga C, Rodriguez AE, Verdejo HE, Ferreira J, Iglewski M, Chiong M, Simmen T, Zorzano A, Hill JA, Rothermel BA, Szabadkai G, Lavandero S (2011) Increased ER-mitochondrial coupling promotes mitochondrial respiration and bioenergetics during early phases of ER stress. *J Cell Sci* **124:** 2143–2152

Brooks C, Wei Q, Feng L, Dong G, Tao Y, Mei L, Xie ZJ, Dong Z (2007) Bak regulates mitochondrial morphology and pathology during apoptosis by interacting with mitofusins. *Proc Natl Acad Sci USA* **104:** 11649–11654

Chami M, Oules B, Szabadkai G, Tacine R, Rizzuto R, Paterlini-Brechot P (2008) Role of SERCA1 truncated isoform in the proapoptotic calcium transfer from ER to mitochondria during ER stress. *Mol Cell* **32:** 641–651

Chen H, Chomyn A, Chan DC (2005) Disruption of fusion results in mitochondrial heterogeneity and dysfunction. *J Biol Chem* **280:** 26185–26192

Chen H, Detmer SA, Ewald AJ, Griffin EE, Fraser SE, Chan DC (2003) Mitofusins Mfn1 and Mfn2 coordinately regulate mitochondrial fusion and are essential for embryonic development. *J Cell Biol* **160:** 189–200

de Brito OM, Scorrano L (2008) Mitofusin 2 tethers endoplasmic reticulum to mitochondria. *Nature* **456:** 605–610

Doroudgar S, Thuerauf DJ, Marcinko MC, Belmont PJ, Glembotski CC (2009) Ischaemia activates the ATF6 branch of the endoplasmic reticulum stress response. *J Biol Chem* **284:** 29735–29745

Friedman JR, Lackner LL, West M, DiBenedetto JR, Nunnari J, Voeltz GK (2011) ER tubules mark sites of mitochondrial division. *Science* **334:** 358–362

Giorgi C, Ito K, Lin HK, Santangelo C, Wieckowski MR, Lebiedzinska M, Bononi A, Bonora M, Duszynski J, Bernardi R, Rizzuto R, Tacchetti C, Pinton P, Pandolfi PP (2010) PML regulates apoptosis at endoplasmic reticulum by modulating calcium release. *Science* **330:** 1247–1251

Guo X, Chen KH, Guo Y, Liao H, Tang J, Xiao RP (2007) Mitofusin 2 triggers vascular smooth muscle cell apoptosis via mitochondrial death pathway. *Circ Res* **101:** 1113–1122

Hailey DW, Rambold AS, Satpute-Krishnan P, Mitra K, Sougrat R, Kim PK, Lippincott-Schwartz J (2010) Mitochondria supply membranes for autophagosome biogenesis during starvation. *Cell* **141:** 656–667

Halterman MW, Gill M, DeJesus C, Ogihara M, Schor NF, Federoff HJ (2010) The endoplasmic reticulum stress response factor CHOP-10 protects against hypoxia-induced neuronal death. *J Biol Chem* **285:** 21329–21340

Harding HP, Novoa I, Zhang Y, Zeng H, Wek R, Schapira M, Ron D (2000) Regulated translation initiation controls stress-induced gene expression in mammalian cells. *Mol Cell* **6:** 1099–1108

Harding HP, Zhang Y, Ron D (1999) Protein translation and folding are coupled by an endoplasmic-reticulum-resident kinase. *Nature* **397:** 271–274

Hetz C, Bernasconi P, Fisher J, Lee AH, Bassik MC, Antonsson B, Brandt GS, Iwakoshi NN, Schinzel A, Glimcher LH, Korsmeyer SJ (2006) Proapoptotic BAX and BAK modulate the unfolded protein response by a direct interaction with IRE1alpha. *Science* **312:** 572–576

Hetz C, Thielen P, Matus S, Nassif M, Court F, Kiffin R, Martinez G, Cuervo AM, Brown RH, Glimcher LH (2009) XBP-1 deficiency in the nervous system protects against amyotrophic lateral sclerosis by increasing autophagy. *Genes Dev* **23:** 2294–2306

Hoppins S, Edlich F, Cleland MM, Banerjee S, McCaffery JM, Youle RJ, Nunnari J (2011) The soluble form of Bax regulates mitochondrial fusion via MFN2 homotypic complexes. *Mol Cell* **41:** 150–160

Hotamisligil GS (2010) Endoplasmic reticulum stress and the inflammatory basis of metabolic disease. *Cell* **140:** 900–917

Inesi G, Wade R, Rogers T (1998) The sarcoplasmic reticulum $Ca2^+$ pump: inhibition by thapsigargin and enhancement by adenovirus-mediated gene transfer. *Ann N Y Acad Sci* **853:** 195–206

Ishihara N, Eura Y, Mihara K (2004) Mitofusin 1 and 2 play distinct roles in mitochondrial fusion reactions via GTPase activity. *J Cell Sci* **117:** 6535–6546

Karbowski M, Norris KL, Cleland MM, Jeong SY, Youle RJ (2006) Role of Bax and Bak in mitochondrial morphogenesis. *Nature* **443:** 658–662

Kouroku Y, Fujita E, Tanida I, Ueno T, Isoai A, Kumagai H, Ogawa S, Kaufman RJ, Kominami E, Momoi T (2007) ER stress (PERK/eIF2alpha phosphorylation) mediates the polyglutamine-induced LC3 conversion, an essential step for autophagy formation. *Cell Death Differ* **14:** 230–239

Leboucher GP, Tsai YC, Yang M, Shaw KC, Zhou M, Veenstra TD, Glickman MH, Weissman AM (2012) Stress-induced phosphorylation

and proteasomal degradation of mitofusin 2 facilitates mitochondrial fragmentation and apoptosis. *Mol Cell* **47**(4): 547–57

Legros F, Lombes A, Frachon P, Rojo M (2002) Mitochondrial fusion in human cells is efficient, requires the inner membrane potential, and is mediated by mitofusins. *Mol Biol Cell* **13:** 4343–4354

Li G, Scull C, Ozcan L, Tabas I (2010) NADPH oxidase links endoplasmic reticulum stress, oxidative stress, and PKR activation to induce apoptosis. *J Cell Biol* **191:** 1113–1125

Lu PD, Harding HP, Ron D (2004a) Translation reinitiation at alternative open reading frames regulates gene expression in an integrated stress response. *J Cell Biol* **167:** 27–33

Lu PD, Jousse C, Marciniak SJ, Zhang Y, Novoa I, Scheuner D, Kaufman RJ, Ron D, Harding HP (2004b) Cytoprotection by pre-emptive conditional phosphorylation of translation initiation factor 2. *EMBO J* **23:** 169–179

Maiuolo J, Bulotta S, Verderio C, Benfante R, Borgese N (2011) Selective activation of the transcription factor ATF6 mediates endoplasmic reticulum proliferation triggered by a membrane protein. *Proc Natl Acad Sci USA* **108:** 7832–7837

McCullough KD, Martindale JL, Klotz LO, Aw TY, Holbrook NJ (2001) Gadd153 sensitizes cells to endoplasmic reticulum stress by down-regulating Bcl2 and perturbing the cellular redox state. *Mol Cell Biol* **21:** 1249–1259

Michelangeli F, East JM (2011) A diversity of SERCA $Ca2^+$ pump inhibitors. *Biochem Soc Trans* **39:** 789–797

Neuspiel M, Zunino R, Gangaraju S, Rippstein P, McBride H (2005) Activated mitofusin 2 signals mitochondrial fusion, interferes with Bax activation, and reduces susceptibility to radical induced depolarization. *J Biol Chem* **280:** 25060–25070

Ngoh GA, Papanicolaou KN, Walsh K (2012) Loss of mitofusin 2 promotes endoplasmic reticulum stress. *J Biol Chem* **287:** 20321–20332

Novoa I, Zeng H, Harding HP, Ron D (2001) Feedback inhibition of the unfolded protein response by GADD34-mediated dephosphorylation of eIF2alpha. *J Cell Biol* **153:** 1011–1022

Ogata M, Hino S, Saito A, Morikawa K, Kondo S, Kanemoto S, Murakami T, Taniguchi M, Tanii I, Yoshinaga K, Shiosaka S, Hammarback JA, Urano F, Imaizumi K (2006) Autophagy is activated for cell survival after endoplasmic reticulum stress. *Mol Cell Biol* **26:** 9220–9231

Pich S, Bach D, Briones P, Liesa M, Camps M, Testar X, Palacin M, Zorzano A (2005) The Charcot-Marie-Tooth type 2A gene product, Mfn2, up-regulates fuel oxidation through expression of OXPHOS system. *Hum Mol Genet* **14:** 1405–1415

Puthalakath H, O'Reilly LA, Gunn P, Lee L, Kelly PN, Huntington ND, Hughes PD, Michalak EM, McKimm-Breschkin J, Motoyama N, Gotoh T, Akira S, Bouillet P, Strasser A (2007) ER stress triggers apoptosis by activating BH3-only protein Bim. *Cell* **129:** 1337–1349

Rao RV, Castro-Obregon S, Frankowski H, Schuler M, Stoka V, del Rio G, Bredesen DE, Ellerby HM (2002) Coupling endoplasmic reticulum stress to the cell death program. An Apaf-1-independent intrinsic pathway. *J Biol Chem* **277:** 21836–21842

Rehman J, Zhang HJ, Toth PT, Zhang Y, Marsboom G, Hong Z, Salgia R, Husain AN, Wietholt C, Archer SL (2012) Inhibition of mitochondrial fission prevents cell cycle progression in lung cancer. *FASEB J* **26:** 2175–2186

Rouschop KM, van den Beucken T, Dubois L, Niessen H, Bussink J, Savelkouls K, Keulers T, Mujcic H, Landuyt W, Voncken JW, Lambin P, van der Kogel AJ, Koritzinsky M, Wouters BG (2010) The unfolded protein response protects human tumour cells during hypoxia through regulation of the autophagy genes MAP1LC3B and ATG5. *J Clin Invest* **120:** 127–141

Rzymski T, Milani M, Pike L, Buffa F, Mellor HR, Winchester L, Pires I, Hammond E, Ragoussis I, Harris AL (2010) Regulation of autophagy by ATF4 in response to severe hypoxia. *Oncogene* **29:** 4424–4435

Santel A, Fuller MT (2001) Control of mitochondrial morphology by a human mitofusin. *J Cell Sci* **114:** 867–874

Schewe DM, Aguirre-Ghiso JA (2008) ATF6alpha-Rheb-mTOR signaling promotes survival of dormant tumour cells *in vivo*. *Proc Natl Acad Sci USA* **105:** 10519–10524

Sebastian D, Hernandez-Alvarez MI, Segales J, Sorianello E, Munoz JP, Sala D, Waget A, Liesa M, Paz JC, Gopalacharyulu P, Oresic M, Pich S, Burcelin R, Palacin M, Zorzano A (2012) Mitofusin 2 (Mfn2) links mitochondrial and endoplasmic reticulum function with insulin signaling and is essential for normal glucose homoeostasis. *Proc Natl Acad Sci USA* **109:** 5523–5528

Seimon TA, Obstfeld A, Moore KJ, Golenbock DT, Tabas I (2006) Combinatorial pattern recognition receptor signaling alters the balance of life and death in macrophages. *Proc Natl Acad Sci USA* **103:** 19794–19799

Shen T, Zheng M, Cao C, Chen C, Tang J, Zhang W, Cheng H, Chen KH, Xiao RP (2007) Mitofusin-2 is a major determinant of oxidative stress-mediated heart muscle cell apoptosis. *J Biol Chem* **282:** 23354–23361

Simmen T, Aslan JE, Blagoveshchenskaya AD, Thomas L, Wan L, Xiang Y, Feliciangeli SF, Hung CH, Crump CM, Thomas G (2005) PACS-2 controls endoplasmic reticulum-mitochondria communication and Bid-mediated apoptosis. *EMBO J* **24:** 717–729

Sperandio S, de Belle I, Bredesen DE (2000) An alternative, non-apoptotic form of programmed cell death. *Proc Natl Acad Sci USA* **97:** 14376–14381

Sugioka R, Shimizu S, Tsujimoto Y (2004) Fzo1, a protein involved in mitochondrial fusion, inhibits apoptosis. *J Biol Chem* **279:** 52726–52734

Sutendra G, Dromparis P, Wright P, Bonnet S, Haromy A, Hao Z, McMurtry MS, Michalak M, Vance JE, Sessa WC, Michelakis ED (2011) The role of Nogo and the mitochondria-endoplasmic reticulum unit in pulmonary hypertension. *Sci Transl Med* **3:** 88ra55

Tabas I, Ron D (2011) Integrating the mechanisms of apoptosis induced by endoplasmic reticulum stress. *Nat Cell Biol* **13:** 184–190

Teske BF, Wek SA, Bunpo P, Cundiff JK, McClintick JN, Anthony TG, Wek RC (2011) The eIF2 kinase PERK and the integrated stress response facilitate activation of ATF6 during endoplasmic reticulum stress. *Mol Biol Cell* **22:** 4390–4405

Timmins JM, Ozcan L, Seimon TA, Li G, Malagelada C, Backs J, Backs T, Bassel-Duby R, Olson EN, Anderson ME, Tabas I (2009) Calcium/calmodulin-dependent protein kinase II links ER stress with Fas and mitochondrial apoptosis pathways. *J Clin Invest* **119:** 2925–2941

Verfaillie T, Rubio N, Garg AD, Bultynck G, Rizzuto R, Decuypere JP, Piette J, Linehan C, Gupta S, Samali A, Agostinis P (2012) PERK is required at the ER-mitochondrial contact sites to convey apoptosis after ROS-based ER stress. *Cell Death Differ* **19**(11): 1880–91

Wang Y, Li X, Wang L, Ding P, Zhang Y, Han W, Ma D (2004) An alternative form of paraptosis-like cell death, triggered by TAJ/TROY and enhanced by PDCD5 overexpression. *J Cell Sci* **117:** 1525–1532

Whelan RS, Konstantinidis K, Wei AC, Chen Y, Reyna DE, Jha S, Yang Y, Calvert JW, Lindsten T, Thompson CB, Crow MT, Gavathiotis E, Dorn 2nd GW, O'Rourke B, Kitsis RN (2012) Bax regulates primary necrosis through mitochondrial dynamics. *Proc Natl Acad Sci USA* **109:** 6566–6571

Wu L, Li Z, Zhang Y, Zhang P, Zhu X, Huang J, Ma T, Lu T, Song Q, Li Q, Guo Y, Tang J, Ma D, Chen KH, Qiu X (2008) Adenovirus-expressed human hyperplasia suppressor gene induces apoptosis in cancer cells. *Mol Cancer Ther* **7:** 222–232

Xu W, Liu L, Charles IG, Moncada S (2004) Nitric oxide induces coupling of mitochondrial signalling with the endoplasmic reticulum stress response. *Nat Cell Biol* **6:** 1129–1134

Yamamoto K, Yoshida H, Kokame K, Kaufman RJ, Mori K (2004) Differential contributions of ATF6 and XBP1 to the activation of endoplasmic reticulum stress-responsive cis-acting elements ERSE, UPRE and ERSE-II. *J Biochem* **136:** 343–350

Yoon MJ, Kim EH, Lim JH, Kwon TK, Choi KS (2010) Superoxide anion and proteasomal dysfunction contribute to curcumin-induced paraptosis of malignant breast cancer cells. *Free Radic Biol Med* **48:** 713–726

Yorimitsu T, Nair U, Yang Z, Klionsky DJ (2006) Endoplasmic reticulum stress triggers autophagy. *J Biol Chem* **281:** 30299–30304

Zhao T, Huang X, Han L, Wang X, Cheng H, Zhao Y, Chen Q, Chen J, Xiao R, Zheng M (2012) Central role of mitofusin 2 in autophagosome-lysosome fusion in cardiomyocytes. *J Biol Chem* **287:** 23615–23625